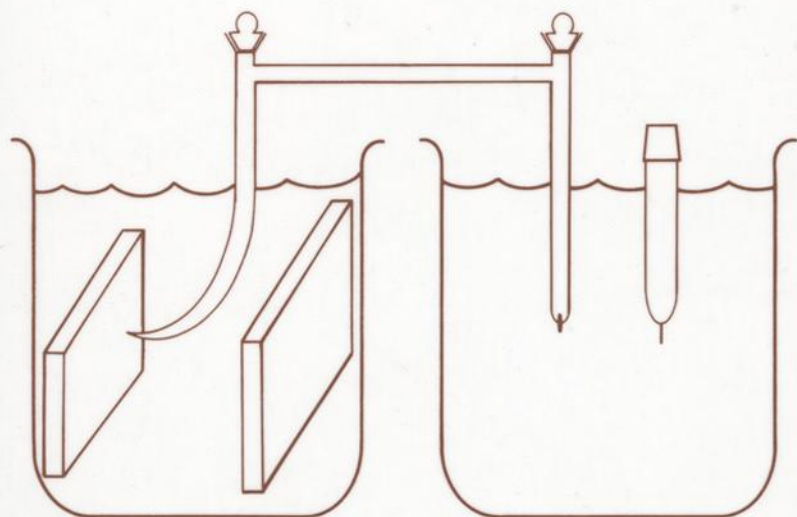


# THE MEASUREMENT AND CORRECTION OF ELECTROLYTE RESISTANCE

## IN ELECTROCHEMICAL TESTS

Scribner/Taylor, editors



ASTM  
STP  
1056

STP 1056

***The Measurement and Correction  
of Electrolyte Resistance in  
Electrochemical Tests***

*L. L. Scribner and S. R. Taylor, editors*



ASTM  
1916 Race Street  
Philadelphia, PA 19103

Library of Congress Cataloging-in-Publication Data

The Measurement and correction of electrolyte resistance in electrochemical tests / L.L. Scribner and S.R. Taylor, editors. (STP ; 1056)

Papers presented at the Symposium on Ohmic Electrolyte Resistance Measurement and Compensation, held at Baltimore, MD, 1988; sponsored by ASTM Committees G-1 on Corrosion of Metals and G1.11 on Electrochemical Measurements in Testing.

Includes bibliographical references.

ISBN 0-8031-1283-1

1. Electrolytes--Conductivity--Measurement--Congresses.
2. Electric measurements--Congresses. 3. Electric resistance--Measurement--Congresses. I. Scribner, L. L. (Louis L.), 1944-II. Taylor, S. R. (S. Ray), 1953- . III. American Society for Testing and Materials. Committee G-1 on Corrosion of Metals.
- IV. ASTM Committee G-11 on Electrochemical Measurements in Testing.
- V. Symposium on Ohmic Electrolyte Resistance Measurement and Compensation (1988 : Baltimore, Md.) VI. Series: ASTM special technical paper ; 1056.

QD565.M43 1990

541.3'72--dc20

89-18322

CIP

Copyright © by AMERICAN SOCIETY FOR TESTING AND MATERIALS 1990

NOTE

The Society is not responsible, as a body,  
for the statements and opinions  
advanced in this publication.

**Peer Review Policy**

Each paper published in this volume was evaluated by three peer reviewers. The authors addressed all of the reviewers' comments to the satisfaction of both the technical editor(s) and the ASTM Committee on Publications.

The quality of the papers in this publication reflects not only the obvious efforts of the authors and the technical editor(s), but also the work of these peer reviewers. The ASTM Committee on Publications acknowledges with appreciation their dedication and contribution of time and effort on behalf of ASTM.

## Foreword

The Symposium on Ohmic Electrolyte Resistance Measurement and Compensation was held at Baltimore, MD on 17 May 1988. ASTM Committees G-1 on Corrosion of Metals and G1.11 on Electrochemical Measurements in Testing sponsored the symposium. L. L. Scribner and S. R. Taylor, University of Virginia, served as chairmen of the symposium and are editors of the resulting publication.

# Contents

<b>Overview</b>	1
<b>THEORY</b>	
<b>Influence of Electrolyte Resistance on Electrochemical Measurements and Procedures to Minimize or Compensate for Resistance Errors—</b> HARVEY P. HACK, PATRICK J. MORAN, AND JOHN R. SCULLY	5
<b>IR Drop in Electrochemical Corrosion Studies—Part I: Basic Concepts and Estimates of Possible Measurement Errors—</b> WILLIAM C. EHRHARDT	27
<b>CRITICAL COMPARISONS OF METHODS</b>	
<b>Theoretical Problems Related to Ohmic Resistance Compensation—</b> KEMAL NISANCIOGLU	61
<b>IR Drop in Electrochemical Corrosion Studies—Part 2: A Multiple Method IR Compensation System—</b> WILLIAM C. EHRHARDT	78
<b>Determination and Elimination of the Uncompensated Resistance in Low Conductivity Media—</b> FLORIAN MANSFELD, Y. C. CHEN, AND H. SHIH	95
<b>MATHEMATICAL APPROACHES</b>	
<b>Correction of Experimental Data for the Ohmic Potential Drop Corresponding to a Secondary Current Distribution on a Disk Electrode—</b> J. MATTHEW ESTEBAN, MARK LOWRY, AND MARK E. ORAZEM	127
<b>Application of Numerical Simulations to Evaluate Components of Potential Difference in Solution—</b> VINCENT FAROZIC AND GEOFFREY PRENTICE	142
<b>APPLICATIONS</b>	
<b>Ohmic Compensation in Desert Soil Using a Galvanostatic DC Bridge—</b> DANIEL ABRAHAM, DENNY A. JONES, MICHAEL R. WHITBECK, AND CLINTON M. CASE	157

<b>Measurements of IR-Drop Free Pipe-to-Soil Potentials on Buried Pipelines—</b> NEIL G. THOMPSON AND JOHN A. BEAVERS	168
<b>Elimination of IR Error in Measurements of Corrosion in Concrete—</b> E. ESCALANTE	180
<b>Comparison of Current Interruption and Electrochemical Impedance Techniques in the Determination of Corrosion Rates of Steel in Concrete—</b> NEAL S. BERKE, DING FENG SHEN, AND KATHLEEN M. SUNDBERG	191
<b>Measurement of the Components of the Ohmic Resistance in Lithium/Iodine (P2VP) Batteries—</b> C. C. STREINZ, R. G. KELLY, P. J. MORAN, J. JOLSON, J. R. WAGGONER, AND S. WICELINSKI	202
<b>The Importance of Ohmic Potential Drop in Crevice Corrosion—</b> BARBARA A. SHAW	211
<b>Index</b>	221

## Overview

---

The measurement of any electrode potential includes an error caused by a voltage drop through the electrolyte. This error is caused by the inherent resistance (IR) of the solution and is proportional to the cell current. It has therefore been referred to as IR drop, ohmic overpotential, IR voltage error, or potential error caused by solution resistance. As the current or solution resistivity increase, or both, the error in electrode potential measurements can become quite large, thus distorting current-potential data and preventing accurate interpretation. Due to the ubiquitous nature of ohmic electrolyte resistance throughout the electrochemical sciences, an understanding of the phenomenon, methods to measure it, and means to correct for its presence are required to obtain precise data.

The purpose of this book is to present, review, and critique new and existing methods for the correction of ohmic electrolyte resistance. Although the 13 papers have been segregated into the areas of Theory, Critical Comparisons, Mathematical Approaches, and Applications, many of the papers are more broadly based, covering more than one of the above areas.

The reader is introduced to the theoretical considerations of ohmic electrolyte resistance measurements by Hack, Scully, and Moran in their review of the impact and methods for correcting IR in electrochemical measurements. This is complemented by Ehrhardt's paper, which includes consideration of cell geometry, current distribution, and the type of experiment on the IR voltage drop.

The next section critically compares several of the commonly available methods for correcting the error associated with IR voltage drop. Nisancioglu compares the current interruption, potential pulse, and electrochemical impedance techniques, and discusses error correction using electrode design, measurement technique, and data analysis. Mansfeld, Chen, and Shih compare correction methods present in commercially available systems and discuss the practical advantages and limitations of the respective techniques and equipment. Ehrhardt also reviews existing correction methods, but compares them experimentally to a new system introduced by the author, which is capable of combining different methods.

Esteban, Lowry, and Orazem introduce a numerical method to adjust current-potential data for the electrolyte resistance. This has provided better agreement between experimental data and mathematical models for the rotating disc electrode. Farozic and Prentice utilize numerical simulation of the potential distribution in more complex systems (for example, multiple electrode, irregular electrode shape) to provide insight into data interpretation and optimization of electrode arrangement.

The last section examines engineering applications of IR voltage drop measurement and correction. Thompson discusses the issues related to potential measurements of buried pipelines under cathodic protection. Abraham, Jones, Whitbeck, and Case use a modified Wheatstone bridge to assess ohmic interference associated with corrosion measurements of nuclear waste containers in desert soil. Another important area in which high-resistivity media complicate electrode potential measurements is that of rebar corrosion in concrete. The paper by Escalante describes the use of current interruption as a means to eliminate

the IR error that arises in the measurement of the potential of steel in concrete under galvanostatic conditions. Berke, Shen, and Sundberg look at the same rebar/concrete system, but compare two correction methods, current interruption and electrochemical impedance measurements. Streinz et al. present a number of methods for determining the sources of ohmic resistance in lithium/iodine batteries. The final paper by Shaw focuses on the importance of ohmic potential drop in crevice corrosion measurements, an area of extreme importance when one realizes its relevance to other areas such as environmentally assisted fracture.

The universal nature of the ohmic electrolyte resistance and its bearing on subsequent electrode potential measurements must be recognized and corrected for by those in the electrochemical sciences. We feel that the depth, range, and relevance of the topics presented here will make this STP an excellent reference and source for the electrochemical scientist and engineer.

*Ray Taylor*

University of Virginia, Department of  
Materials Science, Thornton Hall, Char-  
lottesville, VA 22903; symposium chair-  
man and editor.

*Louie Scribner*

University of Virginia, Department of  
Materials Science, Thornton Hall, Char-  
lottesville, VA 22903; symposium chair-  
man and editor.

# Theory

# Influence of Electrolyte Resistance on Electrochemical Measurements and Procedures to Minimize or Compensate for Resistance Errors

---

**REFERENCE:** Hack, H. P., Moran, P. J., and Scully, J. R., "Influence of Electrolyte Resistance on Electrochemical Measurements and Procedures to Minimize or Compensate for Resistance Errors," *The Measurement and Correction of Electrolyte Resistance in Electrochemical Tests, ASTM STP 1056*, L. L. Scribner and S. R. Taylor, Eds., American Society for Testing and Materials, Philadelphia, 1990, pp. 5-26.

**ABSTRACT:** Electrolyte resistance is receiving increasing attention as a source of error in electrochemical measurements when not properly managed. This paper is designed as an introduction to, and summary of, this topic. A discussion of electrolyte resistance and its effect on the results of electrochemical measurements is presented. A broad spectrum of methods for minimizing or correcting the errors caused by electrolyte resistance is described. Several advanced ideas are also introduced. References are given to lead the reader to additional information.

**KEY WORDS:** corrosion testing, electrochemical testing, electrolyte resistance, IR drop, IR compensation, current distribution, current interruption, electrochemical impedance spectroscopy, AC impedance, potentiostatic testing

## Introduction

Electrolyte resistance and resistances of other components in the electrochemical circuit can have significant effects on the measurements being performed. The IR error in any electrochemical measurement in which there is an applied current, such as in corrosion testing, causes the applied potential (in potentiostatic or potentiodynamic control) or the measured potential (in current control) to deviate from that of the actual potential across the electrode/electrolyte interface being studied. This error can be large for the cases of high currents and/or low electrolyte conductivity. Alternatively, the error may be small enough to be ignored, but it cannot be completely eliminated. This paper is designed to be an introduction to, and summary of, the topic of electrolyte resistance as a source of error in electrochemical measurements.

### *What Effect Does Electrolyte Resistance Have?*

In Figs. 1 and 2, two identical electrodes are electrically connected by external wires of zero resistance, and a battery is used to force a potential difference,  $E_A$ , between them. The

<sup>1</sup> Metallurgists, Marine Corrosion Branch, David Taylor Research Center, Bethesda, MD.

<sup>2</sup> Associate professor, Corrosion and Electrochemistry Research Laboratory, The Johns Hopkins University, Baltimore, MD.

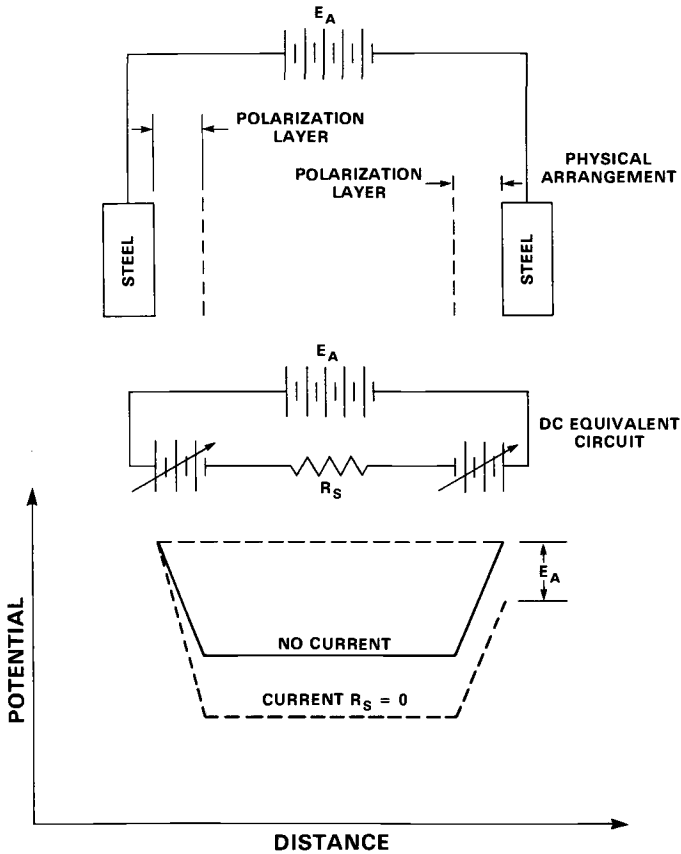


FIG. 1—Potential distribution in a cell with no electrolyte resistance.

resultant current flow will change the magnitude of the initial potential step across each double layer so that these steps sum to  $E_A$ . In the case of zero electrolyte resistance, as in Fig. 1, the potential will be uniform throughout the electrolyte.

Figure 2 illustrates the same situation when the electrolyte resistance is significant. Imposing a potential will cause a current to flow through the resistive electrolyte that generates a potential drop in the electrolyte of  $I$  times the solution resistance  $R_S$ . In a one-dimensional cell, such as a tube of electrolyte with electrodes at both ends, this results in a linear potential gradient through the electrolyte. In more complex three-dimensional geometries, the profile will not be linear. The total imposed cell potential in the case of a significant electrolyte resistance now includes  $I$  times  $R_S$  in the electrolyte as well as the sum of the potential steps at the two electrodes.

Figures 1 and 2 also contain the DC equivalent circuits for the situations described. The applied potential,  $E_A$ , is represented by a battery, potential steps in the polarization layers by variable batteries, and solution resistance by a resistor.

The effect of the potential gradient in the electrolyte on a potentiostatic test, such as that in ASTM Reference Test Method for Making Potentiostatic and Potentiodynamic Anodic Polarization Measurements (G 5), is illustrated in Fig. 3. Between the working electrode surface and the reference electrode position is a portion of the electrolyte resistance,

$R_{S(\text{Uncomp})}$ . Between the working electrode and the counter electrode position is the electrolyte resistance,  $R_S$ . The potentiostat will hold the potential difference between the specimen and the reference electrode position at a constant value,  $E_{\text{SET}}$ . If the electrolyte resistance is significant, then the electrolyte potential gradient will cause an error in the measured working electrode potential of magnitude  $I$  times  $R_{S(\text{Uncomp})}$ . The specimen will not be at the potential set by the potentiostat, but at a potential,  $E_{\text{ACTUAL}}$ , that depends on the location of the reference electrode, the electrolyte resistivity, and the total current flow.

### Other Sources of Error

Any component of the electrical circuit of the electrochemical cell which gives rise to a resistance other than that at the double layers can also introduce similar errors. The most common of these is lead resistance, caused by a significant lead wire resistance that creates a voltage drop that makes the potential at the specimen terminal of the potentiostat different from that actually at the sample. In this case, the potential at the specimen terminal has an error, whereas with electrolyte resistance, the potential at the reference electrode position is in error. The effect, however, is the same.

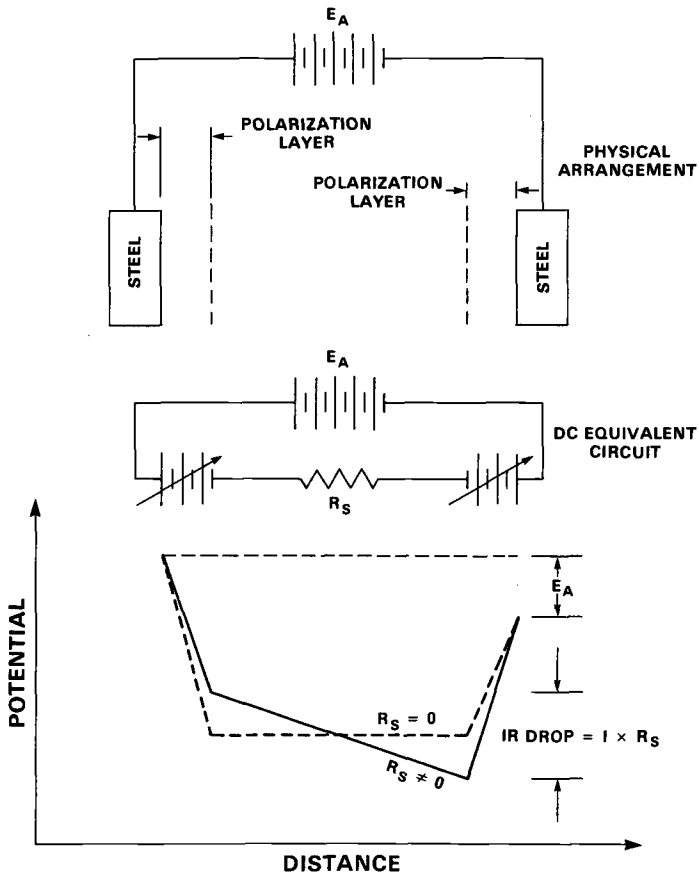


FIG. 2—Potential distribution in a cell with electrolyte resistance.

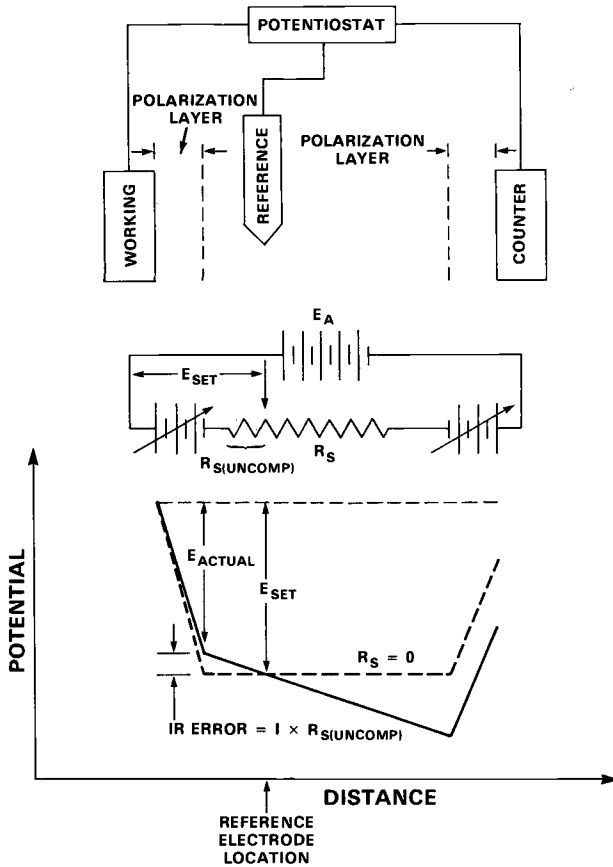


FIG. 3—Potential distribution in a cell with a potentiostat.

If the electrical connection to the working electrode is poor, it adds a high resistance which will result in measurement errors in the working-reference voltage. This can be the result of a cold solder joint, improper cleaning of a threaded connection, insufficient pressure or cleaning of a pressure connection, etc. The current flowing through the resistance at the poor joint creates a potential difference between the metal specimen and the wire connected to it. A long working electrode lead may itself have a significant resistance. Although the reference circuit carries almost no current, a sufficiently high resistance there will still cause a reference potential error. If the glass sheath of a glass-encased reference electrode dries out, a high resistance may be created in the electrolyte path of the reference electrode. These factors can contribute errors to the measurement and are easily avoided by proper experimental technique.

If the specimen material itself is extremely thin or is not a good conductor of electricity, a potential difference may be generated between the wire connection point and the specimen surface at the electrolyte due to the resistance of the bulk specimen material. This is a particularly difficult problem to handle since the resistance between the connection point and a given point on the specimen surface may vary with location, giving a potential error which is not the same everywhere on the specimen surface. This might occur, for example,

on a composite specimen where conductive graphite fibers are in a nonconductive matrix like epoxy.

Finally, surface films on the specimen may also cause an unwanted resistance in the current path. These may be due to air-formed oxides, calcareous deposits, biological layers, etc., and can introduce measurement error. Unlike the previous resistances discussed, a surface film may not generate a potential drop strictly by Ohm's Law, but may have a current-dependent resistance, or may even rectify the current like a diode such that the resistance of the film is different depending on the direction of current flow.

### *What Is a Significant Resistance?*

The significance level for resistance depends on the total current flowing in the cell and the level of potential error (produced by the product of current times resistance) that can be tolerated. This depends on the type of experiment being performed as well as the system being studied. If in doubt, procedures for minimization or correction of these errors should be performed.

### *What Is This Type of Error Called?*

A number of terms have been coined for the above described type of error, but none is perfectly descriptive. "IR drop" error implies that measurement errors are usually due to a current,  $I$ , flowing through a resistance,  $R$ , creating a potential drop via Ohm's Law. The term "uncompensated ohmic resistance" implies that the impedance causing the error is ohmic, with no capacitive or inductive components (unlike most impedances across double layers), and is not compensated for by simple measurement techniques. Since there are many ways used to compensate for this type of error, as described below, this term cannot be applied for a well-conducted test. The term "uncompensated electrolyte resistance" also implies that the test was not conducted with proper compensation, and refers only to electrolyte resistance, thereby ignoring the other causes such as lead resistance. "Ohmic resistance" error implies that impedances leading to these errors have no capacitive or inductive components. This can be confusing since there are ohmic components of polarization resistance that are not part of this error. The term "solution resistance" is vague and unspecific. For the purposes of the remainder of this paper, the term "IR error" will be used.

### *Why Is It Bad?*

IR error is bad for electrochemical measurements because it causes incorrect measurements to be made. Several specific errors associated with specific types of tests are described below:

*Overestimation of Polarization Resistance*—The polarization resistance test, such as in ASTM Practice for Conducting Potentiodynamic Polarization Resistance Measurements (G 59), is designed to measure  $R_p$ . The resistance of the electrolyte between the specimen and the reference electrode position, the resistance of any lead or connection, and the bulk specimen resistance are all in series with the resistance of the double layer being measured. These various resistances cannot be distinguished by the potentiostat in a DC measurement, and therefore the measured resistance will include the sum of all of these terms. If these resistances are not accounted for, they will give a polarization resistance which is higher than the true value [ $I$ ]. This can be seen in Fig. 4. Even small electrolyte resistances can lead to significant errors in polarization resistance for rapidly corroding materials that have low polarization resistances. If IR errors associated with this type of test are not con-

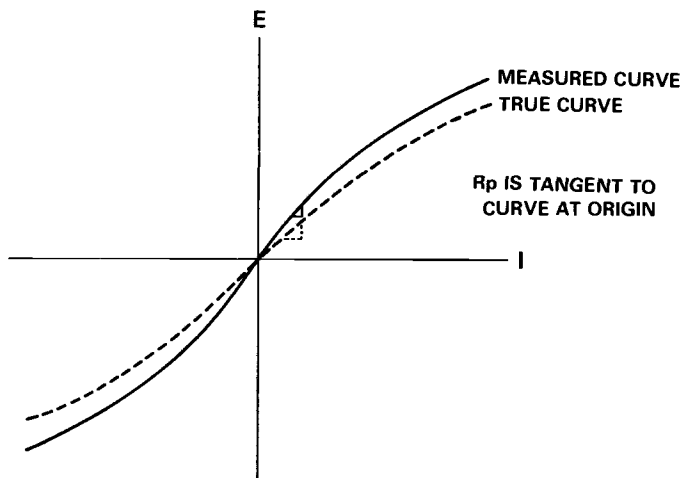


FIG. 4—Effect of IR error on polarization resistance.

sidered, polarization resistance overestimation that will occur will result in an underestimation of corrosion rate due to the reciprocal relationship between these two properties. This will provide measured corrosion rates that are too low.

*Incorrect Polarization Curves*—In the generation of polarization curves, such as the testing described in ASTM G 5 and ASTM Test Method for Conducting Cyclic Potentiodynamic Polarization Measurements for Localized Corrosion Susceptibility of Iron-, Nickel-, or Cobalt-Based Alloys (G 61), IR error will shift the potential by an amount proportional to the current being measured. As shown in Fig. 5, if the specimen is being anodically polarized, the actual potential will be more negative than that set on the potentiostat. If the specimen is being cathodically polarized, the actual potential will be more positive than the set potential. The measured polarization curve will deviate from the true curve by an amount proportional to the current. For tests run to a fixed maximum potential, this will lead to termination of the test at a true potential less than that desired, with resulting loss of data. The remainder of the data can be corrected for as described later. The effect of solution resistance may limit the actual potential that can be applied to an electrode, as additional cell voltage will partially go into additional IR error, and not entirely into electrode polarization.

When an active-passive polarization curve is measured, some data may be lost, that is, not recoverable or correctable [2]. This is illustrated in Fig. 6. The measured curve (dashed line) is shifted away from the true curve (solid line) by a potential proportional to the measured current. The effect of the IR error is to tilt the curve over slightly. By itself, this effect is correctable as described later, but if the shift becomes too pronounced, the measured curve could be forced to double back on itself as shown by the short dashes between points A and B in the figure. A potentiostat will not measure such a curve shape, but will instead jump directly from point A to point B as shown on the long-dashed curve. All information on the real curve between these two points will not be measurable. Only by reducing the sources of the IR error will this portion of the curve be able to be measured.

*Variable "Constant" Potential*—A potentiostat controls the potential between the reference electrode and working electrode by varying the potential applied to the counter electrode, and thus the cell current. The IR error between the reference location and the surface

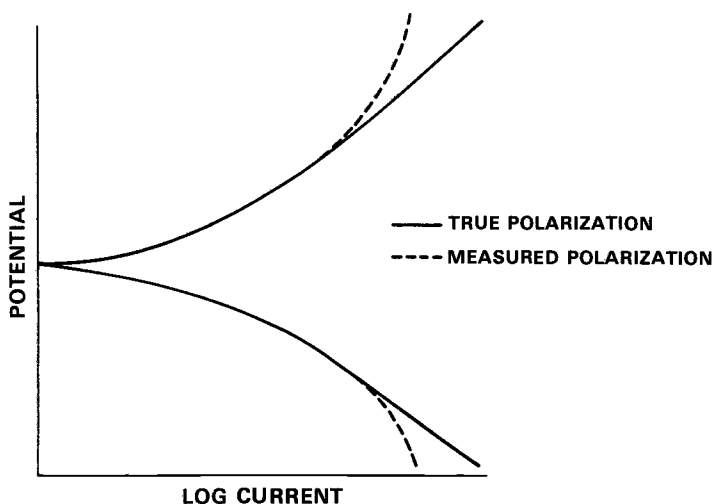


FIG. 5—Effect of IR Error on polarization curves.

## IR EFFECT

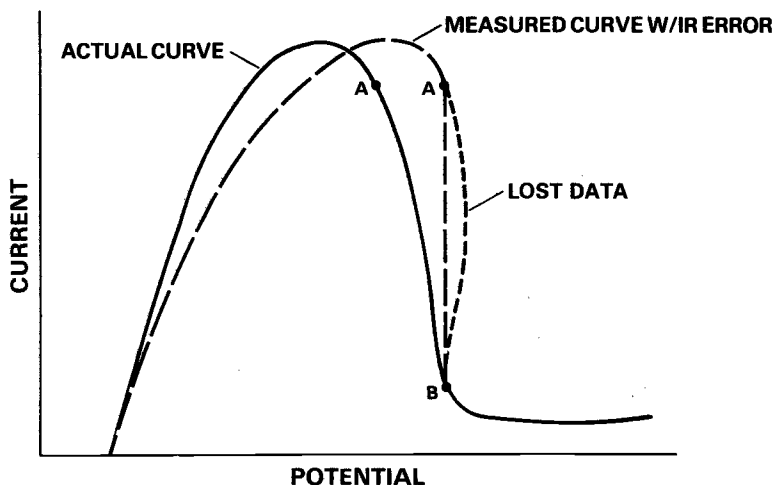


FIG. 6—Loss of data on active nose due to IR error.

of the working electrode is a function of this current, and thus a variable IR error will occur, leading to an uncertain working electrode potential, even though the potentiostat is functioning properly. This is particularly important when monitoring the performance of an electrode material over time, or when trying to hold a constant overpotential during stress corrosion testing.

*Incorrect Sweep Rate*—IR error will cause the potential sweep rate to be different from that expected in a potentiodynamic test [2-4]. In areas of the polarization curve where

current increases as potential is swept away from the freely-corroding potential, the IR error will increase with time, causing the sweep rate to be lower than anticipated. This can lead to a proportionately large amount of time being spent in the high current area of the active nose of an active-passive curve, leading to excessive corrosion before the onset of passivation in an anodic polarization test. In the sections of active-passive curves where current decreases as potential is swept away from the freely-corroding value, the IR error will decrease with time, causing a larger sweep rate than anticipated. The actual sweep rate when IR errors are present will therefore be variable over the course of the test. Although the data itself can be corrected to remove the IR error, additional difficulties may be introduced if the material is highly sweep-rate sensitive. In practice, there are few corrosion systems that are so sweep-rate sensitive that this effect becomes important if proper IR error minimization measures are used during the test.

### *Potential and Current Distribution Effects*

IR error is affected by the distribution of the total current flowing between the working and counter electrodes. If the current flow concentrates in the area between the working and reference electrodes, the potential gradient and resultant IR error will be higher than if the current concentrates outside of this area. This can be seen in Fig. 7. Since both cur-

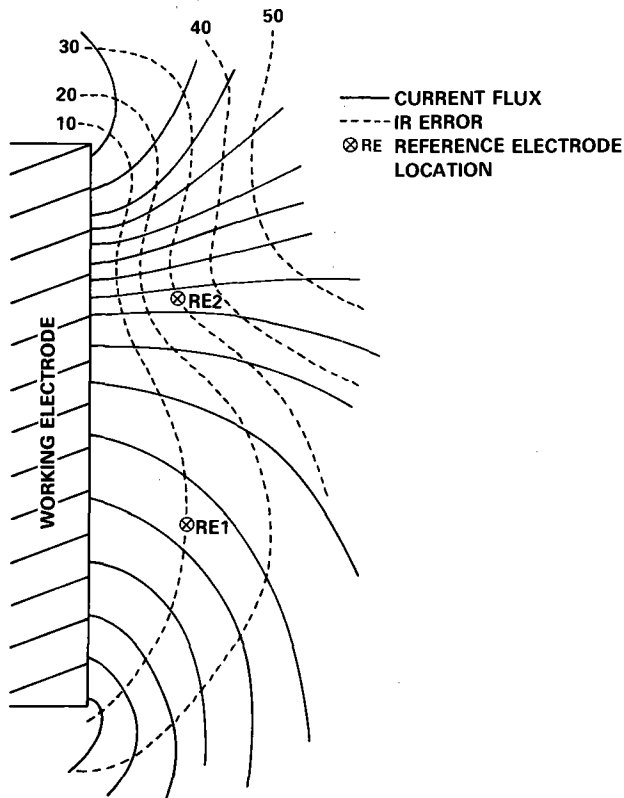


FIG. 7—IR error variation with reference cell placement and current density variations.

rent density and electrolyte resistivity can vary considerably over a large structure, particularly in soils, the amount of IR error can be a function of position on a large working electrode. In such cases the current distribution plays a large role in determining IR error. Current distribution is, itself, controlled by geometry, electrolyte resistivity, and polarization resistance of the working electrode material.

## Dealing with Electrolyte Resistance

### *Minimization Methods*

In this section methods for minimizing IR error and correcting for it are discussed. Because there are a wide variety of methods, they are only briefly described herein.

*Supporting Electrolyte*—In low conductivity electrolytes, conductivity can be increased by the addition of an inert salt which presumably does not influence the electrochemical reactions which occur in its absence. Conductivity of the solution of the inert salt “supports” the ionic current flow, and the salt solution is therefore referred to as a supporting electrolyte. It is usually not good practice to use a supporting electrolyte in corrosion studies because addition of different ionic species to the electrolyte conflicts with the principle of simulation of the corrosive environment. It is usually not possible to be assured that the ions added do not influence the corrosion reactions taking place. However, if the electrolyte resistance is large and no other minimization or correction methods seem adequate, then the use of a supporting electrolyte is an alternative which at least allows electrochemical measurements to be made, even though this can increase the difficulty of the corrosion analysis.

*Capillaries*—A capillary is used to decrease the length of current-carrying electrolyte between the reference electrode and the working electrode, thus decreasing the IR error. A capillary, sometimes called a salt bridge, is illustrated in Fig. 8. It is a long thin hollow glass tube filled with electrolyte and connected to a compartment housing the reference electrode. When an electrometer is used to measure potential there is little current flow in the capillary, and thus any IR drop in the capillary is minimal. The reference electrode will therefore measure the same potential as at the tip of the capillary. Since a capillary can be placed closer to the working electrode than a reference electrode, its use will reduce IR error.

The upper portion of Fig. 8 shows a capillary with an extremely fine tip, a salt bridge with the test electrolyte, and a separate beaker containing the reference cell and an electrolyte compatible with this cell. This setup is useful if it is undesirable to contaminate the test electrolyte with small amounts of the electrolyte in which the reference cell is placed. The bottom of Fig. 8 shows a wider capillary with a porous glass frit at the tip, which is used because of ease in capillary position adjustment. The larger diameter of the capillary tip in the latter configuration is applicable only in lower resistivity electrolytes, as the larger diameter prevents the capillary from being located as close to the working electrode as in the former configuration. There are several disadvantages to the use of capillaries:

1. Capillaries are generally fragile, especially if composed of glass, although more durable ones are available. They can also be expensive.
2. The tip can be clogged by gas bubbles or other substances, increasing the capillary resistance relative to the electrometer resistance. This makes the potential measurements inaccurate or may prevent measurements from being taken due to loss of continuity. This problem is particularly common in elevated temperature testing.
3. Capillaries can distort current flow to the part of the working electrode closest to the tip, which is the area which most influences the measured potential. The error due to this

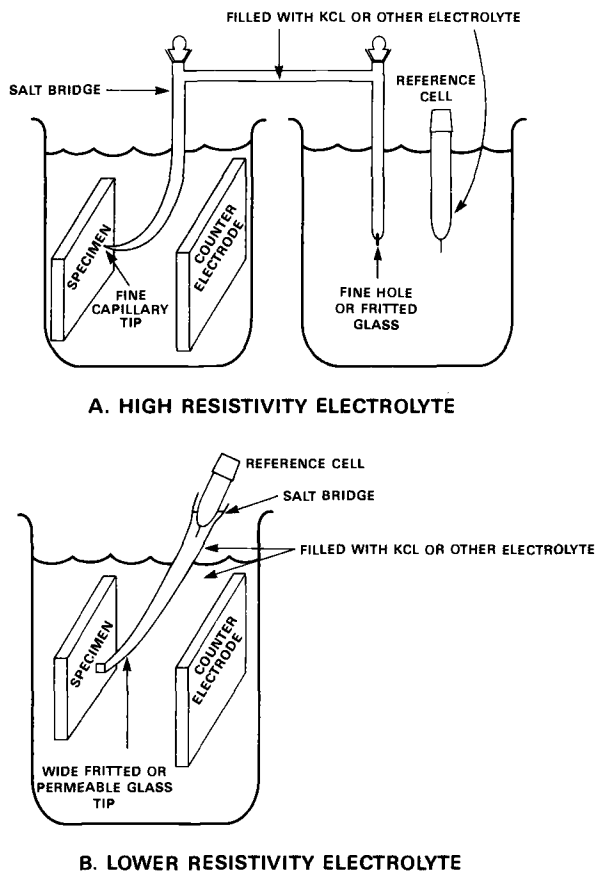


FIG. 8—Use of salt bridges.

current “blocking” depends on the relative values of the electrolyte resistance and the working electrode polarization resistance. A good rule of thumb to minimize current blocking is to keep the capillary away from the working electrode by a distance of at least two times its cross sectional diameter [5–12]. However, for low conductivity electrolytes the distance calculated from this rule may be inadequate.

4. Capillaries do not eliminate IR error, whereas there is often a tendency to assume they do. Therefore the magnitude of the electrolyte resistance that can cause IR error should be determined even if a capillary is used. In many corrosion situations it is easier to measure the electrolyte resistance between the working and reference electrodes and correct for it than to deal with the possibility of problems associated with use of a capillary. In low conductivity media the electrolyte resistance is large enough to require IR measurement and correction even if a capillary is used.

#### *Correcting for Electrolyte Resistance*

Whether a minimization method has been attempted or not, the experimenter must still be concerned with measuring the electrolyte resistance and correcting data for IR error

introduced by it. The resistance is determined by estimation or measurement and a correction applied at any current by shifting the measured potential toward the freely-corroding potential by an amount equal to the product of the electrolyte resistance and the applied current [2]. Correcting for IR error is straightforward once the electrolyte resistance has been determined.

*Estimating Electrolyte Resistance*—It is sometimes possible to estimate the value of the electrolyte resistance between the working and reference electrodes from a knowledge of the cell geometry, electrode placement, and conductivity of the electrolyte determined in separate experiments or obtained from tabulated data. This can be done for a simple geometry by solving the LaPlace Equation directly [13–15], or for more complicated geometries by the use of computer techniques such as finite element or boundary element modeling. A thorough discussion of these methods is beyond the scope of this paper. Complicated cell geometries, which are common in corrosion testing, make such estimation difficult.

Another estimation technique is applied to electrochemical data after a test. If the data appear to deviate from expected Tafel behavior due to electrolyte resistance, then a straight line is fit to the expected or partially exhibited Tafel region, as shown for anodic polarization in Fig. 9. Some knowledge of the expected Tafel slope values is of assistance when available. The deviation between the experimental data and the projected Tafel line at several current values is plotted as a function of the applied current, as shown in Fig. 10. The result should be a straight line with an intercept at zero applied current if the Tafel line was chosen properly, the only error was IR error, and the electrolyte resistance remained constant during the experiment. Plotting the current (calculated as current density times working electrode wetted surface area) instead of current density allows for a calculation of the uncompensated electrolyte resistance from the slope of the line, as illustrated. This estimation procedure is valuable for data where the exact experimental details are unavailable. Caution should be exercised, since bending of potential versus log current density plots away from ideal behavior looks like it is caused by IR error but can also be caused by commonly encountered factors in corrosion testing such as passivation in anodic polarization and diffusion limitation in cathodic polarization. However, the deviations caused by these factors will generally not be linear with current as is the case for IR error, and should be readily apparent by using the above plotting technique. Also, diffusion-lim-

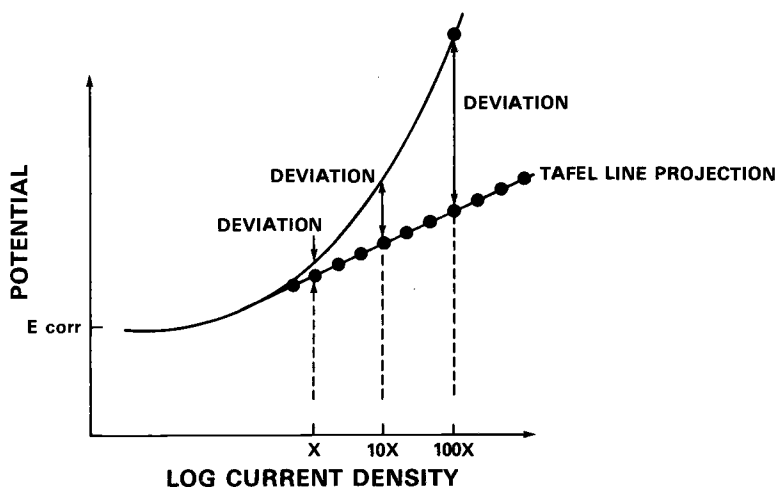


FIG. 9—Deviation of polarization curve from Tafel line due to IR error.

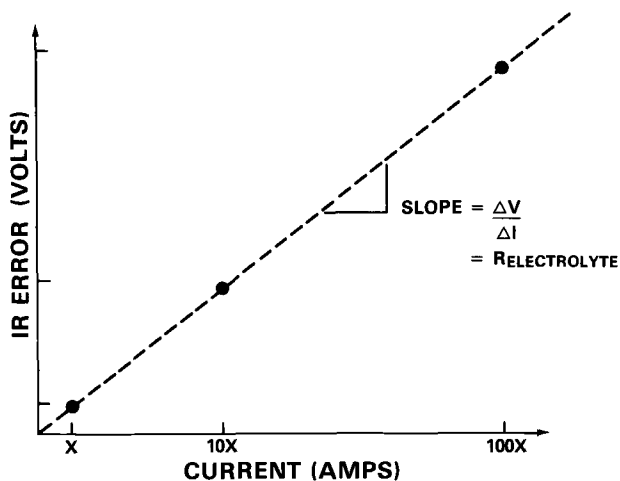


FIG. 10—Estimation of IR error from Tafel deviation plot.

ited behavior will lead to a limiting current density which will usually change when the electrolyte is stirred.

Several other estimation techniques are described elsewhere [2,16]. All other IR error determination methods, as described below, involve at least some direct measurement of electrolyte resistance in the cell.

#### Measurement Methods

**Cell Calibration**—When experiments are often conducted in the same or similar cells, the cell geometry can be calibrated to determine electrolyte resistance. The cell is filled with a known conductivity electrolyte such as 1.0 M potassium chloride (KCl). A conductivity meter is connected to platinum electrodes at the exact positions the working and reference electrodes will occupy during the tests. Once the conductivity of the cell with a known test electrolyte is determined, the conductivity of the test electrolyte is determined in a standard conductivity cell. The resistance of the test electrolyte in the test cell can then be calculated by multiplying the original cell resistance with the standard electrolyte by the ratio of the test electrolyte to the standard electrolyte.

This knowledge can be used to determine the applied current magnitude at which significant errors are encountered. For example, in 3.5 wt% sodium chloride (NaCl) or synthetic seawater in a typical laboratory cell (such as that in ASTM Standard G-5 without the capillary) the resistance of the electrolyte between working and reference electrodes is about 1 to 5  $\Omega$ . Therefore, if errors less than 5 mV are considered negligible, currents less than 1 mA will induce insignificant IR error, whereas currents of 10 mA will cause errors of 10 to 50 mV and some type of correction becomes necessary.

Another example can be given for this same cell configuration, but in tap water or inland cooling waters where the conductivity is two orders of magnitude less than synthetic seawater. The resistance in this case would be 100 to 500  $\Omega$ . Currents of 1 mA would lead to an IR error of 100–500 mV, which requires correction.

Cell calibration will be accurate only for primary current distributions on the working electrode. If the working electrode is expected to vary in potential significantly over its

surface, as would occur if secondary or tertiary current distribution is significant, then the current distribution, and thus the resistance measured, will not be the same as the actual test setup. In such cases cell calibration should not be used, although an order of magnitude estimate of IR error may still be obtained if deviation from primary distribution is not large.

*Position Extrapolation*—In this technique, IR error is determined by translating the reference electrode toward the working electrode while current is held constant. The working versus reference voltage is plotted as a function of distance from the working electrode, Fig. 11. The data is extrapolated to zero distance and the resistance, the IR error, and the corrected potential can be determined. During this procedure the reference should not be brought close enough to the working electrode to block the current.

While this method is possible in principle, there are several disadvantages. Generation of the data for each current is tedious, although data from one current could be used to determine the uncompensated electrolyte resistance at a given distance. This resistance could be used to correct the rest of the data at other currents, under the assumption of a constant electrolyte resistance over the test period. Accurate measurement of distance requires a special translating stage for the reference cell, and performing this measurement in a controlled atmosphere, as is required in some tests, may be impossible. The potential versus distance relationship in most cells will not be truly linear, making extrapolation more difficult. Other methods described herein are usually more direct and more accurate.

*Positive Feedback*—Positive feedback is an electrical method for correcting IR error that is available on many commercial potentiostats. In an electrochemical test, the actual potential of the working electrode deviates from that measured by the IR error as follows

$$E_{\text{actual}} = E_{\text{measured}} - IR_{\text{uncomp}}$$

With positive feedback the applied current is multiplied by some fraction,  $f$ , of the uncompensated resistance, and the result added to the measured potential to offset the IR error

$$E_{\text{actual}} = E_{\text{measured}} - IR_{\text{uncomp}} + IfR_{\text{uncomp}}$$

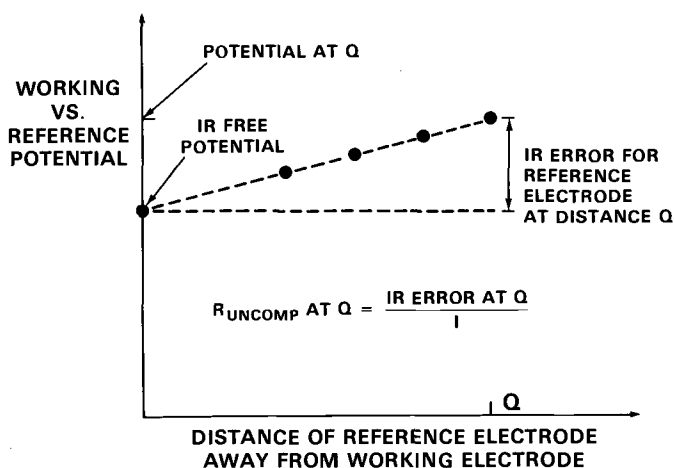


FIG. 11—Reference cell positioning to determine IR error.

When the feedback,  $fR_{uncomp}$  is equal to  $R_{uncomp}$  then the actual and measured potentials are identical.

This technique is applied by increasing  $f$  until the potentiostat output becomes unstable, indicating a net positive feedback condition (overcompensation), then decreasing  $f$  slightly. The technique assumes that the electrolyte resistance will remain constant over the duration of the test. The hardware necessary is seen by comparing Figs. 12 and 13. Figure 12 is a simplified version of a potentiostat, and Figure 13 has added a second operational amplifier, a variable resistor, and additional circuitry to create positive feedback.

Unfortunately, this technique has a number of significant disadvantages besides the requirement for a constant electrolyte resistance over the course of the test. A major dis-

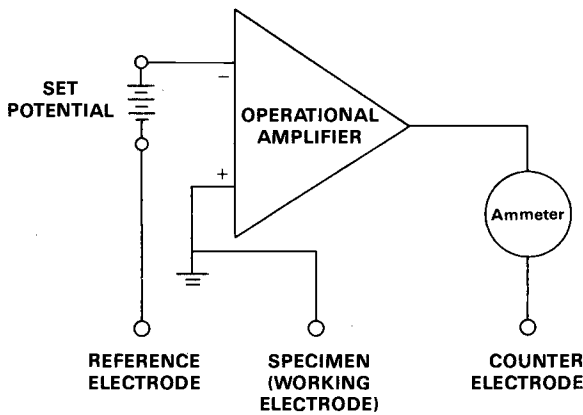


FIG. 12—Schematic of a simple potentiostat.

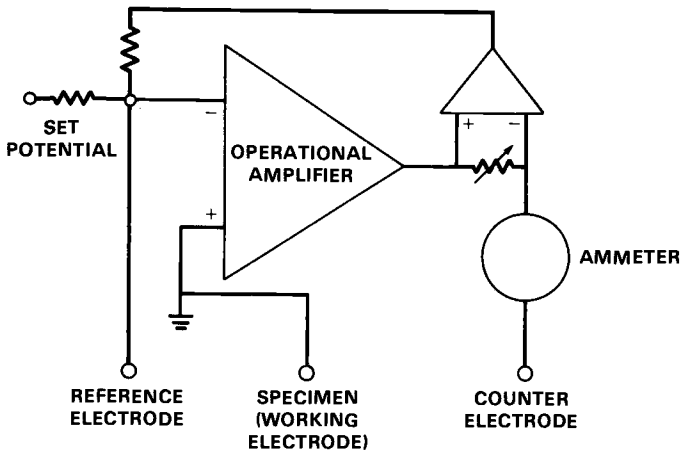


FIG. 13—Schematic of a positive feedback circuit.

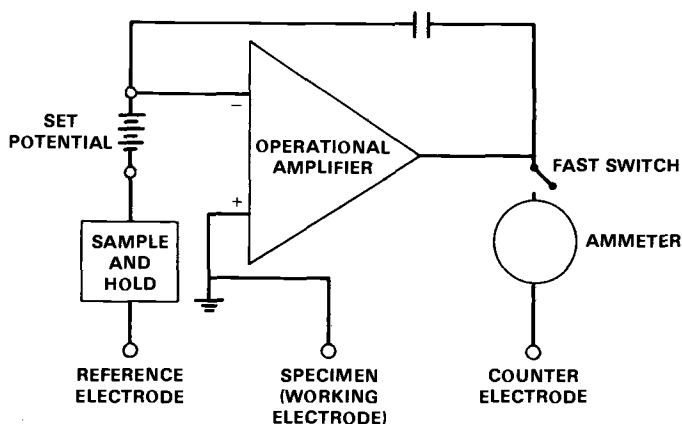


FIG. 14—Schematic of a current interruption circuit.

advantage concerns the procedure for setting  $f$ . The instability of a circuit is related both to the amount of positive feedback and the impedance of the working electrode and potentiostat circuits. Simply increasing  $f$  until instability occurs, then backing off until it stops will usually lead to overcompensation by an amount dependent on the specific reactions taking place in the cell. The initial instability obtained during the setting of  $f$  can lead to large working electrode potential swings which can damage the validity of a test. Finally, information on the final value of the uncompensated resistance determined during the setting procedure is usually not available on most commercial equipment. Additional information on positive feedback can be found elsewhere [2,16].

**Current Interruption**—In the current interruption method, the applied current is interrupted via a fast switch (generally in the counter electrode lead) and the working versus reference potential is monitored with the aid of a fast storage oscilloscope. This is illustrated in Fig. 14. The potential response during an interrupt is shown in Fig. 15. The voltage drop across the electrolyte is purely resistive and is therefore immediately lost upon interruption of the current. Depolarization of the working electrode usually takes some time to occur, as discharging of the double layer has capacitive character. The instantaneous drop in the voltage upon interruption is visually separable on the oscilloscope, and is due only to the IR drop in the electrolyte at the current applied prior to the interruption.

Manual interruption correction is usually best applied after the experiment, although changes can occur in electrolyte resistivity or current distribution during the test which could invalidate a manual post-test correction. Automated current interruption is usually done during the test. To perform interruption correction manually, the electrodes remain fixed during the test and any post-test measurements. After the test has been performed and data taken, a constant current source such as a potentiostat in controlled current mode is used to apply a series of currents throughout the range of the data just taken. At each current an interruption is performed, and the working versus reference electrode response measured. From these measurements, the IR error can be determined as a function of current. Finally, the potential at each current can be corrected by the IR error measured at that current. The corrections may be checked by plotting the measured IR error as a function of the current at which it was measured, as in Fig. 16. This should produce a straight

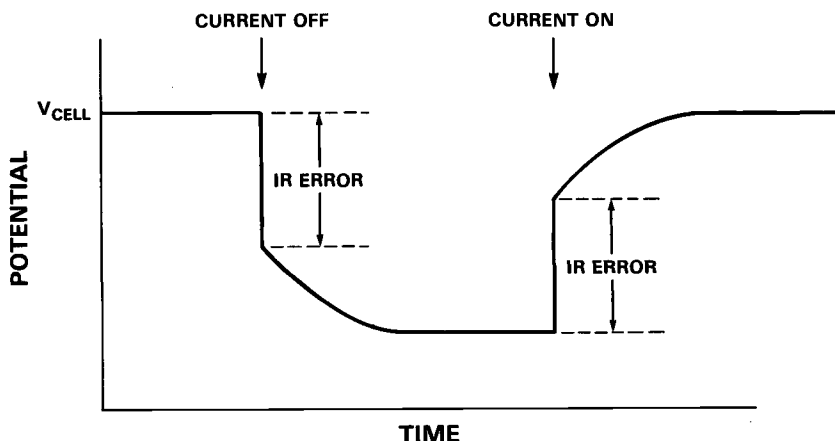


FIG. 15—Determining IR error from an ideal current interruption.

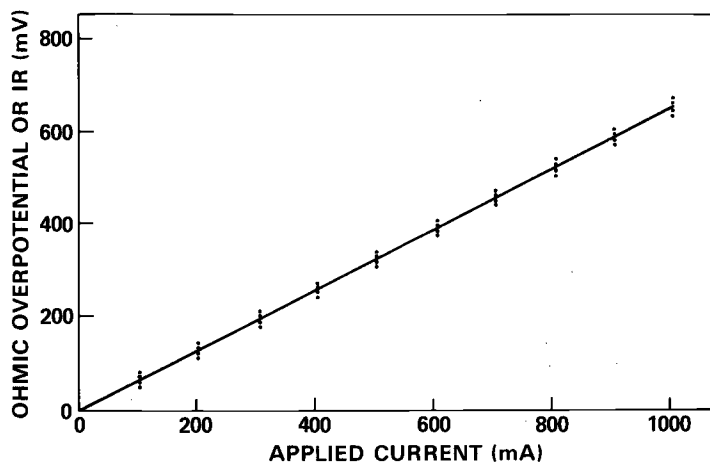


FIG. 16—Actual deviation plot to check IR error.

line with a slope of  $R$ , the electrolyte resistance, and an intercept of zero; no current - no IR error. The sweep rate of the scope should not influence the IR error at a constant applied current.

Several commercial potentiostats now have automated IR correction features based on current interruption and can determine the IR error and correct the data during the test.

There are a number of concerns about the current interruption technique. The high impedance associated with many reference electrodes, especially those with glass frits, can cause slow response of the reference electrode itself during the interrupt. To avoid this problem an inert wire can be capacitively coupled to the reference electrode lead to decrease high frequency impedance which is significant during an interrupt [17]. Alternatively an auxiliary reference electrode can be used to carry the high frequency signal during the interrupt [17,18].

Additional information on the current interruption method can be found elsewhere [2,3,16,19,20].

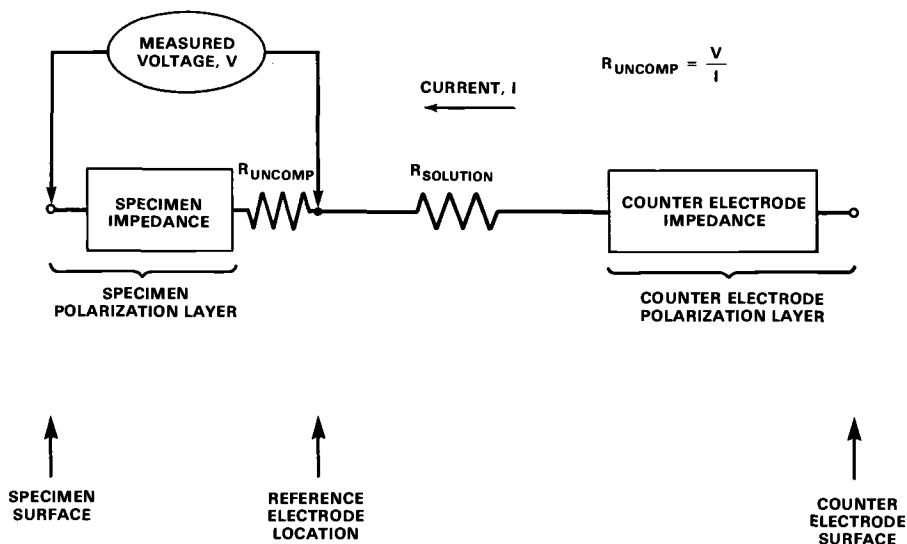


FIG. 17—Simplified electrical equivalent circuit of an electrochemical interface.

*High Frequency Superposition*—An alternative method to determine the electrolyte resistance is the use of a high frequency voltage perturbation superimposed on the DC applied potential. Looking at the equivalent circuit in Fig. 17, the double layer capacitance will act as a very low resistance for high frequency signals. If a high frequency voltage is applied, and the corresponding current measured, the ratio of their amplitudes is the resistance of the electrolyte. This measurement can be applied before, during, or after the test, and if a relatively small amplitude is used, the perturbation does not interfere with the electrochemical reaction being studied.

Selection of the proper frequency is best accomplished by examining the phase difference between the applied voltage and the measured current. When this difference is zero the cell is functioning in a purely resistive manner. This will in general happen at two frequencies. At a sufficiently low frequency, the double layer capacitance acts as an open circuit and the resistance measured is the sum of the polarization resistance and the electrolyte resistance. At a sufficiently high frequency, the double layer capacitance acts as a short circuit and the measured resistance is the electrolyte resistance. Electrochemical Impedance Spectroscopy (EIS), also called AC Impedance, can help to determine the proper frequencies for these phenomena. It involves application of a small sinusoidal voltage perturbation over a broad range of frequencies and measurement of the applied current at each frequency applied. The magnitude and phase of the impedance at each frequency is determined with the aid of a lock-in amplifier, oscilloscope, or spectrum analyzer. EIS is ideal for polarization resistance testing as it imposes the small perturbation required for this test and allows accurate correction for the electrolyte resistance. Additional information on EIS can be found elsewhere [21–25].

### Other Complications

The following concerns are valid regardless of the method used for measuring IR error.

*Changes with Time*

Changes in IR error as a function of specimen exposure time may arise for a variety of reasons. The electrolyte conductivity can change with time. In an aqueous NaCl solution, for example, hydrolysis of metal ions created by oxidation forms metal hydroxides and H<sup>+</sup> ions. The equivalent conductance of the H<sup>+</sup> cation is almost seven times that of many metallic ions and five to seven times that of Cl<sup>-</sup> or Na<sup>+</sup>, respectively. To maintain charge neutrality, Cl<sup>-</sup> ions migrate to the working electrode. Thus, the electrolyte conductivity near the working electrode increases with exposure time. In the case of cathodic polarization in aqueous electrolytes, the reduction of oxygen and water generate OH<sup>-</sup> ions that have a specific conductance that is three to four times that of Cl<sup>-</sup> or Na<sup>+</sup>, respectively. To maintain electroneutrality, cations will migrate to the cathode surface. If the counter electrode is placed in the same cell as the working electrode, then it will contribute to increased conductivity with time. Large counter electrode surface areas or separate counter electrode chambers or both are used to minimize this effect. Buffering agents can minimize excessive pH shifts that occur over time, but the buffer may affect the reactions being studied. Flow and working electrode surface area to electrolyte volume ratio play a strong role in determining whether the bulk electrolyte changes significantly over time.

Development of resistive films over time may block surface area, changing current distribution, and therefore total electrolyte path resistance. This concept is illustrated in Fig. 18.

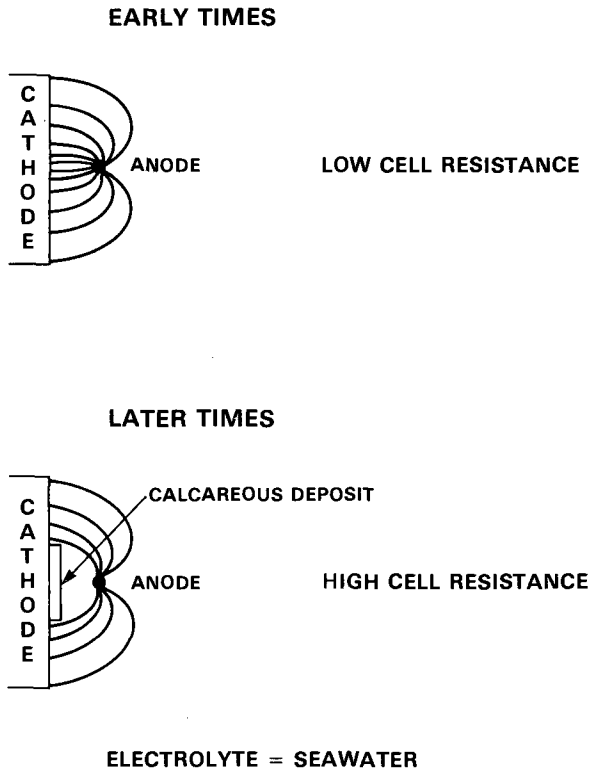


FIG. 18—Current redistribution with time due to calcareous deposit buildup.

### *Reference Electrode Positioning and Current Distribution*

Distribution of current can affect IR error even when the total current and electrolyte resistivity remain constant. Potential gradients will be high in areas with high current densities, leading to high IR errors if the reference cell is placed in such areas. Large gradients also result in greater sensitivity of IR error to reference cell placement. If current densities are low in a given area, IR error will be low and reference cell placement is not critical. Edges and sharp corners have the largest currents and potential gradients, and thus the largest IR error, making these areas to avoid when placing the reference electrode.

Current will flow such as to minimize the total cell voltage [26]. If polarization resistance is negligible compared to the electrolyte resistance, the current distribution will be controlled mainly by the geometry and electrolyte resistivity, a phenomenon called primary current distribution [26,27]. Primary current distributions result in the largest variation in current density over the working electrode surface of all of three types of current distributions. Changes in the type of current distribution from primary to secondary or tertiary will cause the current density to become more uniform over the working electrode [26–29]. This could change the local current density at the location of the reference cell even though total electrolyte resistance and cell current remain constant. This will lead to a change in the amount of IR error with a change in the type of current distribution, and is illustrated in Fig. 7 for sample edges where it is particularly noticeable [28]. A change in the type of current distribution over time could therefore result in a time-dependent IR error.

For these reasons the reference electrode tip should be placed normal to the center of the working electrode but far from it so that the potential at the reference electrode location is not drastically affected by the local variations in the current distribution of the working electrode. The IR error will be larger and must be determined, but the value obtained will be more representative of the average IR error over the entire sample [28–30].

### *The Effect of Bubbles*

Bubbles in electrochemical cells may arise from the evolution of gases from the working and counter electrode surfaces (oxygen, hydrogen, chlorine) or from intentional purging or aerating (nitrogen, argon, helium, air or oxygen). Bubbles cover parts of the working electrode surface, increasing overpotential on the uncovered parts, and take up an appreciable volume fraction of electrolyte, thus changing the effective electrolyte conductivity. Tobias and coworkers have determined the effect of bubbles on both current distribution and ohmic resistance [31–33]. They considered the effect of bubbles on the “apparent” electrolyte resistivity and developed the following expression:

$$p/p_0 = (1 - e)^{-3/2}$$

where  $p_0$  is the electrolyte resistivity at zero gas fraction,  $p$  is the reduced resistivity and  $e$  is the gas void fraction. Thus, a void fraction of 0.3 increases the resistivity by a factor of 1.7. The situation is actually more complex since bubble size will affect the gas void fraction [32,33]. The orientation of the electrode will affect the IR error. For vertical electrodes with rising evolved gases, resistivity is less at the bottom edge, while for horizontal electrodes, resistivity may be more uniform. Both the IR error and the total cell voltage are increased by increasing gas void fraction. Forced or natural convection strongly affects these effects.

The influence of bubbles on the already significant IR drop in the occluded geometry of

a crack tip may be large. This is beyond the scope of this review, and details may be found elsewhere [34].

### *Heating*

Electrode heating occurs because of the presence of a high electrolyte resistance coupled with a high cell current over time. The presence of bubbles promotes heating by raising electrolyte resistivity. Joule heating leads to measurement errors, but these are not all IR errors. Ionic diffusion coefficients and equivalent conductances increase by 2 to 3% for a temperature increase of 1°C, slightly increasing electrolyte conductivity, which will affect IR error.

### *Current Interruption or AC Impedance?*

The choice of IR error measurement method is based on whether the current distribution present during the current interruption or impedance measurement is the same as the current distribution during the DC experiment. The two types of IR error measurement techniques will be discussed separately.

*Current Interruption*—If the same current magnitude is used for the interruption as in the DC electrochemical experiment, then while the current is “on” the current distribution is similar, and the reference electrode is at the same potential before the interruption takes place as in the DC experiment. After the interruption, the reference electrode experiences a potential corresponding to the “true” polarization if the current is zero everywhere on the surface [35]. If, however, the electrode double layer was nonuniformly charged when the current was flowing, then after interruption current will flow through the electrolyte from one part of the electrode surface to the other as charge is redistributed. The current flow just after interruption will create another IR error which will prevent the measured potential from being the “true” potential. This is most likely to occur for primary current distributions, since these are the least uniform. If the polarization resistance of the electrode is large compared with the electrolyte resistance, the current distribution is more uniform and the measured voltage error will be fairly accurate [35]. An additional disadvantage is the inconvenience of performing separate experiments to determine IR error, unless a simultaneous current pulse is used. Finally, it is not always practical or convenient for the current to be interruptible, particularly in field testing.

*Electrochemical Impedance*—In this method, electrolyte resistance is determined from the real component of impedance measured at high frequency. However, since electrolyte resistivity is frequency independent, total electrolyte resistance may change with frequency due to current redistribution. Thus the high frequency value of electrolyte resistance measured by the impedance technique may be somewhat different from the value near DC where the experiment was carried out [22]. This effect is dependent on cell geometry, reference electrode position, and polarization characteristics of the working electrode. At high frequency, cell current is shunted through the double layer capacitance and the electrochemical system is in primary current distribution. At low frequencies approaching DC, the double layer capacitance passes no current, and the faradaic current determines the distribution. The cell is in secondary or tertiary current distribution. Where polarization resistance measurement is desired, the most correct electrolyte resistance is that obtained at low frequency. This quantity is not determined by the AC method. Thus, the AC method offers the convenience of a single experiment, but with the uncertainty associated with changing values of the total electrolyte resistance.

If the impedance measurement is combined with some DC current, the AC signal is now

summed with the applied DC potential (which does not change during the course of the experiment). Thus while the AC component is shunted through the double layer capacitance, the DC current remains unchanged during the high frequency electrolyte resistance measurement. If the AC signal is small compared to the DC level, the current distribution will not change significantly as a function of frequency. The resistance measured in this instance will be similar to that experienced under pure DC and the electrolyte resistance determined with the impedance method will be accurate. Potentiostats and impedance systems capable of performing simultaneous DC and AC polarization are required.

### Summary

This paper presented examples of errors introduced into electrochemical measurements due to electrolyte resistance and methods to minimize or correct for these errors. Additional information is available in the references cited herein.

### References

- [1] F. Mansfeld, "The Effect of Uncompensated IR-Drop on Polarization Resistance Measurements", *Corrosion*, Vol. 32, No. 4, April 1976, p. 143.
- [2] Britz, D., "IR Elimination in Electrochemical Cells", *Journal of Electroanalytical Chemistry and Interfacial Electrochemistry*, Vol. 88, No. 2, April 1978, p. 309.
- [3] Schwabe, K., Oelssner, W., and Suschke, H., *Protection of Metals*, Vol. 15, 1979, p. 126.
- [4] Mansfeld, F., "The Effect of Uncompensated Resistance in the True Scan Rate in Potentiodynamic Experiments", *Corrosion*, Vol. 38, No. 10, October 1982, p. 556.
- [5] Barnartt, S., "Primary Current Distribution Around Capillary Tips Used in the Measurement of Electrolytic Polarization", *Journal of the Electrochemical Society*, Vol. 99, No. 12, December 1952, p. 549.
- [6] Barnartt, S., "Polarization Measurements Made with a Luggin-Haber Capillary Magnitude of IR Drop Corrections in Electrode", *Journal of the Electrochemical Society*, Vol. 108, No. 1, January 1961, p. 102.
- [7] Cahan, B., Nagy, Z., and Genshaw, M., "Cell Design for Potentiostatic Measuring System", *Journal of the Electrochemical Society*, Vol. 119, No. 1, January 1972, p. 64.
- [8] Mumby J., and Perone, S., *Chemical Instrumentation*, Vol. 3, 1971, p. 191.
- [9] Kasper, C., *Transactions of the Electrochemical Society*, Vol. 77, 1940, p. 353.
- [10] Kasper, C., *Transactions of the Electrochemical Society*, Vol. 77, 1940, p. 365.
- [11] Kasper, C., *Transactions of the Electrochemical Society*, Vol. 78, 1940, p. 131.
- [12] Kasper, C., *Transactions of the Electrochemical Society*, Vol. 78, 1940, p. 147.
- [13] Nisancioglu, K., "The Error in Polarization Resistance and Capacitance Measurements Due to Nonuniform Ohmic Potential Drop to Flush-Mounted Probes", Paper 75, Corrosion/85, National Association of Corrosion Engineers, Boston, MA, March 1985.
- [14] Pilla, A., *Computer Chemical Instrumentation*, Mattson, Mark and MacDonald, Eds., Vol. 2, 1972, p. 138.
- [15] Doblhofer K., and Pilla, A., *Journal of the Electrochemical Society*, Vol. 39, 1972, p. 91.
- [16] Hayes, M., Kuhn, A., and Patefield, W., "Techniques for the Determination of Ohmic Drop in Half-Cells and Full Cells: A Review", *Journal of Power Sources*, Vol. 2, 1977/78, p. 121.
- [17] Herrmann, C., Perrault, G., and Pilla, A., "Dual Reference Electrode for Electrochemical Pulse Studies", *Analytical Chemistry*, Vol. 40, No. 7, June 1968, p. 1173.
- [18] Moran, P., "Auxiliary Electrode Method for Determination of Ohmic Resistance," *Corrosion*, Vol. 42, No. 7, July 1986, P. 432.
- [19] McIntyre J., and Peck, Jr., W., "An Interrupter Technique for Measuring the Uncompensated Resistance of Electrode Reactions under Potentiostatic Control," *Journal of the Electrochemical Society*, Vol. 117, No. 6, June 1970, p. 747.
- [20] Flinn, D. Rosen, M., Schuldiner, S., and Fahey, J., "A High-Speed Switch for Isolation of the Reference Electrode Circuit to Hold-Off IR Changes during Current Interruption or Pulsing", *Journal of the Electrochemical Society*, Vol. 117, No. 1, January 1970, p. 79.
- [21] Gabrielli, C., *Identification of Electrochemical Processes by Frequency Response Analysis*, Monograph SI/Dym/001, Solartron Electronic Group, Ltd., England, 1980.
- [22] McKubre, M., "Techniques for AC Impedance Measurements in Corrosion Systems," Paper

- 480, Corrosion/87, San Francisco, CA, National Association of Corrosion Engineers, March 1987.
- [23] Mansfeld, F., "Recording and Analysis of AC Impedance Data for Corrosion Studies", *Corrosion*, Vol. 36, No. 5, May 1981, p. 301.
- [24] McDonald, D. and McKubre, M., "Impedance Measurements in Electrochemical Systems", *Treatise on Modern Electrochemistry*, Yeager, Ed.
- [25] Silverman, D., "Primer on the AC Impedance Technique", *Electrochemical Techniques for Corrosion Engineering*, R. Baboian, Ed., National Association of Corrosion Engineers, Houston, TX, 1986.
- [26] Newman, J., *Electrochemical Systems*, Prentice-Hall, Inc., NJ, 1973.
- [27] Moulton, H., "Current Flow in Rectangular Conductors", *Proceedings of the London Mathematical Society (ser. 2)*, Vol. 3, 1905, p. 104.
- [28] Newman, J., "The Fundamental Principles of Current Distribution and Mass Transfer in Electrochemical Cells", In *Electroanalytical Chemistry*, Chapter 6, A. J. Bard, ED., Marcel Dekker, New York, NY., 1972.
- [29] Newman, J., "Current Distribution on a Rotating Disk Electrode Below the Limiting Current", *Journal of the Electrochemical Society*, Vol. 113, No. 12, December 1966, p. 1235.
- [30] Newman, J., "Resistance for Flow of Current to a Disk", *Journal of the Electrochemical Society*, Vol. 113, No. 5, May 1966, p. 501.
- [31] De La Rue, R. and Tobias, C., "On the Conductivity of Dispersions", *Journal of the Electrochemical Society*, Vol. 106, No. 9, September 1959, p. 827.
- [32] Tobias, C., "Effect of Gas Evolution on Current Distribution and Ohmic Resistance in Electrolyzers", *Journal of the Electrochemical Society*, Vol. 106, No. 9, September 1959, p. 833.
- [33] Meredith, R. and Tobias, C., "Evaluating the Effective Resistances of Diaphragms or Electrolytic Separators", *Journal of the Electrochemical Society*, Vol. 110, No. 12, December 1963, p. 1257.
- [34] Pickering, H., "On the Roles of Corrosion Products in Local Cell Processes", *Corrosion*, Vol. 42, No. 3, March 1986, p. 125.
- [35] Newman, J., "Ohmic Potential Measured by Interrupter Techniques," *Journal of the Electrochemical Society*, Vol. 117, No. 4, April 1970, p. 507.

William C. Ehrhardt<sup>1</sup>

## IR Drop in Electrochemical Corrosion Studies— Part I: Basic Concepts and Estimates of Possible Measurement Errors

---

**REFERENCE:** Ehrhardt, W. C., “IR Drop in Electrochemical Corrosion Studies—Part I: Basic Concepts and Estimates of Possible Measurement Errors,” *The Measurement and Correction of Electrolyte Resistance in Electrochemical Tests*, ASTM STP 1056, L. L. Scribner and S. R. Taylor, Eds., American Society for Testing and Materials, Philadelphia, 1990, pp. 27–58.

**ABSTRACT:** Electrochemical techniques used in the study of corrosion are particularly susceptible to errors due to IR drop when used to study systems such as the corrosion of steel in natural waters. The influence of the electrochemical measurement cell geometry on both the nature and the magnitude of the expected errors is reviewed. Also, the effect of a non-uniform current distribution on the working electrode is examined. Expected errors for a range of corrosion rates and water conductivities that are typical of steel in cooling systems are presented for three types of experiments. These experiments are: simple linear polarization (polarization resistance), small range polarization, which is computer-fit to extract the corrosion rate and Tafel parameters, and full polarization.

**KEY WORDS:** cell constant, corrosion, corrosion probe, curve fitting, current distribution, electrochemical cell, IR compensation, polarization resistance, solution resistance, steels, Tafel slopes

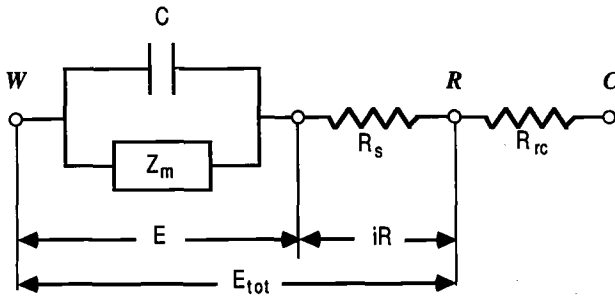
Electrochemical corrosion techniques are powerful tools in the investigation of corrosion inhibitors which are designed for use in cooling water systems. The natural waters in which these inhibitors are used often have low conductivity. Consequently, uncompensated IR drop is frequently a problem, and it must be overcome if useful information is to be obtained. Experiments on low carbon steel (LCS), a metal commonly used in cooling system heat exchangers, are a particular problem because it corrodes at relatively high rates in low conductivity waters.

The general subject of IR drop compensation has been reviewed by Britz [1] and by Hayes et al. [2]. In this paper, the importance and limitations of IR compensation in the area of electrochemical corrosion measurements are outlined. The impact of cell design—particularly the influence of the current distribution—on minimizing the IR drop problem is reviewed. Three commonly used experimental techniques are examined in detail. Illustrations of the magnitude of the errors involved are developed for the specific case of LCS corrosion in natural waters.

### The Metal Electrode Interface and Corrosion Test Cell

Figure 1 depicts an idealized equivalent circuit of an electrochemical corrosion cell. The working electrode has a double layer capacitance  $C$  associated with it which typically has

<sup>1</sup> Senior research scientist, Betz Laboratories, Inc., Somerton Rd., Trevose, PA 19047.



**W** Working electrode  
**R** Reference (Luggin) electrode  
**C** Counter electrode

**C** = Double layer capacitance.

**Z<sub>m</sub>** = Impedance of metal /solution interface (excluding **C**).

**R<sub>s</sub>** = Uncompensated solution resistance. May include component from surface film on metal.

**R<sub>rc</sub>** = Resistance between reference and counter electrodes.

**E<sub>tot</sub>** = Total working vs reference potential (control potential).

**E** = Potential across metal/solution interface.

**iR** = Potential drop due to cell current flowing through **R<sub>s</sub>**

FIG. 1—Idealized equivalent circuit of an electrochemical cell.

a value in the range of 1 to 1000  $\mu\text{F}/\text{cm}^2$ . Charge transfer processes, such as metal oxidation and oxygen reduction, occur on the metal surface. In some cases, these processes can be represented as an electrical impedance  $Z_m$  in parallel to  $C$ . In general, the rates of the electrochemical processes on the metal and the double layer capacitance depend on the electrical potential  $E$  across the metal solution interface, so both  $C$  and  $Z_m$  will be potential dependent.

In many electrochemical corrosion experiments, information about the corrosion rate and the corrosion mechanism is obtained by measuring the current  $I$  that flows across the metal/solution interface as the potential  $E_{\text{tot}}$  is slowly varied. Typical scan rates are in the range of 0.1 to 1.0 mV/s. Under these conditions, the capacitance  $C$  has a very high impedance relative to  $Z_m$  and has essentially no influence on the current  $I$ .

The current flows through the solution in the cell between the working and counter electrodes. The potential at the solution side of the metal/solution interface  $E$  is different than the potential at the “potential sensing” (reference) electrode  $E_{\text{tot}}$  because the intervening solution has some electrical resistance  $R_s$ . The relationship between  $E_{\text{tot}}$  and  $E$  is given by

$$E = E_{\text{tot}} - IR_s \quad (1)$$

The second term on the right-hand side is the  $IR$  drop: it can be a significant fraction of  $E_{\text{tot}}$ . If the  $IR$  drop is not compensated for in some way, the experiment may yield only information about the solution resistance and nothing about the corrosion process.

## Effects of Cell Geometry and Current Distribution

### *Reference Electrode (Luggin Probe)*

To minimize IR drop, reference electrodes are normally coupled into the electrochemical cell through a glass tube that has a fine (capillary) tip, called a Luggin probe. The closer the tip is to the working electrode, the smaller  $R$ , will be. However, if the reference electrode is brought too close to the surface of the working electrode, the reference electrode will distort the current flowing locally on the working electrode, a phenomenon known as "shielding." A rule of thumb used for the traditional glass capillary type of Luggin is that the probe must be kept a distance of at least two times the capillary outer diameter away from the surface to avoid shielding [3–9]. Calculations by Landau et al. [9] support the experimental results of Barnartt [5] regarding the ohmic drop sensed by the Luggin when placed two diameters away. Calculations by Tokuda et al. [8] suggest that a distance of at least one capillary diameter is adequate. They also found that thinner capillary walls caused less distortion of the current distribution.

In minimizing IR drop, capillaries with smaller diameters are desirable because they can be placed closer to the working electrode without causing shielding. The small capillaries also minimize the leakage rate of filling solution into the test solution. Barnartt [5] has reported routinely using 0.2 mm diameter Luggins; Kuhn and Stevenson [6] report using 0.44 and 0.94 mm diameter Luggins. Mumby and Perone [10] were able to produce capillaries with tip diameters between 0.005 and 0.5 mm on 2 mm diameter Pyrex tubing using a commercial microelectrode puller. Since Luggin capillary diameters are not usually reported in the literature, it is not known how typical these values are.

The Luggin probes used in this laboratory and commonly used for corrosion studies are not capillary probes but are commercially supplied (EG&G Princeton Applied Research, P.O. Box 2565-T, Princeton, New Jersey 08540) Vycor (porous glass) tips which are sealed to the end of 4-mm outside diameter (OD) glass tubing. To the author's knowledge, no information has been published that validates the minimum separation guidelines for tips which are relatively large and porous (rather than open-ended). If the guidelines do apply, the minimum separation distance for such probes is between 4 mm (if the Tokuda et al. [8] results are valid) and 8 mm (traditional guidelines).

Due to the minimum distance requirement, an IR drop penalty is associated with larger diameter probes. However, larger diameter probes minimize the AC signal problems that are associated with the high electrical resistance and associated capacitance of small diameter probes [1,2,10–14]. AC characteristics can have a significant impact on electrochemical impedance and current interruption experiments. Mumby and Perone [10] measured the electrical characteristics of reference probes with a range of tip diameters. A 0.005 mm tip had an associated resistance of 340 k $\Omega$ . Vycor tips are reported to have relatively low electrical resistance and share the low leakage rate advantage of the smaller diameter capillaries.

In place of a Luggin probe, metal wire pseudo reference electrodes, used alone or with capacitive coupling to standard reference electrodes [1,6,15–19] have been employed. The wire electrodes have low resistance and can significantly reduce frequency response problems. Due to their small diameters (in some cases, as small as 10 micrometres [6]), they can be placed relatively close to the working electrode.

Metal rods are usually employed as the reference electrode in the three-electrode probes designed for industrial corrosion monitoring [20–25]. For these probes, considerations of probe ruggedness and the possibility of debris lodging between electrodes generally dictate a design with a relatively large working to reference electrode spacing. The associated IR drop related problems will be more severe than for a typical cell designed for laboratory use.

### Primary Current Distribution

The spatial variation in current on the working electrode when the interfacial potential  $E$  is zero is called the primary current distribution.  $E$  will be zero if the electrochemical processes at the working electrode are infinitely fast. For the cell depicted in Fig. 1, this is equivalent to setting  $Z_m$  to zero. In this situation, the potential difference between the working and reference electrodes,  $E_{tot}$ , is due entirely to current flow through the solution resistance.

If the primary current distribution is uniform, the potential sensed by the Luggin probe depends only on the perpendicular distance between the probe and the working electrode,  $z$ . For a non-uniform primary distribution, the sensed potential is a function of either two or three spatial coordinates, depending on the symmetry of the working electrode/counter electrode geometry.

For example, consider the cell geometry consisting of plane working and counter electrodes of length  $L$  placed opposite to each other and embedded flush with insulating walls. When the separation between the planes is much greater than  $L$ , the primary current distribution is given by [26]

$$i(x)/i(\text{avg}) = 1/(\pi[(x/L) - (x/L)^2]^{1/2}) \quad (2)$$

where  $x$  is the distance across the plane measured from the edge of the electrode,  $i(x)$  is the current density at position  $x$ , and  $i(\text{avg})$  is the average current density on the electrode. The current distribution is plotted in Fig. 2. This distribution is highly non-uniform: the current density is infinite at the edges and is about 64% of the average current density on

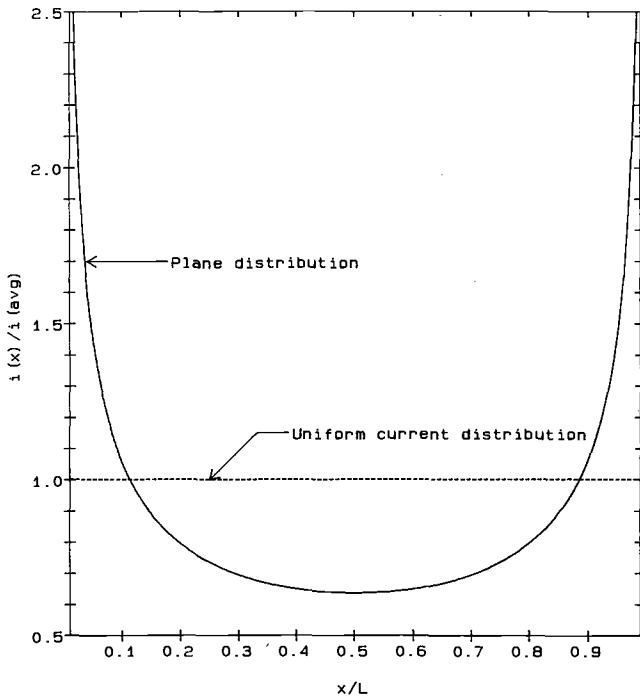


FIG. 2—Primary current distribution for the plane electrode geometry.

plane in the middle. The equipotential surfaces for this geometry [27] are shaped so that the potential difference between the electrode surface (an equipotential) and a plane parallel to the surface is greater at the edges than in the center of the electrode. Further, for any fixed distance  $x$  across the plane, the potential is not proportional to the perpendicular distance,  $z$ , from the plane.

Current distribution non-uniformity is not a phenomenon unique to the above example. Even when the effects of finite electrode kinetics are accounted for, the same qualitative behavior is obtained from detailed models for two [28] and three [29] dimensional plane electrodes and for the disk electrode [30]. The current density for all these geometries is higher on the edges than in the interior. The behavior of the current density at the edge of an electrode can be readily predicted [27]: if the angle between the electrode surface and the surrounding insulator surface is greater than  $90^\circ$ , the current density at the edge will be infinite; if the angle is less than  $90^\circ$ , the current density will be zero; and if it is equal to  $90^\circ$ , the current density will have a finite value that depends on the particular electrode geometry. Consequently, any electrode having a bounding insulator at an angle other than  $90^\circ$  will have a non-uniform primary current distribution.

This edge effect makes it difficult to construct a practical electrochemical cell having a working electrode with a uniform primary current distribution. The commonly used rotating cylinder and rotating disc electrodes both employ electrodes set flush with a surrounding insulator. A superior arrangement (from the standpoint of primary current distribution uniformity) is a working electrode holder where the area of a flat metal specimen exposed to solution is controlled by an insulating ring that presses up against the specimen so that the insulator/metal boundary forms a right angle. An electrode that is recessed in the surrounding insulator with a  $90^\circ$  insulator/electrode boundary will have a finite current density at the electrode edge. However, the current density may not be uniform across the electrode surface. Model calculations [31] have been done to determine the depth a plane electrode needs to be recessed to obtain a uniform current distribution, and to assess the effect of deviations from the  $90^\circ$  insulator/electrode angle.

This emphasis on the nature of the primary current distribution is necessary because, as will be shown, there are difficulties in the interpretation of resistance measurements and real errors in the measurement of corrosion rates and other electrochemical parameters that arise from non-uniform primary distribution. As indicated, the Luggin senses a potential difference caused by the current flow in its immediate vicinity. However, the potentiostat senses the total current,  $I$ , passing through the entire working electrode. When the working electrode current distribution is the primary current distribution,  $R_s$  is given by

$$R_s = E_{\text{tot}}/I \quad (3)$$

Unless the local current around the reference is equal to the average current over the working electrode, the value of  $R_s$  computed will not be a representative value for the electrode geometry. Thus, for the flat plate geometry in Fig. 2, the best Luggin position is at  $x/L = 0.114$ . The problem of optimum Luggin probe positioning for geometries in which the current distribution is non-uniform has been discussed by Britz [1] and others [5,7,9,12,32–37].

## The Cell Constant, $C_k$

### *General Aspects*

The magnitude of the IR drop is directly related to the product of  $R_s$  and the area of the working electrode. For a given cell geometry, that is, shape, size, and relative position of

working, reference, and counter electrodes, solution conductivity,  $\kappa$ , working electrode surface area,  $A$ , and measured solution resistance,  $R_s$ , it is possible to define an empirical cell constant,  $C_k$ , by

$$R_s A = C_k / \kappa \quad (4)$$

For a given solution conductivity, the smaller  $C_k$  is, the smaller the IR drop error.  $C_k$  will be shown below to be interpretable as the effective distance of the reference electrode from the working electrode.

$C_k$  may be computed analytically for certain ideal electrode geometries. For realistic cell geometries, numerical techniques must be used [8,9,29–31,38–44]. The problem involves computing the current distribution between the working and counter electrodes due to an impressed potential difference between them. Then, the fraction of the potential difference sensed by the reference electrode must be determined for the specific working/reference/counter geometry involved. For accurate calculations, the positions of the cell walls and the size and shape of the Luggin probe or other potential sensing electrode must be taken into account.

$C_k$  can be experimentally determined by making the appropriate resistance measurements with known solution conductivity. For a three-electrode cell, the desired resistance,  $R_s$ , is not the resistance obtained by making a measurement directly between the working and reference electrodes [7]. A direct measurement of this type senses a resistance that applies to the case where current flows between the working and reference electrodes. The current and potential distribution in this case can be very different from the current and potential distribution that exists when current flows between the working and counter electrodes.

#### *Analytical Models for $C_k$*

Table 1 contains expressions for the cell constant,  $C_k$ , for four electrode geometries. The first three, the plane, the cylinder, and the sphere, are uniform primary current distribution geometries if the restrictions listed under "Electrode Geometry" are satisfied. These restrictions are difficult to satisfy in practice. The disk geometry, has a non-uniform primary distribution [45]. A more detailed expression for  $C_k$  based on model calculations for a particular disk cell geometry, has been developed and experimentally confirmed [39].

Table 1 shows that for the case of the plane,  $C_k$  is the distance  $z$  of the reference electrode from the electrode surface. The limiting forms for small  $z$  given in Column 4 of the table all reduce to  $C_k$  being proportional to  $z$ . In this small  $z$  limit, the physical distance of the probe,  $z$ , and the probe's "electrical distance,"  $C_k$ , for the uniform distribution geometries are identical. However, for a cylindrical electrode of small diameter (wire electrode) or a spherical electrode that is a small mercury drop, it may be quite difficult to approach the limiting condition because a very small diameter reference electrode would be required.

Except for the case of the plane, the expressions for  $C_k$  depend both on  $z$  and on the working electrode size. In the case of the cylinder,  $C_k$  increases with  $z$ , but only logarithmically. Thus, if the reference is "far away," it has much less effect than for the case of the plane. For the sphere and the disk geometries,  $C_k$  becomes independent of  $z$  at large values of  $z$  (see Column 5 of Table 1). There is a limiting resistance for these geometries, and the effective distance represented by  $C_k$  at large  $z$  is a function of  $r$  (sphere or disk radius) rather than  $z$ .

For the disk geometry, most of the potential drop between the working and counter electrodes occurs close to the disk surface [45], so the limiting resistance is approached quickly.

TABLE 1—Expressions for the cell constant  $C_k$ .

Electrode Geometry	Uniform Current Density	$C_k$	Small $z^a$ Approximation	Large $z^a$ Approximation	Refs
Plane					
Plane counter electrode and perpendicular end walls	yes	$z^a$	...	...	3,4
Cylinder, radius $r$					
Cylindrical counter electrode and perpendicular end walls	yes	$r \ln[(r + z)/r]$	$z$ for $z < r/3$	...	3,4
Sphere, radius $r$					
Concentric sphere counter electrode	yes	$z r/(z + r)$	$z(1 - (z/r))$ for $z < r/4$	$r(1 - (r/z))$ for $z > 4r$	3,4
Disk, radius $r$					
Counter electrode at infinity reference on disk axis	no	$(r/2) \arctan(z/r)$	$z/2$ for $z < r/2$	$(r/2)[(\pi/2) - (r/z)]$ for $z > 2r$	45

<sup>a</sup>  $z$  = distance from electrode surface

For a disk with a radius of 0.25 cm, the apparent resistance measured by a probe placed on the disk axis 5 disk diameters below the disk is 94% of the limiting resistance.

### Values of $C_k$ for Real Cells

The discussion above indicates that many factors influence the value of  $C_k$  for a given cell.  $C_k$  is not reported as such in the literature. However,  $C_k$  was computed from literature data using the reported values of  $R_s$ , solution conductivity, and working electrode area. An assumption was made that the reported ohmic resistance is due solely to the solution resistance.

Marsh [20] has made measurements with a two electrode corrosion rate meter (CRM) probe geometry (1 cm spacing between electrodes) over a wide range of conductivities. These data correspond to a  $C_k$  of approximately 0.5 cm over the range of conductivities relevant here.  $C_k$  is not independent of  $\kappa$ ; it is 2.0 cm at a conductivity of 10 000  $\mu\text{S}/\text{cm}$  ( $1 \mu\text{S} = 1 \mu\text{mho} = 1 \times 10^{-6} \Omega^{-1}$ ). Hubbe [46] made measurements using similar electrodes with 3.3 cm distance between electrode centers; a  $C_k$  of 0.45 cm is representative of these data. Data obtained by Rhoades [23] for a CRM geometry in tap water yield a  $C_k$  of 0.5 cm.

Measurements by Mansfeld [47] using a Luggin with a typical corrosion cell correspond to a  $C_k$  between 0.1 and 0.16 cm. Data obtained by Walter [48] using a Luggin probe placed between 0.2 and 0.5 cm from the working electrode correspond to  $C_k$  of 0.18 cm.

Mansfeld et al. [49] made measurements using a rotating cylinder cell. An interrupter technique was used in conjunction with a gold wire reference electrode positioned close to the cylinder surface. Their low conductivity data (500  $\mu\text{S}/\text{cm}$ ) correspond to a  $C_k$  of 0.2 cm; data for a conductivity of 100 000  $\mu\text{S}/\text{cm}$  correspond to a  $C_k$  of 0.36 cm.

Kajimoto et al. [50] made measurements on a disk-like geometry—a low carbon steel rod with only the end exposed. The corresponding  $C_k$  is 0.17 cm. McIntyre et al. [15] used

a disk geometry; their data yields a  $C_k$  of 0.13 cm. The  $C_k$  of 0.32 cm obtained from the disk data of Wruck et al. [51] corresponds to the theoretical prediction of the limiting resistance for the disk. In their experiments, the Luggin probe was 4 cm from a disk with a 0.375 cm radius.

Note that in some cases the "constant"  $C_k$  varies with conductivity. This indicates that effects other than those discussed thus far are important in some systems.

Data obtained in this laboratory for a typical ASTM type corrosion cell yielded  $C_k$  values in the range of 0.15 to 0.35 cm. A 5 cm<sup>2</sup> area, low carbon steel cylindrical working electrode and a Vycor-tipped Luggin probe positioned within 1 cm from the working electrode was used.

The "Luggin-less" cell designed by Cahan et al. [13] for studies requiring good high frequency response is a model of what can be achieved in obtaining a low inherent  $R_s$  and uniform current distribution in a three-electrode cell. The  $C_k$  for this cell is in the range of 0.008 to 0.01 cm. This is more than an order of magnitude lower than for the more typical cells cited above. However, this cell design is impractical for use in routine corrosion studies.

In summary, most of the cell geometries typically used for corrosion studies are expected to have a  $C_k$  in the range of 0.1 to 0.5 cm. The low end of the range corresponds to a good cell design for laboratory use; the high end corresponds to the types of probes often used in industrial corrosion monitoring situations (where Luggin probes are not used). The  $C_k$  range is consistent with the values one would estimate using the  $C_k$  expressions for the model geometries listed in Table 1 if  $z$  values are used which are representative of the typical Luggin probe diameters used in routine corrosion studies and the minimum separation guidelines are followed.

### Other Contributions to Ohmic Resistance

The use of a cell constant to determine the magnitude of the uncompensated cell resistance is appropriate only when  $R_s$  is due to the solution conductivity alone, which is assumed to be constant throughout the experiment. However, processes can occur that cause the resistance to vary.

The solution conductivity can be time dependent [39]. When an anodic current is passed through a working electrode, metal ions are produced. If they remain soluble, they will raise the conductivity in the vicinity of the electrode above that of the bulk value and lower the resistance.

The formation of a nonconductive surface layer on the electrode will raise the resistance [52]. This type of layer is likely to form when cathodic polarization measurements are made in oxygen containing waters which are supersaturated with respect to calcium carbonate (CaCO<sub>3</sub>). A locally higher pH at the metal surface is generated by the reduction of dissolved oxygen to hydroxyl ion. This can cause CaCO<sub>3</sub> to precipitate on the metal surface. Bubbles formed during the course of gas evolution reactions, that is, reduction of hydrogen ion to hydrogen gas, also can lower the effective conductivity, even when the bubbles are so small as to be invisible to the naked eye [6,44,53].

When time-dependent effects are present, in most cases it is useful to use a compensation technique capable of adjusting to a changing  $R_s$ . However, sometimes a process such as the formation of a resistive film is an important part of the system being studied. In such a situation, one would not want the information about this process removed by an adaptive IR compensation technique.

### Secondary and Tertiary Current Distributions

Thus far the discussion regarding current and potential distributions in a cell has been limited to the effects of cell geometry and solution conductivity; the electrochemical reactions occurring at the metal/solution interface have been assumed to take place at whatever rate is needed to carry the ohmically controlled current without generating any interfacial potential drop. In order to introduce a model for a corrosion reaction at the interface, it is convenient to reference all potentials to the corrosion potential,  $E_c$ . The polarization,  $\Delta E$ , is defined by

$$\Delta E = E - E_c \quad (5)$$

An overpotential is normally defined as the deviation of a potential from an equilibrium value. Although  $E_c$  is not an equilibrium potential, the polarization defined above is referred to here as the overpotential. It will also be referred to as the true overpotential, when it must be distinguished from the total overpotential. The total overpotential (total polarization) is defined by

$$\Delta E_{\text{tot}} = E_{\text{tot}} - E_c \quad (6)$$

Making certain assumptions about the nature of the corrosion process which are sometimes met in practice [54,55], the dependence of the external current  $I$  on the overpotential can be written as

$$I = I_c \{ \exp(\Delta E \ln(10)/b_a) - \exp(-\Delta E \ln(10)/b_c) \} \quad (7)$$

where  $b_a$  and  $b_c$  are the anodic and cathodic Tafel constants and  $I_c$  is the corrosion current. The assumptions underlying the derivation of Eq 7 limit its applicability. In particular, other equations must be used if transport [56–59] or double layer [60] effects are important, or if the corrosion process is spatially inhomogeneous [59,61]. For these and other reasons, Eq 7 is, in most cases, not an accurate model for the current vs. potential response of the steel corrosion process in natural waters. However, it is a frequently used model and does allow analyses to be made that otherwise could not be made without greatly increased complexity.

It is instructive to examine the consequences of introducing an interfacial potential drop such as described by Eq 7 on the current distribution on the electrode surface and the resulting effect on IR drop measurements and interpretations. The current passing through the working electrode generates an overpotential across the double layer given by Eq 7. The current distribution that satisfies both Eq 7 on the electrode surface and the equations governing the primary current distribution (which apply to the entire cell) is called the secondary distribution.

As the overpotential increases, a point is reached at which the electron transfer rate of the electrochemical process is greater than the rate at which electrochemical reactants and products can be transported to and from the electrode surface. At this point the current is limited by transport processes (convective and diffusive mass transport), and the resulting current distribution is called the tertiary distribution.

The literature describes in detail secondary and tertiary distributions, the interactions between them, and the decomposition of total overpotentials into ohmic, surface, and concentration components [27,41,62,63]. Some points of particular interest to IR compensation are presented here.

If the primary current distribution is uniform, the secondary distribution will also be uniform. Therefore, the solution side of the double layer is an isopotential surface. The IR drop in this instance will simply be the IR drop from the solution side of the double layer to the reference electrode.

A geometry with a nonuniform primary current distribution will also have a nonuniform secondary distribution, although the secondary distribution will in general be more uniform than the primary. For instance, regions of infinite primary current density on the electrode necessarily have finite secondary current density due to the finite rate of electrochemical reactions.

The presence of a nonuniform secondary distribution causes difficulties with IR compensation. The solution side of the double layer is not an isopotential surface: the overpotential varies with position on the working electrode. For a given position of the reference electrode, there exists a range of IR drops corresponding to the range of overpotentials on the working electrode. Given this situation, two questions naturally arise: (1) Which IR drop is really being measured by a given experimental technique? (2) If some method is available to measure some particular IR drop within the range, which one is the best one to measure?

Unfortunately, these questions have not, in general, been answered. The universal recommendation is that cells with non-uniform primary current distributions should be avoided [1,7,9]. However, an extensive amount of analysis has been done on the disk geometry [27,30,32,36,39,45,64-76]. These results can be used as a guide to the kinds of effects that result from nonuniform current distributions.

Model calculations for the rotating disk using an approximation of Eq 7 valid for small overpotentials and assuming no mass transport limitations (infinitely fast disk rotation) predict that for the case of rapid electrochemical kinetics (high corrosion rates), the variation between the potential at the disk edge to the potential at the disk center can be a factor of two or more [27]. Under the model assumptions, the ratio of current densities at these locations will be the same as the potential ratio.

For the case of the disk geometry, Newman has analyzed the problem of which IR drop is measured when the current interrupt technique is used [65]. The reference electrode senses the local potential corresponding to the secondary distribution while the current is flowing. However, the IR drop sensed by the reference electrode when the cell current is interrupted is equal to the IR drop that would be measured at that reference electrode for the primary current distribution at the same total current and same reference electrode position. This result has been experimentally verified [72].

In general, secondary current distribution nonuniformities and their attendant IR compensation and experiment interpretation problems are minimized when the interfacial electrochemical processes are slow (low corrosion rates). Problems can be reduced by decreasing the size of the working electrode and increasing the solution conductivity.

The effect of mass transport on current and potential distributions varies. Tertiary current distributions for the rotating disk and cylinder geometries are uniform, although the potential distributions are not. Convective mass transport effects for cell geometries involving pipe or channel flow tend to have asymmetric current distributions: transport rates are higher on the leading edge of the electrode where fresh reactant is supplied.

As indicated, the shape (degree of nonuniformity) of a nonuniform secondary distribution depends on corrosion rate. Thus, the anticipated range of corrosion rates and solution conductivities for which a measurement cell will be used must be accounted for in order to choose an optimum position for the reference electrode. To optimize their correction factor approach to IR drop compensation, Rizzi and Ronchetti [38] computed the secondary current distributions for an electrochemical probe designed for on-line corrosion mon-

itoring. Figure 4 of their work shows the effect of the corrosion rate on the potential distribution on a working electrode for a fixed solution conductivity and working/counter electrode geometry. It has been observed that such detailed analyses are necessary in order to properly characterize potential measurement errors for cells with nontrivial geometries [9].

A nonuniform current distribution has been identified as the source of significant problems in certain experiments. Mears et al. [34] in studying the breakdown of passivity on a sheet of stainless steel masked off to a square one cm<sup>2</sup> in area, found a gradient of up to 60 mV between the center and edge of the working area. This gradient caused preferential pitting to occur on the electrode. The electrolyte for this study was 0.2 M sodium chloride; the nonuniformity is expected to be larger in less conductive electrolytes.

Harrar and Shain [35] mapped the isopotentials in an electrolysis cell and found potential differences of several 100 mV across the working electrode. It has been found that interpretable linear sweep voltammograms can only be obtained from thin layer cells that have been specifically designed to have a uniform current distribution [77,78].

In summary, there are IR drop related errors that are not solved by any IR compensation technique. The simple picture of the equivalent circuit of the electrochemical cell given in Fig. 1 is inadequate when current nonuniformities are present. The resulting errors in potential control and the associated errors in the parameters derived from the measured current/potential curves are difficult to quantify without detailed analysis. In some cases, these errors are probably comparable in magnitude to the more quantifiable errors that will be discussed in this paper.

## Electrochemical Corrosion Experiments

### *Range of Conductivities and $R_s$*

The range of solution conductivities usually encountered in open system cooling systems using fresh water as a water supply is 200  $\mu\text{S}/\text{cm}$  (uncycled, good quality water at relatively low temperatures) to 10 000  $\mu\text{S}/\text{cm}$  (high tower cycles, water with relatively high chloride and sulfate content at high temperatures). In the analysis that follows, Eq 4 is assumed to

TABLE 2—*Extreme values of variables used in analysis of errors.*

Variable	Unit	Extreme Values	
Solution conductivity	$\mu\text{S}/\text{cm}$	high	low
$C_k$ (measure of cell quality)		10 000	200
$R_s$ , $A$ (from Eq 4)	cm	good	poor
	$\Omega \text{ cm}^2$	0.1	0.5
Steel corrosion rate	mpy <sup>c</sup>	min <sup>a</sup>	max <sup>b</sup>
		10	2500
$R_p$ , $A$ (from Eq 12)	$\Omega \text{ cm}^2$	low	high
		1	20
$R_s/R_p$	—	max <sup>d</sup>	min <sup>e</sup>
		16 529	826.4
		min	max
		$6.0 \times 10^{-4}$	3.0

<sup>a</sup> Corresponds to HIGH conductivity, GOOD cell.

<sup>b</sup> Corresponds to LOW conductivity, POOR cell.

<sup>c</sup> 1 mpy = 0.0254 mm/y.

<sup>d</sup> Corresponds to LOW corrosion rate.

<sup>e</sup> Corresponds to HIGH corrosion rate.

be an accurate predictor of solution resistance for an electrochemical cell. It is also assumed that there are no other contributions to the ohmic resistance. For the conductivity range cited above, a good quality cell ( $C_k = 0.1$  cm) will have  $R_s A$  values between 10 and 500  $\Omega$  cm<sup>2</sup>. The corresponding range for a poor quality cell ( $C_k = 0.5$  cm) is 50 to 2500  $\Omega$  cm<sup>2</sup>. The extreme values of the above quantities are listed in Table 2.

Following common practice in the field of electroanalytical measurements, some workers have sought to minimize IR drop problems by adding "inert" electrolytes such as sodium perchlorate ( $\text{NaClO}_4$ ) to the test solution to raise the conductivity. Mansfeld et al. [49] compared IR drop compensated polarization curves of low carbon steel in tapwater with uncompensated curves in tapwater containing 1 M  $\text{NaClO}_4$ . The character of the polarization curves was completely changed: the  $\text{NaClO}_4$  induced a passivation behavior not present in the original solution. Similarly, dramatic changes were observed in curves where sodium nitrite ( $\text{NaNO}_2$ ) was added to these solutions as an inhibitor. This modification of the electrochemical processes on iron by  $\text{NaClO}_4$  has been confirmed by other investigators [39]. The results show that adding electrolytes is not a good approach to the IR compensation problem when the corrosion of steel in natural waters is being studied.

### The Polarization Resistance

In the analysis that follows, a uniform primary current distribution geometry cell is assumed. With this assumption the simple lumped parameter model equivalent circuit depicted in Fig. 1 can be used to represent the cell. If the control signal is limited to small, slow perturbations about some fixed value of the overpotential,  $\Delta E^*$ , the interfacial impedance  $Z_m$  can be replaced by a resistance,  $R_m$ , given by

$$R_m = (\partial \Delta E / \partial I) \text{ at } \Delta E = \Delta E^* \quad (8)$$

and the effect of the double layer capacitance,  $C$ , can be ignored.  $R_m$  is a function of the overpotential,  $\Delta E^*$ . The value of  $R_m$  at zero overpotential is the polarization resistance,  $R_p$ , given by

$$R_p = (\partial \Delta E) / (\partial I) \text{ at } \Delta E = 0 \quad (9)$$

Under these conditions, the equivalent circuit model of Fig. 1 reduces to that of Fig. 3. This model is approximately valid for overpotentials of plus or minus a few millivolts.

Using Eq 7,  $R_p$  is given by

$$R_p = B / I_c \quad (10)$$

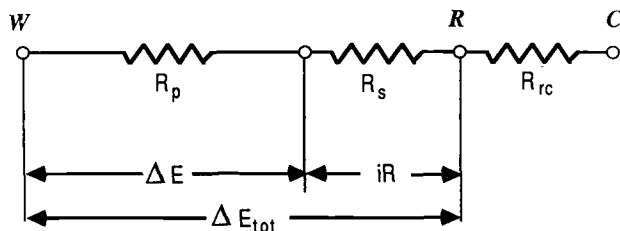
where the constant  $B$  is

$$B = b_a b_c / [\ln(10)(b_a + b_c)] \quad (11)$$

Of the metals commonly used in cooling water systems, low carbon steel (LCS) is the material that corrodes at the highest rates and has the most severe IR drop problems in electrochemical measurements. Therefore, the numerical examples presented in the remainder of this paper are for the specific case of LCS corrosion.

For LCS, the relationship between  $R_p$  and corrosion rate is given by

$$CR = 456.6B / (R_p A) \text{ for LCS} \quad (12)$$



**W** Working electrode  
**R** Reference (Luggin) electrode  
**C** Counter electrode

$R_p$  = Polarization resistance..

$R_s$  = Uncompensated solution resistance. May include component from surface film on metal.

$R_{rc}$  = Resistance between reference and counter electrodes.

$\Delta E_{tot}$  = Total overpotential.

$\Delta E$  = True overpotential.

$iR$  = Potential drop due to cell current flowing through  $R_s$ .

FIG. 3—Idealized DC signal equivalent circuit of an electrochemical cell for small overpotentials.

where  $CR$  is the corrosion rate in mils per year (mpy) ( $1 \text{ mpy} = 0.0254 \text{ mm/y}$ ), and  $A$  is the area of the working electrode in  $\text{cm}^2$ . A LCS density of  $7.87 \text{ g/cm}^3$  and a two-electron oxidation process for iron have been assumed.

### The B Value

If the Tafel constants ( $b_a$  and  $b_c$  in Eq 7) are known,  $B$  can be computed. From theoretical considerations, an appropriate range for the anodic Tafel constant,  $b_a$ , is from 30 to 120 mV [54]. For natural waters, however, values near and beyond the high end of the range are more common. A  $b_a$  of 120 mV has been reported for iron in tap water [49]. When the pH is neutral to alkaline, as in the air-saturated waters found in typical cooling water systems, the cathodic reaction is oxygen reduction. The appropriate range for  $b_c$  under these conditions is from 120 mV to infinity. The latter limit corresponds with the case where oxygen reduction is mass transport controlled. Within these limits for the Tafel constants,  $B$  assumes the range of values from 10.4 mV ( $b_a = 30$ ,  $b_c = 120$ ) to 52.1 mV ( $b_a = 120$ ,  $b_c = + \text{infinity}$ ). Values in the high end of this range are more likely.

In practice, rather than being computed from measured or mechanistically reasonable values of the Tafel constants,  $B$  is often used as an empirical scale factor which is selected to give a reasonable correspondence between electrochemically measured corrosion rates and corrosion rates measured by other means (usually weight loss) [23–25, 54, 79–81]. This is the approach used in setting a scale factor for the readout of commercial corrosion rate meters that are based on the polarization resistance technique. One vendor of such meters

has chosen a  $B$  value of 36.2 mV [80–81]. Another has selected a value of 27.5 mV [23–24], yet in some models the default value can be adjusted. Data obtained in this laboratory and data published by Rizzi and Ronchetti [38] for steel in cooling waters indicate that in some cases  $B$  values as high as 70 mV are needed to obtain good correlation between weight loss and LCS corrosion rates computed from Eq 12.

For the purposes of illustration, a  $B$  value of 36.2 mV will be used in the following discussion. Substituting this value in Eq 12 yields

$$CR = 16\,529/(R_p A) \quad \text{for LCS} \quad (13)$$

Solving for  $R_p A$  yields

$$R_p A = 16\,529/CR \quad \text{for LCS} \quad (14)$$

with the LCS corrosion rate,  $CR$ , being expressed in mpy (1 mpy = 0.0254 mm/y) and  $R_p A$  being expressed in  $\Omega \text{ cm}^2$  in both of the above equations.

For many cooling systems, a  $CR$  for LCS of 1 mpy is a low value, and is routinely achieved with modern cooling treatment programs. LCS corrosion rates can be in the 100–200 mpy range in some uninhibited waters with high conductivity. However, in treated systems, a value of 20 mpy is considered unacceptably high. It is possible to sustain a  $CR$  near 20 mpy for the lowest conductivity waters considered here (see Table 2). Thus, most of the examples presented will be limited to a consideration of the 1 to 20 mpy  $CR$  range. These limits and the corresponding values of  $R_p A$  from Eq 14 are listed in Table 2.

### IR Drop Errors for Common Experiments

In what follows the IR drop related error parameters appropriate for three types of experiments are examined. The experiments considered are as follows:

1. **Linear polarization.** In this experiment the parameter of interest is the corrosion rate, which is computed from  $R_p A$ . Overpotentials in the range of  $\pm 10$  mV are generally employed.
2. **Small range polarization.** The purpose of this experiment is to extract both the corrosion rate and the Tafel constants by using nonlinear fitting techniques. Overpotentials in the range of  $\pm 30$  to  $\pm 60$  mV are generally used.
3. **Full polarization.** Data obtained from the full polarization experiment can be analyzed to extract the same parameters as the small range polarization experiment. In addition, the technique is used to test the validity of various models for the corrosion process (such as Eq 7) and to uncover the existence of other phenomena occurring in the corrosion system (that is, passivation). Overpotentials of 100 to 2000 mV are used.

#### *Linear Polarization (Polarization Resistance)*

Mansfeld [47,54] has presented a detailed analysis of the effect of uncompensated IR drop on polarization resistance measurements. Experimental results from both high [21,82] and low [21,38,49,83–86] conductivity solutions have confirmed the necessity of compensating for IR drop to obtain accurate corrosion rates.

Mansfeld [47,54] has shown that the  $R_p$  measured in a linear polarization experiment,  $R_p(\text{meas})$ , is related to the true  $R_p$  by

$$R_p(\text{meas}) = R_p + R_s \quad (15)$$

This can also be seen by examination of Fig. 3. Equation 15 can be rewritten as

$$R_p(\text{meas}) = R_p(1 + R_s/R_p) \quad (16)$$

$R_p(\text{meas})$  and  $R_p$  will be nearly equal only when the ratio  $R_s/R_p$  is small. This dimensionless ratio is called the Wagner number [62]; it can be interpreted as an indicator of the relative importance of ohmic and kinetic effects in determining the current distribution of the cell. Using Eqs 4 and 14, the ratio for LCS is

$$R_s/R_p = 60.5C_kCR/\kappa, \text{ for LCS} \quad (17)$$

where  $C_k$  is in cm,  $CR$  is in mpy, and  $\kappa$  is expressed in  $\mu\text{S}/\text{cm}$ . The range of  $R_s/R_p$  that corresponds to the previously stated extremes of the variables in Eq 17 is listed in Table 2 and is shown graphically in Fig. 4. As is well known, the combination of low conductivity and high corrosion rates yields high  $R_s/R_p$  ratios.

The corrosion rate measured in a linear polarization experiment done without IR compensation,  $CR(\text{meas})$ , is obtained by assuming that  $R_s$  is zero, that is, that  $R_p(\text{meas}) = R_p$ . Replacing  $R_p$  in Eq 13 with  $R_p(\text{meas})$  from Eq 16 and re-arranging terms yields

$$CR(\text{meas}) = CR/(1 + R_s/R_p) \quad (18)$$

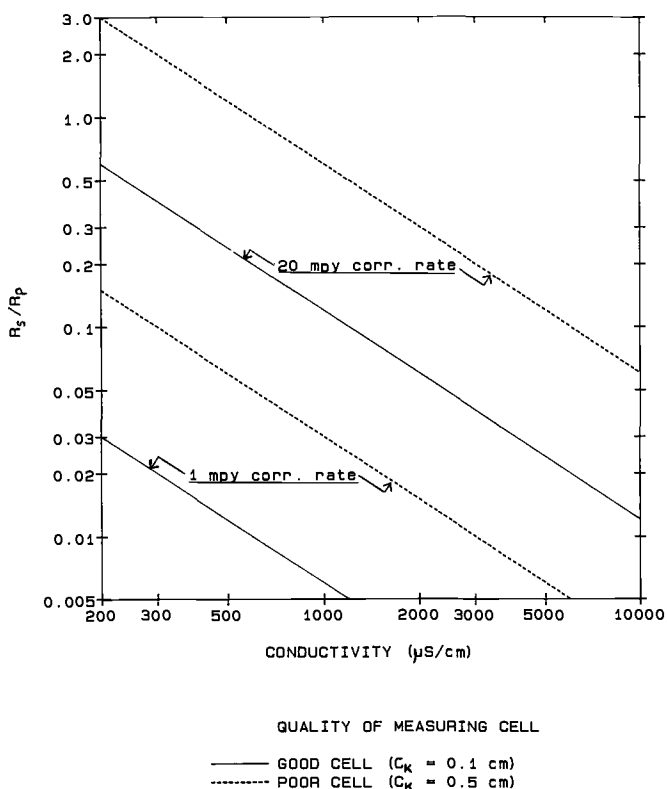


FIG. 4—Dependence of  $R_s/R_p$  for low carbon steel on solution conductivity, cell quality, and corrosion rate, assuming a  $B$  value of 36.2 mV (1 mpy = 0.0254 mm/y).

Equation 18 indicates that, unless  $R_s$  is zero, the measured corrosion rate  $CR(\text{meas})$  will always be less than the true corrosion rate,  $CR$ . Substituting Eq 17 for  $R_s/R_p$ , results in

$$CR(\text{meas}) = CR/(1 + 60.5C_k CR/\kappa) \text{ for LCS} \quad (19)$$

where all quantities retain the same units as in Eq 17.

Corrosion in cooling tower systems is often monitored with corrosion rate meters (CRMs) which utilize the polarization resistance technique. As previously indicated, the probes for these meters have larger cell constants (typically in the 0.3 to 0.5 cm range) than do typical laboratory corrosion cells. Since, until recently, the CRMs had no provision for automatic IR compensation [23], an examination of the practical limits of an uncompensated CRM for measuring LCS corrosion rates is of interest.

Equation 19 has been plotted for a range of solution conductivities for a  $C_k$  of 0.3 cm in Fig. 5a, and 0.5 cm in Fig. 5b. The fractional error in the measured corrosion rate,  $f_{\text{err}}$ , is defined by

$$CR(\text{meas}) = CR(1 - f_{\text{err}}) \quad (20)$$

Combining Eqs 19 and 20 yields

$$\kappa = 60.5CRC_k(1 - f_{\text{err}})/f_{\text{err}} \text{ for LCS} \quad (21)$$

Contours of constant fractional error defined by Eq 21 have been plotted in Fig. 6a for  $C_k = 0.3$  cm and in Fig. 6b for  $C_k = 0.5$  cm. The curves have been marked with the percent error,  $100f_{\text{err}}$ . Figures 5 and 6 reveal that there is a large region of practical interest where IR drop errors are significant. If the maximum measurement error that can be tolerated is set at 20% ( $f_{\text{err}} = 0.2$ ), the region can be described using Eq 21 and the solution resistivity  $\rho$  via the inequality

$$\rho CR \leq 4132/C_k \text{ for 20\% error limit, LCS} \quad (22)$$

where  $\rho$  is expressed in  $\Omega$  cm. To stay within this limit, the product of the resistivity and the corrosion rate ( $\Omega$  cm mpy) should not exceed 8264 (for  $C_k = 0.5$  cm) or 13 773 (for  $C_k = 0.3$  cm). These values bracket the value for  $\rho CR$  of 10 000 (mpy  $\Omega$  cm) cited by Townsend [21] as the limit of the useful range of two-electrode and wide-spaced three-electrode CRM probes when a conductivity correction factor is not used.

### Limits to IR Compensation

The most common type of industrial CRM probe used in cooling systems has electrodes which consist of parallel metal cylinders [22]. The primary current distribution for these probes is definitely nonuniform; the current density on the working electrode is highest on the part of the electrode closest to the counter electrode. Using the appropriate instrumental techniques a value of  $R_s$  can be obtained and used to correct  $R_p$ ; however, a residual error in the computed corrosion rate will remain because a single value of  $R_s$  cannot account for the distribution of potentials at the electrode surface. Results available from analysis of the disk geometry by Tiedemann et al. [70] and (more recently) by Nisancioglu [36] give an indication of the magnitude of these nonuniformity errors.

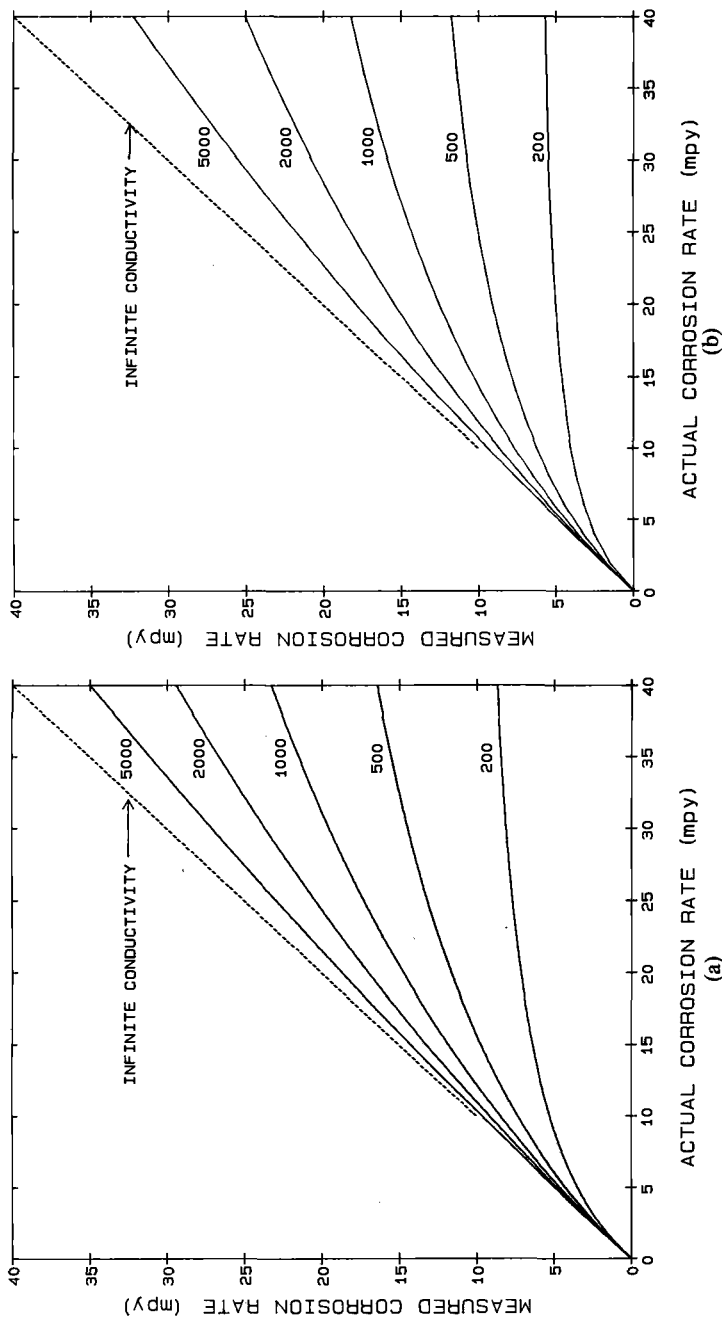


FIG. 5—Measured versus actual low carbon steel corrosion rate as a function of solution conductivity, assuming a B value of 36.2 mV, for (a)  $C_x = 0.3 \text{ cm}$  and (b)  $C_x = 0.5 \text{ cm}$ . Curve labels are conductivity,  $\mu\text{S/cm}$  ( $1 \text{ mpy} = 0.0254 \text{ mm/y}$ ).

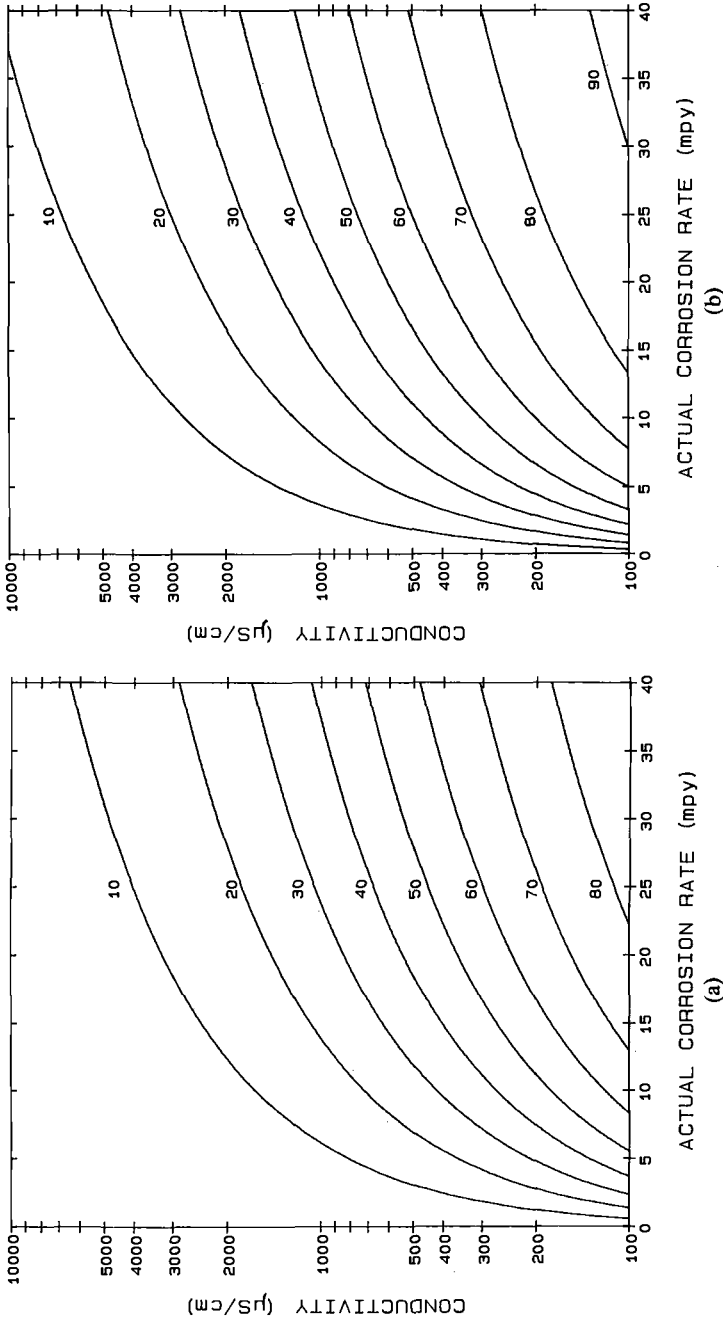


FIG. 6—Percent error in the measured low carbon steel corrosion rate as a function of solution conductivity and actual corrosion rate, assuming a B value of 36.2 mV, for (a)  $C_k = 0.3$  cm and (b)  $C_k = 0.0254$  mm/y. Curve labels are percent error (1 mpy = 0.0254 mm/y).

Tiedemann et al. [70] computed the secondary distribution for the disk under linear polarization conditions as a function of a dimensionless parameter  $J$  given by

$$J = r/(\kappa R_p A) \quad (23)$$

where  $r$  is the disk radius.  $J$  is analogous to the ratio  $R_s/R_p$  previously examined. Hypothetical experiments were considered where the IR drop is measured with an instrumentally perfect current interrupter and a very small (ideal) reference electrode is placed in three different locations: far from the disk, close to the disk at the disk center, and close to the disk at the disk edge. Due to the nonuniform distribution, the IR drops measured by the interrupter are different in all three locations and, therefore, the measured overpotential also varies with location. The overpotential is used along with the total current to compute an apparent  $R_p$  value. From this, using an exactly known  $B$  value, an apparent corrosion current density,  $i_c(\text{apparent})$ , is obtained. The ratio of the true corrosion current density,  $i_c(\text{true})$ , to  $i_c(\text{apparent})$  is a function of both  $J$  and the reference electrode location.

This analysis demonstrates that when  $J$  is small (low corrosion rates, high conductivity) the secondary current distribution is uniform, the reference electrode position has little effect, and  $i_c(\text{true})/i_c(\text{apparent})$  is close to one. As  $J$  becomes large, the distribution becomes more like the primary distribution, where infinite current density exists at the disk edge. For large  $J$ ,  $i_c(\text{true})/i_c(\text{apparent})$  deviates from unity. The error for the edge reference position is significantly larger than for the other positions.

$J$  is 3.0 when the solution conductivity is  $200 \mu\text{S}/\text{cm}$ , the  $R_p A$  value is  $826 \text{ ohm cm}^2$  (see Table 2), and the disk radius is 0.5 cm. For this  $J$  value,  $i_c(\text{true})/i_c(\text{apparent})$  is 0.8 for the reference at disk center, 1.1 for the reference far away, and 1.5 for the reference at the disk edge. These are significant errors considering that theoretically "perfect" IR compensation is being assumed. Using the same low conductivity with a  $R_p A$  value of  $16\,529 \Omega \text{ cm}^2$  (see Table 2),  $J$  is equal to 0.076. At this extreme, the non-uniformity errors are small.

### Small Range Polarization

In the linear polarization experiment a  $B$  value (Eq 11) is needed to convert  $R_p$  to the corrosion current,  $I_c$  (Eq 10). Rather than estimate  $B$  or measure Tafel constants in separate experiments, the Tafel constants and  $I_c$  can be determined in a single experiment by applying nonlinear fitting techniques to the current/overpotential curve obtained from a small range polarization scan [58,87–95]. Generally, a scan range of  $\pm 30$  to  $\pm 60$  mV is required to obtain enough curvature in the response to reliably determine the parameters. Much attention has been paid to the fitting algorithm and other details of the method. Yet, most of the analyses to date on the errors in the fitted parameters have ignored the possible errors due to uncompensated IR drop. The exceptions are the comprehensive study by Williams and Taylor [87] and the brief treatment by Mansfeld and Kendig [90].

The total overpotential,  $\Delta E_{\text{tot}}$ , applied between working and reference electrodes is related to the true overpotential,  $\Delta E$  by

$$\Delta E_{\text{tot}} = \Delta E + I R_s \quad (24)$$

Using a range of  $b_a$  between 30 and 120 mV,  $b_c$  values of 120 mV and infinity, and for a range of  $R_s/R_p$  between 0 and 10, Williams and Taylor [87] computed curves of  $I$  versus  $\Delta E_{\text{tot}}$  for a range of  $\pm 30$  mV in  $\Delta E_{\text{tot}}$  (in 2 mV steps) from Eqs 7, 10, 11, and 24. The computed curves were then fit to Eq 7 by assuming that  $\Delta E_{\text{tot}}$  was actually  $\Delta E$ ; this simulates the process of fitting Eq 7 to a polarization curve obtained without IR compensation. Some of the results derived from their analysis are:

TABLE 3—Results of fits to computed polarization curves for several polarization ranges.

$R_p/R_c$	$b_a$ mV	$b_c$ mV	$I^*(app)$	$S_{dev}^a$	$b_a = 60$ mV, $b_c = 60$ mV					$I^*(a00)$	$S_{dev}$	
					$b_a$ mV	$b_c$ mV	$I^*(app)$	$S_{dev}$	$b_a$ mV			$b_c$ mV
	$\pm 20$ mV											
0.00	60.0	60.0	1.00	7.05e-13	60.0	60.0	1.00	7.98e-13	60.0	60.0	1.00	1.08e-12
0.01	61.0	61.0	1.01	2.02e-05	61.1	61.1	1.01	1.53e-04	61.3	61.3	1.01	6.87e-04
0.02	62.0	62.0	1.01	3.75e-05	62.3	62.3	1.02	2.81e-04	62.6	62.6	1.03	1.24e-03
0.05	65.0	65.0	1.03	7.50e-05	65.6	65.6	1.04	5.47e-04	66.5	66.5	1.06	2.32e-03
0.10	70.1	70.1	1.06	1.05e-04	71.1	71.1	1.08	7.43e-04	72.7	72.7	1.11	3.00e-03
0.20	80.3	80.3	1.12	1.10e-04	82.1	82.1	1.14	7.46e-04	84.7	84.7	1.18	2.85e-03
0.50	112.8	112.8	1.25	5.57e-05	115.9	115.9	1.29	3.60e-04	120.1	120.1	1.34	1.31e-03
1.00	173.0	173.0	1.44	1.53e-05	177.0	177.0	1.48	9.66e-05	182.3	182.3	1.52	3.53e-04
2.00	313.9	313.9	1.74	3.82e-06	319.6	319.6	1.78	1.19e-05	325.6	325.6	1.81	4.48e-05
	$\pm 50$ mV											
0.00	60.0	60.0	1.00	1.60e-12	60.0	60.0	1.00	2.50e-12	60.0	60.0	1.00	6.60e-12
0.01	61.6	61.6	1.02	2.32e-03	62.0	62.0	1.03	6.59e-03	63.4	63.4	1.08	3.82e-02
0.02	63.2	63.2	1.04	4.10e-03	64.0	64.0	1.06	1.13e-02	66.5	66.5	1.14	5.99e-02
0.05	67.7	67.7	1.09	7.28e-03	69.4	69.4	1.13	1.87e-02	74.3	74.3	1.27	8.33e-02
0.10	74.8	74.8	1.15	8.88e-03	77.5	77.5	1.21	2.13e-02	85.1	85.1	1.40	8.12e-02
0.20	88.0	88.0	1.24	7.91e-03	92.1	92.1	1.32	1.77e-02	102.7	102.7	1.53	5.89e-02
0.50	125.3	125.3	1.40	3.44e-03	131.6	131.6	1.48	7.31e-03	146.7	146.7	1.69	2.20e-02
1.00	188.9	188.9	1.58	9.30e-04	196.7	196.7	1.65	1.99e-03	215.2	215.2	1.82	6.10e-03
2.00	332.9	332.9	1.85	1.22e-04	341.6	341.6	1.90	2.73e-04	362.5	362.5	2.02	9.13e-04
	$\pm 80$ mV											
0.00	60.0	60.0	1.00	1.60e-12	60.0	60.0	1.00	2.50e-12	60.0	60.0	1.00	6.60e-12
0.01	61.6	61.6	1.02	2.32e-03	62.0	62.0	1.03	6.59e-03	63.4	63.4	1.08	3.82e-02
0.02	63.2	63.2	1.04	4.10e-03	64.0	64.0	1.06	1.13e-02	66.5	66.5	1.14	5.99e-02
0.05	67.7	67.7	1.09	7.28e-03	69.4	69.4	1.13	1.87e-02	74.3	74.3	1.27	8.33e-02
0.10	74.8	74.8	1.15	8.88e-03	77.5	77.5	1.21	2.13e-02	85.1	85.1	1.40	8.12e-02
0.20	88.0	88.0	1.24	7.91e-03	92.1	92.1	1.32	1.77e-02	102.7	102.7	1.53	5.89e-02
0.50	125.3	125.3	1.40	3.44e-03	131.6	131.6	1.48	7.31e-03	146.7	146.7	1.69	2.20e-02
1.00	188.9	188.9	1.58	9.30e-04	196.7	196.7	1.65	1.99e-03	215.2	215.2	1.82	6.10e-03
2.00	332.9	332.9	1.85	1.22e-04	341.6	341.6	1.90	2.73e-04	362.5	362.5	2.02	9.13e-04
	$\pm 120$ mV											
0.00	60.0	60.0	1.00	1.37e-17	60.0	60.0	1.00	1.36e-17	60.0	60.0	1.00	2.74e-17
0.01	61.3	61.3	1.01	5.62e-05	61.5	61.5	1.02	2.97e-04	61.8	61.8	1.02	1.05e-03
0.02	62.7	62.7	1.02	1.04e-04	63.0	63.0	1.03	5.44e-04	63.5	63.5	1.04	1.90e-03
0.05	66.7	66.7	1.06	2.10e-04	67.5	67.5	1.07	1.06e-03	68.6	68.6	1.09	3.55e-03
0.10	73.7	73.7	1.12	3.01e-04	75.0	75.0	1.14	1.46e-03	76.8	76.8	1.17	4.63e-03
0.20	88.1	88.1	1.22	3.29e-04	90.2	90.2	1.25	1.52e-03	93.0	93.0	1.29	4.56e-03
0.50	137.4	137.4	1.52	1.89e-04	140.2	140.2	1.55	8.46e-04	144.0	144.0	1.58	2.41e-03
1.00	241.6	241.6	2.00	6.11e-05	243.7	243.7	2.01	2.74e-04	246.6	246.6	2.02	7.87e-04
2.00	535.0	535.0	2.95	9.74e-06	535.0	535.0	2.94	4.44e-05	533.4	533.4	2.91	1.31e-04

	±50 mV		±60 mV		±80 mV	
0.00	60.0	120.0	60.0	120.0	60.0	120.0
0.01	62.2	124.2	62.7	125.2	64.5	128.5
0.02	64.2	128.1	65.2	130.0	68.4	135.7
0.05	70.1	139.3	72.2	142.8	78.0	152.3
0.10	79.3	156.3	82.5	161.2	90.8	173.1
0.20	96.7	187.6	101.0	193.3	111.9	206.1
0.50	148.7	281.0	154.3	285.1	167.5	294.4
1.00	250.3	465.4	254.9	462.1	266.6	458.5
2.00	531.7	986.1	530.2	959.0	529.8	909.7
			$b_a = 60 \text{ mV}, b_c = \text{infinity}$			
			±30 mV			
0.00	60.0	2.5e+06	60.0	2.5e+06	60.0	5.1e+06
0.01	61.4	5.8e+10	61.6	9.7e+14	62.0	3.8e+16
0.02	62.8	5.8e+10	63.3	9.7e+14	64.0	3.8e+16
0.05	67.0	5.8e+10	68.0	9.7e+14	69.6	3.8e+16
0.10	74.0	5.8e+10	75.8	9.7e+14	78.2	3.8e+16
0.20	88.5	5.8e+10	91.1	9.7e+14	94.5	3.8e+16
0.50	137.3	5.8e+10	140.0	9.7e+14	143.7	3.8e+16
1.00	240.6	5.8e+10	241.4	9.7e+14	242.6	3.8e+16
2.00	536.9	5.8e+10	533.2	9.7e+14	528.5	3.8e+16
			±60 mV			
0.00	60.0	5.1e+06	60.0	1.0e+07	60.0	1.0e+07
0.01	62.6	1.1e+17	63.4	8.1e+10	66.1	1.4e+11
0.02	65.1	1.1e+17	66.5	8.1e+10	71.0	1.4e+11
0.05	71.7	1.1e+17	74.5	8.1e+10	82.1	1.4e+11
0.10	81.5	1.1e+17	85.5	8.1e+10	95.7	1.4e+11
0.20	98.8	1.1e+17	104.0	8.1e+10	116.4	1.4e+11
0.50	148.3	1.1e+17	153.8	8.1e+10	166.8	1.4e+11
1.00	244.5	1.1e+17	247.0	8.1e+10	254.3	1.4e+11
2.00	522.7	1.1e+17	516.2	8.1e+10	502.7	1.4e+11
			±80 mV			
0.00	60.0	5.1e+06	60.0	1.0e+07	60.0	1.0e+07
0.01	62.6	1.1e+17	63.4	8.1e+10	66.1	1.4e+11
0.02	65.1	1.1e+17	66.5	8.1e+10	71.0	1.4e+11
0.05	71.7	1.1e+17	74.5	8.1e+10	82.1	1.4e+11
0.10	81.5	1.1e+17	85.5	8.1e+10	95.7	1.4e+11
0.20	98.8	1.1e+17	104.0	8.1e+10	116.4	1.4e+11
0.50	148.3	1.1e+17	153.8	8.1e+10	166.8	1.4e+11
1.00	244.5	1.1e+17	247.0	8.1e+10	254.3	1.4e+11
2.00	522.7	1.1e+17	516.2	8.1e+10	502.7	1.4e+11

<sup>a</sup> S<sub>dev</sub> = Standard deviation of the fit.

Some of the results derived from their analysis are:

1. For a wide range of  $R_s/R_p$  values, the fit of Eq 7 to the synthetic data is excellent. The appearance of the fit does not indicate that the curve is distorted by IR drop.
2. The apparent Tafel constants,  $b_a(\text{app})$  and  $b_c(\text{app})$ , are larger than their true values.
3. The apparent corrosion current,  $I_c(\text{app})$ , is larger than the true corrosion current,  $I_c$ . This is the opposite of the effect that uncompensated resistance has on a simple linear polarization experiment.
4. Fits to curves with  $b_c = \text{infinity}$  converge with a negative  $b_c(\text{app})$ .
5. The parameter errors depend on  $b_a$ ,  $b_c$ , and  $R_s/R_p$ , but are independent of  $I_c$ .

Result 5 was obtained by numerical testing. This result can be derived solely by examining the form of the equations in modified form. The reduced current,  $I^*$ , is defined by

$$I^* = I/I_c \quad (25)$$

Equation 7 in reduced form becomes

$$I^* = \exp[\Delta E \ln(10)/b_a] - \exp[-\Delta E \ln(10)/b_c] \quad (26)$$

and Eq 24 can be rewritten

$$\Delta E_{\text{tot}} = \Delta E + I^*(R_s/R_p)B \quad (27)$$

The form of the  $\Delta E_{\text{tot}}$  versus  $I^*$  curve defined by Eqs 26 and 27 depends only upon  $b_a$ ,  $b_c$ , and  $R_s/R_p$ , but not on  $I_c$ .

The effect of changing the polarization range on the above results was determined. As the range increases a point must be reached where the shape of a true Tafel response (Eq 7) and the shape of an IR drop distorted response are noticeably different. Curves were computed from Eqs 26 and 27 in 2 mV increments of  $\Delta E_{\text{tot}}$  for  $\Delta E_{\text{tot}}$  ranges between  $\pm 20$  and  $\pm 80$  mV, for a  $b_a$  of 60 mV and  $b_c$  values of 60 mV, 120 mV, and infinity, and for a range of  $R_s/R_p$  values of between 0 and 2. The resulting curves were fit to

$$I = I_c^*(\text{app})I^* \quad (28)$$

$I^*$  is given by Eq 26, and the apparent reduced corrosion current  $I_c^*(\text{app})$  is defined by

$$I_c^*(\text{app}) = I_c(\text{app})/I_c \quad (29)$$

$I_c^*(\text{app})$  is one if  $R_s/R_p$  is zero (no IR drop). The curves were fit using a general purpose nonlinear regression program which allowed  $b_a$ ,  $b_c$ ,  $I_c^*(\text{app})$ , and the corrosion potential,  $E_c$ , to vary. In order to speed convergence, the cases were fit (for fixed overpotential range,  $b_a$ , and  $b_c$ ) sequentially in order of increasing  $R_s/R_p$ , using the results from the preceding fit as a starting point for the next fit.

The results of these fits are shown in Table 3. The corrosion potential was zero to within  $\pm 2$  mV in all cases and is not shown. The  $\pm 60$  mV range results for  $b_a = 60$  mV,  $b_c = 120$  mV as a function of  $R_s/R_p$  are plotted in Fig. 7; the results for the same Tafel constants and  $R_s/R_p = 0.2$  are plotted for polarization ranges between  $\pm 20$  mV and  $\pm 80$  mV in Fig.

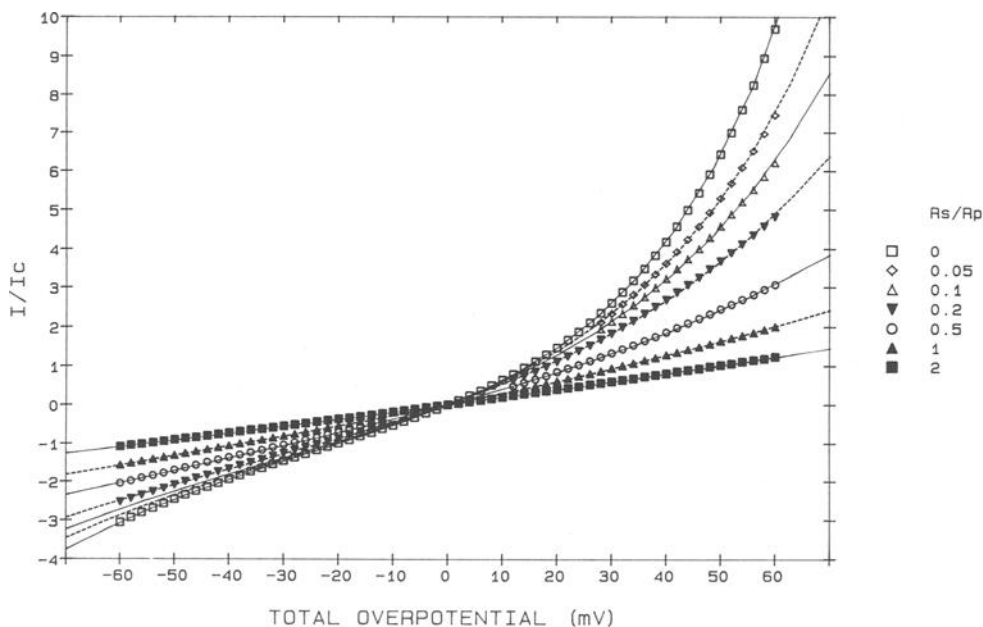


FIG. 7—Computed reduced current versus total overpotential curves as a function of  $R_s/R_p$  for  $b_a = 60$  mV, and  $b_c = 120$  mV. Solid and dashed continuous lines are backfits computed assuming no IR drop.

#### 8. The following conclusions can be drawn:

1. The trends noted above for the apparent Tafel constants and corrosion current as a function of  $R_s/R_p$  hold for all polarization ranges considered. The fit standard deviation initially increases with  $R_s/R_p$ , reaches a maximum at about the 0.1 to 0.2 range, then decreases.

2. The overall quality of the fit—as judged from the appearance of the backfit—remains high even up to the  $\pm 60$  mV range (see Fig. 8). The  $R_s/R_p$  value of 0.2 for the curves in Fig. 8 is at or near the value that produces the maximum standard deviation in all of the ranges. Yet, deviations between the backfit curve and the data points are only evident in the vicinity of zero overpotential in the  $\pm 60$  and  $\pm 80$  mV ranges and in the extremes of the  $\pm 80$  mV range curve. These deviations might easily be masked by experimental noise.

3. Convergence with positive  $b_c$  values can be obtained from the curves synthesized using  $b_c = \text{infinity}$ . A few cases were forced to converge at the negative  $b_c$  value parameter sets obtained by Williams and Taylor [87]. These sets produced very slightly smaller fit standard deviations, but the appearance of the plotted backfits were almost indistinguishable.

4. For  $b_c = 60$  and 120 mV with  $b_a = 60$  mV, the parameter errors are not strong functions of the overpotential range.

5. For this type of analysis, significant parameter errors ( $>10\%$ ) can result from  $R_s/R_p$  ratios that are as low as 0.05. Limitations on the conductivity/corrosion rate combinations that are amenable to study without using IR compensation can be assessed by examining Fig. 2.

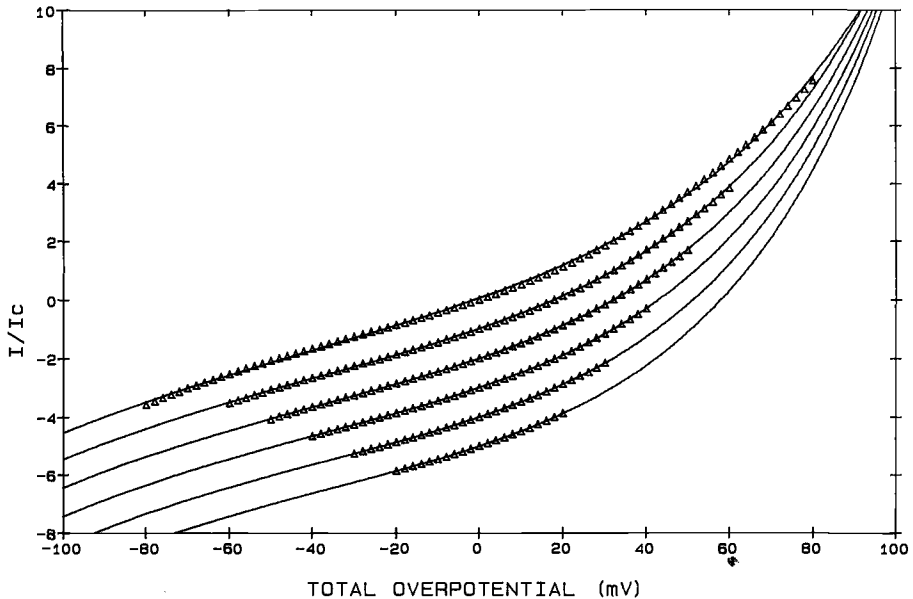


FIG. 8—Computed reduced current versus total overpotential curves for a range of total overpotentials for  $R_s/R_p = 0.2$ ,  $b_a = 60$  mV, and  $b_c = 120$  mV. Continuous curves are back-fits computed assuming no IR drop. Successive curves are displaced by  $-1.0$  current units for clarity.

The improvement in the quality of the fit for  $R_s/R_p$  ratios exceeding some critical value is a necessary consequence of the forms of the equations involved. As  $R_s/R_p$  becomes large, the electrochemical process contributes a negligible amount to the total current and the shape of the polarization curve approaches a straight line. When  $b_a$  and  $b_c$  are large relative to  $\Delta E$ , Eq 26 is very well approximated by a linear equation. Thus, for large  $R_s/R_p$ , the fitting algorithm is able to generate excellent fits by setting  $b_a$  and  $b_c$  to large values and setting  $I_c^*(app)$  to whatever value is needed to match the slope of the polarization curve.

#### IR Drop Errors For Full Polarization

Figure 9 shows the anodic portion of the computed total overpotential versus log reduced current curves computed from Eqs 26 and 27 for a range of  $R_s/R_p$  ratios for the case  $b_a = 60$  mV,  $b_c = 120$  mV. On the figure is marked the point on the undistorted curve ( $R_s/R_p = 0$ ) where this curve becomes truly linear. Also shown is the extrapolation of this linear portion back to the reduced corrosion current. Identifying a linear region on a polarization curve and computing the slope is probably the most common method of obtaining Tafel constants. Although there is no universal agreement on the current range over which the curve should be linear if it is to qualify as a true Tafel region, generally a range of at least a half a decade of current is used.

As  $R_s/R_p$  increases, the computed curves in Fig. 9 break away from the undistorted curve at lower values of the reduced current. For  $R_s/R_p$  ratios greater than 0.02, the break point occurs at currents below the current at which the undistorted curve becomes linear. Even for  $R_s/R_p = 0.01$ , the range of the polarization curve which can be considered linear falls

between reduced current values of 5 and 15—a range of less than half a decade. On most of the curves shown in Fig. 9, one could select a region that is mostly linear. These regions have slopes higher than the true Tafel slope and would extrapolate back to zero overpotential at currents higher than the true corrosion current. The trend in the errors in Tafel slope and corrosion current as  $R_s/R_p$  increase is the same as described above for the extended linear polarization experiment.

Uncompensated IR drop in a polarization experiment will cause the effective scan rate (change in true overpotential per unit time)  $S(\text{eff})$ , to be less than the applied scan rate (change in total overpotential per unit time),  $S(\text{appl})$ . This problem, including the effect of varying  $R_s$ , has been examined by Mansfeld [96]. It is assumed here that  $R_s$  is constant. Referring to Fig. 3, it can be seen that  $R_s$  and  $R_p$  form a voltage divider, and so at zero overpotential

$$S(\text{eff}) = S(\text{appl}) / (1 + R_s/R_p) \text{ at } \Delta E = 0 \tag{30}$$

As the true overpotential becomes larger, the differential interfacial resistance is no longer  $R_p$  (Eq 9), but  $R_m$  (Eq 8). At some arbitrary overpotential,  $\Delta E^*$ , the effective scan rate is

$$S(\text{eff}) = S(\text{appl}) / (1 + R_s/R_m) \text{ at } \Delta E = \Delta E^* \tag{31}$$

As long as the Tafel constants are finite,  $R_m$  will decrease with increasing overpotential as will  $S(\text{eff})$ .

To quantify the IR drop related errors, polarization curves were computed from Eqs 7 and 24 in the same manner as described for the extended range linear polarization experiment. A total overpotential range of 400 mV was used; only anodic curves were generated.

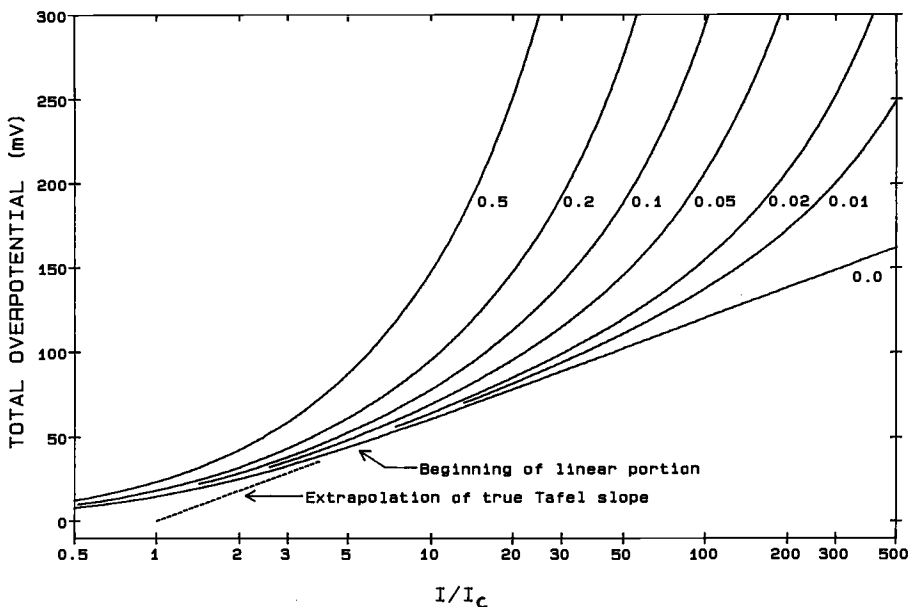


FIG. 9—Computed total overpotential versus reduced current polarization curves for  $b_a = 60 \text{ mV}$ ,  $b_c = 120 \text{ mV}$  as a function of  $R_s/R_p$  (curve label).

Three different measures of error were extracted from these curves:

1. The total overpotentials at which the IR drop is equal to 10, 20, 50, 100, and 200 mV.
2. The total overpotentials at which the IR drop is equal to 10, 20, 25, 50, 75, and 80 percent of the total overpotential.
3. The total overpotentials at which  $S(\text{eff})$  is equal to 75, 50, 25, and 10 percent of  $S(\text{appl})$ .

The measures of error for a  $b_a = 60$  mV,  $b_c = \text{infinity}$  case have been plotted in Figs. 10 through 12 for a range of  $R_s/R_p$  values. A LCS corrosion rate of 0.254 mm/y (10 mpy) and an area of 1 cm<sup>2</sup> were chosen to illustrate the magnitude of the quantities involved. As with all the previous analyses, the error parameters are functions only of  $b_a$ ,  $b_c$ , and  $R_s/R_p$ . Similar analyses done for  $b_a = 30, 60,$  and 120 mV with  $b_c = 120$  mV or infinity obtained generally similar results.

Figures 10 and 11 indicate that even at an  $R_s/R_p$  of 0.01, the range of overpotential that can be scanned before the polarization curve is significantly distorted is less than 150 mV. Note that the error parameters have an essentially linear dependence on the log of  $R_s/R_p$ ; therefore, an order of magnitude reduction in  $R_s/R_p$  using an IR compensation method gains only a modest increase in the range of overpotential where an undistorted polarization curve can be acquired. For  $b_a$  values in the range of 30 to 120 mV and for solution conductivities within the cooling water limits, anodic polarization curves with good quality IR compensation are limited at best to a few 100 mV of overpotential before distortion. This limits linear regions on polarization curves in most circumstances to two decades of current.

It can be seen from Fig. 12 that the effective scan rate drops quickly with increasing

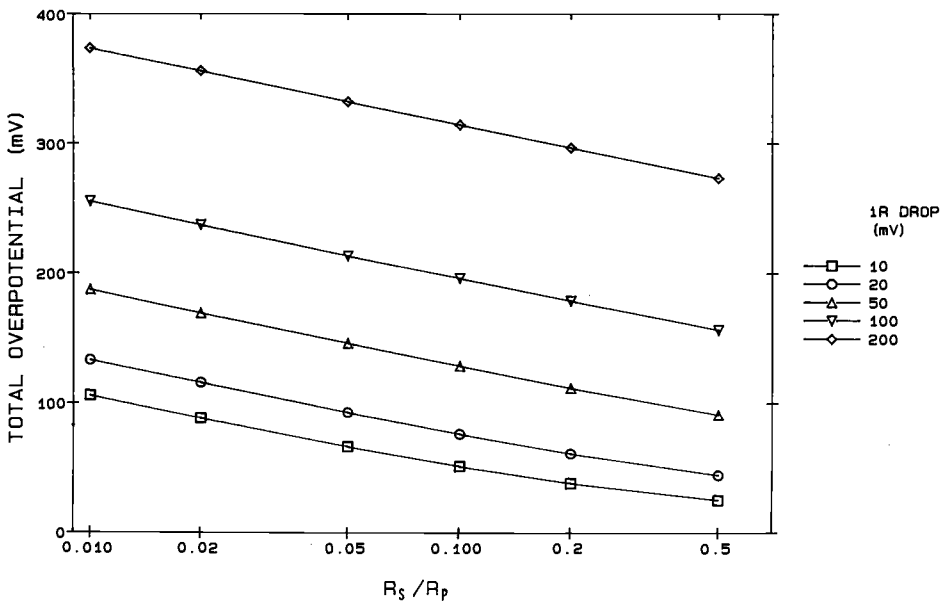


FIG. 10—Dependence of IR drop in a low carbon steel polarization scan on the total overpotential and  $R_s/R_p$ .

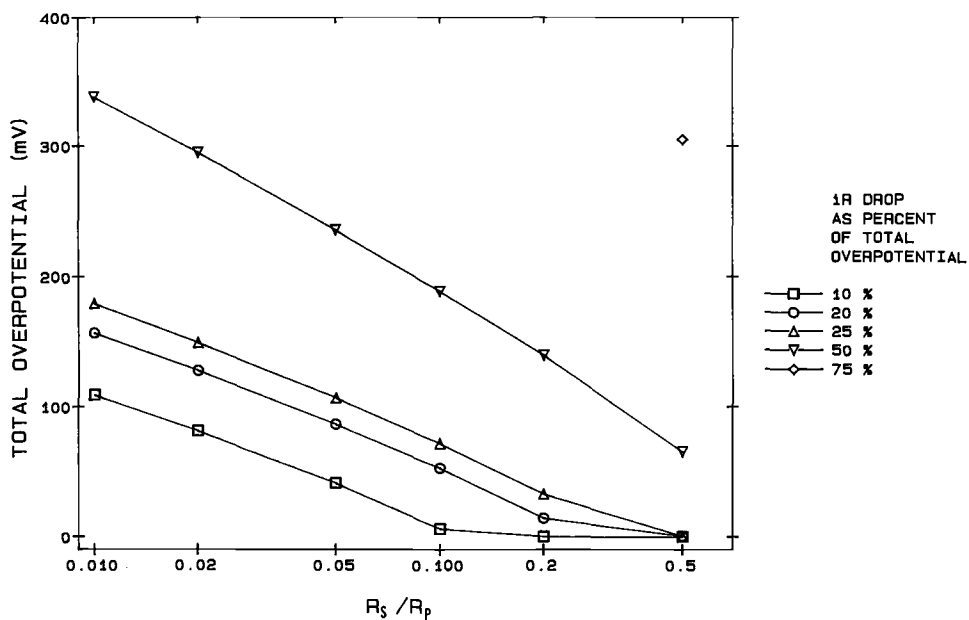


FIG. 11—Dependence of IR drop (expressed as a percent of the total overpotential) in a low carbon steel polarization scan on the total overpotential and  $R_s/R_p$ .

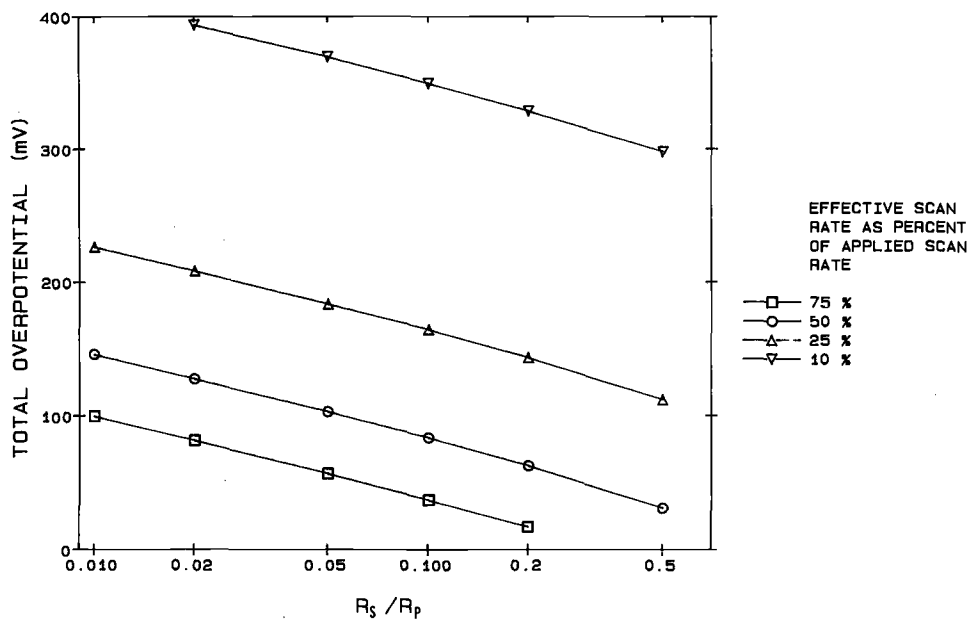


FIG. 12—Dependence of the effective scan rate (expressed as a percent of the applied scan rate) in a low carbon steel polarization scan on the total overpotential and  $R_s/R_p$ .

overpotential. For the same true overpotential range, a non-IR compensated polarization scan will take considerably longer than one obtained using a real time IR compensation technique.

The decrease in  $R_m$  (Eq 8) that occurs with increasing overpotential has an additional deleterious effect on experiments conducted in cells with non-uniform primary distributions. As the polarization scan proceeds to higher overpotentials, the electrochemical reaction rate increases rapidly ( $R_m$  decreases) and the overall current distribution on the working electrode becomes increasing nonuniform, eventually approaching the primary distribution. Potential control errors will arise that cannot be corrected for even with IR compensation.

West and Newman [76] have analyzed the errors in the exchange current density and the Tafel slope that result from analysis of polarization data taken on an electrode with a nonuniform current distribution in the potential region where Tafel kinetics are valid. The disk electrode with current interruption IR compensation was used as the model system. The disk edge, at the disk center, and at infinity reference electrode positions were considered. A dimensionless average current density was shown to be the important parameter governing the current density distribution. Plots of IR compensated overpotential versus log current for this model system are generally non-linear. Thus, a situation similar to the uniform current distribution, non-IR compensated experiment results; no unique Tafel slope can be extracted from the data. West and Newman concluded that the optimum reference electrode position for this system is at infinity, but that a uniform primary current distribution electrode geometry must be used if accurate kinetic parameters are to be obtained.

#### *Compensation Accuracy and Electrode Area*

The importance of  $R_s/R_p$  in determining the magnitude of errors in the above experiments has been demonstrated. Errors are small when  $R_s/R_p$  is less than 0.01. An IR compensation technique can reduce the effective value of  $R_s/R_p$  of a cell, but there are practical limits to this reduction.

Consider the Max  $R_s/R_p$  from Table 2 of 3.0, corresponding to a value of  $R_sA$  of 2500  $\Omega$  cm<sup>2</sup> and an  $R_pA$  value of 826.4  $\Omega$  cm<sup>2</sup>. In order for the effective  $R_s/R_p$  to be 0.01, the compensation technique must reduce  $R_sA$  to 8.26  $\Omega$  cm<sup>2</sup>, and thus must be able to measure  $R_sA$  with a 0.3% accuracy. This is usually possible if the electrode area is small, for example, 1 cm<sup>2</sup>, but becomes difficult if the electrode area is 10 cm<sup>2</sup> or more. In this case, the compensation system must be accurate to better than 1  $\Omega$ ; this accuracy can be difficult to achieve in some of the electrical environments in which corrosion tests are conducted.

#### **Conclusions**

All of the experiments commonly used to study LCS corrosion in natural waters can be effected by IR drop related problems. The criteria set forth in this paper can be used to decide if these problems are of significance in a given experiment. The presence of non-uniform current distribution on the working electrode can seriously limit the ability of IR drop compensation techniques to reduce IR drop induced errors. Such errors can only be minimized by using a properly designed cell.

#### *Acknowledgments*

The author gratefully acknowledges Betz Laboratories, Inc. for permission to prepare and to publish this paper.

## References

- [1] Britz, D., "iR Elimination in Electrochemical Cells," *Journal of Electroanalytical Chemistry*, vol. 88, 1978, pp. 309–352.
- [2] Hayes, M., Kuhn, A. T., and Patefield, W., "Techniques for the Determination of Ohmic Drop in Half-Cells and Fuel Cells: A Review," *Journal of Power Sources*, vol. 2, 1977/78, pp. 121–136.
- [3] Vetter, K. J., *Electrochemical Kinetics*, Academic Press, 1967, pp. 385–395.
- [4] Barnartt, S., "Magnitude of IR-Drop Corrections in Electrode Polarization Measurements Made with a Luggin-Haber Capillary," *Journal of the Electrochemical Society*, vol. 108, 1961, pp. 102–104.
- [5] Barnartt, S., "The Oxygen-Evolution Reaction at Gold Anodes I. Accuracy of Overpotential Measurements," *Journal of the Electrochemical Society*, vol. 106, No. 8, 1959, pp. 722–729.
- [6] Kuhn, A. T., and Stevenson, M., "Over-Potential Measurement at Gas-Evolving Electrodes," *Electrochimica Acta*, vol. 27, No. 3, 1982, pp. 329–337.
- [7] Sundheim, B. R., "Two Remarks on the Resistive Contribution to Overpotential," *Journal of the Electrochemical Society*, vol. 115, No. 2, 1968, pp. 158–160.
- [8] Tokuda, K., Gueshi, T., Aoki, K., and Matsuda, M., "Finite-Element Method Approach to the Problem of the IR-Potential Drop and Overpotential Measurements by Means of a Luggin-Haber Capillary," *Journal of the Electrochemical Society*, vol. 132, No. 10, 1985, pp. 2390–2398.
- [9] Landau, U., Weinberg, N. L., and Gileadi, E., "Three-Electrode Measurements in Industrial Cells," *Journal of the Electrochemical Society*, vol. 135, No. 2, 1988, pp. 396–403.
- [10] Mumby, J. E., and Perone, S. P., "Potentiostat and Cell Design for the Study of Rapid Electrochemical Systems," *Chemical Instrumentation*, vol. 3, No. 2, 1971, pp. 191–227.
- [11] Meyer, J.-J., Poupard, D., and Dubois, J.-E., "Potentiostat with a Positive Feedback iR Compensation and a High Sensitivity Current Follower Indicator Circuit for Direct Determination of High Second-Order Rate Constants," *Analytical Chemistry*, vol. 54, 1982, pp. 207–212.
- [12] Harrar, J. E., and Pomernacki, C. L., "Linear and Nonlinear System Characteristics of Controlled-Potential Electrolysis Cells," *Analytical Chemistry*, vol. 45, No. 1, 1973, pp. 57–79.
- [13] Cahan, B. D., Nagy, Z., and Genshaw, M. A., "Cell Design for Potentiostatic Measuring System," *Journal of the Electrochemical Society*, vol. 119, No. 1, 1972, pp. 64–69.
- [14] Gohr, G., Mirink, M., and Shiller, C. A., "Distortions of High Frequency Electrode Impedance. Their Causes and How to Avoid Them," *Journal of Electroanalytical Chemistry*, vol. 180, 1984, pp. 273–285.
- [15] McIntyre, J. D. E., and Peck, W. F., "An Interrupter Technique for Measuring the Uncompensated Resistance of Electrode Reactions under Potentiostatic Control," *Journal of the Electrochemical Society*, vol. 117, No. 6, 1970, pp. 747–751.
- [16] Robinson, R. S., McCurdy, C. W., and McCreery, R. L., "Microsecond Spectroelectrochemistry by External Reflection from Cylindrical Electrodes," *Analytical Chemistry*, vol. 54, No. 13, 1982, pp. 2356–2361.
- [17] Herrmann, C. C., Perrault, G. G., and Pilla, A. A., "Dual Reference Electrode for Electrochemical Pulse Studies," *Analytical Chemistry*, vol. 40, No. 3, 1968, pp. 1173–1174.
- [18] Moran, P. J., "Auxiliary Electrode Method for Determination of Ohmic Resistance," *Corrosion*, vol. 42, No. 7, 1986, pp. 432–434.
- [19] Mansfeld, F., Lin, S., Chen, Y. C., and Shih, H., "Minimization of High-Frequency Phase Shifts in Impedance Measurements," *Journal of the Electrochemical Society*, vol. 135, No. 4, 1988, pp. 906–907.
- [20] Marsh, G. A., "The Measurement of Instantaneous Corrosion Rates," Second International Congress on Metallic Corrosion, New York, NY, National Association of Corrosion Engineers, 1963, pp. 936–941.
- [21] Townsend, C. R., "Comparison of the 2- and 3-Electrode Polarization Resistance Methods of Corrosion Measurement," *Corrosion/74*, National Association of Corrosion Engineers, paper no. 64, 1974.
- [22] Dean, S. W., "Overview of Corrosion Monitoring in Modern Industrial Plants," *Corrosion Monitoring in Industrial Plants Using Nondestructive Testing and Electrochemical Methods*, ASTM STP 908, G. C. Moran and P. Labine, Eds., American Society for Testing and Materials, Philadelphia, 1986, pp. 197–220.
- [23] Rhoades, R. V., "Applying Microcomputer Technology to Two-Frequency Polarization Resistance Measurements," *Computers in Corrosion Control, Proceedings*, Corrosion/86 Symposium, NACE, 1986, pp. 129–138.
- [24] Model 9030 Corrat Corrosion Rate Monitor, User's Manual, Rohrback Cosasco Systems, Santa Fe Springs, CA, 1987.

- [25] Annand, R. R., and Eaton, P. E., "Modern Developments in Polarization Techniques for Corrosion Rate Measurement," *Corrosion/73*, Conference, National Association of Corrosion Engineers, paper no. 4, 1973.
- [26] Wagner, C., "Theoretical Analysis of the Current Density Distribution in Electrolytic Cells," *Journal of the Electrochemical Society*, vol. 98, No. 3, 1951, pp. 116-128.
- [27] Newman, J. S., *Electrochemical Systems*, Prentice-Hall, 1973, chapter 18 (Applications of Potential Theory), pp. 340-352.
- [28] Parrish, W. R., and Newman, J., "Current Distributions on Plane, Parallel Electrodes in Channel Flow," *Journal of the Electrochemical Society*, vol. 117, No. 1, 1970, pp. 43-48.
- [29] Shih, H., and Pickering, H. W., "Three-Dimensional Modeling of the Potential and Current Distributions in an Electrolytic Cell," *Journal of the Electrochemical Society*, vol. 134, No. 3, 1987, pp. 551-558.
- [30] Smyrl, W. H., and Newman, J., "Current Distribution at Electrode Edges at High Current Densities," *Journal of the Electrochemical Society*, vol. 136, No. 1, 1989, pp. 132-139.
- [31] Diem, C. B., Newman, B., and Orazem, M. E., "The Influence of Small Machining Errors on the Primary Current Distribution at a Recessed Electrode," *Journal of the Electrochemical Society*, vol. 135, No. 10, 1988, pp. 2524-2530.
- [32] Newman, J., and Harrar, J. E., "Potential Distribution in Axisymmetric Mercury-Pool Electrolysis Cells at the Limiting Current," *Journal of the Electrochemical Society*, vol. 120, No. 8, 1973, pp. 1041-1044.
- [33] Goldberg, I. B., Bard, A. J., and Feldberg, S. W., "Resistive Effects in Thin Electrochemical Cells: Digital Simulation of Electrochemistry in Electron Spin Resonance Cells," *Journal of Physical Chemistry*, vol. 76, No. 18, 1972, pp. 2550-2559.
- [34] Mears, D. C., and Rothwell, G. P., "Effects of Probe Position on Potentiostatic Control during the Breakdown of Passivity," *Journal of the Electrochemical Society*, vol. 115, No. 1, 1968, pp. 36-38.
- [35] Harrar, J. E., and Shain, I., "Electrode Potential Gradients and Cell Design in Controlled Potential Electrolysis Experiments," *Analytical Chemistry*, vol. 38, No. 9, 1966, pp. 1148-1158.
- [36] Nisancioglu, K., "The Error in Polarization Resistance and Capacitance Measurements Resulting from Nonuniform Ohmic Potential Drop to Flush-Mounted Probes," *Corrosion*, vol. 43, No. 5, 1987, pp. 258-265.
- [37] Fiaud, C., Keddou, M., Kadri, A., and Takenouti, H., "Electrochemical Impedance in a Thin Surface Electrolyte Layer. Influence of the Potential Probe Location," *Electrochimica Acta*, vol. 32, No. 3, 1987, pp. 445-448.
- [38] Rizzi, R., and Ronchetti, C., "On-Line Monitoring of the True Corrosion Rate in Problems Related to Power Plants," *Corrosion Monitoring in Industrial Plants Using Nondestructive Testing and Electrochemical Methods, ASTM STP 908*, G. C. Moran and P. Labine, eds., American Society for Testing and Materials, Philadelphia, 1986, pp. 314-338.
- [39] Athayde, M. G., Mattos, O. R., and Sathler, L., "The Anodic Behaviour of Iron in Ethanol-Water Solutions in the Presence and Absence of  $\text{NaClO}_4$  as the Supporting Electrolyte," *Electrochimica Acta*, vol. 22, No. 6, 1987, pp. 909-913.
- [40] Dimpault-Darcy, E. C., and White, R. E., "Secondary Current Distributions Using TOPAZ2D and Linear Kinetics," *Journal of the Electrochemical Society*, vol. 135, No. 3, 1988, p. 656-658.
- [41] Smyrl, W. H., "Current and Potential Distributions in Corrosion Systems," *American Institute of Chemical Engineering Symposium Series*, vol. 77, No. 204, 1981, pp. 152-160.
- [42] Matlosz, M., Creton, C., Clerc, C., and Landolt, D., "Secondary Current Distributions in a Hull Cell," *Journal of the Electrochemical Society*, vol. 134, No. 12, 1987, pp. 3015-3021.
- [43] Menon, M. M., and Landau, U., "Modeling of Electrochemical Cells Including Diffusion, Migration, and Unsteady-State Effects," *Journal of the Electrochemical Society*, vol. 134, No. 9, 1987, pp. 2248-2253.
- [44] Dukovic, J. O., "Studies on Current Distribution in Electrochemical Cells," Ph.D. thesis, Lawrence Berkeley Laboratory, University of California, Berkeley, CA., LBL-22084, August, 1986.
- [45] Newman, J., "Resistance for Flow of Current to a Disk," *Journal of the Electrochemical Society*, vol. 113, 1966, pp. 501-502.
- [46] Hubbe, M. A., "Polarization Resistance Corrosivity Test with a Correction for Resistivity," *British Corrosion Journal*, vol. 15, No. 4, 1980, pp. 193-197.
- [47] Mansfeld, F., "The Effect of Uncompensated IR-Drop on Polarization Resistance Measurements," *Corrosion*, vol. 32, No. 4, 1976, pp. 143-146.
- [48] Walter, G. W., "The Effect of IR-Drop on Corrosion Rates Calculated from Low Polarization Data," *Corrosion Science*, vol. 18, 1978, pp. 927-945.

- [49] Mansfeld, F., Kendig, M. W., and Tsai, S., "Corrosion Kinetics in Low Conductivity Media. I. Iron in Natural Waters," *Corrosion Science*, vol. 22, No. 5, 1982, pp. 455–471.
- [50] Kajimoto, Z. P., Wolyneć, S., and Chagas, H. C., "IR Drop Compensation for Corrosion Rate Determination of Carbon Steel in Acid Solutions," *Corrosion Science*, vol. 25, No. 1, 1985, pp. 35–41.
- [51] Wruck, W. J., Machado, R. M., and Chapman, T. W., "Current Interruption—Instrumentation and Applications," *Journal of the Electrochemical Society*, vol. 134, No. 3, 1987, pp. 539–546.
- [52] Glass, G. K., "The Effect of a Change in Surface Conditions Produced by Anodic and Cathodic Reactions on the Passivation of Mild Steel," *Corrosion Science*, vol. 26, No. 6, 1986, pp. 441–454.
- [53] Leistra, J. A., and Sides, P. J., "Voltage Components at Gas Evolving Electrodes," *Journal of the Electrochemical Society*, vol. 134, No. 10, 1987, pp. 2442–2446.
- [54] Mansfeld, F., "The Polarization Resistance Technique for Measuring Corrosion Currents," *Advances in Corrosion Science and Technology*, vol. 6, M. G. Fontana, R. W. Staehle, Eds., Plenum, 1976, pp. 163–262.
- [55] Smyrl, W. H., "Electrochemistry and Corrosion on Homogeneous and Heterogeneous Metal Surfaces," *Comprehensive Treatise of Electrochemistry*, J. O'M. Bockris, B. E. Conway, E. Yeager, R. E. White, Eds., vol. 4, 1981, pp. 97–149.
- [56] Nagy, Z., and Thomas, D. A., "Effect of Mass Transport on the Determination of Corrosion Rates from Polarization Measurements," *Journal of the Electrochemical Society*, vol. 133, No. 10, 1986, pp. 2013–2017.
- [57] Britz, D., and Hougaard, P., "Effects of Mixed Activation and Control of the Cathodic Process on Corrosion Current Measurements," *Corrosion Science*, vol. 23, No. 9, 1983, pp. 987–994.
- [58] Hougaard, P., and Britz, D. H., "Corrosion Rate Measurements and Calculations: Calculation of Error Limits and Transport Effects," *Corrosion Science*, vol. 23, No. 3, 1983, pp. 271–283.
- [59] Kiss, L., *Kinetics of Electrochemical Metal Dissolution* (Studies in Physical and Theoretical Chemistry 47), Elsevier, 1988.
- [60] Nagy, Z., and Schultz, P. F., "Effect of Double Layer Structure on the Determination of Corrosion Rates from Polarization Measurements," *Journal of the Electrochemical Society*, vol. 135, No. 11, 1988, p. 2700.
- [61] Lorenz, W. J., and Heusler, K. E., "Anodic Dissolution of Iron Group Metals," *Corrosion Mechanisms*, F. Mansfeld, Ed., Marcel Dekker, 1987, pp. 1–83.
- [62] Ibl, N., "Current Distribution," *Comprehensive Treatise of Electrochemistry*, vol. 6 (Electrodics: Transport), E. Yeager, J. O'M. Bockris, B. E. Conway, S. Sarangapani, Eds., Plenum Press, 1983, pp. 239–315.
- [63] Hine, F., *Electrode Processes and Electrochemical Engineering*, Plenum Press, 1985, chapter 13 (Current Distribution and Potential Distribution), pp. 313–338.
- [64] Newman, J., "Current Distribution to a Rotating Disk Below the Limiting Current," *Journal of the Electrochemical Society*, vol. 113, No. 12, 1966, p. 1235–1241.
- [65] Newman, J., "Ohmic Potential Drop Measured by Interrupter Techniques," *Journal of the Electrochemical Society*, vol. 117, 1970, pp. 507–508.
- [66] Newman, J., "Frequency Dispersion in Capacity Measurements at a Disk Electrode," *Journal of the Electrochemical Society*, vol. 117, No. 2, 1970, pp. 198–203.
- [67] Nanis, L., and Kesselman, W., "Applications of Current and Potential Distributions in Disk Electrode Systems," *Journal of the Electrochemical Society*, vol. 118, No. 3, 1971, pp. 454–461.
- [68] Newman, J., "Discussion," *Journal of the Electrochemical Society*, vol. 118, No. 12, 1971, pp. 1966–1967.
- [69] Nanis, L., and Kesselman, W., "Discussion," *Journal of the Electrochemical Society*, vol. 118, No. 12, 1971, pp. 1967–1968.
- [70] Tiedemann, W. H., Newman, J., and Bennion, D. N., "The Error in Measurements of Electrode Kinetics Caused by Nonuniform Ohmic-Potential Drop to a Disk Electrode," *Journal of the Electrochemical Society*, vol. 120, No. 2, 1973, pp. 256–258.
- [71] Pierini, P., and Newman, J., "Potential Distribution for Disk Electrodes in Axisymmetric Cylindrical Cells," *Journal of the Electrochemical Society*, vol. 126, No. 8, 1979, pp. 1348–1352.
- [72] Miller, B., and Bellavance, M. I., "Measurement of Current and Potential Distribution at Rotating-Disk Electrodes," *Journal of the Electrochemical Society*, vol. 120, No. 2, 1973, pp. 42–53.
- [73] Wan, H. H., and Cheh, H. Y., "The Current Distribution on a Rotating Disk Electrode in Galvanostatic Pulsed Electrolysis," *Journal of the Electrochemical Society*, Vol. 135, No. 3, 1988, pp. 643–650.
- [74] Wan, H. H., and Cheh, H. Y., "The Current Distribution on a Rotating Disk Electrode in Poten-

- tiostatic Pulsed Electrolysis," *Journal of the Electrochemical Society*, vol. 135, No. 3, 1988, pp. 658-660.
- [75] Law, C. G., and Newman, J., "Corrosion of a Rotating Iron Disk in Laminar, Transition, and Fully Developed Turbulent Flow," *Journal of the Electrochemical Society*, vol. 133, No. 1, 1986, pp. 37-42.
- [76] West, A. C., and Newman, J., "Corrections to Kinetic Measurements Taken on a Disk Electrode," *Journal of the Electrochemical Society*, vol. 136, No. 1, 1989, pp. 139-143.
- [77] Hinman, A. S., Pons, S., and Cassidy, J., "Voltammetry and Coulometry with Immersed Thin Layer Electrodes—I. Model for Effects of Solution Resistivity in Linear Sweep Voltammetry," *Electrochimica Acta*, vol. 130, No. 1, 1985, pp. 89-94.
- [78] Fedkiw, P. S., Weidner, J. W., and Kang, M. P., "Ohmic Distortion of Reversible Voltammograms in Thin-Layer Cells," *Electrochimica Acta*, vol. 33, No. 3, 1988, pp. 421-424.
- [79] Prazak, M., "The Polarization Resistance Method for Corrosion Testing," *Werkstoffe und Korrosion*, vol. 25, No. 2, 1974, pp. 104-112.
- [80] Hausler, R. H., "On the Use of Linear Polarization Measurements for the Evaluation of Corrosion Inhibitors in Concentrated HCl at 200 F (93 C)," *Corrosion*, vol. 42, No. 12, 1986, pp. 729-739.
- [81] Yeske, R. A., "Electrochemical Techniques for Monitoring Corrosion Rates in Simulated Kraft White Liquors," *Corrosion Monitoring in Industrial Plants Using Nondestructive Testing and Electrochemical Methods*, ASTM STP 908, G. C. Moran and P. Labine, Eds., American Society for Testing and Materials, Philadelphia, 1986, pp. 266-288.
- [82] Medina, E., Pizarro, R., Salas, G., Rauchle, F., and Gonzalez, J. A., "Some Errors in the Estimation of Corrosion Rates in High Conductivity Media Due to Neglect of the Ohmic Drop Compensation" (in Spanish), vol. 22, No. 6, *Revista del Metal Madrid*, 1986, pp. 352-358.
- [83] Scully, J. R., and Bundy, K. J., "Electrochemical Methods for Measurement of Steel Pipe Corrosion Rates in Soil," *Materials Performance*, vol. 24, No. 4, 1985, pp. 18-25.
- [84] Kasahara, K., and Kajiyama, F., "Determination of Underground Corrosion Rates from Polarization Resistance Measurements," *Corrosion*, vol. 39, No. 12, 1983, pp. 475-480.
- [85] Scully, J. R., Moran, P. J., and Gileadi, E., "Electrochemical Measurements of Corrosion Rates in Media of Low Conductivity," *Journal of the Electrochemical Society*, vol. 133, No. 3, 1986, pp. 579-581.
- [86] Mansfeld, F., and Tsai, S., "Corrosion Kinetics in Low Conductivity Media. II. Iron and Nickel in Ethanolic HCl," *Corrosion Science*, vol. 27, No. 8, 1987, pp. 873-877.
- [87] Williams, L. F. G., and Taylor, R. J., "iR Correction. Part II. Effect on Corrosion Monitoring," *Journal of Electroanalytical Chemistry*, vol. 108, 1980, pp. 305-316.
- [88] Massiani, Y., Crousier, J.-P., Crousier, J., Galea, J., and Romanetti, G., "Determination of Polarization Curve Parameters with the Aid of a Nonlinear Regression Program. Application to the Corrosion of a Metal in Acid Solution in the Presence of Dissolved Oxygen" (in French), *Electrochimica Acta*, vol. 29, No. 12, 1984, pp. 1679-1683.
- [89] Reingeverts, M. D., and Semenyuk, E. Ya., "Computer Processing of Polarization Curves in Order to Determine Corrosion Rates," *Protection of Metals*, vol. 18, No. 5, 1982, pp. 647-649.
- [90] Mansfeld, F., and Kendig, M., "Calculation of Corrosion Rates from Polarization Data with a Microcomputer," *Materials Performance*, vol. 22, No. 12, 1983, pp. 40-42.
- [91] Gerchakov, S. M., Udey, L. R., and Mansfeld, F., "An Improved Method for the Analysis of Polarization Resistance Data," *Corrosion*, vol. 37, No. 12, 1981, pp. 696-700.
- [92] Lindemuth, J. R., Rodgers, R., and Fosdick, L., "The Evaluation of Electrochemical Corrosion Data by Non-Linear Chi-Squared Minimization," in Proc. Symposium on Computer Aided Acquisition and Analysis of Corrosion Data, M. W. Kendig, U. Bertocci, and J. E. Strutt, Eds., *Electrochemical Society Proceedings*, vol. 85-3, 1985, pp. 23-31.
- [93] Damborenea, J. J., Ruiz, J., and Vazquez, A. J., "Calculation of Corrosion Rates in Inhibited Acid Electrolytes by Computer," *Proceedings*, 6th European Symposium on Corrosion Inhibitors (6SEIC), Ann. Univ. Ferrara, N. S., Sez. V, Suppl. No. 8, 1985, pp. 859-871.
- [94] Skinner, W., "Influence of Experimental Inaccuracies on Corrosion Rates and Tafel Slopes Determined from Electrochemical Measurements in Different Overpotential Ranges," *British Corrosion Journal*, vol. 22, No. 3, 1987, pp. 172-175.
- [95] Dnyashev, V. S., and Dnyasheva, V. L., "Determination of the Parameters of the Polarization-Curve Equation by the Method of Least Squares," *Protection of Metals*, vol. 22, No. 4, 1987, pp. 523-526.
- [96] Mansfeld, F., "The Effect of Uncompensated Resistance on the True Scan Rate in Potentiodynamic Experiments," *Corrosion*, vol. 38, No. 10, 1982, pp. 556-559.

# **Critical Comparisons of Methods**

## Theoretical Problems Related to Ohmic Resistance Compensation

---

**REFERENCE:** Nisancioglu, K., "Theoretical Problems Related to Ohmic Resistance Compensation," *The Measurement and Correction of Electrolyte Resistance in Electrochemical Tests, ASTM STP 1056*, L. L. Scribner and S. R. Taylor, Eds., American Society for Testing and Materials, Philadelphia, 1990, pp. 61–77.

**ABSTRACT:** Current interruption, potential pulse methods, and the AC impedance technique are well accepted means of measuring the ohmic potential drop to an electrode for ohmic resistance compensation. An interpretation of the measured quantities is given, and the relationship between the measured and true parameters is established. Theoretical calculations indicate that a significant discrepancy may exist between the measured and the true corrosion rate, although the data are corrected for the ohmic resistance in the solution by conventional means. The cause of the error is a nonuniform ohmic potential drop to the electrode surface, and its magnitude is determined by geometry, position of the reference electrode, solution conductivity, and corrosion rate. Such errors in practice are specific to low-conductivity media and occluded cells with gaps or crevices. The magnitude of expected error is calculated for a few typical geometries. Possible ways of correcting the error are discussed. These include probe design, measurement technique, and methods of data analysis.

**KEY WORDS:** current distribution, nonuniform ohmic drop, polarization resistance, disk electrode, crevice corrosion, current interruption, AC impedance, corrosion monitoring, probe design

### Nomenclature

$b_a, b_c$	Tafel slope, V
$E$	Electrode potential, V
$E_{\text{corr}}$	Corrosion potential, V
$E_{\text{eff}}$	Measured E, V
$h$	Crevice height, cm
$i$	Current density, A cm <sup>-2</sup>
$i_{\text{ave}}$	Average current density, A cm <sup>-2</sup>
$i_{\text{corr}}$	Corrosion current density, A cm <sup>-2</sup>
$i_x$	Current density in the x-direction, A cm <sup>-2</sup>
$I$	Current, A
$J$	Dimensionless corrosion rate, Eq 20
$L_c$	Length of crevice, cm
$L_m$	Length of metal, cm
$r_o$	Disk radius, cm

<sup>1</sup> Professor, department of chemistry, Laboratories of Industrial Electrochemistry, Norwegian Institute of Technology, N-7034 Trondheim, Norway.

$R_{\text{eff}}$	Measured polarization resistance, $\Omega \text{ cm}^2$
$R_{\Omega}$	Ohmic resistance in the solution, $\Omega \text{ cm}^2$
$R_p$	True polarization resistance, $\Omega \text{ cm}^2$
$x$	Coordinate along the length of the crevice, cm
$V$	Potential of the metal, V
$\Delta\phi_{\Omega}$	Measured ohmic potential drop in the solution, V
$\varepsilon_1, \varepsilon_2$	Equations 10 and 11
$\kappa$	Solution conductivity, $\Omega^{-1} \text{ cm}^{-1}$
$\eta$	$E - E_{\text{corr}}$ , V
$\eta_{\text{eff}}$	Measured $\eta$ , V
$\xi$	$x/L_m$
$\varphi$	Potential defined in Eq 18, V
$\phi$	Potential in the solution, V
$\phi^p$	Potential in the solution adjacent to the metal surface, V

## Introduction

The ohmic potential drop in the solution may be an important factor to consider in the electrochemical measurement of corrosion rates in low conductivity environments, in occluded corrosion cells, and in the presence of high rates of corrosion. Although the ohmic resistance is properly taken into account by a well-accepted, experimental technique, a significant discrepancy may still remain uncompensated for in the calculated rates. The error is a result of a nonuniform ohmic potential drop to the electrode surface, and it cannot be corrected by conventional experimental means. The problem has caused difficulties in the determination of kinetic parameters in electroanalytical chemistry and is well documented in the electrochemical literature [1-3]. Its possible significance in electrochemical corrosion monitoring has been recently discussed [4].

The present paper reviews the theoretical factors that cause this type of error, with numerical examples for the disk electrode and a one-dimensional model for crevice corrosion. An experimental verification is given for crevice corrosion. Possible ways of reducing or eliminating the error are suggested.

## Interpretation of Experimentally Measured Parameters

In measuring corrosion rates, the parameter sought is usually the polarization resistance, which is inversely proportional to the corrosion rate. The polarization resistance is defined as

$$R_p = \frac{1}{(\partial i / \partial E)_{E = E_{\text{corr}}}} = \left( \frac{\partial E}{\partial i} \right)_{i=0} \quad (1)$$

where  $E$  is the electrode potential, and  $i$  is the net current density. The measurement of polarization resistance is based on the assumption that the current-potential relationship can be linearized around the corrosion potential, such that Eq 1 can be written in the simple form

$$R_p = \eta / i \text{ (linear kinetics)} \quad (2)$$

where

$$\eta = E - E_{\text{corr}} \tag{3}$$

Both  $\eta$  and  $i$  may be nonuniform, that is, position dependent, at the electrode surface. However, the quantities  $\eta$  and  $i$  in Eq 2 correspond to the same location on the metal surface. Independent of position on the metal surface, therefore, the ratio  $\eta/i$  is a constant and a property of the corroding metal-environment system.

Since the measurement of the local values of  $\eta$  and  $i$  is not straightforward, the measured polarization resistance  $R_{\text{eff}}$  is based on an effective  $\eta$ , dependent on the location of the reference electrode, and the average current density

$$R_{\text{eff}} = \eta_{\text{eff}}/i_{\text{ave}} \tag{4}$$

The relationship between  $R_p$  and  $R_{\text{eff}}$  can then be expressed by

$$\frac{R_p}{R_{\text{eff}}} = \left( \frac{\eta}{\eta_{\text{eff}}} \right) \left( \frac{i_{\text{ave}}}{i} \right) \tag{5}$$

Let us assume that  $\eta_{\text{eff}}$  is determined with respect to a reference electrode positioned at A in Fig. 1. The electric potentials in the solution at A and adjacent to the metal surface, respectively, are given by  $\phi_A$  and  $\phi_o$ . Both potentials depend on the position they are measured at in the solution. Thus, the potential measured by the reference electrode at A, before correction for the ohmic potential drop, is given by

$$E_{\text{eff}} = E + \phi_o - \phi_A \tag{6}$$

The experimental quantity  $\eta_{\text{eff}}$  is obtained by correcting  $E_{\text{eff}}$  for the experimentally measured ohmic potential drop

$$\eta_{\text{eff}} = E_{\text{eff}} - E_{\text{corr}} - \Delta\phi_\Omega \tag{7}$$

$\Delta\phi_\Omega$  is measured also with respect to the reference electrode at A.

Before proceeding further with the analysis, a few words are in order concerning the significance of the measured ohmic potential drop. Newman has shown rigorously that the ohmic potential drop measured by current interruption [5] and the ohmic resistance obtained from the high frequency limit of AC impedance data [6] correspond to the primary distribution. The latter exists under reversible conditions at the electrode (i.e., with no polarization). Therefore, the primary potential distribution in the solution adjacent to the metal surface  $\phi_o$  is uniform. Let us denote this quantity as  $\phi_o^p$  to distinguish it from  $\phi_o$ , which describes the local ohmic drop to a polarized surface (Eq 6). The ohmic potential drop as measured with respect to the reference electrode A (Fig. 1) is then given by

$$\Delta\phi_\Omega = \phi_o^p - \phi_A^p \tag{8}$$

where  $\phi_A^p$  is the potential at A corresponding to the primary distribution.

Combination of Eqs 3 and 5 through 8 gives

$$\frac{R_p}{R_{\text{eff}}} = \epsilon_1 \epsilon_2 \tag{9}$$

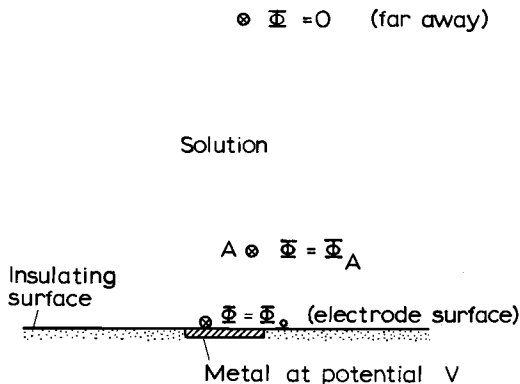


FIG. 1—Potentials measured by reference electrode (Luggin probes) positioned at various locations in the solution. The potentials are referred to a reference electrode positioned far away from the metal surface (point of zero potential). Crossed circles indicate reference electrode locations.

where

$$\epsilon_1 = \frac{1}{1 + \frac{\phi_o - \phi_o^p}{\eta} + \frac{\phi_A^p - \phi_A}{\eta}} \tag{10}$$

$$\epsilon_2 = i_{ave}/i \tag{11}$$

As indicated by Eq 9, the error in  $R_{eff}$  can be considered as a combination of two factors.  $\epsilon_1$  arises directly from the nonuniformity of ohmic drop to the metal surface, and  $\epsilon_2$  is due to the nonuniformity of current distribution at the surface. In principle, the two factors are related, since both result from ohmic effects; a high ohmic drop in the solution may also cause a nonuniform current distribution at the electrode surface. Both factors depend on the placement of the reference electrode. The same applies to  $R_{eff}$  if the reference electrode is placed close to the metal surface. The positional dependence of  $R_{eff}$  becomes less important as the reference electrode is moved away from the metal surface. If the reference electrode is placed adjacent to the metal surface, however, the value of  $\epsilon_1$  becomes unity, and the error in  $R_{eff}$  becomes directly proportional to the nonuniformity of current distribution at the metal surface.

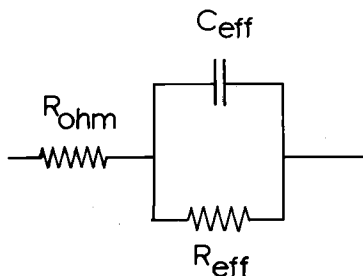


FIG. 2—Equivalent circuit representing the metal-solution interface in the experimental determination of ohmic potential drop, double-layer capacitance, and polarization resistance.

Independent of the measurement technique, the metal-solution interface is modeled in essence according to the simple equivalent circuit shown in Fig. 2. A possible way of obtaining the experimental parameters is by using pulse techniques equivalent to the linear polarization method. The response of the electrode to a current or a potential pulse is shown, respectively, in Figs. 3 and 4. As is well known, the step response in the potential to a step change in the applied current corresponds to the ohmic resistance in the solution [7]. This is followed by the capacitive charging of the electric double layer. The measured quantity  $\eta_{\text{eff}}$  is obtained from the difference  $E_{\text{eff}} - E_1$  after the charging process reaches a steady state as indicated in Fig. 3. If a potential pulse is applied, the ohmic resistance is obtained from the ratio of pulse amplitude to the peak current response (Fig. 4)

$$\frac{R_{\Omega}}{\text{Area}} = \frac{E_{\text{eff}} - E_{\text{corr}}}{I_1} \tag{12}$$

The polarization resistance is then obtained from

$$R_{\text{eff}} = \frac{E_{\text{eff}} - E_{\text{corr}}}{I/\text{Area}} - R_{\Omega} \tag{13}$$

where  $I$  is the steady-state current attained after charging the double layer.

Figure 5 schematically illustrates the complex plane impedance diagram (Nyquist plot) for the metal-solution interface. In the ideal case in which  $R_{\text{eff}} = R_p$  and  $C_{\text{eff}} = C$  (the true double-layer capacitance), the impedance plot will be represented by a semicircle. A non-uniform ohmic drop to the surface of the electrode will in many cases ( $R_p/R_{\text{eff}} < 1$ ) enlarge the frequency dispersion of the impedance resulting in larger diameter semicircles [4,6,8]. An opposite effect is expected for  $R_p/R_{\text{eff}} > 1$ . A slight distortion is also introduced such

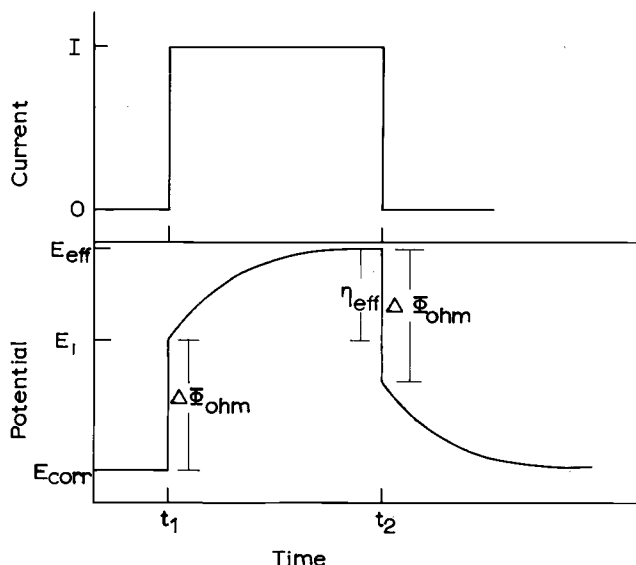


FIG. 3—Response of electrode potential to a square current pulse applied by an external source (schematic).

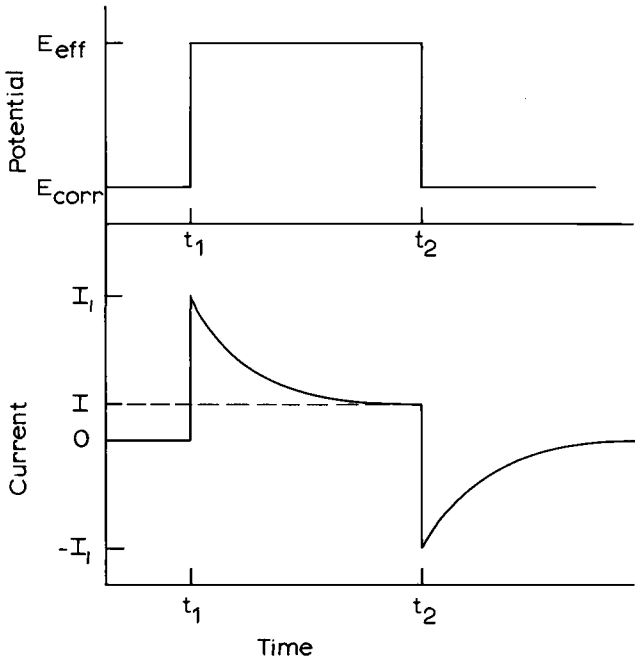


FIG. 4—Response of measured current to a square potential pulse applied by a potentiostat (schematic).

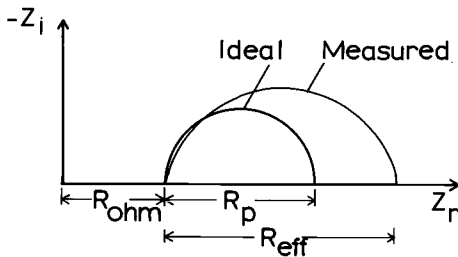


FIG. 5—Complex plane impedance plots for the ideal circuit in Fig. 2 and for a realistic electrochemical interface in the presence of nonlinear ohmic drop to the metal surface (schematic.)

that the experimental data cannot be fitted exactly to a semicircle. Nevertheless, the zero frequency limit of the curve, after compensating for the ohmic resistance, is related unambiguously to  $R_{eff}$  as long as inductive loops caused by adsorption effects do not complicate the data analysis.

The measured response of the working electrode to a DC or and AC signal may deviate from the foregoing description as a result of perturbations introduced by the external power source or by the reference electrode, especially at short periods during DC measurements and at high frequencies in AC measurements. A discussion of instrumental errors and their correction is outside the scope of this paper. These issues have been discussed in detail by other authors contributing to this symposium [9,10].

**Magnitude of Error in  $R_{eff}$**

*Narrow Crevice*

Localized corrosion and corrosion in restricted geometries such as in crevices and under thin films of electrolyte often exhibit a highly nonuniform current distribution. As a result,  $\epsilon_2$  is by far the dominating factor in determining the error associated with the measurement of polarization resistance. Although the experimental data are corrected for ohmic resistance, the error in  $R_{eff}$  can become significantly larger than the corresponding error for an electrode exposed to a bulk electrolyte, especially if the corrosive environment has a low conductivity.

We would like to estimate analytically the magnitude of this error for a narrow, two-dimensional crevice model depicted in Fig. 6. The metal in the crevice is embedded in an insulating plane of length  $L_c - L_m$ , which gives a certain degree of occlusion to the corroding metal. The treatment is applicable also to a metal exposed to a thin film of electrolyte (Fig. 7).

Since the electrolyte is restricted to a thin layer, the potential drop across the crevice height can be neglected relative to the potential gradient in the  $x$ -direction. As a consequence,  $\epsilon_1$  for this system is approximately unity because the potential differences  $\phi_A^p - \phi_o^p$  are very small relative to the magnitude of  $\eta$  in Eq 11. Thus, the size of error is determined strictly by the nonuniformity of current distribution in the crevice. Moreover, the thin layer approximation reduces the mathematical problem to a one-dimensional equation.

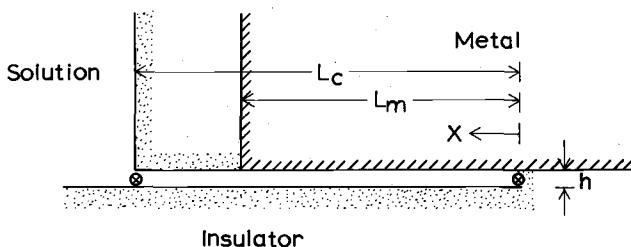


FIG. 6—Crevice model. Crossed circles indicate reference electrode locations.

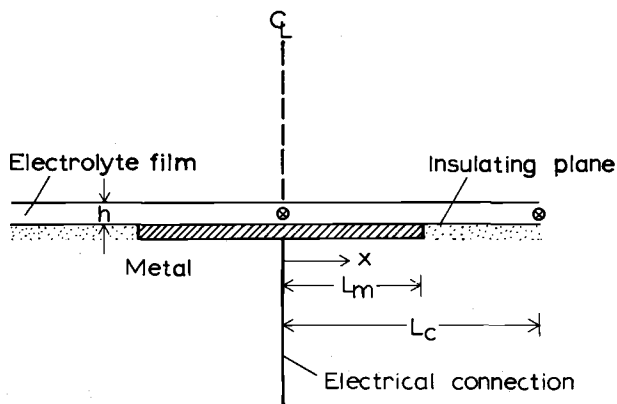


FIG. 7—Metal wetted by a thin layer of corrosive solution. Crossed circles indicate reference electrode locations.

Neglecting the effect of any concentration gradient that may exist in the solution, a current balance for the system gives

$$\int_0^x i \, dx = i_x h \quad (14)$$

where  $i$  is the current density on the metal surface, and  $i_x$  is the current density in the electrolyte. The latter obeys Ohm's law according to the equation

$$i_x = -\kappa \frac{d\phi}{dx} \quad (15)$$

Combining the two equations and differentiating, we obtain

$$i = -\kappa h \frac{d^2\phi}{dx^2} \quad (16)$$

For linearized kinetics, the current density on the metal is expressed by

$$\begin{aligned} i &= 2.3 i_{\text{corr}} \left( \frac{1}{b_a} + \frac{1}{|b_c|} \right) \varphi \\ &= \varphi / R_p \end{aligned} \quad (17)$$

where  $b$  is the Tafel slope. The potential  $\varphi$  is given by

$$\varphi = V - \phi - E_{\text{corr}} \quad (18)$$

where  $V$  is the potential of the metal. Equation 16 can be reduced to the form

$$\frac{d^2\varphi}{d\xi^2} = J\varphi \quad (19)$$

where

$$J = \frac{L_m^2}{\kappa h R_p} \quad (20)$$

and

$$\xi = x/L_m$$

The parameter  $J$  can be regarded as a dimensionless corrosion rate.

Equation 19 can readily be solved for the boundary conditions

$$\frac{d\varphi}{dx} = 0 \quad \text{at } x = 0 \quad (21)$$

$$\varphi = \varphi_m \quad \text{at } x = L_m \quad (22)$$

The potential and current distributions, then, are given by, respectively,

$$\frac{\varphi}{\varphi_m} = \frac{\cosh\left(\sqrt{J}\frac{x}{L_m}\right)}{\cosh\sqrt{J}} \tag{23}$$

$$\frac{i}{i_{ave}} = \frac{\sqrt{J}\cosh\left(\sqrt{J}\frac{x}{L_m}\right)}{\sinh\sqrt{J}} \tag{24}$$

Eq 24 is plotted in Fig. 8. The current distribution on the metal becomes increasingly non-uniform as  $J$  becomes large. As  $J$  increases, the current density and the potential in the solution attain their primary distributions. By taking the limit of Eq 24 as  $J \rightarrow \infty$ , we obtain the primary current distribution on the metal

$$i = \begin{cases} 0 & \text{for } x < L_m \\ \infty & \text{for } x = L_m \end{cases} \tag{25}$$

Thus, the primary current distribution is zero everywhere on the metal surface except at the edge.

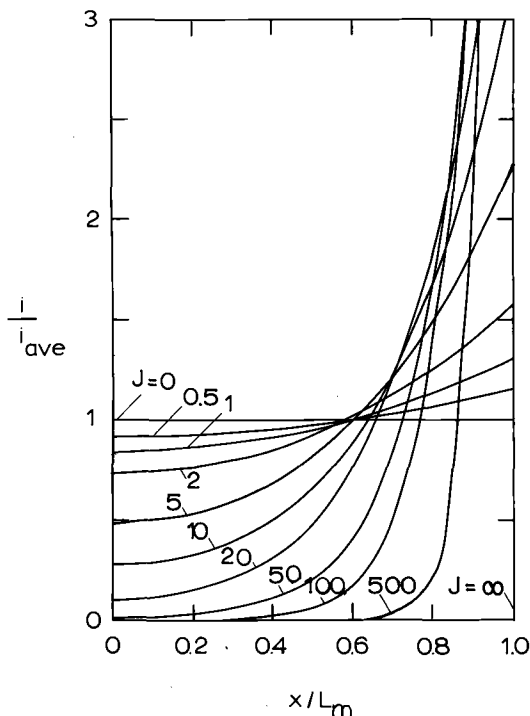


FIG. 8—Current distribution in a narrow crevice for linear electrode kinetics.

The potential distribution for  $L_c \geq x \geq L_m$  can be expressed as

$$\frac{\varphi}{\varphi_c} = \frac{1 + \left(\frac{x}{L_m} - 1\right) \sqrt{J} \tanh \sqrt{J}}{1 + \left(\frac{L_c}{L_m} - 1\right) \sqrt{J} \tanh \sqrt{J}} \tag{26}$$

Using these results, we obtain for the measured resistance

$$\begin{aligned} R_{\text{meas}} &= \varphi/i_{\text{ave}} \\ &= \frac{L_m}{Kh} (x - L_m) + \frac{L_m^2}{Kh} \frac{1}{\sqrt{J} \tanh \sqrt{J}} \end{aligned} \tag{27}$$

where the first term can be recognized as the ohmic resistance between  $x = L_m$  and  $L_m < x \leq L_c$ . This is the resistance that can be compensated for by experiment, and it corresponds to the primary current distribution expressed by Eq 25. The second term then cor-

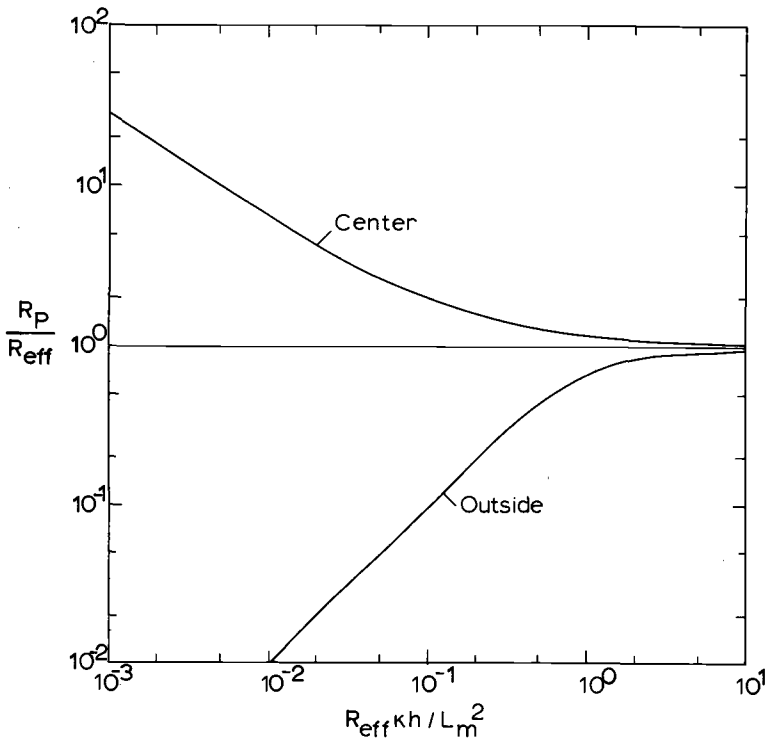


FIG. 9—Calculated error in the measured polarization resistance for the crevice model depicted in Fig. 5.

responds to the measured polarization resistance  $R_{\text{eff}}$ . From these results, we obtain for the model

$$\frac{R_p}{R_{\text{eff}}} = \frac{\sinh \sqrt{J}}{\sqrt{J} \cosh \left( \sqrt{J} \frac{x}{L_m} \right)} \tag{28}$$

The equation is plotted in Fig. 9 for reference electrode positions (Fig. 6) at  $x = 0$  and  $x = L_c$ . The figure indicates that the polarization resistance measured with respect to a reference electrode placed outside the crevice will be larger than the true value, and vice versa—a hypothetical probe positioned at the crevice tip will measure smaller values than the true value.

A similar analysis was carried out earlier [4] for a circular crevice model, and the results are given in Fig. 10 in view of the significance of this geometry for crevice corrosion under screws and gaskets and for the experimental model discussed in the following section.

It should be emphasized again that the above analysis and results in principle are applicable to a narrow crevice ( $h \ll L_m$ ). Separate analysis [12] of a two-dimensional crevice model indicated, however, that the one-dimensional model gives a good approximation for the current distribution as long as  $h < 0.1 L_m$ .

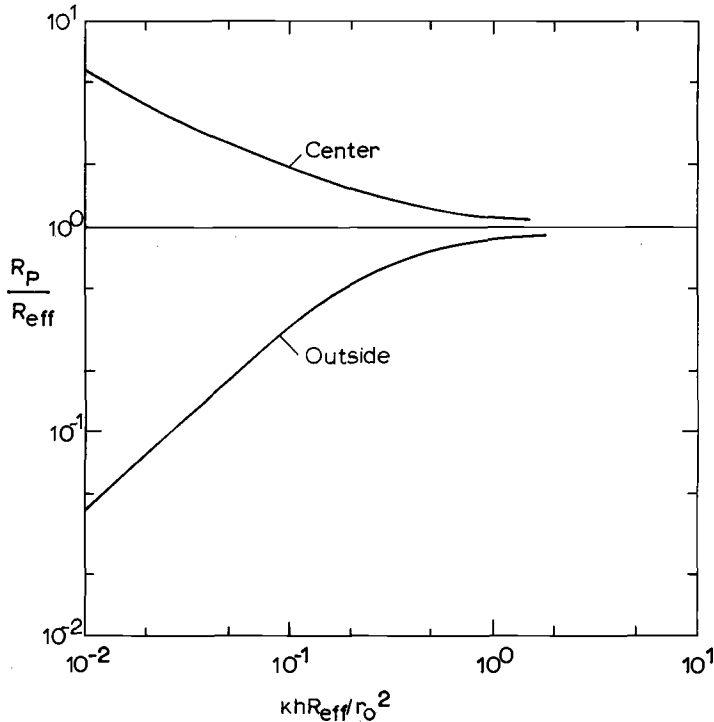


FIG. 10—Calculated error in the measured polarization resistance of a thin circular crevice.

*Disk Electrode*

The nature of nonuniform ohmic drop to a disk electrode and its effect on experimental data have been amply discussed [1-5] and the subject is also treated in a separate paper presented at this conference [11]. The calculated error in  $R_{\text{eff}}$  for linear kinetics is shown in Fig. 11. These results indicate that the placement of the reference electrode close to the disk surface can cause a larger error than its placement at a certain distance away from the disk. In the former case,  $\epsilon_1$  becomes unity, and the error is proportional to the nonuniformity of current distribution at the surface. This suggests that  $\epsilon_1$  and  $\epsilon_2$  act in opposing directions as the reference electrode is removed from the surface, such that the resulting error is smaller than either of its components. This is illustrated for a specific location of the reference electrode in Fig. 12.

**Experimental Verification***Apparatus and Procedure*

A brief experimental verification of the theoretical results was attempted by using an artificial crevice cell developed in a separated study [13] for investigating the crevice corrosion of steels. The design is based on an earlier investigation by McCafferty [14]. The cell is sketched in Fig. 13. The crevice is formed between an optically polished glass disk and a disk specimen positioned parallel to the glass surface. The specimen is attached to a micrometer assembly employed to align the two surfaces and produce an accurate setting of the crevice height. The glass disk (6 cm in diameter) was embedded at the bottom surface of the cell, and it contained three, 1-mm diameter holes placed radially at 1-cm intervals starting with the hole at the center. A fourth hole, collinear with the other holes, was drilled through the plexiglass surface adjacent to the glass disk. These served as Luggin

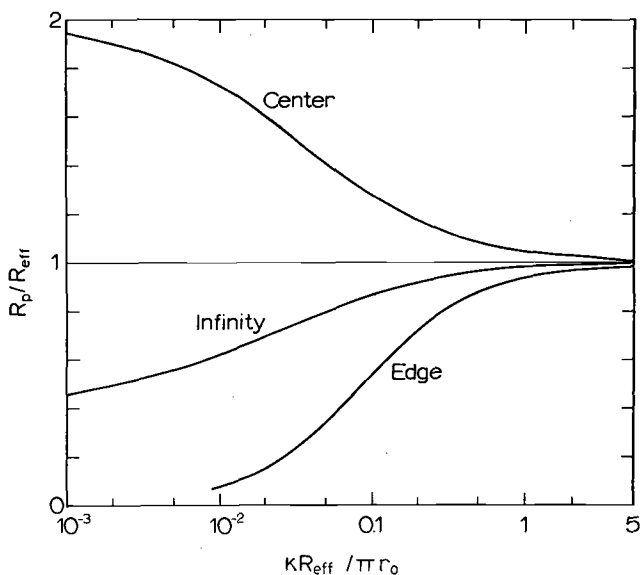


FIG. 11—Calculated error in the measured polarization resistance of a disk electrode exposed to a large volume of electrolyte (Ref 4).

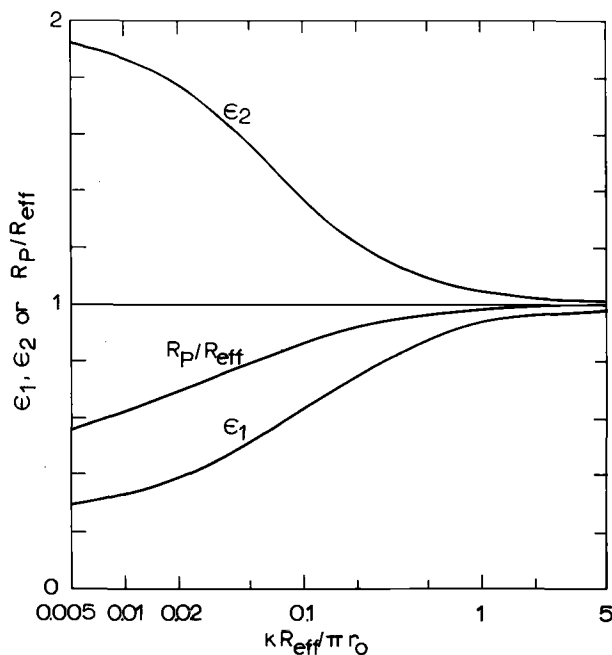


FIG. 12—Magnitude of opposing factors  $\epsilon_1$  and  $\epsilon_2$ , which affect the magnitude of error in  $R_{eff}$ . Calculations are based on a reference electrode placed on the axis of disk far from the surface.

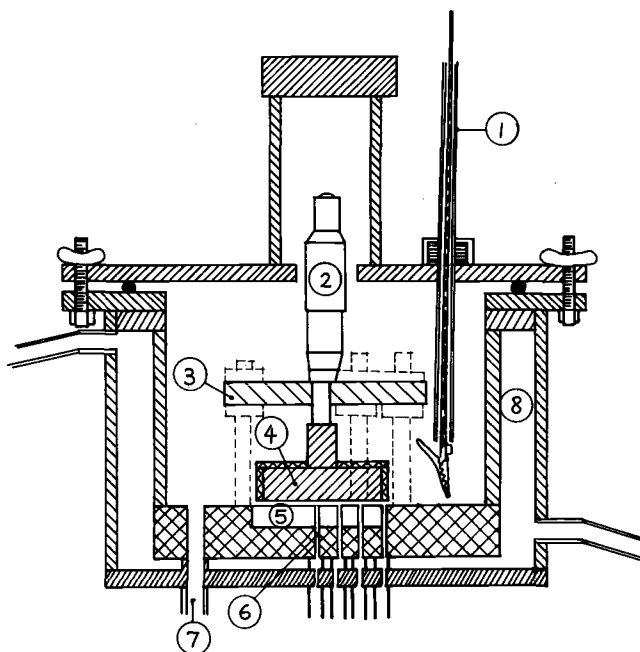


FIG. 13—Experimental crevice cell. 1—Electrical connection to specimen. 2—Micrometre. 3—Micrometre stand. 4—Specimen. 5—Glass disk. 6—Luggin capillary. 7—Electrolyte inlet/outlet. 8—Water jacket for temperature control.

capillaries for potential measurements. Further details about the cell can be found in Ref 13.

The experiments were performed with pure iron under open circuit conditions in deaerated 0.1 M sulfuric acid solution at 25°C. The diameter of the metal specimen was 2 cm. The metal was embedded in epoxy with an outer diameter of 6 cm. The AC impedance technique was employed by using a Solartron 1172 Frequency Response Analyzer and the well-established procedure for such measurements as reviewed by Mansfeld [15].

### Results

Since hydrogen evolution was a problem, measurements were taken immediately after the crevice was flooded with the solution. Replicate runs were not too reproducible because true steady-state was not attained during the measurements. However, the results give a correct picture of the error related to the nonuniformity of ohmic drop to the surface when simultaneous measurements of the working electrode impedance with respect to different reference electrode positions are compared.

Typical Nyquist plots for the complex impedance measured with respect to two Luggin capillary positions are shown in Figs. 14 and 15. Distorted semicircles are obtained, and the  $R_{\text{eff}}$  values measured with respect to the inner (center of metal disk) and outer (edge of epoxy mounting) reference electrode locations for a given crevice height vary as predicted by the analytical calculations. The  $R_{\text{eff}}$  values measured with respect to the outer electrode are appreciably smaller than the values recorded with respect to the inner electrode. The true value ( $R_p$ ) lies somewhere in between the two measurements. For example, the  $R_{\text{eff}}$  values measured in Fig. 14 are about 480 and 850  $\Omega \text{ cm}^2$ , respectively, with respect to the Luggin probes at the center and outside of crevice. Correcting these values by using Fig. 9 gives about 650  $\Omega \text{ cm}^2$  for the true polarization resistance  $R_p$ .

### Discussion

Electrochemical corrosion monitoring is probably the only way of measuring the instantaneous corrosion rate in situ. Increased application of the electrochemical techniques in

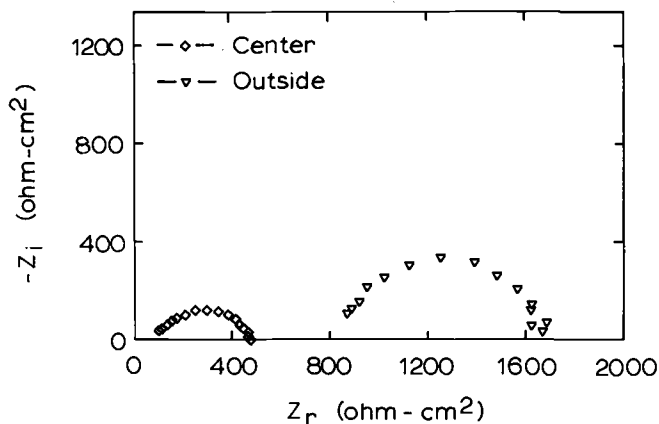


FIG. 14—Nyquist plots of the impedance of an iron electrode in a narrow circular crevice. Diameter of metal: 2 cm. Solution: 0.1 M  $\text{H}_2\text{SO}_4$ . Crevice height: 1 mm.

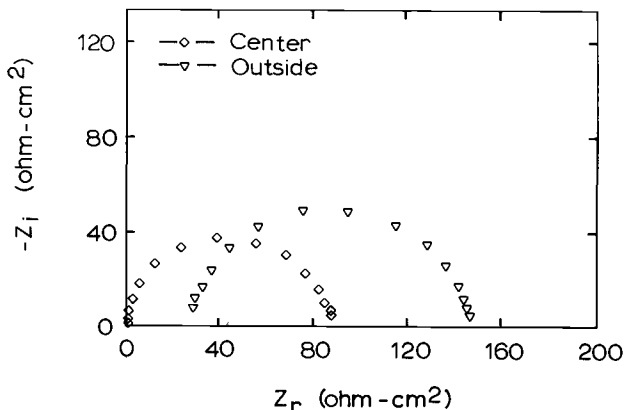


FIG. 15—Nyquist plots of the impedance of an iron electrode in a narrow circular crevice. Diameter of metal: 2 cm. Solution: 0.1 M  $H_2SO_4$ . Crevice height: 5 mm.

low conductivity media and to estimate corrosion rates under thin electrolyte layers and in occluded areas brings to the fore the problem of adequate ohmic resistance compensation. We tried to show here that the conventional means of resistance compensation may not be satisfactory in such applications. A systematic error may result in the presence of a nonuniform ohmic drop to the electrode surface, and correcting the error by purely experimental means is at best not straightforward. The problem is compounded because the measured corrosion rate is often lower than the actual rate.

In discussing the nature of problems associated with the electrochemical technique, it is necessary to distinguish between direct measurements on a corroding surface and indirect measurements performed by using small corrosion monitoring probes.

Electrochemical techniques are unsuitable for measuring rates of localized corrosion. This is partly related to a lack of a priori knowledge about the actual geometry of corroding sites. Even in laboratory cells with well-defined geometry, the  $R_p$  value obtained in the proper manner corresponds to the corrosion rate at the location where the net local current density is zero. The corrosion rate, which is nonuniformly distributed, has to be obtained by calculation. This can be accomplished by using the equations derived from the fundamental principles as demonstrated above for a specific geometry. The task is made even simpler if the potential distribution in the crevice can be measured by a multiprobe set-up as in the laboratory cell described above [13].

Another difficulty in estimating corrosion rates in occluded cells is a lack of information about the conductivity in the occluded area, which can be quite different than the conductivity of the bulk environment. Moreover, this study did not treat the problem of concentration variations in the solution and its effect on the nonuniformity of the ohmic potential drop. This matter deserves further study.

Electrochemical methods are more suitable for monitoring situations approximating uniform corrosion. In practice such measurements are performed by using corrosion probes that contain the reference and counter electrodes and a working electrode constructed from the same metal as the structure under investigation. Although corrosion may be uniformly distributed over the actual structure, the current distribution on the probe-working electrode may become nonuniform during measurement. Correcting the error caused by a nonuniform ohmic drop to the probe surface should not pose great difficulties, because the geometry of the working electrode and location of the reference electrode rel-

ative to the working electrode are known. In addition, the conductivity of corrosive environment has to be estimated. It is necessary to have information about the thickness of electrolyte film if corrosion occurs under thin layers of corrosive liquids. With this information, the magnitude of error can be estimated from correction charts (Figs. 9 through 11) calculated for the particular probe geometry. If the information required to use the figures is not readily available, it is still worthwhile to perform an order-of-magnitude estimate with guessed quantities to assess if this type of error is of any significance for the measured quantities.

The best way of avoiding the problem is by designing probes with a uniform primary distribution. The uniformity of primary current distribution is directly related to the electrode geometry, and the basic geometric factors that affect the distribution have been discussed [1,16]. Edge effects which lead to a nonuniform current distribution are maximized when the working electrode and the surrounding insulating material are placed in the same plane by using flush-mounted probes. A 90°-angle between the metal and an insulating surface usually eliminates such edge effects. For example, a hemispheric electrode mounted on an insulating plane exhibits a uniform current and potential distribution even in the presence of concentration polarization effects [17]. Placement of the reference electrode adjacent to the working electrode edge, as practiced in certain flush-mounted probe designs [18], should be avoided. In fact, the error resulting from positioning the reference electrode a few diameters away from the working electrode is smaller than that resulting from placing it adjacent to the surface, if the means for ohmic resistance compensation are available.

## Conclusions

The existing methods of data analysis for ohmic resistance compensation may not be adequate in measurements involving low conductivity media, high corrosion rates, occluded cells, or some combination thereof. Depending also on the electrochemical probe geometry or the morphology of localized corrosion, a significant nonuniformity may exist in the ohmic potential drop to the active surface, and this cannot be compensated for readily by the available experimental techniques. The resulting error in the measured corrosion rate can be corrected in certain cases by using correction factors derived from the fundamental principles. These cases include measurements performed by electrochemical probes with simple geometry. The error can also be avoided by proper probe design. Estimating the corrosion rates in occluded cells is a difficult task, mainly because the morphology of the active site and properties of the local environment, which affect the current and potential distributions, usually are not known.

## Acknowledgment

Liv Odden assisted with the experimental work. This work was supported by the Foundation for Industrial and Scientific Research at the Norwegian Institute of Technology (SINTEF).

## References

- [1] Tiedemann, W. H., Newman, J., and Bennion, D. N., *Journal of the Electrochemical Society*, Vol. 120, No. 2, 1973, pp. 256-258.
- [2] Smyrl, W. H. and Newman, J., *Journal of the Electrochemical Society*, Vol. 119, No. 2, 1972, pp. 208-212.
- [3] Miller, B. and Bellavance, M. I., *Journal of the Electrochemical Society*, Vol. 120, No. 1, 1973, pp. 42-53.

- [4] Nisancioglu, K., *Corrosion*, Vol. 43, No. 5, 1987, pp. 258–265.
- [5] Newman, J., *Journal of the Electrochemical Society*, Vol. 117, No. 4, 1970, pp. 507–508.
- [6] Newman, J., *Journal of the Electrochemical Society*, Vol. 117, No. 2, 1970, pp. 198–203.
- [7] Nisancioglu, K. and Newman, J., *Journal of the Electrochemical Society*, Vol. 120, No. 10, 1973, pp. 1339–1346, 1356–1358.
- [8] Glarum, S. H., *Journal of the Electrochemical Society*, Vol. 124, No. 4, 1977, pp. 518–524.
- [9] Rogers, R. S., “Instrumental Implementation and Limitations of Potential Correction Methods—Part I: Theoretical,” ASTM STP 1056, *Ohmic Electrolyte Resistance Measurement*, American Society for Testing and Materials, Philadelphia, 1989.
- [10] Mansfeld, F., Chen, Y. C., and Shih, H., “Determination and Elimination of the Uncompensated Resistance in Low Conductivity Media,” ASTM STP 1056, *Ohmic Electrolyte Resistance Measurement and Compensation*, American Society for Testing and Materials, Philadelphia, 1989.
- [11] Esteban, J. M., Lowry, M., and Orazem, M. E., “Correction of Experimental Data for the Ohmic Potential Drop Corresponding to a Secondary Distribution on a Disk Electrode,” ASTM STP 1056, *Ohmic Electrolyte Resistance Measurement and Compensation*, American Society for Testing and Materials, Philadelphia, 1989.
- [12] Nisancioglu, K., “Crevice Corrosion on Stainless Steels: Modeling for Experimental Design,” SINTEF Report No. STF34 F79022, Trondheim, Norway, April 1979.
- [13] Nisancioglu, K. and Andersen, T. R., “An Electrochemical Cell for Crevice-Corrosion Testing of Steels,” SINTEF Report No. STF34 A82026, Trondheim, Norway, March 1982.
- [14] McCafferty, E., *Journal of the Electrochemical Society*, Vol. 121, No. 8, 1974, pp. 1007–1013.
- [15] Mansfeld, F., *Corrosion*, Vol. 36, No. 5, 1981, pp. 301–307.
- [16] Newman, J., in *Localized Corrosion*, R. W. Staehle, B. F. Brown, J. Kruger, and A. Agrawal, Eds., National Association of Corrosion Engineers, Houston, 1974, p. 45.
- [17] Nisancioglu, K. and Newman, J., *Journal of the Electrochemical Society*, Vol. 121, No. 2, 1974, pp. 241–246.
- [18] Strømmen, R., “Corrosion Monitoring Probe Designs,” paper presented during ICOSM 83, London, 1983.

William C. Ehrhardt<sup>1</sup>

## IR Drop in Electrochemical Corrosion Studies— Part 2: A Multiple Method IR Compensation System

---

**REFERENCE:** Ehrhardt, W. C., “IR Drop in Electrochemical Corrosion Studies—Part 2: A Multiple Method IR Compensation System,” *The Measurement and Correction of Electrolyte Resistance in Electrochemical Tests, ASTM STP 1056*, L. L. Scribner and S. R. Taylor, Eds., American Society for Testing and Materials, Philadelphia, 1990, pp. 78–94.

**ABSTRACT:** The experimental methods available for IR drop correction in electrochemical corrosion experiments are briefly reviewed. A computer-controlled system that incorporates several different methods of IR compensation is described and some examples of its performance are presented.

**KEY WORDS:** corrosion, current interruption, electrochemical impedance, feedback, instrumentation, IR compensation, polarization, solution resistance

In order to obtain usable results from many electrochemical corrosion experiments, some form of IR drop correction must be employed.<sup>2</sup> A variety of techniques are available to make this correction [1–3]. In this paper, the principles behind and limitations to the various experimental approaches to IR compensation are reviewed. The details and performance of an IR compensation system developed as an add-on to a conventional potentiostat are described.

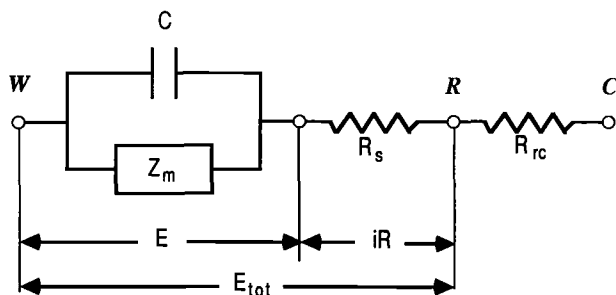
### The Compensation Process

Figure 1 depicts an idealized equivalent circuit of an electrochemical cell. The working electrode is made of the metal that is being tested. The potential of interest in the experiment is  $E$ : the potential across the metal/solution interface (also referred to here as the true potential). A reference electrode is placed in the solution close to the working electrode to minimize the resistance,  $R_s$ , of the solution between it and the working electrode surface. The size, shape, and relative placement of all electrodes in the cell have an effect on the interpretability of the current/potential curves obtained from the cell. Of particular importance is the degree of uniformity of the current distribution on the working electrode. These considerations have been described in a previous paper.<sup>2</sup> The development here assumes that Fig. 1 is an adequate equivalent circuit for the actual cell response.

In an electrochemical experiment, the cell is connected to a potentiostat which controls the potential difference between the working and reference electrodes at a potential  $E_{tot}$ .

<sup>1</sup> Senior research scientist, Betz Laboratories, Inc., Somerton, Rd., Trevose, PA 19047.

<sup>2</sup> Ehrhardt, W. C., Part 1, this publication, pp. 27–58.



**W** Working electrode  
**R** Reference (Luggin) electrode  
**C** Counter electrode

**C** = Double layer capacitance.  
**Z<sub>m</sub>** = Impedance of metal /solution interface (excluding C).  
**R<sub>s</sub>** = Uncompensated solution resistance. May include component from surface film on metal.  
**R<sub>rc</sub>** = Resistance between reference and counter electrodes.  
**E<sub>tot</sub>** = Total working vs reference potential (control potential).  
**E** = Potential across metal/solution interface.  
**iR** = Potential drop due to cell current flowing through R<sub>s</sub>

FIG. 1—Idealized equivalent circuit of an electrochemical cell.

The relationship between  $E_{tot}$  and  $E$  is given by

$$E = E_{tot} - IR_s \quad (1)$$

where the second term on the right hand side is the IR drop. The IR drop can be directly measured by some experimental techniques. With other techniques  $I$  and  $R_s$  are individually determined and the IR drop is computed.

An additional voltage drop is generated by the cell current flowing through the solution resistance between the reference and counter electrodes,  $R_{rc}$ .  $R_{rc}$  is usually larger than  $R_s$ . For DC or slowly varying signals, this additional voltage drop usually does not cause a problem unless it forces the potential between the working and counter electrodes to exceed the voltage supply capability (compliance) of the potentiostat. However, as will be shown later,  $R_{rc}$  can cause problems with higher frequency AC signals and affect certain IR compensation measurements.

In the usual electrochemical experiment, one wishes to set the true potential,  $E$ , equal to a particular value, the control potential,  $E_{con}$ . IR compensation techniques employing positive electrical feedback correct  $E_{tot}$  using a feedback potential,  $E_{fb}$ ,

$$E_{\text{tot}} (\text{corrected}) = E_{\text{con}} + E_{\text{fb}} \quad (2)$$

where

$$E_{\text{fb}} = FCIR_s \quad (3)$$

and 100  $FC$  is the percent compensation.  $FC$  is one if “perfect” (100%) IR compensation is applied. With perfect feedback compensation, at any instant in time  $E$  is equal to  $E_{\text{con}}$ .

$E_{\text{fb}}$  can be either a continuous analog signal or a discrete signal generated using a digital to analog (D/A) converter. The correction process (feedback loop) must adjust to the variations in current that result from potential changes. At the same time, the correction process must not be overly sensitive to the natural fluctuations in the current that can occur even when the potential is held fixed, otherwise the control system can be driven into oscillation. This is especially likely to happen when  $FC$  is near one.

An alternative to using feedback is the mathematical correction technique. No correction is applied to  $E_{\text{tot}}$ . In this case,  $E_{\text{tot}}$  is equal to  $E_{\text{con}}$ .  $E$  is computed from Eq 1 using the measured value of  $E_{\text{tot}}$  and either the measured or the computed IR drop. The feedback and mathematical correction techniques may be combined if  $0 < FC < 1$ .

In summary, the IR compensation process consists of two steps:

1. Determination of the IR drop. The options are:
  - a. direct measurement
  - b. computation from measured values of  $R_s$  and  $I$
2. Correction of  $E_{\text{tot}}$ . The options are:
  - a. electronic (real time) correction
  - b. mathematical (post-measurement) correction

Because the control potential,  $E_{\text{con}}$ , is usually a function of time (for example, a linear ramp), both of these steps need to be repeated during the course of the experiment. If option 1(b) is used in the determination step, either  $R_s$  can be assumed to be constant [4] or its value can be periodically updated to adjust for variations with time. Possible causes of a time-varying  $R_s$  have been previously discussed.<sup>2</sup>

With the mathematical correction approach, the true potential scan rate and scan range will not be the same as the control potential scan rate and scan range. Consequently, the real time (feedback) approach to compensation is preferred.

### Methods for $R_s$ Measurement and IR Compensation

#### *Wide Bandwidth Analog Feedback* [1–3,5,6]

Analog feedback was essentially the only instrumental method for IR compensation available in the first generation of commercial potentiostats. This technique is much more suited for certain electroanalytical experiments than it is for electrochemical corrosion experiments. The feedback signal is obtained from the output of the potentiostat's current follower,  $V_i$ .  $V_i = IR_{\text{meas}}$ , where  $I$  is the current through the cell and  $R_{\text{meas}}$  is the current measuring resistor used in the current follower. An adjustment is made, usually manually, to set the degree of feedback,  $DF$ , so that  $E_{\text{fb}} = DFV_i$ . If the  $DF$  adjustment is accomplished using a voltage divider circuit (the usual arrangement), then  $DF$  will be in the range  $0 < DF < = 1$ .  $E_{\text{fb}}$  is supplied as an additional control input to the potentiostat's potential control amplifier, thus forming a positive feedback loop.

The designation "wide bandwidth" used here is meant to denote that  $E_{fb}$  is not low pass filtered in any significant way. With this IR compensation method, compensation can be provided for control signals which change rapidly with time.

Using Eq 3, one obtains

$$DF = FCR_s/R_{meas} \quad (4)$$

Thus, for fixed  $R_{meas}$ , adjusting  $DF$  is equivalent to adjusting the product  $FCR_s$ . Usually,  $R_s$  is not known. Note that even if  $DF$  is constrained to values between 0 and 1,  $FC$  is not. One of the method's difficulties is that no universally acceptable technique exists for setting  $DF$ . One approach often used is to monitor the current versus time response of the system to an applied square wave voltage using an oscilloscope.  $DF$  is adjusted until the response resembles that expected for the smooth charging of a pure capacitor. However, it has been observed that this adjustment procedure can result in the corresponding  $FC$  being near or even exceeding one. Overcompensation and potentiostat oscillations can result. The severity of the problem depends in a detailed way on the gain and phase shift versus frequency characteristics of the amplifiers in the potentiostat's control circuitry and of the electrochemical cell [2,3]. The latter is dependent on the particular electrochemical system under study.

Note that the  $DF$  obtained from the adjustment process is only appropriate for a particular value of  $R_{meas}$  (see Eq 4). With most potentiostats, the current sensitivity cannot be changed once  $DF$  has been set without changing the effective value of  $FC$ . This is a distinct disadvantage in many corrosion experiments where the current varies over several orders of magnitude and accurate data cannot be obtained unless  $R_{meas}$  is varied. Further, the  $DF$  adjustment procedure requires that the potential be set in a region where no Faradaic reaction occurs [5], an impossible requirement for most corrosion reactions. It is partly because of the inadequacies of the wideband analog feedback method that other instrumental approaches to IR compensation have been developed.

### *Damped Analog Feedback*

As indicated above, severe problems with control stability can arise if a wide-band analog feedback loop is used and  $FC$  is at or near one. Britz [2,7] has shown that if the frequency response of the feedback system is limited through low pass filtering—an approach called "damped positive feedback"—100% IR compensation may be achieved while still maintaining stable potential control. This approach lowers the effective potentiostat bandwidth. Electrochemical corrosion experiments use slow voltage ramps as the control signals (typical ramp rates less than 60 mv/min). For these experiments, adequate potentiostat bandwidth can be maintained even with heavy filtering.

### *Digital Feedback*

Digital feedback has been used in the system to be described below. The stability characteristics of positive analog feedback have been thoroughly analyzed [2,3]. No analysis of the stability of a digital feedback approach was found in the literature. The rate at which the D/A is updated should determine the effective bandwidth of the feedback. The minimum time between D/A updates is the total time required to determine the IR drop (see Step 1 above) plus the D/A settling time.

If the update rate is too slow, the response of the compensation system will be too sluggish and  $E_{fb}$  will lag behind the control signal by an excessive amount of time. If the update

rate is too fast or if the D/A resolution is too coarse, stability problems can arise. The correction ( $E_{fb}$ ) is applied as digital voltage step which will generate a current transient. The transient is partly due to the charging of the double layer and other capacitances and partly due to the finite equilibration time of the electrochemical processes occurring at the working electrode. If the current transient has not died out before the next update cycle occurs, the measured IR drop will be larger than it would be if a steady state current had been achieved. To compensate for the larger IR drop, a larger correction voltage will be applied, which will generate an even larger current transient. After a few cycles the whole correction process will become unstable.

### *Current Interruption [2,8-25]*

The current interruption method is conceptually straightforward. If the current flowing through the cell is suddenly interrupted, the IR drop must disappear instantaneously with the current. The voltage  $E$  cannot vanish instantaneously, but must decay at a rate determined by the discharge rate of the double layer capacitance (see Fig. 1). If the time constant for the discharge is long compared to the time required to accurately measure  $E$ , the potential measured at the reference electrode during the time that the current is off will be the true potential across the metal solution interface at the time of interrupt. If  $E_{tot}$  prior to the interruption is also measured, the IR drop can be determined by taking the difference,  $E_{tot} - E$ .

Some practical difficulties with the interruption technique exist. The switching time for turning the current on and off in most interruption systems is less than a microsecond. However, the potentiostat, the cell connection wiring, the cell itself, the type of reference electrode used, and the magnitude of the current being interrupted all affect the settling time of the potential response waveform. Thus, there is a minimum waiting time (delay time) required before an accurate potential measurement can be made. If the settling time were the only consideration in the measurement, the delay time could simply be set to a large value for all experiments. However, it is also necessary to choose a delay time that is short enough so that no significant discharge of the potential across the double layer capacitance occurs. These conflicting requirements dictate that the interrupt waveform be monitored if an optimum delay time is to be selected. In some cases, no single point on the waveform yields an accurate IR drop, and extrapolation techniques [10,17] must be applied to the interrupt waveform to determine the true electrode potential at the instant of interrupt.

It should be noted that there are limitations associated with the use of current interruption as a technique for the measurement of  $R_s$ . Generally speaking, it is difficult to determine the IR drop to better than 1 or 2 mV. Assuming an IR drop of 10 mV (for example,  $R_s = 100 \Omega$ ,  $I = 100 \mu A$ ) and negligible uncertainty in the measured value of  $I$ , a 2 mV uncertainty in the IR drop is equivalent to a 20% (20  $\Omega$ ) uncertainty in  $R_s$ . The error can be reduced by increasing the current; the  $R_s$  error in this example would be reduced to 2% if the cell current were increased to 1 mA. However, the use of large currents to obtain an accurate  $R_s$  is generally inadvisable if additional measurements must be made on the system, since the corrosion characteristics of the test electrode can be significantly and irreversibly altered.

### *Transient Techniques*

Transient techniques involve monitoring the response of an electrochemical cell to an applied voltage [5,26,27] or current [28,29] square wave or pulse. The resulting waveform

is analyzed to extract  $R_s$  and, in some cases,  $C$  and  $Z_m$ . Although these techniques are useful for measurement of  $R_s$ , they do not lend themselves easily to automatic operation. Unless very small perturbations are used, they cannot be applied during a polarization experiment. In addition, the applied current methods require switching from potentiostatic to galvanostatic control.

### *Sine Wave (Electrochemical Impedance)*

Electrochemical impedance techniques are now commonly used in electrochemical corrosion studies. A complete impedance experiment requires measuring the complex cell impedance over a broad range of frequencies. When only  $R_s$  is of interest, a small amplitude sinusoidal voltage of frequency  $f$  is applied to the cell. A high enough frequency is used so that the magnitude of the impedance of the double layer capacitance,  $1/(2\pi fC)$ , is small compared to the magnitude of  $Z_m$ . At this frequency, the capacitor shorts out  $Z_m$  and the effective impedance between the working and reference electrodes is  $R_s$ . The appropriate frequency can be determined by monitoring the magnitude of the impedance of the cell as the frequency is increased. For a cell like the one depicted in Fig. 1, the magnitude should decrease and then reach a plateau where it remains independent of frequency. The impedance at this point should have zero phase shift, that is, it should appear to be a pure resistance. For most corrosion systems, frequencies between 100 Hz and 10 kHz are adequate to reach the plateau region. In some systems using the impedance technique for  $R_s$  measurement, a fixed frequency within this range is employed [4,30,31].

An advantage of the sine wave approach is that  $R_s$  can be determined accurately even at zero DC current. The corrosion system is only slightly perturbed during the measurement. However, the measurement frequency must be properly chosen. Like the square wave and pulse methods, the sine wave technique is usually not appropriate to use during an ongoing polarization scan. However, as will be shown, it is possible to halt the scan in progress, measure  $R_s$ , and then continue the scan from that point.

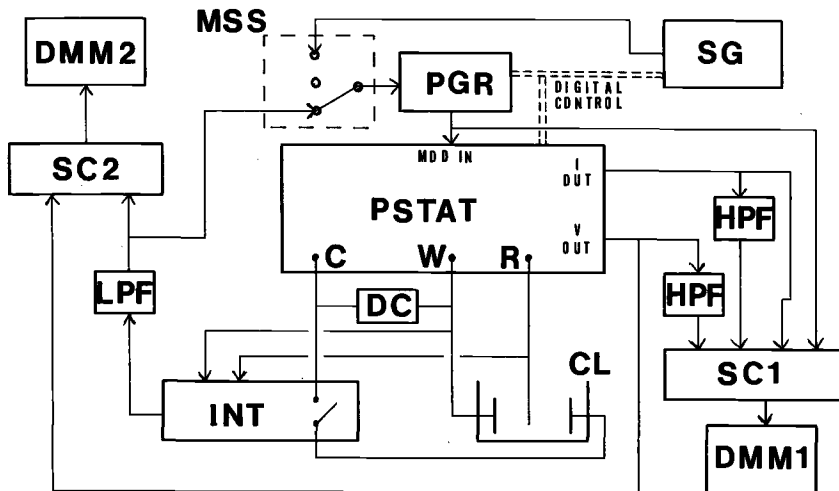
## **Potentiostat and IR Compensation System**

### *System Components*

The system shown in Fig. 2 was developed as an "add-on" to a potentiostat without adequate built-in IR compensation capabilities. Most of the system components are computer controlled (Hewlett Packard Model HP 86). The system was designed to only operate with slow polarization ramp rates: 0.5 mV/s or less. Four different modes of operation are possible when making polarization measurements:

1. Uncompensated.
2. Digital feedback correction of the analog polarization voltage ramp. A value of  $R_s$  obtained from a sine wave measurement and the most recently measured value of  $I$  are used to digitally generate  $E_{fb}$  using a D/A convertor.
3. Digital feedback correction of the analog polarization voltage ramp. The most recently measured value of the low pass filtered IR drop signal obtained from the current interrupter is used to digitally generate  $E_{fb}$ .
4. Analog feedback correction of the analog polarization voltage ramp.  $E_{fb}$  is the low pass filtered IR drop signal obtained from the current interrupter.

The system components common to all modes of operation are: the modulation select



- SG Signal generator (Wavetek, Model 20)  
 MSS Modulation select switch (3 pole manual switch)  
 PGR Waveform programmer (Princeton Applied Research Model 175)  
 PSTAT Potentiostat (ECO instruments model 552/EPU)  
 C Counter electrode  
 W Working electrode  
 R Reference electrode  
 DC Diode clamp  
 CL Cell  
 HPF High pass filter (A. P. Circuit Corp Model APH, 8-pole Butterworth)  
 SC1 Scanner card number 1 (Keithley Model 705 Scanner)  
 DMM1 Digital multimeter number 1 (Hewlett Packard Model 3478A)  
 INT Interrupter (Electrosynthesis Co. Model 800, bipolar, with analog output)  
 LPF Low pass filter (Frequency Devices Model 901F, 8-pole Butterworth)  
 SC2 Scanner card number 2 (Keithley Model 705 Scanner)  
 DMM2 Digital multimeter number 2 (Keithley Model 192)

FIG. 2.—Schematic of IR compensation system.

switch, waveform programmer, potentiostat, scanner, digital multimeters, and the computer system.

The waveform programmer provides either a positive or negative analog ramp that starts from a manually set DC offset value. The standard ramp rate is 10 mV/min. The position of the modulation control switch determines the source of the modulation voltage applied to the programmer. If a modulation voltage is supplied, it is superimposed on the analog ramp. The ramp start, ramp reset, and ramp hold functions of the programmer are controlled via digital logic signals derived from the potentiostat and controlled by the system computer.

The potential difference between the working and reference electrodes of the cell connected to the potentiostat is controlled at a value equal to the sum of the potential supplied at the potentiostat's modulation input and the potential obtained from the potentiostat's computer controlled internal D/A converter. An analog signal equal to the total control voltage is provided at the voltage out connector and an analog voltage signal proportional to the measured current is provided at the current output connector. The cell on/off function and current range resistor selection are under computer control. The counter electrode

circuit of the potentiostat was wired so that the circuit is completed through the current interrupt switch of the interrupter. This switch remains closed when the interrupter is not in use.

The computer-controlled scanner routes selected signals to two separate computer-controlled digital multimeters, designated DMM1 and DMM2. Both multimeters are used to measure DC volts. In the sine wave measurement mode, DMM1 is also used to measure AC volts. The system has the usual peripherals for displaying, plotting, and storing data.

## Operational Modes of the System

### *Uncompensated Mode*

In the uncompensated mode the modulation select switch is set so that no modulation is applied to the analog ramp from the waveform programmer. The potentiostat internal D/A is set at zero. The DC offset control of the programmer is set to the corrosion potential,  $E_c$ , and the programmer scan is set either for a positive-going ramp terminating at +10 V or a negative-going ramp terminating at -10 V.

DMM1 monitors the unfiltered current output signal of the potentiostat, and DMM2 monitors the voltage output. When the polarization scan is initiated, the cell is turned on. At this point the control potential is equal to  $E_c$ . The internal D/A of the potentiostat is slowly ramped to the desired starting point of the experiment relative to  $E_c$ . In other words, if the start point is +30 mV relative to  $E_c$ , the D/A is ramped to +30 mV. After an adjustable hold time, the computer triggers the start of the analog ramp and records the data via DMM1 and DMM2. A sample is taken every 3 s for small range scans and every 4 s for longer scans (generally for 100 mV range or more), corresponding to a sample every 0.5 mV and 0.67 mV, respectively, for a 10 mV/min ramp rate. The current sensitivity is adjusted as needed during the scan. When the measured potential reaches the desired final potential for this experiment, the cell is turned off and the ramp is reset to its initial value.

### *Digital Feedback Mode—R<sub>s</sub> Determined via Sine Wave Measurement*

In the digital feedback, sine wave mode the signal generator, high pass filters, and an oscilloscope (Panasonic Digital Storage Oscilloscope Model VP-5730P) are used. The signal generator output is a sine wave and is gated on or off as needed under computer control using a digital input-output (IO) line. The minimum generator frequency used is 250 Hz.

DMM1 is switched to its AC volts mode to measure sine wave amplitudes. The meter can measure AC signals between 20 Hz and 300 kHz. Maximum accuracy is attained between 100 Hz and 20 kHz, and is 0.3% in this range. The high pass filters have a filter cutoff of 200 Hz, so AC power line components up to the third harmonic (180 Hz) are removed from the filtered signals.

The programmer DC offset is adjusted as in uncompensated operation. Then the modulation select switch is set so that the signal generator is connected to the programmer modulation input and the generator is gated on. DMM1 is switched to AC volts operation and the scanner is set to route the programmer output signal directly to DMM1. The generator output is manually adjusted to between 10.3 and 10.9 mV RMS (nominal 15 mV peak amplitude), and is then gated off.

Operation proceeds as in uncompensated mode until the cell is turned on. At this point the DC current is measured and the current sensitivity is adjusted. The generator is gated on, and the AC current is measured by DMM1 at the output of the high pass filter. The current sensitivity is adjusted so that the peak voltage (AC plus DC) of the current output

signal is between 20 and 400 mV. The signal generator frequency is then adjusted to the minimum frequency ( $\geq 250$  Hz) that produces a zero phase shift condition between the voltage and current waveforms monitored on the oscilloscope. When this frequency has been set, five second averages of the high pass filtered current and potential signals are obtained via DMM1;  $R_s$  is computed from their ratio. The generator is then gated off and DMM1 is again set to monitor the DC current output voltage signal. Accurately identifying a true zero phase shift condition from the oscilloscope display can sometimes be difficult. However, the difference between the magnitude of the impedance and the real part of the impedance is only 1.5% at  $10^\circ$  of phase shift; thus  $R_s$  can be accurately determined even if the frequency adjustment is not perfect.

As in the uncompensated mode, the potentiostat D/A is ramped to the experiment starting potential relative to  $E_c$ . At this point an IR correction loop is entered. In this loop, the potential from the D/A is adjusted until the potential  $E$  (see Eq 1) is within 2 mV of the desired experiment starting potential. For example, if a starting potential of +30 mV relative to  $E_c$  is required and  $R_s$  is 10  $\Omega$ , the correction loop would terminate if the D/A voltage were +40 mV at a current of 1 mA. The correction process is analogous to solving for a root of a nonlinear equation by successive approximations. If the response of the current to potential changes is erratic or is strongly time dependent, the correction loop exit criterion may never be met. Thus far no difficulties have been encountered; the correction loop usually terminates within four iterations.

When the correction loop is exited, the analog ramp is started. The correction voltage supplied by the D/A is updated to correct for changes in IR drop as each point is acquired. The potential value stored at a given point is the difference between the voltage measured by DMM2 and the computed IR drop. The scan is terminated when the true potential reaches the desired final value.

An option is provided for a "no feedback" mode of operation. In this mode, the correction loop is entered at the beginning so that the initial potential  $E$  is at its proper (compensated) value. However, once the ramp is started, the D/A voltage remains fixed as in uncompensated operation. The scan is terminated at the desired final  $E$ . Although the same true potential range is scanned as in the feedback mode of operation, the true scan rate varies during the experiment.

Finally, an option is also provided to halt the analog ramp periodically during the scan and to re-measure  $R_s$  at that point using the sine method. Use of this option improves compensation accuracy when  $R_s$  varies during the course of the experiment.

#### *Digital Feedback Mode—IR Drop Determined from Interrupter*

In the digital feedback, interrupter mode, the interrupter, diode clamp, low pass filter, and oscilloscope are used. No modulation is provided to the waveform programmer. When the interrupter is active, it provides an analog voltage signal equal to the measured value of the IR drop at the selected interrupt delay time (up to 99  $\mu$ s). This signal is updated every interrupt (10 times/s). The IR drop signal is routed to the low pass filter to remove all of the high frequency noise; a filter cutoff frequency of 0.2 Hz is usually used. At the appropriate times, the low pass filter output is routed by the scanner to DMM2 for measurement. The oscilloscope is used to monitor the interrupt waveform.

Operation proceeds as in the uncompensated mode until the initial starting (uncorrected) potential has been set. At this point an optimum interrupter delay time is manually set by observing the interrupt waveform. In most cases, a value of 40  $\mu$ s is suitable. This value is used as a default if the IR drop at the adjustment time is so small that no interrupt

decay can be observed. Once this adjustment has been made, operation proceeds as in the previously described digital feedback mode with two exceptions:

1. DMM2 is toggled back and forth by the scanner between measuring the IR drop from the low pass filter and measuring the total applied voltage.
2. The measured value of the IR drop, rather than a computed value, is used to adjust the potentiostat D/A to compensate the analog ramp.

In both analog and digital feedback interrupter modes a value of  $R_s$  is computed at the beginning and at the end of the polarization scan. These values are obtained from 5 s averages of the IR drop and of  $I$ .

#### *Analog Feedback Mode—IR Drop Determined From the Interrupter*

In the analog feedback mode the same system components as in the previously described mode are used. However, the modulation select switch is set so that the IR drop signal from the low pass filter is applied to the waveform programmer as a modulation voltage. The potentiostat D/A is used only to establish the initial start potential—as in uncompensated operation. The IR drop is continuously compensated from the time that the cell is turned on. As in the digital feedback mode, a provision is made for the adjustment of the interrupt delay setting prior to starting the analog ramp.

#### *All Compensated Modes*

It should be noted that all three of the compensated modes employ damped feedback. Obviously, in the interrupter modes, the low pass filter is the filtering element in the feedback loop. In the case of the sine wave mode, the filtering is provided by the digital multimeter used to measure the current, DMM1. This meter filters out higher frequencies from the current signal by an internal averaging process.

#### **Dummy Cells**

Dummy cells used for these tests were configured in the same way as the components in Fig. 1, but  $Z_m$  was replaced by a resistor. Capacitors between 5 and 50  $\mu\text{F}$  were used. The latter value was used for interrupter testing, and is large enough so that potential changes observed during the interrupt period reflect primarily the influence of the settling time of the measuring circuitry.

#### *$R_s$ Measurement Accuracy—Sine Wave*

AC signal measurement accuracy at high frequencies ( $>500$  Hz) is strongly influenced by the current measuring resistor,  $R_{\text{meas}}$ , used to monitor the current. If a measurement is made by applying a voltage  $V_{\text{in}}$  across the terminals of a simple resistor,  $R$ , the voltage supplied at the current monitor output of the potentiostat,  $V_{\text{out}}$ , is given by

$$V_{\text{out}} = V_{\text{in}}(R_{\text{meas}}/R) \quad (5)$$

The term in parenthesis is the gain of the current measuring circuitry,  $G_i$ . The available current measuring resistors vary by factors of ten from 1  $\Omega$  to 1 M $\Omega$  and correspond to a

TABLE 1—Effect of  $R_{rc}$  on the sine wave mode measurements of the impedance ( $\Omega$ ) of a dummy cell.<sup>a,b</sup>

Measurement Frequency kHz	$R_{rc}$ ( $\Omega$ )		
	0	100	1000
0.5	139	139	164
1.0	117	120	236
2.0	106	125	375
5.0	102	145	534
10.0	...	156	582
20.0	102	161	597

<sup>a</sup>  $R_s$  actual = 100  $\Omega$ .

<sup>b</sup> Expected plateau frequency for  $R_{rc} = 0$  is  $\sim 5$  kHz.

full scale current value in the range from 1 A to 1  $\mu$ A, with  $V_{out} = 1$  V being full scale. Data presented by Mansfeld et al. [33] (see Table 1 and Fig. 2 of the reference) and tests performed with this system clearly demonstrate that systematic, high-frequency measurement errors caused by potentiostat non-idealities are minimized when  $G_i \leq 1$ . The peak  $V_{in}$  for the sine wave is 15 mV. In the sine wave measurement mode, a tradeoff is made between the systematic errors that occur at high gain and the poor measurement accuracy that occurs at low gain by setting  $R_{meas}$  so that the peak value of  $V_{out}$  is between 20 and 400 mV. The equivalent gains are between 1.3 and 27.

Measurements were made on dummy cells at 5 and 10 kHz;  $R_s$  was varied between 1  $\Omega$  and 10 k $\Omega$ .  $R_{rc}$  was zero in these tests. At a frequency of 5 kHz, the agreement between the actual and measured values of  $R_s$  was  $\pm 3\% \pm 0.5 \Omega$ .

The measured values of  $R_s$  obtained from initial testing of the sine-based system on real cells were too large. The source of this problem was found to be the influence of  $R_{rc}$  on the measurement of  $R_s$ . For most corrosion cell geometries, the distance between the Luggin probe and the counter electrode is much greater than between the Luggin and the working electrode, so  $R_{rc}$  is usually larger than  $R_s$ . Dummy cell tests were performed to examine the effect of nonzero values of  $R_{rc}$  on the  $R_s$  measurement. The results of one of these tests are shown in Table 1.

It is apparent from this table that for this potentiostat,  $R_{rc}$  has a significant influence on  $R_s$ , and causes  $R_s$  to be overestimated. The magnitude of the error increases with frequency. For  $R_{rc}$  equal to 1000  $\Omega$ , no plateau region (region where the magnitude of the impedance does not change with frequency) exists.

Some potentiostat non-idealities are clearly effecting the higher frequency measurements when  $R_{rc}$  is large. Gohr et al. [33] have analyzed the effect of the various components of the equivalent circuit of a cell/potentiostat system on high frequency impedance measurements. They found that certain stray impedances in the system could cause measurement errors which increased with frequency. Models of real cell/potentiostat systems are very complex [3,6,33–35]. The circuit element characteristics which need to be known in order to use these models have not been measured for this compensation system. However, the data in Table 1 indicate that for this system, measurements of  $R_s$  must be made at as low a frequency as possible.

*IR Drop Measurement Accuracy—Interrupter*—Table 2 contains representative IR drop data for the interrupter system as a function of delay time and DC current level for  $R_{rc}$  values of 0 and 1000  $\Omega$ . The measured values should be compared to the theoretical values

TABLE 2—Effect of current, delay time, and  $R_{rc}$  on the interrupter measured IR drop for a dummy cell.<sup>a,b,c</sup>

Applied Voltage, mV	Current, mA	IR Drop Theory, mV	Interrupter Delay Time ( $\mu$ s)					
			6	10	15	20	30	40
100	0.092	9.2	2 (3)	4 (6)	5 (8)	7 (8)	8 (9)	9 (9)
200	0.183	18.3	5 (9)	9 (13)	12 (17)	16 (17)	17 (17)	18 (18)
500	0.453	45.3	21 (38)	31 (40)	38 (41)	41 (42)	43 (43)	44 (44)
1000	0.907	90.8	50 (83)	71 (83)	81 (87)	86 (88)	89 (89)	90 (89)

<sup>a</sup> Dummy cell:  $C = 50 \mu\text{F}$ ,  $R_p = 1000 \Omega$ ,  $R_s = 100 \Omega$ ,  $R_{rc}$  either  $0 \Omega$  or  $1000 \Omega$ .

<sup>b</sup> Table entries are measured in IR drops (mV) for  $R_{rc} = 1000 \Omega$ .

<sup>c</sup> Values in parenthesis are IR drops for  $R_{rc} = 0 \Omega$ .

in column three of the table. These data indicate that, provided an adequate delay time is used, the interrupter measured values of IR drop are not affected by  $R_{rc}$ .

As shown in the table, a minimum delay time of  $20 \mu\text{s}$  is needed for the interrupt waveform to settle to within 10% of the true IR drop. The settling time becomes shorter as the magnitude of the current increases. For the  $6 \mu\text{s}$  delay, the measured IR drop ranges from 33% to 91% of the true IR drop as the current is varied from  $92 \mu\text{A}$  to  $907 \mu\text{A}$ .

A delay of  $40 \mu\text{s}$  is usually adequate to allow the interrupt waveform to completely settle. When using dummy cells, the measured IR drop is usually within  $\pm 2 \text{ mV}$  of the true value, this being the noise level on the analog signal from the interrupter. For real cells, the noise level increases to about  $\pm 5 \text{ mV}$ .

### Feedback Stability

The multimeter used to measure the DC current (DMM1) has good noise rejection characteristics for one of the major sources of noise in the system—AC pickup at power line frequencies and its harmonics (normal mode rejection at  $60 \text{ Hz} \geq 60 \text{ dB}$ ). Thus, variations in the measured DC current accurately reflect variations in the true DC current. This is essential for operation of the sine wave method feedback loop, since the correction voltage is derived from the current measurement. Smooth curves are obtained from the sine wave method-based measurements on dummy cells (see Fig. 3).

The interrupter analog output is relatively noisy. Polarization curves obtained with no filtering applied to the interrupter analog output exhibited erratic behavior, as illustrated in Fig. 3 for the digital feedback mode. The feedback stability of both the analog and digital feedback interrupter modes was improved when the interrupter output is passed through a low pass filter with a cutoff frequency of  $0.2 \text{ Hz}$ . The analog feedback mode has a smoother response than the digital feedback mode.

### Real Corrosion Cells

Figure 4 shows the results of two  $\pm 60 \text{ mV}$  polarization, linear polarization experiments. These tests were run using a flat low carbon steel (LCS) working electrode immersed in a jet of water flowing parallel to its surface. The test solution was Philadelphia tap water with a conductivity of  $260 \mu\text{S}/\text{cm}$  ( $1 \mu\text{S} = 1 \mu\text{mho} = 1 \times 10^{-6} \Omega^{-1}$ ). A Vycor tipped 4-mm glass tube was used as the Luggin probe in conjunction with a saturated calomel electrode (SCE) reference. The compensated curve was obtained using the interrupter in analog feedback mode, a  $40\text{-}\mu\text{s}$  interrupter delay time was used. The initial measured resistance was

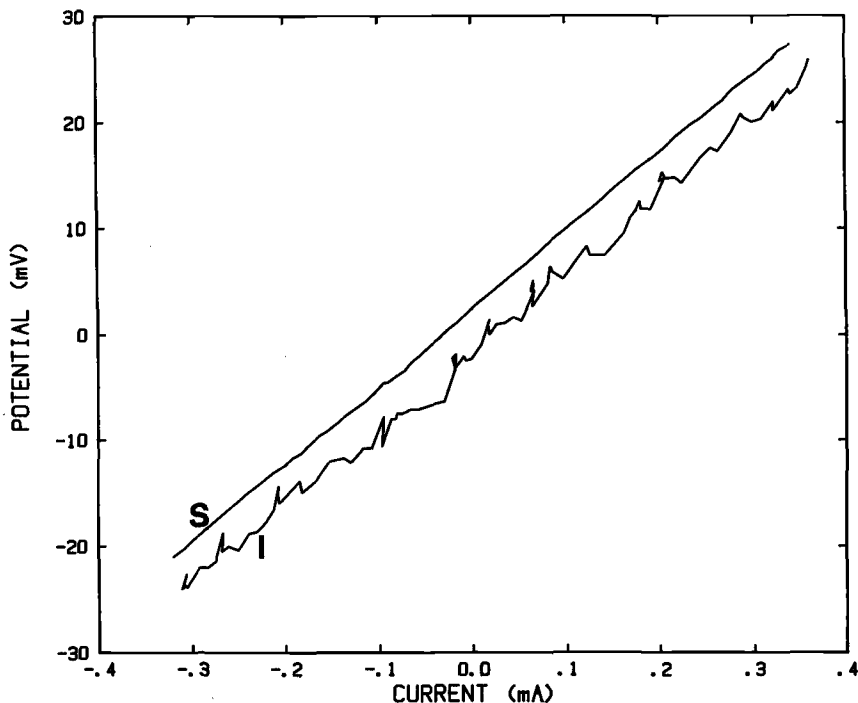


FIG. 3—Dummy cell polarization curves obtained using digital feedback IR compensation.

S—sine wave mode

I—interrupter mode using unfiltered interrupter analog output (curve displaced by  $-2$  mV for clarity)

$122 \Omega$ ; the final resistance was  $139 \Omega$ . In addition to having a distinctly different polarization resistance (slope at zero polarization), the compensated curve also exhibits a definite curvature. The uncompensated curve is almost perfectly straight, an indication that the response is dominated by IR drop<sup>2</sup>.

Linear polarization experiments were also conducted on this system using the digital feedback interrupter and sine wave modes. The digital interrupter mode was very stable for this system, and produced results that can be superimposed on the compensated curve shown in Fig. 4. The measured initial  $R_p$  was  $120 \Omega$ , and the final  $R_p$  was  $140 \Omega$ .

An  $R_p$  of  $167 \Omega$  was obtained from a sine-wave mode measurement at 500 Hz on this same electrode, a value higher than for any of the interrupter measurements. In both the interrupter and sine wave measurement modes, the values of  $R_p$  at  $-60$  mV polarization were lower than those obtained at  $+60$  mV polarization by as much as  $30 \Omega$ . Repeated measurements on the same electrode confirmed that these differences were not due to irreversible changes of the electrode surface produced by the previous polarization scan.

The use of wire electrodes in place of ordinary reference electrodes can improve high frequency response in current interrupt and electrochemical impedance experiments<sup>2</sup>. Some data were obtained using the interrupter with a reference electrode consisting of an insulated platinum wire with approximately a millimeter of its tip exposed. The wire tip was positioned close to the tip of the Luggin probe. Only the potentiostat was connected to the SCE reference. The only significant difference between the platinum wire and Luggin

probe reference interrupter experiments was that the interrupt waveform was considerably noisier with the wire. The  $R_s$  values were essentially identical.

Further tests were conducted in tap water with the conductivity raised to  $890 \mu\text{S}/\text{cm}$  by the addition of potassium perchlorate ( $\text{KC10}_4$ ). The results of uncompensated, interrupt compensated (analog feedback,  $40 \mu\text{s}$  delay), and sine wave compensated (500 Hz measure frequency, with periodic remeasure) anodic polarization curves are presented in Fig. 5. The steps in the sine wave curve occur at the points at which the ramp was halted and  $R_s$  remeasured. As with the lower conductivity results, the  $R_s$  values obtained from the interrupter mode measurements ( $33.1$  to  $36.6 \Omega$ ) are consistently lower than those obtained from the sine wave mode ( $42.5$  to  $45.4 \Omega$ ). The curve obtained using sine wave mode compensation demonstrates approximate Tafel like behavior with a slope of  $90 \text{ mV}$ .

## Discussion

Both sine wave and interrupter mode measurements yield essentially identical IR compensated polarization scans if the potentiostat is connected to a dummy cell. The  $R_s$  values obtained from sine wave measurements on low carbon steel in flowing tap water are consistently higher than those from the interrupter measurements.

The noted dependence of  $R_s$  on polarization is of interest. Because of its reversibility and reproducibility, it is possible that it is due to a dependence of the working electrode current distribution on the electrode polarization.

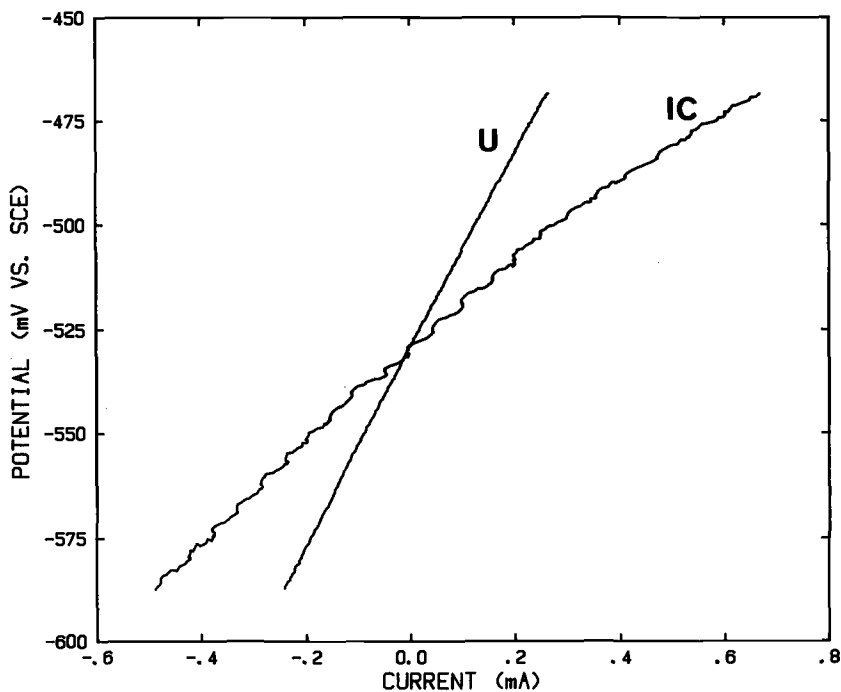


FIG. 4—Low carbon steel polarization curves obtained in flowing water with a conductivity of  $260 \mu\text{S}/\text{cm}$ .

U—uncompensated.

IC—interrupter mode IR compensated, analog feedback, low pass filter cutoff at  $0.2 \text{ Hz}$ .

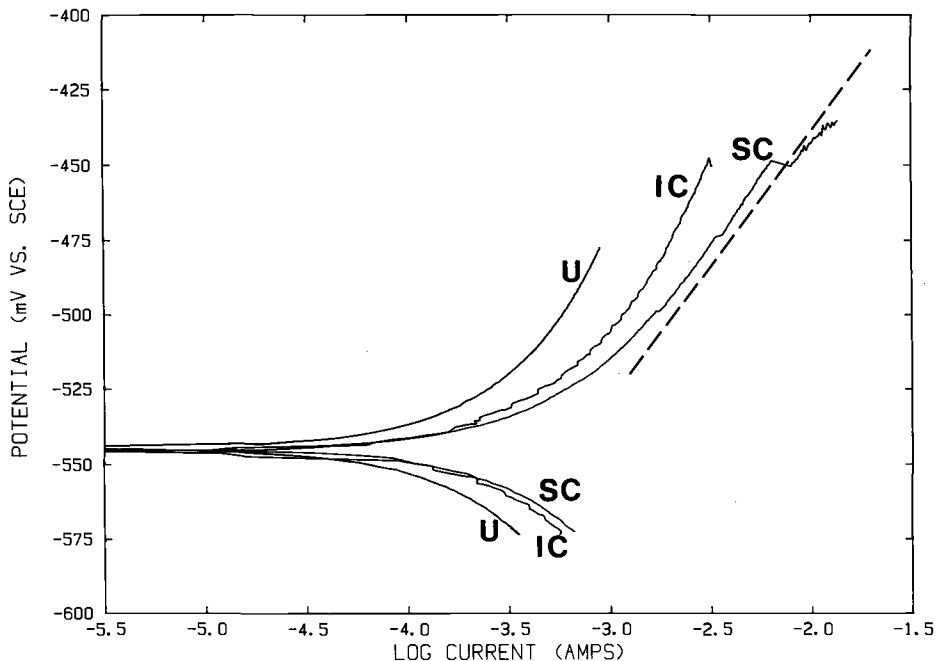


FIG. 5—Low carbon steel polarization curves obtained in flowing water with a conductivity of  $890 \mu\text{S}/\text{cm}$ . Dashed line has a slope of  $90 \text{ mV}/\text{decade}$ .

U—uncompensated,  
 IC—interrupter mode compensated, analog feedback, and  
 SC—sine wave mode compensated with periodic re-measurement of  $R_s$ .

## Conclusions

1. The limited bandwidth feedback technique, using either analog or digital feedback, can be used in a computer based measurement system to obtain stable IR compensation for slow ( $\sim 10 \text{ mV}/\text{min}$ ) polarization ramp experiments.
2. IR compensation systems should be tested on dummy cells having an  $R_{rc} > R_s$ , otherwise misleading results on compensation accuracy could be obtained.
3. In this system, consistent  $R_s$  measurements for dummy cells obtained with both the sine wave and interrupter measurement modes did not carry over to tests on a real corrosion system. Further work needs to be done to resolve the discrepancies in the results. A standard test system (electrode, electrolyte, cell design, etc.) for IR compensated polarization measurements would be extremely valuable in resolving this problem.

## Acknowledgments

The author gratefully acknowledges Betz Laboratories, Inc. for permission to prepare and to publish this paper.

## References

- [1] Hayes, M., Kuhn, A. T., and Patefield, W., "Techniques for the Determination of Ohmic Drop in Half-Cells and Fuel Cells: A Review," *Journal of Power Sources*, vol. 2, 1977/78, pp. 121–136.

- [2] Britz, D., "IR Elimination in Electrochemical Cells," *Journal of Electroanalytical Chemistry*, vol. 88, 1978, pp. 309–352.
- [3] Roe, D. K., "Overcoming Solution Resistance with Stability and Grace in Potentiostatic Circuits," *Laboratory Techniques in Electroanalytical Chemistry*, P. T. Kissinger and W. R. Heineman, Eds., Marcel Dekker, 1984, chapter 7, pp. 193–234.
- [4] Peterson, W. M., and Siegeman, H., "A Microprocessor-Based Corrosion Measurement System," *Electrochemical Corrosion Testing, ASTM STP 727*, F. Mansfeld and U. Bertocci, Eds., American Society for Testing and Materials, Philadelphia, 1981, pp. 390–406.
- [5] He, P., and Faulkner, L. R., "Intelligent, Automatic Compensation of Solution Resistance," *Analytical Chemistry*, vol. 58, 1986, pp. 517–523.
- [6] Meyer, J.-J., Poupard, D., and Dubois, J.-E., "Potentiostat with a Positive Feedback IR Compensation and a High Sensitivity Current Follower Indicator Circuit for Direct Determination of High Second-Order Rate Constants," *Analytical Chemistry*, Vol. 54, 1982, pp. 207–212.
- [7] Britz, D., "100% IR Compensation by Damped Positive Feedback," *Electrochimica Acta*, vol. 25, 1980, pp. 1449–1452.
- [8] Scully, J. R., and Bundy, K. J., "Electrochemical Methods for Measurement of Steel Pipe Corrosion Rates in Soil," *Materials Performance*, vol. 24, No. 4, 1985, pp. 18–25.
- [9] Mansfield, F., Kendig, M. W., and Tsai, S., "Corrosion Kinetics in Low Conductivity Media. I. Iron in Natural Waters," *Corrosion Science*, vol. 22, No. 5, 1982, pp. 455–471.
- [10] Elsner, B., and Bohni, H., "Computer-Assisted D.C. and A.C. Techniques in Electrochemical Investigations of the Active-Passive Transition," *Corrosion Science*, vol. 23, No. 4, 1983, pp. 341–352.
- [11] Britz, D., and Brocke, W. A., "Elimination of IR-Drop in Electrochemical Cells by the Use of a Current-Interruption Potentiostat," *Journal of Electroanalytical Chemistry*, vol. 58, 1975, pp. 301–311.
- [12] Oelssner, W., "Effect of Ohmic Resistance and Automatic IR Compensation on Polarization Rate in Potentiodynamic Measurements" (in German), *Korrosion*, Dresden, vol. 14, No. 1, 1983, pp. 19–30.
- [13] Cassoux, P., Dartiguepeyron, R., Fabre, P.-L., and de Montauzon, D., "Automatic IR Drop Correction for Studies of Electrochemical Systems," *Electrochimica Acta*, vol. 30, No. 11, 1985, pp. 1485–1490.
- [14] Gsellmann, J., and Kordesh, K., "An Improved Interrupter Circuit for Battery Testing," *Journal of the Electrochemical Society*, vol. 132, No. 4, 1985, pp. 747–751.
- [15] Reinhard, G., and Ziems, J., "Voltammetric Studies on Layered Metal Electrodes in Aqueous Electrolytes with the Interrupter Method" (in German), *Zeitschrift Physikalische Fuer Chemie*, Leipzig, vol. 264, No. 1, 1983, pp. 91–105.
- [16] Berthold, M., and Herrmann, S., "Investigation of Corrosion with Measurement and Compensation of the Ohmic Drop," *Corrosion*, vol. 38, No. 5, 1982, pp. 241–245.
- [17] Williams, L. F. G., and Taylor, R. J., "IR Correction. Part I. A Computerized Interrupt Method," *Journal of the Electroanalytical Chemistry*, vol. 108, 1980, pp. 293–303.
- [18] Agladze, T., Dobos, L., Suschke, H., Makarow, V., Meszaros, L., and Elsner, W., "Automatic Compensation of Ohmic Potential Difference in Potentiostatic Measurements," *Protection of Metals*, vol. 15, No. 3, 1979, pp. 213–219.
- [19] Schwabe, K., Elsner, W., and Zushke, Kh. D., "Automatic Compensation of Ohmic Potential Drop by the Interruption Method in Potentiostatic Measurements," *Protection of Metals*, vol. 15, No. 2, 1979, pp. 126–133.
- [20] Moors, M., and Demedts, G., "An Automatic Resistance Polarization Compensator," *Journal of Physics E, Journal of Scientific Instruments*, vol. 9, No. 12, 1976, pp. 1087–1090.
- [21] Farkas, J., Dobos, L., and Kovacs, P., "Potentiostat with Automatic IR-Compensation," *Acta Chimica Hungarica*, vol. 120, No. 1, 1985, pp. 63–71.
- [22] McIntyre, J. D. E., and Peck, W. F., "An Interrupter Technique for Measuring the Uncompensated Resistance of Electrode Reactions under Potentiostatic Control," *Journal of the Electrochemical Society*, vol. 117, No. 6, 1970, pp. 747–751.
- [23] Moran, P. J., "Auxiliary Electrode Method for Determination of Ohmic Resistance," *Corrosion*, vol. 42, No. 7, 1986, pp. 432–434.
- [24] Bezman, R., "Sampled-Data Approach to the Reduction of Uncompensated Resistance Effects in Potentiostatic Measurements," *Analytical Chemistry*, vol. 44, No. 11, 1972, pp. 1781–1785.
- [25] Wruck, W. J., Machado, R. M., and Chapman, T. W., "Current Interruption—Instrumentation and Applications," *Journal of the Electrochemical Society*, vol. 134, No. 3, 1987, pp. 539–546.
- [26] Hishida, M., Takabayashi, J., Kawakubo, T., and Yamashina, Y., "Polarization Curve Measure-

ment in High Purity Water at Elevated Temperatures," *Corrosion*, vol. 41, No. 10, 1985, pp. 570-574.

- [27] Asakura, S., and Nobe, K., "Electrodissolution of Zinc in Acid Chloride Solutions," *Corrosion*, vol. 40, No. 5, 1984, pp. 227-231.
- [28] Kasahara, K., and Kajiyama, F., "Determination of Underground Corrosion Rates from Polarization Resistance Measurements," *Corrosion*, vol. 39, No. 12, 1983, pp. 475-480.
- [29] Asakura, S., and Endo, M., "Square Wave Current Method for Monitoring Corrosion," *New Materials and New Processes*, vol. 2, 1983, pp. 446-451.
- [30] Rhoades, R. V., "Applying Microcomputer Technology to Two-Frequency Polarization Resistance Measurements," *Computers in Corrosion Control* (Proceedings of a Corrosion/86 Symposium), National Association of Corrosion Engineers, 1986, pp. 129-138.
- [31] Harayama, S., and Tsuru, T., "A Corrosion Monitor Based on Impedance Method," *Electrochemical Corrosion Testing, ASTM STP 727*, F. Mansfeld and U. Bertocci, Eds., American Society for Testing and Materials, Philadelphia, 1981, pp. 167-186.
- [32] Mansfeld, F., Kendig, M. W., and Tsai, S., "Recording and Analysis of AC Impedance Data for Corrosion Studies. II. Experimental Approach and Results," *Corrosion*, vol. 38, No. 11, 1982, pp. 570-580.
- [33] Gohr, G., Mirink, M., and Shiller, C. A., "Distortions of High Frequency Electrode Impedance. Their Causes and How to Avoid Them," *Journal of the Electroanalytical Chemistry*, vol. 180, 1984, pp. 273-285.
- [34] Harrar, J. E., and Pomernacki, C. L., "Linear and Nonlinear System Characteristics of Controlled-Potential Electrolysis Cells," *Analytical Chemistry*, vol. 45, No. 1, 1973, pp. 57-79.
- [35] Harrar, J. E., and Shain, I., "Electrode Potential Gradients and Cell Design in Controlled Potential Electrolysis Experiments," *Analytical Chemistry*, vol. 38, No. 9, 1966, pp. 1148-1158.

## Determination and Elimination of the Uncompensated Resistance in Low Conductivity Media

---

**REFERENCE:** Mansfeld, F., Chen, Y. C., and Shih, H., "Determination and Elimination of the Uncompensated Resistance in Low Conductivity Media," *The Measurement and Correction of Electrolyte Resistance in Electrochemical Tests*, ASTM STP 1056, L. L. Scribner and S. R. Taylor, Eds., American Society for Testing and Materials, Philadelphia, 1990, pp. 95-124.

**ABSTRACT:** The positive feedback and the interrupter technique have been used for the continuous elimination of the uncompensated resistance  $R_u$  during the recording of potentiodynamic polarization curves. The positive feedback technique was evaluated with a PAR model 173 potentiostat and a Solartron model 1286 potentiostat. The Solartron potentiostat was also used with the interrupter technique. The application of both techniques was initially evaluated with suitable dummy cells followed by the tests with steel and stainless steel in ethanolic hydrochloric acid (HCl) and in hydrazine. It was found that great care has to be used to determine the optimum parameters for the interrupter technique such as potentiostat bandwidth and interrupter frequency. The potential-time trace in the interrupter period needs to be observed on an oscilloscope in order to determine the optimum conditions. The saturated calomel electrode and similar reference electrodes cannot be used with the interrupter technique. Wire electrodes such as the silver/silver chloride (Ag/AgCl) or platinum give satisfactory results. The positive feedback technique is easier to use, however 100% compensation cannot be achieved in the PAR potentiostat. Since in most cases  $R_u$  will decrease during the recording of a polarization curve, it is difficult to obtain satisfactory results with this technique.

**KEY WORDS:** polarization curves, potentiostats, ohmic drop, positive feedback, interrupter technique, reference electrode, steel, stainless steel, hydrazine

Electrochemical corrosion research is presently limited to solutions of good to moderate conductivity such as dilute acids and neutral solutions of chlorides or sulfates. Experimental problems with the uncompensated resistance ("ohmic drop") have apparently discouraged many researchers from investigating corrosion phenomena in low conductivity media such as very dilute aqueous solutions or organic media. In some cases, the errors in the electrochemical measurements caused by the low conductivity of the corrosive environment were apparently not recognized. Therefore, the conclusions reached were often not valid. In other cases, such as the technologically important area of nuclear reactors, so-called supporting electrolytes, such as sodium perchlorate ( $\text{NaClO}_4$ ) or sodium sulfate ( $\text{Na}_2\text{SO}_4$ ), have been added to distilled water in order to make an electrochemical measurement possible. However, evidence is mounting that these supporting electrolytes can take part in the corrosion reaction and alter the corrosion mechanism.

<sup>1</sup> Professor, graduate student, and research assistant professor, respectively, Department of Materials Science, University of Southern California, Los Angeles, CA 90089-0241.

In order to carry out electrochemical studies in very dilute aqueous solutions or in fairly pure nonaqueous media, a number of experimental problems have to be solved. The low conductivity of the corrosive environment leads to distortion of the measured electrochemical data such as polarization curves, polarization resistance data, etc. It has been shown that characteristic parameters, such as the pitting potential of stainless steels, cannot be determined if the ohmic drop is not completely eliminated. The low conductivity also increases problems with noise and makes appropriate cell design extremely important. Often reference electrodes which work satisfactorily in media of good conductivity cannot be used.

Modern electrochemical equipment contains provisions for elimination of the uncompensated resistance such as positive feedback or the interrupter technique. However, the application of these techniques is quite complicated and requires careful calibration for each metal/environment combination to be studied. Very few studies using the interrupter technique, which has the advantage of elimination of the ohmic drop during an electrochemical measurement, have been published. Electrochemical impedance spectroscopy (EIS) has the advantage that the ohmic drop does not affect the measurement adversely, but in fact provides information concerning solution conductivity and its changes during the experiment. The various techniques which are available for electrochemical studies of corrosion kinetics and mechanisms in low conductivity media have been evaluated in this preliminary investigation.

In potentiostatic and potentiodynamic measurements the applied potential  $E_{\text{appl}}$  includes the ohmic drop  $IR_u$  as a result of which the true electrode potential  $U_{\text{we}}$  deviates from  $E_{\text{appl}}$ . Even for a potentiostatic experiment  $U_{\text{we}}$  can vary with time if the current  $I$  is not constant and the ohmic drop  $IR_u$  changes with time. Since a linear term  $IR_u$  is added to the logarithmic term in the Tafel region, a current-dependent distortion of the polarization curve occurs which—if not recognized and eliminated—can lead to erroneous calculation of Tafel slopes and corrosion currents  $I_{\text{corr}}$  as obtained by Tafel extrapolation. Similarly, in measurements of the polarization resistance  $R_p$ , which is inversely proportional to the corrosion rate, the experimental value  $R'_p$  is the sum of  $R_p$  and  $R_u$ . The error in the value of  $I_{\text{corr}}$  is given by  $R_u/R_p [1]$ .

Another experimental difficulty arises from the effect of the uncompensated resistance  $R_u$  on the true scan rate in a potentiodynamic experiment [2]. Since the ohmic drop becomes more and more dominant with increasing current, the true potential  $U_{\text{we}}$  increases slower than the applied potential  $E_{\text{appl}}$ . On the other hand, in the active-passive transition region the true scan rate can be larger than the applied scan rate. The scan rate error is given by  $R_u/(R_u + R_p) [2]$ .

A number of possibilities exist to eliminate or at least reduce the effects of the uncompensated resistance discussed above. However, despite the fact that most commercial potentiostats now offer techniques such as the positive feedback and the interrupter technique, very few investigations have been reported in which full use has been made of these techniques. This disappointing result might be due mainly to the difficulties in applying these techniques, but also due to an unawareness of the problems which can occur not only in media of low conductivity, but also in many other environments. As shown above, the errors in the determination of  $R_p$  and in the true scan rate depend on the ratio  $R_u$  and  $R_p$  and not on the value of  $R_u$  alone.

The techniques available for the correction of ohmic drop effects can be divided into those in which  $R_u$  is measured and eliminated during the measurement and those in which the ohmic drop is subtracted from the polarization curves after their measurement. In the second case, the scan rate error cannot be eliminated. This group includes a variation of the interrupter technique as used by Boehni and co-workers [3] and numerical subtraction of the ohmic drop using a fixed value of  $R_u$ .

In this investigation emphasis has been placed on the evaluation of techniques which allow continuous compensation of the ohmic drop during the electrochemical experiment. This requirement is especially significant in corrosion systems where  $R_u$  can change during the test due to corrosion and increasing dissolution rates during anodic polarization. The techniques available in commercial equipment are the positive feedback technique and the interrupter technique. Both techniques have been evaluated in this project using potentiostats by PAR model 173 potentiostat and Solartron model 1286 potentiostat and corrosion systems such as steel and stainless steel in ethanolic hydrochloric acid (HCl) which combine low conductivity with varying levels of corrosivity. Some tests have been performed for stainless steel in pure hydrazine.

Since very little information concerning the application of the compensation techniques in low conductivity systems is available at present, EIS (Electrochemical Impedance Spectroscopy) was included as an additional experimental technique. EIS gives information about the electrochemical reactions occurring in a corrosion system and can be used to characterize the frequency response of such a system [4]. During the course of this study it was found that optimization of the interrupter technique was made easier when EIS data had been recorded previously. Such data could then be used to determine the experimental parameters for the interrupter technique.

### Experimental Approach

Various electrochemical techniques have been investigated in the present corrosion studies in low conductivity media. In order to apply these different methods, two dc measurement systems and one ac measurement system have been used. Polarization resistance measurements and the recording of potentiodynamic polarization curves are carried out with the dc measurement systems. The ohmic drop can be compensated by means of the positive feedback technique or the interrupter technique. The ac measurement system is used for the performance of electrochemical impedance spectroscopy (EIS).

### Measurement Systems

Two dc measurement systems have been used to apply the positive feedback technique. System 1 includes a Solartron model 1286 potentiostat, Tektronix 2213A oscilloscope, HP 7470A graphics plotter, digital voltmeters, and the test cell as shown in Fig. 1. System 2 includes the PAR model 173 potentiostat with the model 276 interface, the PAR model 175 universal programmer, a X-Y recorder and the test cell as shown in Fig. 2. The interrupter technique has been applied with System 1. The ac measurement system includes a Solartron model 1286 potentiostat and a 1250 frequency response analyzer, an IBM-XT computer system with GPIB card, and a HP 7470A graphics plotter. A computer program has been developed to run the experiments. Data analysis is done on an IBM-AT computer system and main frame computers at University of Southern California (for example, VAX, CMS, and ACMVS). Results obtained with the interrupter unit PU1 (Meinsberg, East Germany) have been discussed elsewhere [5,6].

### Positive Feedback Technique

*Background*—The application of the positive feedback technique for the compensation of the ohmic drop has been discussed by several researchers [7-9]. A number of potentiostats have been designed to perform this technique [10,11]. The performance of the technique can be described by a schematic of the potentiostatic circuit (Fig. 3a) [12] and the block diagram of the control loop (Fig. 3b). The potentiostat applies a controlled poten-

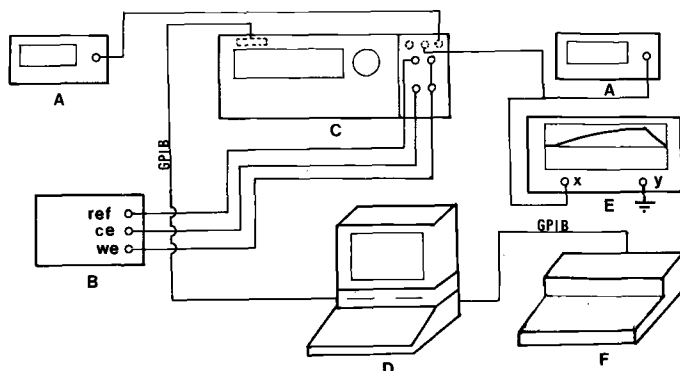


FIG. 1—Experimental arrangement for DC measurements with the positive feedback and current interrupter techniques using the Solartron model 1286 potentiostat. (a) voltmeter, (b) cell, (c) Solartron 1286 potentiostat, (d) IBM-XT computer, (e) oscilloscope, and (f) HP 7470A plotter.

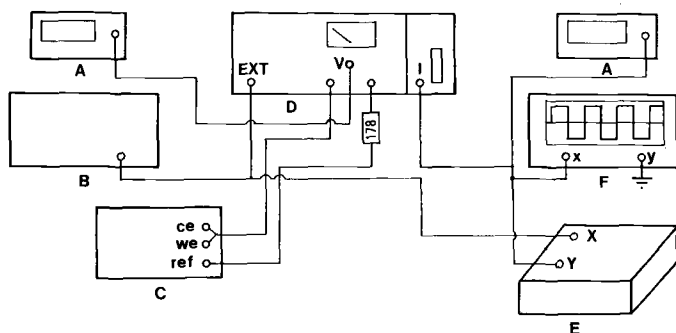


FIG. 2—Experimental arrangement for DC measurements using PAR model 173 potentiostat. (a) voltmeter, (b) PAR 175 universal programmer, (c) cell, (d) PAR 173 potentiostat and 276 interface, (e) X-Y recorder, and (f) oscilloscope.

tial to the working electrode (WE) by driving a current  $I$  via the counter electrode (CE) through the cell. The uncompensated resistance  $R_u$  causes a potential control error which is equal to  $I \times R_u$ . In a three-electrode cell, the potential difference  $\Delta RE$  between the reference electrode (REF) and the working electrode is the sum of the ohmic drop  $IR_u$  and the true electrode potential  $U_{we}$ . In order to eliminate the ohmic drop, the controlled potential has to be increased to a potential which is equal to the sum of the input polarization voltage  $POL$   $V$  and the ohmic drop. The ohmic drop is added to the applied potential as the product of the measured cell current  $I$  times a preset value of the compensation resistance  $R_{comp}$  using a current-voltage converter. Therefore,  $R_{comp}$  has to be equal to the actual  $R_u$  in order to completely compensate the ohmic drop (Fig. 3). In the positive feedback technique, increasing the fraction of compensation of the ohmic drop will decrease the stability margin. However, oscillations do not necessarily occur with 100% compensation [5, 10] because the stability of the system is affected by the properties of the test cell, the bandwidth of the control amplifier which can be adjusted in the Solartron Model 1286 potentiostat and the fraction of the ohmic drop compensation [10, 11, 13–15].

The voltage response waveforms for a square wave polarization voltage can be used for the selection of the optimum bandwidth of the control amplifier in the Solartron poten-



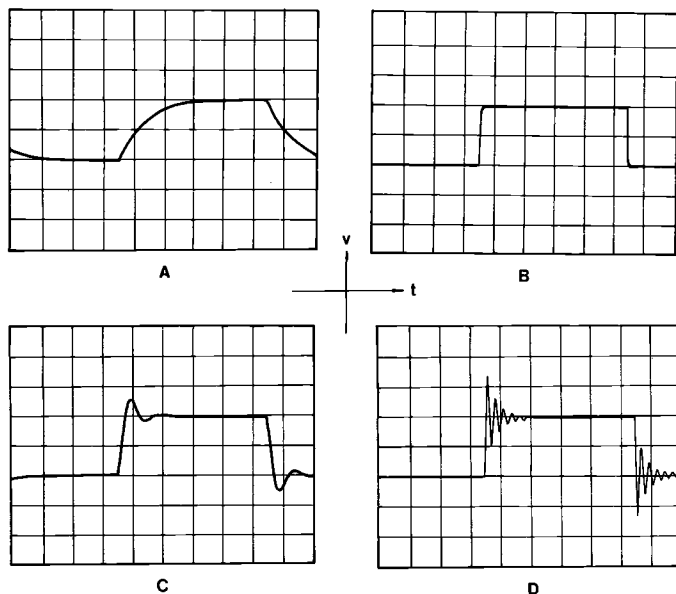


FIG. 4—Voltage response waveforms for evaluating the selection of the optimum bandwidth (schematic). (a) Bandwidth too narrow and overdamped, (b) Optimum bandwidth and an ideal response, (c) Bandwidth close to optimum and underdamped, and (d) Bandwidth too wide and excessive ringing.

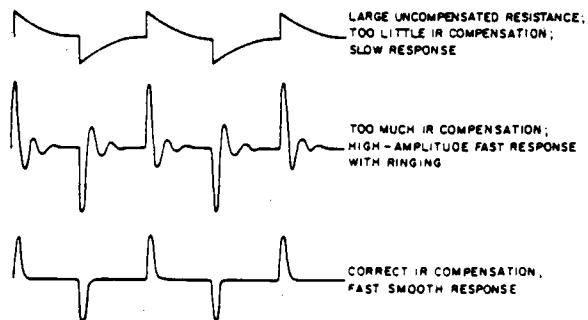


FIG. 5—Current output waveforms for the compensation of the ohmic drop by the positive feedback technique (from Ref 17).

will make the compensation of the ohmic drop less accurate. The measurement needs to be stopped in order to adjust the potentiostat settings. A more serious problem occurs when  $R_u$  changes during the measurement. In this case, the ohmic drop cannot be compensated exactly because the preset value of  $R_{comp}$  is fixed in the potentiostat. If  $R_u$  decreases at a fixed  $R_{comp}$ , oscillations will occur due to overcompensation and the experiment has to be stopped. These problems can only be solved by the application of the interrupter technique.

*Tests with Dummy Cells*—Different dummy cells have been used for testing of the positive feedback technique with the two different potentiostats. The schematic of these dummy cells is shown in Fig. 6. The actual  $R_u$  of the dummy cell cannot be selected as the

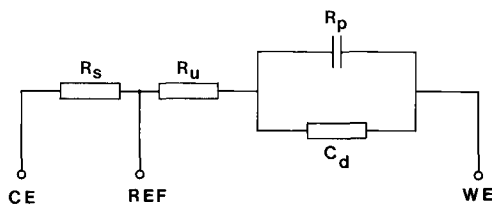


FIG. 6—Circuit schematic of the dummy cell.

preset  $R_{comp}$  in the PAR model 173 potentiostat because it will cause unstable operation. Therefore, the following procedure is suggested for the determination of the optimum value of  $R_{comp}$  when the positive feedback technique is used [17]:

- (1) Apply a constant electrode potential in the cathodic region.
- (2) Generate a small (for example, 10 to 50 mV peak-to-peak) square wave signal at 1 kHz or lower and add this to the applied potential. The frequency of the signal should be in the capacitive region of the system and give a response as shown in Fig. 5a.
- (3) Apply the positive feedback technique.
- (4) Select increasing values of  $R_{comp}$ .
- (5) Monitor the current-time trace of the electrode response from the current output of the potentiostat with the oscilloscope.
- (6) Adjust the preset value of  $R_{comp}$  to obtain the fast smooth response as shown in Fig. 5c.
- (7) If Step 6 does not succeed, lower the frequency of the applied signal.

The frequency of the square wave signal will determine the impedance of the cell and also affect the output current response waveform. In order to determine the optimum setting for the ohmic drop compensation from the current-time traces as shown in Fig. 5, the frequency of the square wave signal has to be selected within the capacitive region of the system. This frequency can be determined from the impedance spectrum for the system under study.

Experimental parameters and results of the tests with dummy cells and a PAR model 173 potentiostat are listed in Table 1. It was found that 90 to 95% compensation could be achieved with a fast, smooth current response. It was also observed that oscillations would occur at 100% ohmic drop compensation. For dummy cells with known parameters, the residual uncompensated resistance  $\Delta R$  can be calculated from the difference between the actual  $R_u$  and the applied  $R_{comp}$ . In addition, polarization resistance measurements can be carried out with and without compensation of the ohmic drop in order to evaluate the

TABLE 1—Maximum values of  $R_{comp}$  for dummy cell tests with positive feedback technique. (PAR model 173 potentiostat,  $E_{applied} = -100$  mV).

Number	$R_s$ ( $\Omega$ )	$R_u$ ( $\Omega$ )	$C_d$ ( $\mu$ F)	$R_p$ ( $\Omega$ )	$R_{comp}$ ( $\Omega$ )	Response
1	10k	1000	50	1000	950	correct
2	33k	3300	50	2200	3100	correct
3	11k	11k	50	11k	10k	correct
4	200k	20k	300	300k	19k	correct
5	100k	120k	300	300k	110k	correct

TABLE 2—*Experimental results of dummy cell tests for positive feedback technique in Solartron potentiostat (POL V = +100 mV and f = 50 Hz) ( $R_u = R_p = 1000 \Omega$ ,  $R_s = 10 R_u$ , and  $C_d = 50 \mu F$ ).*

Test Number	$R_{comp} \Omega$	$\Delta R^a \Omega$	BW Range <sup>b</sup>	$\Delta RE$ (mV)	$I$ (uA)	Response
1	0	1000	J to B	100	50	...
2	950	50	E & B	192	96	correct
3	975	25	E & B	195	97.6	correct
4	995	5	E & B	199	99.6	start ringing
5	1000	0	E & B	200	100	ringing
6	1050	-50	H to B	...	...	oscillation
7	1050	-50	J & I	214	108	ringing

<sup>a</sup>  $\Delta R = R_u - R_{comp}$ .

<sup>b</sup> Unity gain frequencies of the bandwidth BW are that: B (360 KHz), C (>1 MHz), E (24 KHz), F (8 KHz), G (2.4 KHz), H (800 Hz), I (80 Hz), J (8 Hz).

performance of the positive feedback technique. Since the experimental  $R'_p$  without compensation equals the sum of the true  $R_p$  and  $R_u$  ( $R'_p = R_p + R_u$ ) [1], the degree of compensation can be determined from the difference between the  $R'_p$ -values obtained with compensation and without compensation.

In the evaluation of the positive feedback technique with the Solartron model 1286 potentiostat, a dummy cell with  $R_u$  equal to 1 K $\Omega$  was used. The experimental parameters and results are listed in Table 2. The performance of the positive feedback technique was found to be determined by the preset value of  $R_{comp}$  and the bandwidth of the control amplifier in the potentiostat. Since the bandwidth of the control amplifier can be adjusted in this case, as a first step the optimum bandwidth has to be determined. The selection of the optimum bandwidth can be carried out by using a stimulus square wave with a frequency of 50 Hz. It was found that the optimum bandwidth should be two orders of magnitude higher than the frequency of the stimulus square wave in order to obtain the critical damped waveforms. When the positive feedback technique is applied, the optimum value of  $R_{comp}$  can be determined by the same procedures as for the PAR potentiostat. It was found that 99% compensation could be achieved with a fast, smooth current response for bandwidths between 24 kHz and 360 kHz. The current response would show ringing at 99.5% to 100% compensation. Overcompensation could also be obtained without oscillation when a narrow bandwidth of the control amplifier was selected. In this case, the current response waveforms were ringing (Fig. 5b) and an erroneous current value was observed.

### Interrupter Technique

**Background**—The application of the interrupter technique for the compensation of the ohmic drop has been discussed by several groups [3,18–20]. The principle of the interrupter technique can be described as follows. For a three-electrode cell, the potential difference between REF and WE is the sum of the ohmic drop  $IR_u$  and the electrode potential  $U_{we}$ . The ohmic drop vanishes immediately when the cell current is interrupted. The voltage-time relationship of the electrode response for the interrupter technique can be monitored with an oscilloscope from the voltage output of the potentiostat. The discharge of the double layer capacitance causes the decay of the electrode potential as shown in Fig. 7. The voltage spikes are caused by the switching of the interrupter. The ohmic drop  $IR_u$  can

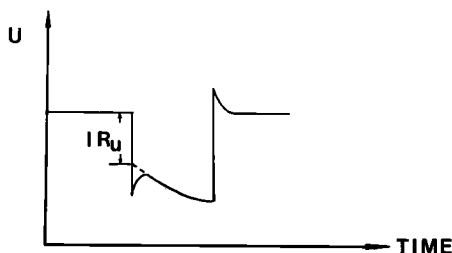


FIG. 7—Potential-time transients during the interrupter period.

be determined from the potential transient during the interrupter period. This ohmic drop can be immediately fed back to the potentiostat and then compensated using a positive feedback control loop. An alternative approach is the computer-assisted extrapolation method to determine the ohmic drop continuously and then compensate it after completion of the test [3,20].

The compensation of the ohmic drop with the interrupter technique can also be carried out in a different way [7,12,19,21]. Since the double layer capacitance usually takes a relatively long time to discharge with respect to the interruption time, the electrode potential  $U_{we}$  can be measured directly during the interrupter period. This electrode potential is sampled before the end of the current interruption and then fed back for comparison with the input polarization voltage ( $POL V$ ). A negative feedback control loop is applied to eliminate the error between  $POL V$  and  $U_{we}$  and keep the electrode potential stable. A circuit schematic and the block diagram of the negative feedback control loop are shown in Figs. 8a [12] and 8b. From the basic concepts of process control [22], it follows that the performance of the interrupter technique will be influenced by the following factors:

- (1) The bandwidth of the control amplifier.
- (2) The interrupter frequency.
- (3) The impedance of the test electrode.
- (4) The characteristics of the reference electrode.

When the ohmic drop is compensated with the interrupter technique, 100% compensation can be achieved in certain frequency regions so that the system shows the behavior which is similar to that of a cell without  $R_u$  [7]. The stability and the accuracy of the interrupter technique will be affected by the bandwidth of the control amplifier and the impedance of the test electrode. Since bandwidth is a description of the control amplifier response as a function of frequency and the impedance of the test electrode is frequency dependent, the measurement frequency becomes an important factor for the interrupter technique. The analysis of these factors will be discussed in the following paragraphs in detail.

*Interrupter Frequency and Potentiostat Bandwidth*—The proper selection of the interrupter frequency is a very important factor for the correct compensation of the ohmic drop. The interrupter frequency equals the inverse of the interrupter period which is the time  $t_{on} + t_{off}$  for an interrupter cycle (Fig. 9) [12]. According to signal and system theory [23], the potential transient of the electrode is determined by the impedance of the electrode and the interrupter frequency. If the interrupter period is selected to be short enough, the electrode response will only show pure resistive behavior. The decay of the electrode potential due to double layer discharge will not occur and a plateau of the voltage-time relationship can be observed on the oscilloscope as shown in Fig. 10b. In this manner, the ohmic drop and the true electrode potential can be determined accurately. For the selection of the inter-

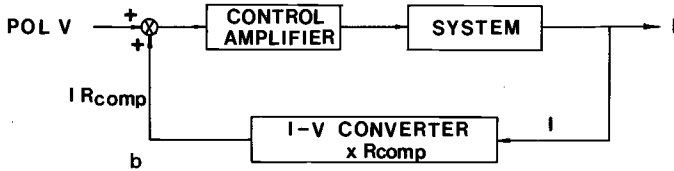
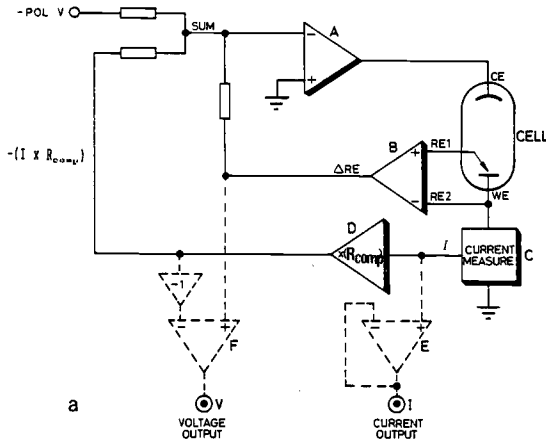


FIG. 8—(a) Circuit schematic of the interrupter technique (from Ref 12) and (b) block diagram of the negative feedback control loop.

rupter frequency in different frequency regions of the impedance spectrum, which is shown schematically in Fig. 10, the potential-time traces are also shown in Fig. 10. From these potential-time traces, it can be concluded that an erroneous value of the ohmic drop will be obtained when the interrupter frequency is selected at very high frequencies where a phase shift occurs (Region A). The optimum interrupter frequency has to be selected in the frequency Region B where the impedance is determined by  $R_u$ . The lower frequency limit of this region can be calculated from the break-point frequency,  $f_b$  [4]

$$f_b = \frac{1}{4\pi R_u C_d} \left( 1 + \frac{1}{R_p} \sqrt{R_p^2 - 4R_u R_p - 4R_u^2} \right) \quad (1a)$$

which can be simplified to

$$f_b = (2\pi R_u C_d)^{-1}, \text{ if } R_p \gg R_u. \quad (1b)$$

For the dummy cell used in Tables 2 and 3 this value is about 3 Hz (Eq 1). It can be seen from Eq 1 that the resistive region increases when the solution conductivity decreases.

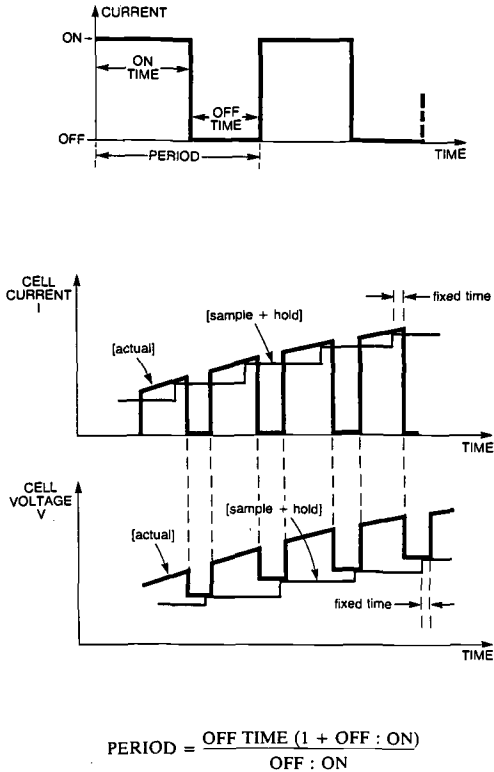


FIG. 9—Interrupter current and voltage waveforms (from Ref. 12).

Since the values of  $R_u$  and  $C_d$  determine the range of this region, the optimum interrupter frequency will vary from system to system. When the interrupter frequency is selected in the frequency region between C and D where the impedance shows capacitive behavior (Fig. 10), the electrode potential will decay during the interrupter period. In this case, the true electrode potential cannot be determined accurately by sampling the data  $5\mu\text{s}$  before the end of the interrupter period in the Solartron potentiostat and the ohmic drop will not be correctly compensated at this interrupter frequency.

Since the frequency dependence of the impedance of the cell can be determined from EIS, it is possible to select the interrupter frequency in a frequency region where no phase shift occurs and where only an ohmic component  $R_u$  determines the measured impedance. The interrupter time and the ratio of the current-off to the current-on times can then be adjusted to select the optimum interrupter frequency. As a result, the electrode potential can be sampled without errors caused by the discharge of the double layer. The value of  $R_{\text{comp}}$  is calculated from the ratio of the ohmic drop measured on the oscilloscope and the measured cell current ("Sample + Hold" mode). The value of  $\Delta RE$  measured in the "Sample + Hold" mode (Fig. 9) has to be equal to the applied potential  $POL V$  for 100% compensation (Table 3).

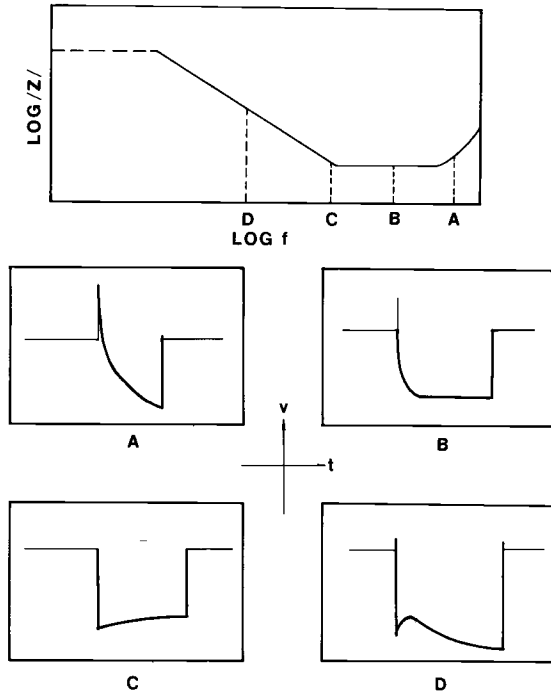


FIG. 10—Impedance spectra and the corresponding potential-time traces for the interrupter technique. (a) phase shift region, (b) resistive region, (c) resistive and capacitive region, and (d) capacitive region.

TABLE 3—Experimental results of dummy cell tests for interrupter technique with Solartron potentiostat (POL V = +100 mV) ( $R_u = R_p = 1000 \Omega$ ,  $R_s = 10 R_u$ , and  $C_d = 50 \mu\text{F}$ ).

Test Number	Off-time (msec)	On:Off Ratio	$f_{\text{int}}$ (Hz) <sup>a</sup>	BW Type	$\Delta RE$ (mV)	$I$ ( $\mu\text{A}$ )	$R'_u \Omega$	$R'_p \Omega$	Response
1	0.027	1	18 500	B	100.6	173.0	983	1163	...
2	0.1	1	5 000	B	99.7	192.2	1041	1037	...
3	0.5	1	1 000	B	97.5	189.9	1027	1027	...
4	1.0	1	500	B	97.9	195.4	1024	1002	...
5	0.027	9	3 700	B	87.5	89.0	1011	1092	...
6	0.1	9	1 000	B	93.2	101.9	1030	1016	correct
7 <sup>b</sup>	0.27	9	350	B	96.8	107.8	1020	998	correct
8 <sup>b</sup>	0.5	9	200	B	97.8	109.9	1001	989	correct
9	0.5	9	200	I	65.8	73.6	1050	993	...
10	1.0	9	100	B	98.3	111.1	1000	983	...
11	1.0	9	100	I	71.9	81.0	1049	986	...
12	0.27	99	37	B	95.6	97.8	1022	987	...
13	0.5	99	20	G	91.4	93.8	1013	984	...
14 <sup>c</sup>	1.0	99	10	G	99.5	102	1000	985	...
15	1.0	99	10	F					oscillation

<sup>a</sup>  $f_{\text{int}}$  is the interrupter frequency.

<sup>b</sup> Recommended parameters.

Note: The measured current  $I$  has to be multiplied by the correction factor CCF ( $R'_p = \Delta RE/I \times \text{CCF}$ ). Current Correction Factor:  $\text{CCF} = \frac{1}{t_{\text{OFF}}/t_{\text{ON}} + 1}$ .

*Tests with Dummy Cells*—A Solartron model 1286 potentiostat was used to evaluate the performance of the interrupter technique. Two different ways of data output can be selected in the potentiostat. One is the “Actual” mode and the other is the “Sample + Hold” mode (Fig. 9). In the “Actual” mode, the output of current and potential is the interrupted waveform which consist of a series of pulses. The voltage-time trace of the electrode response can be monitored with an oscilloscope. The potential difference  $\Delta RE$  is the sum of the ohmic drop and the electrode potential. In the “Sample + Hold” mode, the electrode potential is sampled  $5 \mu\text{s}$  before the end of the current interruption period. The reading of the potential difference  $\Delta RE$  is the sampled electrode potential. The measured cell current has to be corrected by a current correction factor ( $CCF$ ) due to the recharging of the double layer capacitance [12]. The  $CCF$  is calculated by the ratio of the current-on time  $t_{\text{on}}$  to the interrupter period ( $CCF = t_{\text{on}}/(t_{\text{on}} + t_{\text{off}})$ ). The control potential error can be determined by the difference between the values of  $\Delta RE$  and  $POL V$  in the “Sample + Hold” mode.

As a result of tests with dummy cells, the following experimental procedure for the determination of the proper bandwidth and the interrupter frequency has been established:

- (1) Use the shortest interrupter time ( $27 \mu\text{s}$ ) and start at an on:off ratio of 1:1.<sup>2</sup>
- (2) Select the bandwidth  $BW$  of the potentiostat considering that the unity gain of  $BW$  has to be larger than the interrupter frequency.
- (3) Apply a constant cathodic potential.
- (4) Apply the interrupter technique in the “Actual” mode.
- (5) Monitor the potential-time trace from the voltage output with the oscilloscope.
- (6) Adjust the interrupter frequency by increasing the interrupter time to obtain an ideal response with a plateau in the potential-time trace (Fig. 10b).
- (7) If ideal response is not obtained, increase on:off ratio.
- (8) Change to the “Sample + Hold” mode.
- (9) Read the sampled electrode potential  $\Delta RE$  in the “Sample + Hold” mode and compare with the input value of  $POL V$ .
- (10) Increase the bandwidth of the potentiostat to reduce the difference between the true electrode potential  $\Delta RE$  and  $POL V$  without causing oscillations.

A dummy cell with  $R_u = 1000 \Omega$  was used for the testing of the interrupter technique. The tests were carried out at a constant potential of  $-100 \text{ mV}$ . The interrupter frequency was selected in different frequency regions where the impedance of the electrode shows phase shift, pure resistive or capacitive behavior. The experimental results for these tests are listed in Table 3. When an interrupter frequency was selected in the pure resistive region (for example, 20 000 to 100 Hz), a plateau of the potential-time trace as in Fig. 10b was obtained during the interrupter period. The experimental value of  $Ru^*$  was calculated from the ratio of the ohmic drop  $\Delta V$  and cell current  $I$  in the “Sample + Hold” mode. This should be equal to the actual  $Ru$  in order to obtain the correct compensation of the ohmic drop. The sampled true electrode potential during current interruption was the reading of  $\Delta RE$  in the “sample + hold” mode as in Table 3. A control potential error between input  $POL V$  and  $\Delta RE$  was observed when a narrow bandwidth such as  $I(80 \text{ Hz})$  had been selected. It was reduced by increasing the potentiostat bandwidth to  $B(360 \text{ kHz})$  at an

<sup>2</sup> Although the manufacturer of this instrument suggests using an on:off ratio of 1:1, the ratio should never be less than 10:1, and ratios in the range of 1000:1 are quite satisfactory for adequate measurement of the IR component. Large on to off times insures the minimum disturbance of the polarization of the working electrode.

interrupter frequency of 200 Hz or 100 Hz (Tests 8 to 11). Selecting a lower interrupter frequency such as 10 Hz (Tests 14 to 15) reduced the stability margin and caused oscillations. At 10 Hz the maximum bandwidth was  $G$  (2.4 kHz). Since 10 Hz is located in the capacitive region, the correct potential-time trace such as shown in Fig. 10*b* was not observed. The optimum interrupter frequency was found to be between 200 Hz to 1000 Hz (Tests 6 to 8).

The performance of the interrupter technique has also been evaluated by polarization resistance measurements. The compensation resistance  $R_{\text{comp}}$  can be determined from the difference between the  $R'_p$  values obtained with and without the compensation of the ohmic drop. A number of dummy cells have been used for these tests. The dummy cell parameters and the experimental results for  $R_{\text{comp}}$  are listed in Table 4. It was found that the performance of the interrupter technique was very good except at high value of  $R_s$  and  $R_u$ , where it was limited by excessive noise (Test 7).

*Choice of the Reference Electrode*—The proper selection of the reference electrode is a very important factor not only for the interrupter technique, but also for the accurate determination of the electrode potential in low conductivity media [24,25]. The aqueous calomel electrode (SCE) is commonly used in aqueous media. In nonaqueous media, the SCE is not suitable because of the drift of potential and the crystallization of potassium chloride (KCl) of the aqueous-nonaqueous liquid junction. A platinum wire can be used as reference electrode, but its redox potential is not stable in the deaerated ethanolic HCl solutions which serve as model systems in the present study. The silver-silver chloride reference electrode is preferred in nonaqueous media containing chloride ion because a relatively stable potential can be obtained.

A problem which has not been recognized widely until now is due to the high-frequency phase shift resulting from the slow response of the SCE which limits the available interrupter frequency range (see Fig. 10). The platinum wire and the silver-silver chloride (Ag/AgCl) wire have faster response and the high-frequency phase shift can, therefore, be reduced. It was also found in this study that the wire electrodes produce better performance of the interrupter technique due to the faster response for changes of the electrode potential. As shown earlier, using the SCE coupled to a platinum wire by a small capacitor can reduce the high-frequency phase shift [26] in impedance measurements, but it was found in this study that it can cause instability problems in the use of the interrupter technique. For optimum performance of the interrupter technique it is therefore necessary to use wire electrodes such as Ag/AgCl or Pt as *REF*.

### Experimental Results

Based on the procedures which were developed in the dummy cell tests, potentiodynamic polarization curves have been recorded for 1018 carbon steel and 430 stainless

TABLE 4—*Experimental results of polarization tests with dummy cells using interrupter technique with Solartron potentiostat.*

Number	$R_s$ ( $\Omega$ )	$R_u$ ( $\Omega$ )	$C_d$ ( $\mu F$ )	$R_p$ ( $\Omega$ )	$R_{\text{comp}}$ ( $\Omega$ )
1	10k	1k	50	1k	1k
2	33k	3.3k	50	2.2k	3.3k
3	11k	11k	50	11k	11k
4	22k	14.3k	50	2.2k	14.1k
5	10k	100k	100	100k	100k
6	300k	100k	300	100M	100k
7	2.2M	100k	300	2.2M	excessive noise

steel in ethanolic HCl solutions with compensation of the ohmic drop by the positive feedback and interrupter techniques. EIS measurements were applied first in order to determine the optimum parameters for the interrupter technique. The performance of the interrupter technique was then evaluated by polarization resistance measurements with and without compensation of the ohmic drop. The corrosion kinetics of 304 stainless steel in hydrazine have been studied in the same manner.

*Preliminary Tests*

*Choice of REF*—The effects of the type of reference electrode on the performance of the interrupter technique was studied for three types of reference electrodes. The SCE, a Pt wire and a Ag/AgCl wire electrode were used for SS430 in  $10^{-3}$  N ethanolic HCl. The  $R_u$  value for  $10^{-3}$  N was  $1.54 \Omega$  as determined from EIS-data. The potential-time traces were recorded from the oscilloscope by using a CRT camera (Fig. 11). The values of  $R_u$  were

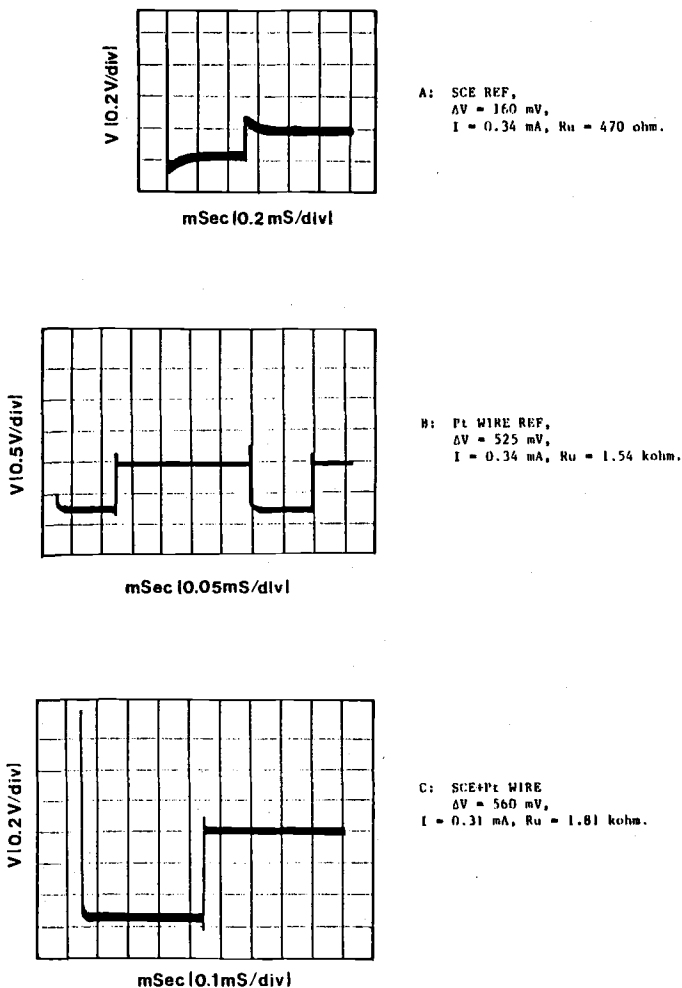


FIG. 11—Interrupter traces for SS430 in  $10^{-3}$  N ethanolic HCl using different reference electrodes.

calculated from these potential-time traces. Curve *A* for the SCE showed an inadequate potential-time response and only about  $\frac{1}{2}$  of the correct value of  $R_u$ . When a Pt wire was coupled to the SCE with a small capacitor, the potential-time trace showed the correct response, but an erroneous  $R_u$  was obtained from curve *C*. This result shows that observation of a "correct" interrupter trace alone does not necessarily guarantee accurate compensation. Only the narrowest bandwidth  $J(8 \text{ Hz})$  could be selected in this case. This is due to the phase shift of the SCE which reduces the stable phase margin. A Pt wire or a Ag/AgCl wire as the reference electrode produced the perfect potential-wire trace as shown in curve *B* and a correct value of  $R_u$ . The selection of a wire electrode as *REF* is therefore necessary for the interrupter technique in these solutions. This restriction has not been recognized in most published reports.

*Positive Feedback Technique and Numerical Analysis*—Anodic polarization curves for SS430 in  $10^{-4} \text{ N}$  ethanolic HCl are shown in Fig. 12. A Pt wire was used as the reference electrode. Curve 1 is the polarization curve which was recorded without the compensation of the ohmic drop. Curve 2 was recorded with the positive feedback technique using the PAR 173 potentiostat. Curve 3 was obtained by numerical subtraction of the ohmic drop from Curve 1 using a  $R_u$  value equal to  $15 \text{ k}\Omega$  which was estimated from EIS data determined at the beginning of the experiment. Curve 4 was obtained from Curve 2 after subtraction of the residual ohmic drop ( $R_u = 3.4 \text{ k}\Omega$ ) which was determined by plotting the potential difference between Curve 2 and a hypothetical Tafel line versus the current. The fact that all points fell on a straight line which went through the origin shows that the Tafel line was drawn correctly and that the potential difference was indeed due to residual ohmic

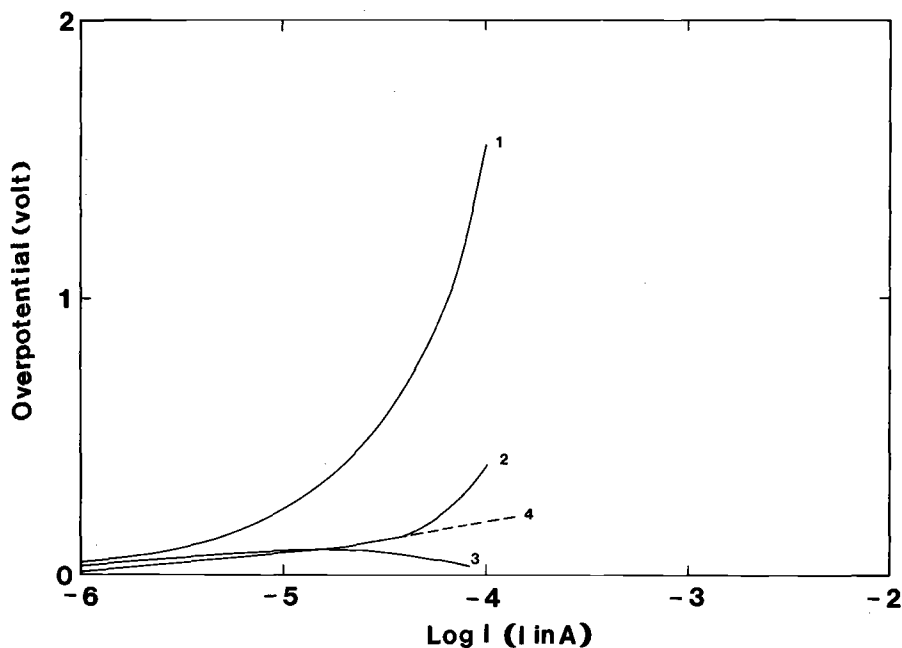


FIG. 12—Anodic polarization curves for SS430 in  $10^{-4} \text{ N}$  ethanolic HCl recorded with and without compensation. (1) uncompensated, (2) positive feedback, (3) numerical subtraction of the ohmic drop from Curve 1, and (4) numerical subtraction of the residual ohmic drop from Curve 2.

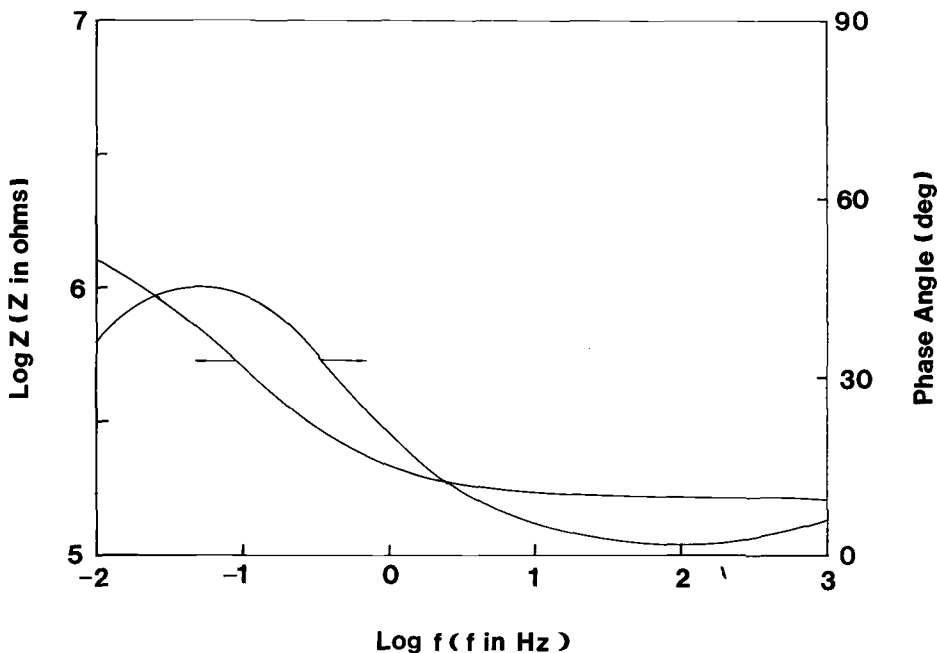


FIG. 13—Bode-plots for SS304L in  $10^{-4}$  N ethanolic HCl.

drop. This result can be understood when it is considered that it is not possible to compensate 100% of the ohmic drop using the PAR model 173 potentiostat. The  $R_u$  value decreased during recording of the polarization curve due to anodic dissolution of the electrode and as a result Curve 3 is overcompensated as indicated by the bending of the curve in the cathodic direction. From the results in Fig. 12, one can see that a fixed value of  $R_{comp}$  can distort the polarization curves since 100% compensation is not possible. Numerical subtraction of the ohmic drop using a constant value of  $R_{comp}$  can produce errors particularly in anodic polarization. These are disadvantages of the positive feedback technique.

*Effect of Electrode Area*—A small test cell with a SS304L working electrode of  $0.06 \text{ cm}^2$  surface area, a large counter Pt electrode and a planar Pt reference electrode with  $0.2 \text{ cm}^2$  surface area was used in  $10^{-4}$  N ethanolic HCl deaerated by pure argon for the initial tests of cell performance. For the EIS measurements (Fig. 13), the current-measuring resistor  $R_m$  was set at  $100 \text{ k}\Omega$  and the galvanostatic mode was used in the low-frequency region in order to avoid the problems due to polarization of the electrode resulting from a shift of  $E_{corr}$  during the measurement. This approach improves the EIS data in the low frequency region to a certain extent [27]. Since the imaginary part of the impedance ( $Z_{imag}$ ) in the EIS data does not reach a maximum value in the measured frequency range, the integration method [28] could not be used to obtain  $R_p$  and  $C_d$ . New fitting procedures are under development to calculate  $R_p$  and  $C_d$  from EIS data of systems which have very low corrosion rates [29].

The potential-time traces for different interrupter frequencies which fall into the resistive region of the spectra in Fig. 13 are shown in Fig. 14, which shows that the  $R_u$  values determined from these traces are very similar for three interrupter frequencies. This is due to the choice of interrupter frequencies which are in the pure resistance range. The  $R_u$  values at 380Hz, 80Hz and 75Hz are all about  $130 \text{ k}\Omega$ . There is minimal phase shift at these

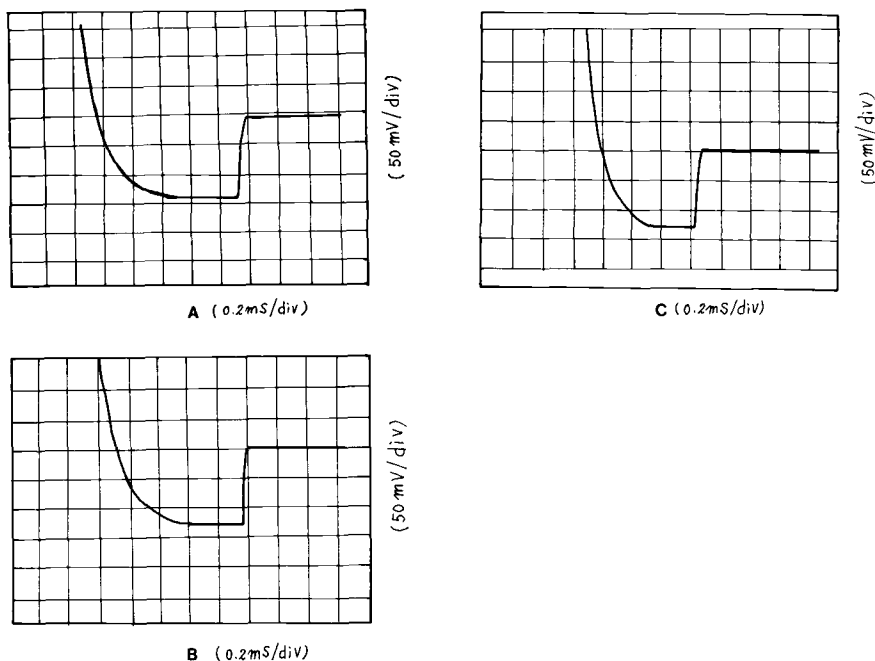


FIG. 14—Potential-time traces for SS304L in  $10^{-4}$  N ethanolic HCl with different interrupter frequencies (a)  $f_{int} = 380$  Hz, (b)  $f_{int} = 80$  Hz, and (c)  $f_{int} = 75$  Hz.

frequencies (Fig. 13). The  $R_u$  values determined from EIS (158 k $\Omega$ ) and from the voltage-time traces are of the same order. Therefore, in this frequency region, adequate ohmic drop compensation (above 82%) can be obtained.

The effects of electrode size have also been investigated. Typical results show that a small size electrode will make EIS measurements and the interrupter technique more difficult to perform. For SS430 with 0.6 cm<sup>2</sup> surface area impedance values in the order of  $6 \times 10^6 \Omega$  at  $10^{-2}$  Hz and  $R_u$  values in the order of 120 k $\Omega$  were obtained in  $10^{-4}$  N ethanolic HCl. Due to these large impedances, the spectra showed large scatter at low frequencies. This situation will make the compensation of the ohmic drop more difficult. On the contrary, SS430 with 4.6 cm<sup>2</sup> surface area gave only  $1 \cdot 10^5 \Omega$  at  $10^{-2}$  Hz and  $R_u = 800 \Omega$ . The impedance spectra for the two electrode sizes are shown in Fig. 15. Based on these results relatively large electrodes are recommended although it is realized that the maximum current density possible in polarization experiments will decrease when large WEs are used.

#### 1018 Carbon Steel in Ethanolic HCl

Electrochemical impedance spectra for 1018 carbon steel in  $10^{-1}$  N,  $10^{-2}$  N,  $10^{-3}$  N, and  $10^{-4}$  N ethanolic HCl solutions were recorded after one hour immersion. The working electrode was a cylindrical rod with a surface area of 4.6 cm<sup>2</sup>. The electrode was prepared according to standard steps which include wet polishing continuously up to 600 grit, degreasing in hot hexane, and rinsing with distilled water. The PAR model K0047 Corrosion Cell and a SCE were used for these initial tests which were carried out before a more

detailed investigation revealed the problems which can occur when a SCE is used as *REF* in the impedance and interrupter techniques (see Choice of Reference Electrode). The impedance spectra are plotted as Bode-plots in Fig. 16. The value of  $R_u$  and the suitable interrupter frequency ranges can be obtained from these impedance spectra. The interrupter frequencies for each solution are selected in the high frequency ranges in which the phase angle is zero. These frequency ranges are limited by phase shift at high frequencies and the start of the capacitive region at lower frequencies. As the conductivity of the electrolyte becomes smaller, the phase shift becomes more serious so that the determination of the suitable interrupter frequency becomes more difficult. The spectra in Fig. 16 show that for all four solutions  $R_u$  and  $R_p$  have values of the same order of magnitude. The experimental values of  $R_u$  and  $R_p$  determined from these EIS measurements are listed in Table 5.

Polarization resistance measurements have been used for evaluation of the interrupter technique in these low conductivity solutions. The polarization resistance was determined with and without compensation of the ohmic drop using a potential scan from  $-30$  mV to  $+30$  mV through the corrosion potential  $E_{corr}$  at a scan rate of  $10$  mV/min. The current was plotted versus the applied potential  $POL$   $V$  in the "Sample + Hold" mode during the measurements. The  $R'_p$  values were determined from the slope of the curves at  $E_{corr}$ . The  $R_u$  values determined from the potential-time traces on the oscilloscope are compared with  $R_{comp}$ , which is the difference of the  $R_p$  values determined with ( $R_p$ ) and without ( $R'_p$ ) the compensation of the ohmic drop ( $R_{comp} = R'_p - R_p$ ). The residual uncompensated resistance ( $\Delta R$ ) is the difference between  $R_u$  and  $R_{comp}$  (Table 5). Since the determination of the optimum interrupter parameters is a trial-and-error method, only some typical results of the evaluation of the interrupter parameters are listed in Table 5. The experimental results

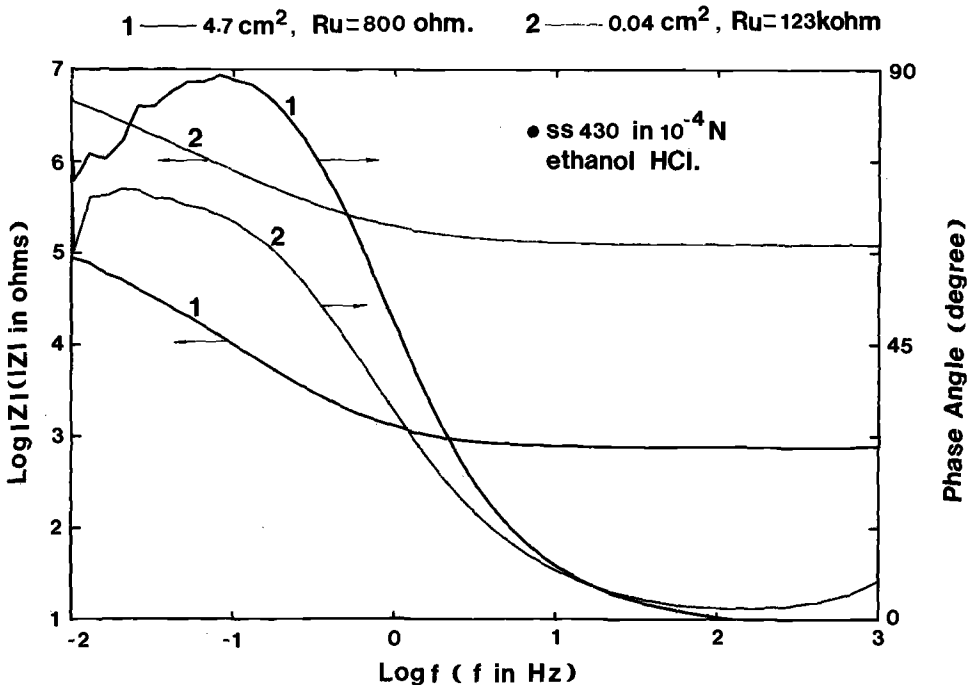


FIG. 15—Effect of electrode area on the magnitude of the impedance and the phase angle.

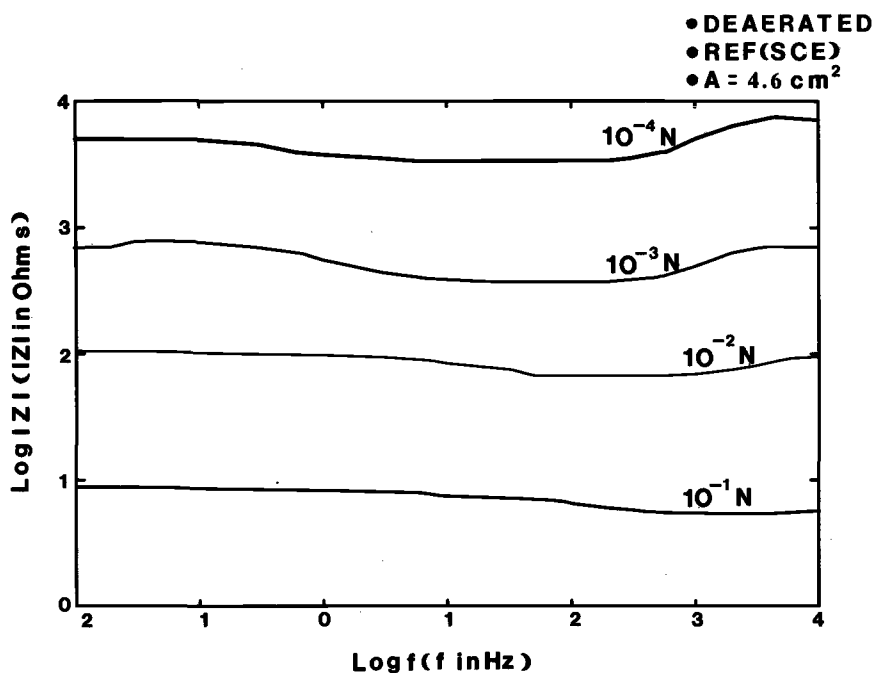


FIG. 16—Electrochemical impedance spectra for 1018 carbon steel in deaerated ethanolic HCl.

TABLE 5—Experimental results of EIS and polarization resistance measurements for 1018 carbon steel in ethanolic HCl.

HCl Conc. (N)	$R_u$ (EIS) $\Omega$	$R_p$ (EIS) $\Omega$	$R_u$ (trace) $\Omega$	$f_{int}^a$ (Hz)	BW Type	$R_{comp}$ $\Omega$	$\Delta R$ $\Omega$	$R'_p$ $\Omega$	$R_p$ $\Omega$
0.1	5.6	3.0	5.2	2000	C	5.5	- 0.3	8.1	2.6
0.01	36	39	36	250	F	49.0	- 13	64	15
0.001	360	448	360	100	I	232	128	429	197
0.0001	3350	1750	2780	100	H	3525	-745	4375	850
0.0001	3350	1750	3300	42	H	3230	70	4375	1145

<sup>a</sup>  $f_{int}$  is the interrupter frequency.

show that the compensation of the ohmic drop was very good for  $10^{-1}$  N ethanolic HCl, but overcompensation was observed for  $10^{-2}$  N HCl and  $10^{-4}$  N HCl and undercompensation for  $10^{-3}$  N HCl. Apparently the potentiostat bandwidth F(8 kHz) used for  $10^{-2}$  N HCl was too wide such that overcompensation occurred, while for  $10^{-3}$  N HCl it was too narrow (I 180 Hz) leading to undercompensation. In the case of  $10^{-4}$  N HCl, selecting a narrower bandwidth such as I or a lower interrupter frequency could have produced more satisfactory results. It was concluded that the optimum settings for the interrupter technique in these solutions need to be determined very carefully in further experiments in order to fully compensate the ohmic drop. The optimum values for the off-time, on-off ratio and potentiostat bandwidth for these solutions are listed in Table 6, which also includes the value of the measuring resistor  $R_m$  which was used in each measurement.

TABLE 6—Optimum experimental parameters for the interrupter technique (1018 carbon steel in ethanolic HCl).

HCl Conc. (N)	$R_m$ ( $\Omega$ )	Off-time (msec)	On:Off Ratio	$f_{int}$ (Hz)	BW Type	Frequency of BW (Hz)
0.1	1	0.05	9	2000	C	>1 M
0.01	10	0.4	9	250	G	2.4 k
0.001	10	1.1	9	91	I	80
0.0001	1000	1.0	9	100	I	80

For the same systems, potentiodynamic polarization curves have been recorded with continuous compensation of the ohmic drop by the interrupter technique (Fig. 17). Cathodic limiting currents  $I_{lim}$  which increase with the HCl concentration were obtained for the four solutions. A pitting potential  $E_{pit}$  was observed for  $10^{-1}$  N and  $10^{-2}$  N HCl. At the lower concentrations, the pitting potential can only be determined when the ohmic drop is fully compensated which was not possible with the experimental approach used in these tests. The polarization curves also provide information concerning the corrosion kinetics of the systems. Corrosion rates were estimated by Tafel extrapolation from the polarization curves for those cases where full compensation of the ohmic drop was possible. The experimental results are listed in Table 7. The polarization curves show that the cathodic reaction is under mass transport control of the hydrogen ion.

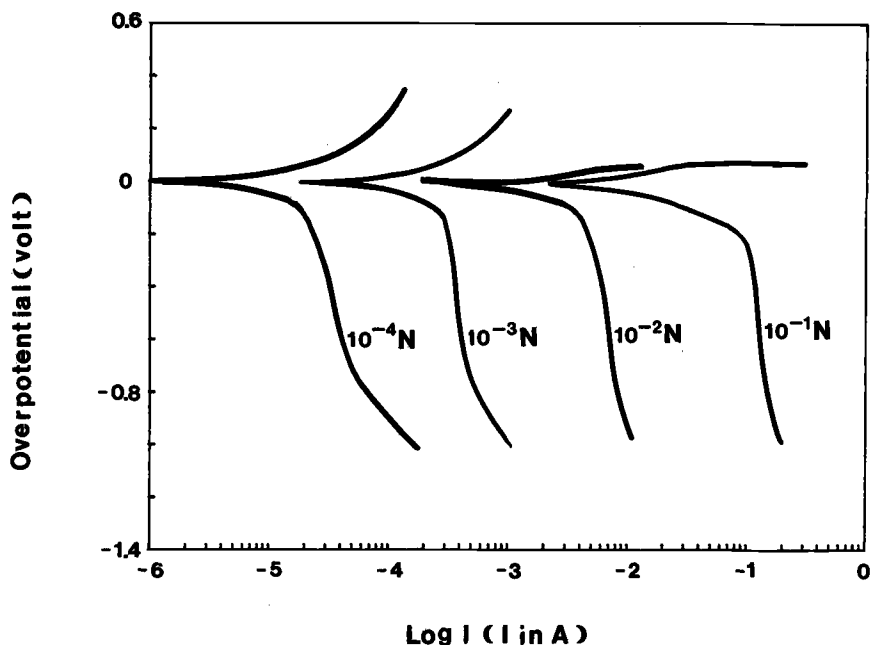


FIG. 17—Potentiodynamic polarization curves recorded with the interrupter technique for 1018 carbon steel in ethanolic HCl.

TABLE 7—Analysis of potentiodynamic polarization curves for 1018 carbon steel in ethanolic HCl (SCE as REF).

HCl Conc. (N)	$E_{\text{corr}}$ (mV)	$I_{\text{lim}}$ (mA/cm <sup>2</sup> )	$E_{\text{pit}}$ (mV)	Corrosion Rate (mm/y)
0.1	-465	29.0	-286	25.8
0.01	-486	1.56	-310	1.0
0.001	-500	0.082	... <sup>a</sup>	0.10
0.0001	-630	0.0073	... <sup>a</sup>	0.008

<sup>a</sup> The pitting potential could not be determined.

### Stainless Steel in Ethanolic HCl

The EIS data for SS430 in the four ethanolic HCl are shown in Fig. 18. The high-frequency phase shift was eliminated using a Pt wire as the reference electrode. This results in a very wide frequency range for the interrupter frequency which increases with increasing  $R_w$ . The results of the evaluation of the interrupter parameters by EIS measurements and polarization resistance measurements are listed in Table 8. The reference electrodes were SCE or a Pt wire. When a SCE was used as the REF, the performance of the interrupter technique was not satisfactory because of the slow response of the SCE. The overcompensation of the ohmic drop for  $10^{-3}$  N HCl is due to the selection of an interrupter frequency which was too high (3.3 kHz). The undercompensation of the ohmic drop for  $10^{-4}$  N HCl is due to the selection of a too narrow bandwidth ( $J(8$  Hz)). Therefore, a wide bandwidth ( $H(800$  Hz)) was selected in the measurement of polarization curves.

Table 8 shows a large discrepancy between the  $R_p$  values determined from the impedance spectra ( $R_p(\text{EIS})$ ) and the polarization curve recorded with compensation of the ohmic drop ( $R_p$ ). Several factors can contribute to this problem. As shown in Fig. 18b, the dc limit of the impedance was not reached even at 0.3 mHz. In addition, the slope of the curve in the capacitance region is  $-0.7$  which suggests that the simple model used in the analysis of this curve with the integration method (Table 8) might not be valid. The inhomogeneous surface model [30] seems to be more appropriate in the determination of  $R_p$  which was too fast. As shown elsewhere [31] the maximum scan rate  $s_{\text{max}}$  can be calculated from the lower break-point frequency  $f_b^1$  in the impedance diagram and the peak-to-peak amplitude  $\Delta E$  of the scan. For the case in Fig. 18b,  $f_b^1$  is about 1 mHz and  $\Delta E = 30$  mV, which results in  $s_{\text{max}} = 0.01$  mV/s. The scan rate used in the present tests was 0.17 mV/s which is close to the lowest scan rate of 0.1 mV/s available in the potentiostat. Since it is therefore not possible to apply the scan rate  $s_{\text{max}} = 0.01$  mV/s which would result in an accurate value of  $R_p$ , the experimental  $R_p'$  values will always be too small. The discrepancy in Table 8 is most likely due to both problems. This discussion shows the difficulties which can arise in media of low conductivity and low corrosivity.

Polarization curves have been recorded with automatic and continuous compensation of the ohmic drop by the interrupter technique (Fig. 19). The experimental parameters for the interrupter settings and bandwidths are listed in Table 9. The values of  $I_{\text{lim}}$ ,  $E_{\text{pit}}$ , and the corrosion rates which were determined from these curves are listed in Table 10. A pitting potential could not be observed in  $10^{-4}$  N HCl due to the distortion of the polarization curve by the residual ohmic drop.

The dependence of the cathodic limiting current  $I_{\text{lim}}$  on the concentration of HCl in ethanol is shown in Fig. 20, where a linear relationship is found between  $\log I_{\text{lim}}$  and  $\log$  con-

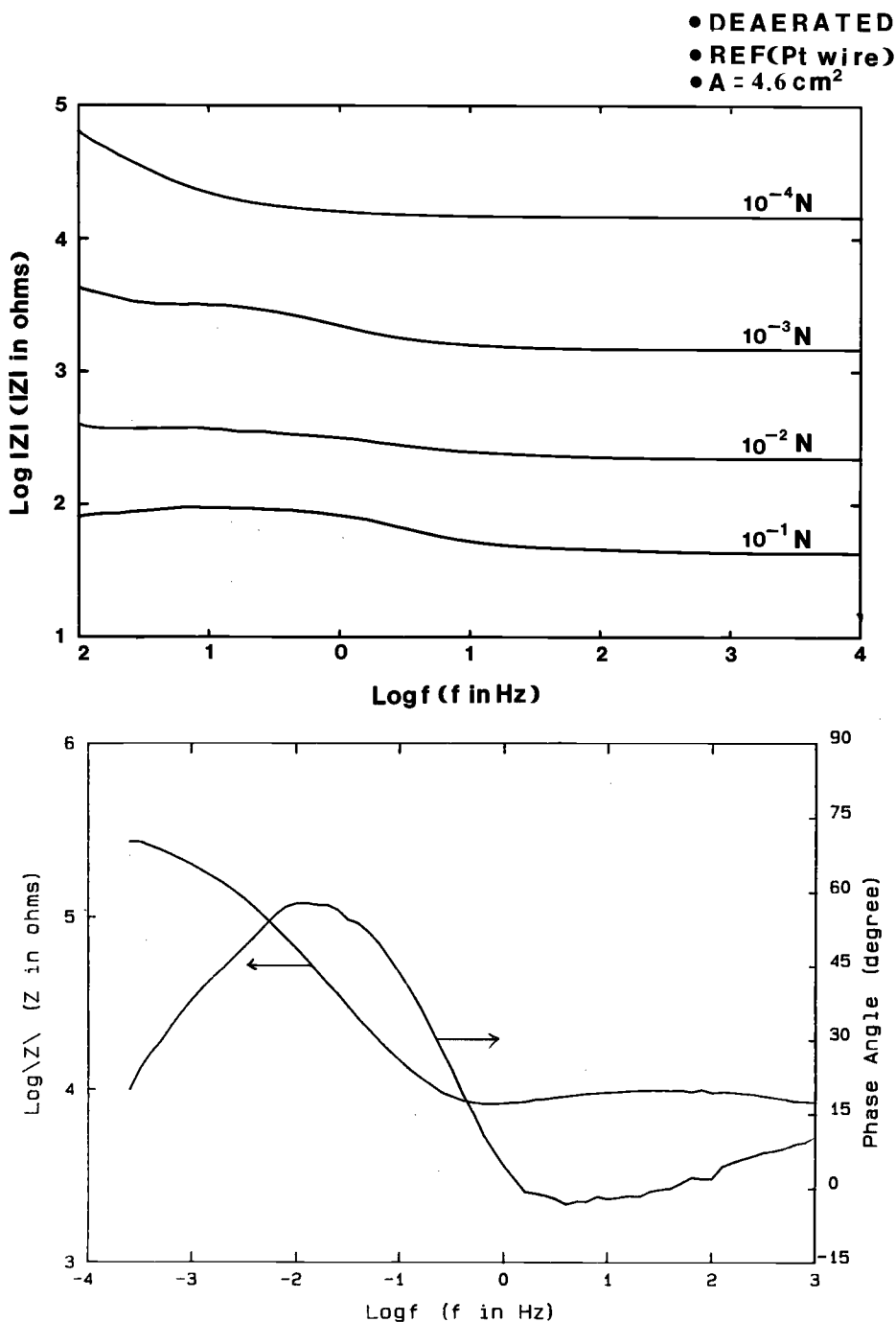


FIG. 18—Electrochemical impedance spectra for SS430 in deaerated ethanolic HCl. (a) for four concentrations of HCl and (b) for  $10^{-4}$  N HCl/EtOH with extended low frequency range.

TABLE 8—Experimental results of EIS measurements and polarization resistance measurements for SS430 in ethanolic HCl.

HCl Conc. (N)	REF	$R_u$ (EIS) $\Omega$	$R_p$ (EIS) $\Omega$	$R_u$ (trace) $\Omega$	$f_{int}$ (Hz)	BW Type	$R_{comp}$ $\Omega$	$\Delta R$ $\Omega$	$R'_p$	$R_p$
0.1	SCE	10.6	7.4	10.0	250	E	10.8	-0.8	17.5	6.7
0.01	SCE	224	152	60.0	100	G	29.0	31.0	86	57
0.001	Pt	1 530	1660	1 530	3330	E	2250	-720	5 840	3 590
0.0001	Pt	10 500	17K	10 500	200	J	5900	4600	29 700	23 800

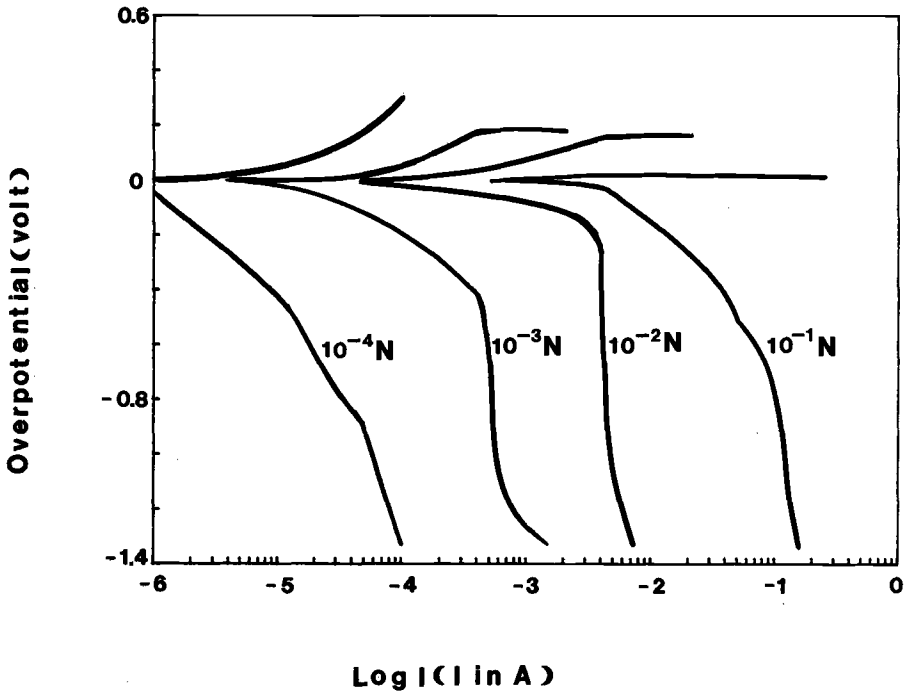


FIG. 19—Potentiodynamic polarization curves obtained with the interrupter technique for SS430 in ethanolic HCl solutions.

TABLE 9—Experimental parameters of the recording of the potentiodynamic polarization curves with the interrupter technique for SS430 in ethanolic HCl.

HCl Conc. (N)	$R_m$ $\Omega$	$t_{off}$ (msec)	On:Off Ratio	$f_{int}$ (Hz)	BW Type	Frequency of BW (Hz)
0.1	0.1	0.03	2	11 000	C	>1M
0.01	1.0	0.05	9	2 000	F	8k
0.001	100	0.10	2	3 300	E	24k
0.0001	1000	0.30	9	330	H	800

TABLE 10—Analysis of potentiodynamic polarization curves for SS430 in ethanolic HCl (Pt wire as REF).

HCl Conc. (N)	$E_{\text{corr}}$ (mV)	$I_{\text{lim}}$ (mA/cm <sup>2</sup> )	$E_{\text{pit}}$ <sup>a</sup> (mV)	Corrosion Rate (mm/y)
0.1	-36	27.8	34	10.0
0.01	-40	0.92	167	0.23
0.001	-30	0.11	179	0.05
0.0001	-550	0.03	.. <sup>b</sup>	0.002

<sup>a</sup>  $E_{\text{pit}}$  is determined as overpotential.

<sup>b</sup> Pitting potential could not be determined.

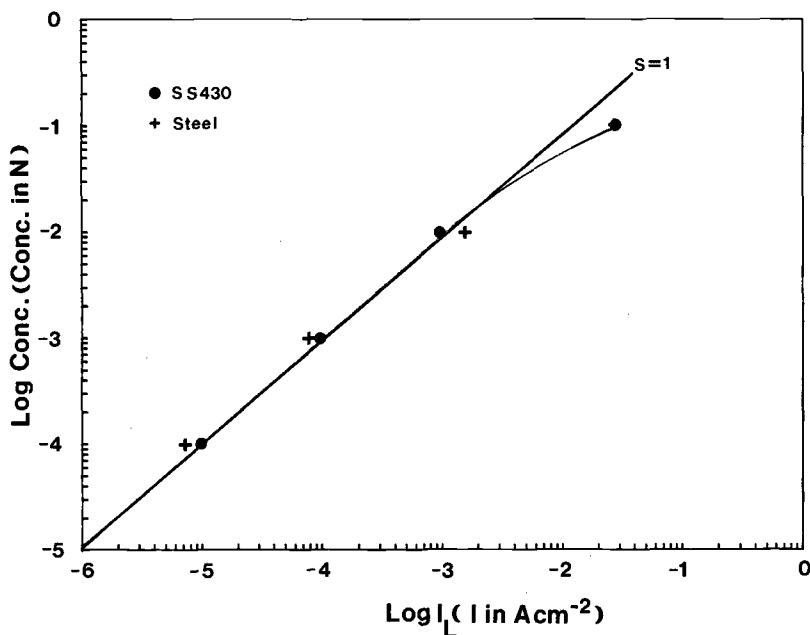


FIG. 20—The dependence of the cathodic limiting current on the concentration of HCl in ethanol.

centration except for  $10^{-1}$  N HCl/ethanol (EtOH). The relationship between the cathodic limiting current and the conductivity of HCl in ethanol is plotted in Fig. 21, and the conductivity of different electrolytes is shown in Table 11. Deviations from linearity have been observed for  $10^{-1}$  N ethanolic HCl solutions. These results show that the cathodic reaction is controlled by diffusion of the hydrogen ion.

### SS304L in Hydrazine

For SS304L in deaerated hydrazine EIS measurements have been carried out for a fifteen-day exposure period. Typical impedance spectra are plotted in Fig. 22, where curve 1, 2, and 3 are the spectra measured during the first, fifth, and twelfth day, respectively. One time constant is observed for all the impedance spectra between 65 KHz and  $10^{-3}$  Hz. The slopes of the spectra in the capacitive region are about  $-0.7$  similar to SS430 in  $10^{-4}$

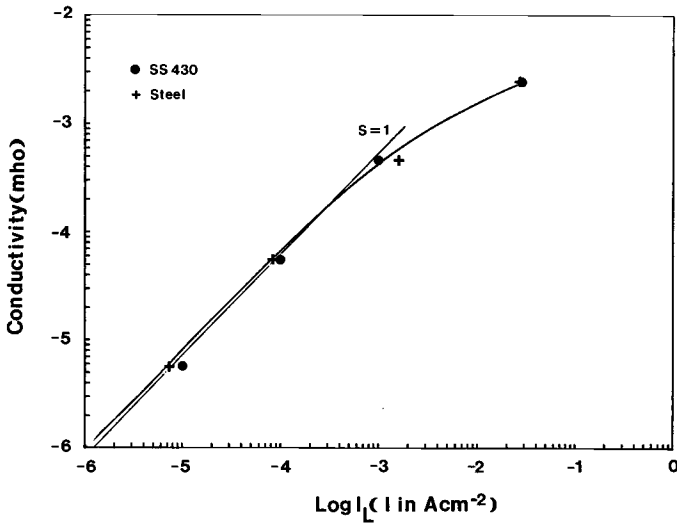


FIG. 21—The dependence of the cathodic limiting current on the conductivity of HCl in ethanol.

TABLE 11—Conductivities of different electrolytes.

Electrolyte	Conductivity (Mho)	Resistivity $\Omega$
Pure Ethanol	$8.5 \times 10^{-7}$	$1.18 \times 10^6$
0.0001N HCl/EtOH	$5.69 \times 10^{-6}$	$1.76 \times 10^5$
0.001N HCl/EtOH	$5.69 \times 10^{-5}$	$1.76 \times 10^4$
0.01N HCl/EtOH	$4.69 \times 10^{-4}$	$2.13 \times 10^3$
0.1N HCl/EtOH	$2.50 \times 10^{-3}$	$4.00 \times 10^2$
1.0N KCl (water)	$1.31 \times 10^{-1}$	7.6
Deionized Water	$5.0 \times 10^{-6}$	$2.50 \times 10^5$
Hydrazine (99%)	$6.0 \times 10^{-7}$	$1.70 \times 10^6$

N ethanolic HCl in Figs. 13 and 15. The mechanisms and the interface models which explain such behavior need further investigation.

Polarization resistance measurements and potentiodynamic polarization curves have been measured for two months. The experimental results are shown in Fig. 23 and Fig. 24. In Fig. 23, Curve 1 was recorded without compensation after 15 days immersion and Curve 2 was recorded with compensation after two months immersion. Since the ohmic drop was smaller than 0.5 mV due to the small cell current resulting from very low corrosion rates, the measurement for Curve 1 was performed without the compensation of the ohmic drop. After two months' immersion, the cell current increased and the ohmic drop (about 2 mV) became more significant. Therefore, the measurement had to be carried out with compensation of the ohmic drop by the interrupter technique. The experimental results showed that  $R_p$  values were  $120 \text{ k}\Omega\text{-cm}^2$  and  $30 \text{ k}\Omega\text{-cm}^2$ , respectively. Since the cell current may contain contributions from the decomposition of hydrazine on the electrode, the dissolution of the SS304, or both, the  $R_p$  values obtained from EIS and  $R_p$  measurements are considered as reaction resistance and the corresponding corrosion currents are considered as reaction currents. It is obvious that the reaction current increases with

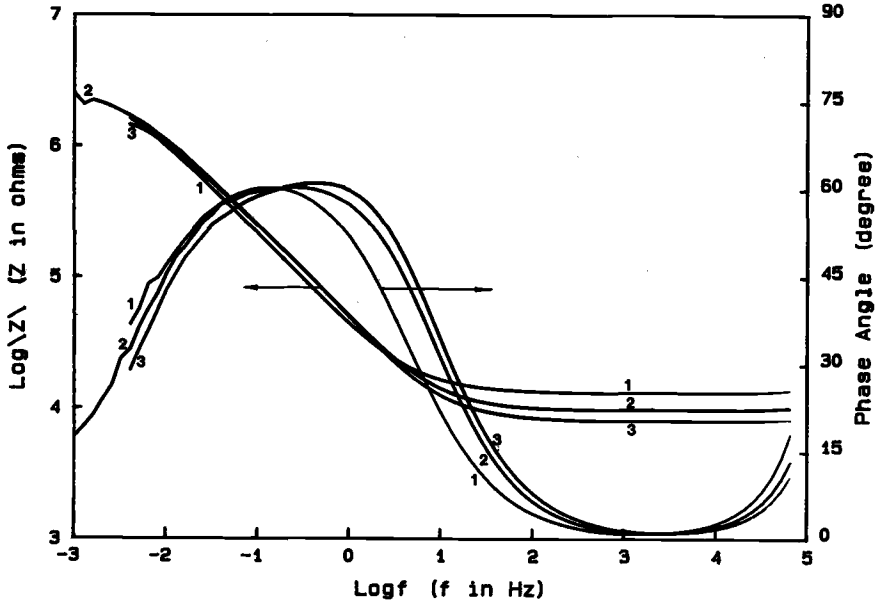


FIG. 22—Bode-plots for SS304L as function of exposure time in  $N_2H_4$ . (1) one day's immersion, (2) five days' immersion, and (3) twelve days' immersion.

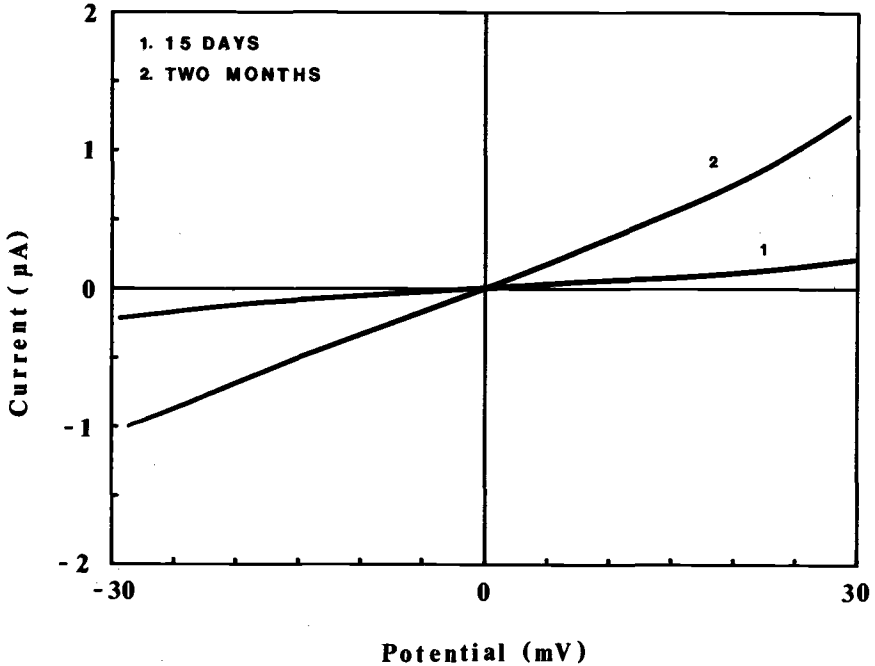


FIG. 23—Polarization resistance measurements for SS304L in  $N_2H_4$  (with compensation of the ohmic drop by the interrupter technique for Curve 2), Area = 0.06 cm<sup>2</sup>.

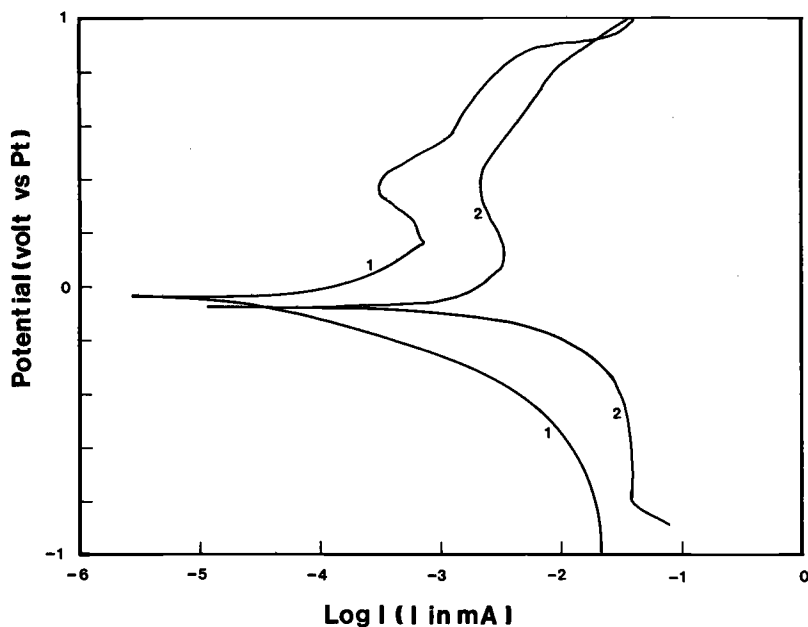


FIG. 24—Potentiodynamic polarization curves for SS304L in  $N_2H_4$ . (1) after 23 days' immersion and (2) after 2 months' immersion.

immersion time. Similar results were observed for the potentiodynamic polarization curves as shown in Fig. 24. Curve 1 was recorded after 23 days of immersion without compensation and Curve 2 was recorded with the compensation of the ohmic drop by the interrupter technique after two months' immersion. The interrupter parameters were off-time 0.03 msec, On:Off ratio = 9 and bandwidth type  $J$ . Curve 2 was plotted as  $\Delta RE$  versus  $\log I$ . Reaction current densities were determined by Tafel extrapolation as  $0.2 \mu A/cm^2$  and  $8 \mu A/cm^2$ , respectively. An active-passive transition and a cathodic limiting current were observed in these curves. The cathodic limiting current densities of  $0.32 mA/cm^2$  and  $0.64 mA/cm^2$ , respectively, are fairly large compared to values for dilute acid solutions or even the limiting current for the reduction of oxygen in neutral media. The increase of  $I_{lim}$  and the increase of the anodic reaction rates with time suggest significant changes in the system which need further examination.

### Summary and Conclusions

1. The results of this study have shown that it is possible to perform electrochemical studies in low conductivity solutions such as pure hydrazine with existing instrumentation provided a number of experimental considerations are followed.

2. A thorough evaluation of the interrupter technique for continuous elimination of the uncompensated resistance  $R_u$  with the Solartron potentiostat model 1286 has shown that the experimental parameters such as interrupter frequency and potentiostat bandwidth have to be carefully selected for each corrosion system. Recording of impedance spectra provides information concerning the frequency dependence of the corrosion cell which can be used to select these parameters.

3. An important finding of this study is the need for the correct choice of the reference electrode. Only wire electrodes such as the Ag/AgCl electrode or a Pt or gold (Au) wire can be used with the interrupter technique.

4. Cell design plays a very important role in electrochemical studies of the corrosion behavior in low conductivity media. This aspect could not be studied in sufficient detail in this study. However, it was found that it is advantageous to use large-size working electrodes in order to lower the experimental values of the polarization resistance and  $R_u$  and to increase the capacitance. Since the use of larger electrodes lowers the maximum available current density, the choice of the electrode size will have to depend on what kind of experiment the investigator wants to perform.

5. The positive feedback technique has been evaluated for the Solartron model 1286 and the PAR 173 potentiostat. The design of the model 1286 allows almost 100% compensation provided the proper adjustments are made on the instrument. For the PAR model 173, less than 100% compensation has to be chosen since the instrument will oscillate at 100% compensation. The residual ohmic drop can be eliminated by numerical methods after the test. The main problem with the positive feedback technique is that a constant compensation resistance has to be used which gives erroneous results or causes oscillations of the potentiostat when  $R_u$  changes during the experiment. This will occur most likely in the recording of anodic polarization curves.

6. The interrupter technique has been applied to the model systems steel or stainless steel in ethanolic HCl in which the conductivity and corrosivity can be varied by varying the HCl concentration. It was found that a cathodic limiting current and a passive region which was limited by the pitting potential could only be observed when the ohmic drop was completely eliminated. The polarization curves for SS304L in hydrazine showed a cathodic limiting current which increased with exposure time and an active-passive transition in the anodic polarization curve. Tafel extrapolation resulted in a reaction current density which reached several  $\mu\text{A}/\text{cm}^2$  after a few days of exposure. However, it is not clear from these data alone whether this value is due to corrosion of the stainless steel, decomposition of the hydrazine, or both.

#### Acknowledgment

This work has been performed for the Jet Propulsion Laboratory, California Institute of Technology, and was sponsored by the Air Force Rocket Propulsion Laboratory through an agreement with the National Aeronautics and Space Administration.

#### References

- [1] Mansfeld, F. *Corrosion*, vol. 32, 1976 p. 143.
- [2] Mansfeld, F. *Corrosion*, vol. 38, 1982 p. 556.
- [3] Elsener B. and Boehni H., *Corrosion Science*, vol. 23, 1983 p. 341.
- [4] Mansfeld, F. *Corrosion*, vol. 37, 1981 p. 301.
- [5] Mansfeld, F. Kendig, M. W. and Tsai, S. *Corrosion Science* vol. 22, 1982 p. 455.
- [6] Mansfeld F. and Tsai, S. *Corrosion Science*, vol. 27, 1987 p. 873.
- [7] Britz, D. *Journal of Electroanalytical Chemistry*, vol. 88, 1978 p. 309.
- [8] Mansfeld, F. *Advanced Corrosion Science Technology*, vol. 6, 1976, p. 163, Plenum Press.
- [9] Bard A. J. and Faulkner, L. R. *Electrochemical Methods*, John Wiley & Sons, Inc., New York (1980).
- [10] Lamy C. and Herrmann, C. C. *Journal of Electroanalytical Chemistry*, vol. 59, 1975, p. 113.
- [11] Garreau D. and Saveant, J. M. *Journal of Electroanalytical Chemistry*, vol. 35, 1972, p. 309.
- [12] "1286 Electrochemical Interface Operating Manual," Solartron Instruments, 1985.
- [13] Garreau D. and Saveant, J. M. *Journal of Electroanalytical Chemistry*, vol. 86, 1978, p. 63.

- [14] Garreau D. and Saveant, J. M., *Journal of Electroanalytical Chemistry*, vol. 50, 1974, p. 1.
- [15] Bewick, A. Bewick, A. Fleischmann, M. and Liler, M., *Electrochimica Acta*, vol. 1, 1959 p. 83.
- [16] Bode, H. W. *Network Analysis and Feedback Amplifier Design*, Van Nostrand, Princeton, N. J., 1945.
- [17] "Model 276 Interface Operating and Service Manual," EG&G Princeton Applied Research, 1983.
- [18] Schwabe, K. Oelssner W. and Suschke, H. D., *Prot Metals*, vol. 15, 1979 p. 126.
- [19] Britz D. and Brocke, W. A. *Journal of Electroanalytical Chemistry*, vol. 58, 1975 p. 301
- [20] Kuhn, M. Schuetze, K. G. Kreysa, G. and Heitz, E. in *Electrochemical Corrosion Testing*, Dechema Monographs, Vol. 101, 1986 p. 265. Frankfurt, FRG.
- [21] Cassoux, P. Dartiguepeyron, R. Fabre, P.-L. de Montauzon, D. *Electrochimica Acta*. vol. 30, 1985, p. 1485.
- [22] Coughanowr D. R. and Koppel, L. B. *Process Systems Analysis and Control*, McGraw-Hill, 1965.
- [23] Cooper G. R. and McGillem, C. D. *Methods of Signal and System Analysis*, Holt, Rinehart and Winston, 1967.
- [24] Ives D. J. G. and Janz, G. J. *Reference Electrodes*, Academic Press, New York 1961.
- [25] Butler, J. N. *Advances in Electrochemistry and Electrochemical Engineering*, Vol. 7, 1970 p. 77.
- [26] Mansfeld, F. Lin, S. Chen, Y.-C. and Shih, H. *Journal of Electrochemical Society*, vol. 135, 1988, p. 906.
- [27] Mansfeld, F. Chen, Y-C. Lin S. and Shih, H., "Recording of Impedance Spectra Under Galvanostatic Control," to be submitted to *Corr. Sci.*
- [28] Kendig M. and Mansfeld, F. *Corrosion*, vol. 39, 1983 p. 455.
- [29] Shih H. and Mansfeld, F. "A New Fitting Procedure for Impedance Data of Systems with Very Low Corrosion Rates," *Corrosion Science* (in press).
- [30] Juttner, K. Lorenze, W. J. Kendig, M. W. and F. Mansfeld, *Journal of the Electrochemical Society*, vol. 135, 1988 p. 332.
- [31] Mansfeld F. and Kendig, M., *Corrosion*, vol. 37, 1981, p. 545.

# **Mathematical Approaches**

## Correction of Experimental Data for the Ohmic Potential Drop Corresponding to a Secondary Current Distribution on a Disk Electrode

**REFERENCE:** Esteban, J. M., Lowry, M., and Orazem, M. E., "Correction of Experimental Data for the Ohmic Potential Drop Corresponding to a Secondary Current Distribution on a Disk Electrode," *The Measurement and Correction of Electrolyte Resistance in Electrochemical Tests*, ASTM STP 1056, L. L. Scribner and S. R. Taylor, Eds., American Society for Testing and Materials, Philadelphia, 1990, pp. 127-141.

**ABSTRACT:** A numerical method is presented for adjusting experimental current-potential curves for the ohmic resistance corresponding to a secondary current distribution on a (rotating) disk electrode. The nonuniform current and potential distributions on the disk electrode cause the electrolyte resistance itself to be a function of measured current. The method described here is employed after the experiments are conducted and yields the Tafel slope as well as adjusted values for current density and surface overpotential that apply to the center of the disk. This facilitates the comparison of the experimental data to those obtained using mathematical models of the rotating disk electrode that, in the secondary current regime, apply strictly only to the center of the electrode. The Tafel slopes obtained agree to within 3 mV/decade with standard techniques for ohmic correction such as current interruption because, at the high current densities where the ohmic correction is most significant, the resistance correction approaches the primary resistance obtained by current interruption. The Tafel slope values for the two methods differ most for solutions of low conductivity. The major advantages of the ohmic correction method described here are that the experimental condition is never perturbed and that the method indicates the extent to which the current distribution is nonuniform.

**KEY WORDS:** ohmic resistance, electrodes, Tafel slopes, electrochemical systems

### Nomenclature

- $a$  Constant in Tafel line equation defined in Eq 3
- $b$  Tafel slope, V/decade
- $F$  Faraday's constant, 96 487 °C/equiv
- $I$  Total current, A
- $i$  Current density, A/m<sup>2</sup>
- $i_{\text{corr}}$  Exchange current density of a freely corroding system, A/m<sup>2</sup>
- $i_o$  Exchange current density, A/m<sup>2</sup>
- $n$  Number of electrons transferred in reaction
- $R$  Gas constant, 8.314 J/K-mole
- $r$  Radial position, m

<sup>1</sup> Graduate research assistant and associate professor, respectively, Department of Chemical Engineering, University of Florida, Gainesville, FL 32611.

<sup>2</sup> Graduate research assistant, department of chemical engineering, University of Virginia, Charlottesville, VA 22901.

$r_o$	Radius of a disk-electrode, m
SCE	Saturated calomel electrode
$T$	Temperature, K
$\alpha$	Apparent transfer coefficient, dimensionless
$\beta$	Apparent anodic or cathodic transfer coefficient (see also Eq 12)
$\delta$	Parameter defined in Eq 8
$\eta_c$	Concentration overpotential, V
$\eta_s$	Surface overpotential, V
$\kappa_\infty$	Conductivity, S/m
$\Phi_o$	Ohmic potential drop, V
$\Phi$	Potential, V

### Subscripts

$a$	Anodic
app	Applied
avg	Average
$c$	Cathodic
corr	Corrosion
$\infty$	Bulk condition far from the electrode surface

### Introduction

The reaction mechanisms governing an electrochemical system are commonly identified by comparing experimentally determined Tafel slopes or apparent transfer coefficients with "theoretical values" obtained from simplifications of specific reaction mechanisms. An analysis of experimental data must include a treatment of the contribution to the measured potential of the electric resistance of the electrolyte, a term that can be significant at large currents or in dilute solutions of low conductivity. A number of techniques are available for making this correction. The ohmic contribution, for example, can be reduced but not eliminated by placing the reference electrodes close to the working electrode. A disadvantage of this approach is that exact placement of the reference electrode is critical, and uncertainty in the electrode location can be a significant source of error. Another approach is to place the reference electrode sufficiently far from the working electrode so that the distance can be considered to approach infinity. This allows the ohmic contribution to the measured potential to be calculated mathematically. Current interruption can also be used to obtain the ohmic contribution to the cell potential.

This paper describes a numerical technique used by Lowry [1,2] to correct the polarization data for the ohmic resistance corresponding to a secondary current distribution on a disk electrode. This procedure was suggested by Newman in his analysis of the current and potential distribution on a rotating disk electrode [3,4]. The treatment presented here does not require perturbation of the electrochemical system and takes into account the nonuniform current and potential distribution present on a disk electrode in the Tafel regime. The analysis can therefore be used to determine the extent to which the coupling of ohmic and kinetic effects causes the current distribution on the electrode to be nonuniform. This information could facilitate the interpretation of spatial variations of surface morphology or of electrode profiles after corrosion experiments. The use of this technique is restricted to a disk electrode with a reference electrode located infinitely far away and at currents below values at which mass-transfer effects are seen. Accurate values of solution conduc-

tivity and disk radius are also needed. The Tafel slopes are estimated by an iterative procedure using data within the Tafel region, where the ohmic resistance typically cannot be neglected.

A brief discussion of the use of polarization measurements to measure corrosion rates and Tafel slopes is presented. The method is illustrated by analyzing data taken by Lowry et al. [2] and the results are compared with those obtained from other ohmic compensation methods.

### Theoretical Development

The analysis of experimental data is usually based on a simplification of the general Butler-Volmer kinetic expression. The discussion here follows the Butler-Volmer expression, a summary of Newman's analysis of the secondary current distribution on a disk electrode, and the numerical method developed for ohmic compensation.

### Identification of Tafel Parameters

The rate at which reversible electrochemical reactions proceed can be described by a Butler-Volmer type equation

$$i = i_o \left\{ \exp \left( \frac{\alpha_a F}{RT} \eta_s \right) - \exp \left( - \frac{\alpha_c F}{RT} \eta_s \right) \right\} \quad (1)$$

The current density  $i$  is the sum of the anodic and cathodic contributions where  $i_o$  is the exchange current density,  $\alpha_a$  and  $\alpha_c$  are the apparent anodic and cathodic transfer coefficients, respectively, and  $\eta_s$  is the surface overpotential. The kinetic parameters  $i_o$ ,  $\alpha_a$ , and  $\alpha_c$  can be determined from experimental data through use of Eq 1. The exchange current density is a function of the electrolyte composition adjacent to the electrode surface and is large for reactions that are fast or reversible [5]. The surface overpotential provides the driving force for the reaction and is a measure of departure from the equilibrium potential  $\Phi_{eq}$ . For reversible reaction,  $\Phi_{eq}$  is given by the Nernst equation.

Electrode kinetic studies are performed by applying an external potential  $\Phi_{app}$  such that

$$\Phi_{app} = \Phi_{eq} + \eta_s + \Phi_o + \eta_c \quad (2)$$

These potentials are measured relative to a known potential of a reference electrode such as the saturated calomel electrode (SCE). The concentration overpotential  $\eta_c$  is due to changes in concentration and conductivity at the electrode surface relative to the bulk. This term can be neglected for currents sufficiently below the limiting current and will not be treated in this work. The ohmic potential drop  $\Phi_o$  is attributed to the solution resistance and is a measure of the driving force necessary to pass current through the electrolyte. At low current densities and close to the equilibrium potential,  $\Phi_o$  is negligible; the contrary is true at high currents. The objective of the ohmic compensation techniques discussed here is to identify the current-potential characteristics of a given system in the absence of this term.

When the surface overpotential becomes large, either the anodic or cathodic current dominates. Equation 1 reduces to an expression in which the surface overpotential becomes linear with respect to the logarithm of the current density. This is called the Tafel

polarization within this regime is essentially activation controlled. In the anodic Tafel region

$$\eta_s = \frac{2.303RT}{\alpha_a F} \log \left( \frac{i}{i_o} \right) = a_a + b_a \log i \quad (3)$$

where

$$a_a = - \frac{2.303RT}{\alpha_a F} \log i_o$$

and the anodic Tafel slope (in units of V/decade) is given by

$$b_a = \frac{2.303RT}{\alpha_a F}$$

Analogous expressions for the cathodic Tafel region can be obtained.

Tafel extrapolations can also be applied to corrosion reactions through the use of the mixed-potential theory [6]. The basis of the polarization techniques found in the literature [7-15] for evaluating kinetic parameters is that the current density for a corroding system consisting of individual reversible reactions can be approximated by

$$i = i_{\text{corr}} \left\{ \exp \left( \frac{2.303\eta_s}{b_a} \right) - \exp \left( - \frac{2.303\eta_s}{b_c} \right) \right\}, \quad (4)$$

where the surface overpotential is defined to be

$$\eta_s = \Phi_{\text{app}} - \Phi_{\text{corr}} - \Phi_o, \quad (5)$$

and  $i_{\text{corr}}$  and  $\Phi_{\text{corr}}$  are the corrosion current and corrosion potential, respectively. These potentials are likewise measured relative to a reference electrode; the value of  $\Phi_{\text{corr}}$  will shift accordingly with the choice of reference potential. The corrosion potential has a value that falls between the reversible potentials of the individual reaction pairs, and represents the dynamic equilibrium state of the freely corroding system. The principal assumption inherent in Eq 4 is that the major contributors to the overall current are the metal dissolution reaction and the reduction of some electroactive species. For this approximation to be valid,  $\Phi_{\text{corr}}$  must be sufficiently far from the two reversible potentials [8].

The techniques described in Ref 7 to 15 use current-potential data in the pre-Tafel region. The measurements are performed at low currents and close to  $\Phi_{\text{corr}}$ , where the ohmic contribution to the potential in Eq 5 is negligible. The experimental data are fitted into Eq 4 to yield values for  $i_{\text{corr}}$ ,  $b_a$ ,  $b_c$ , and  $\Phi_{\text{corr}}$ . The methods Mansfeld and coworkers [8-12] used to analyze polarization data, and Barnart's three-point method [13,14] and its variation [15], do not require the assumption of a linear polarization curve near the corrosion potential.

### The Secondary Current Distribution on a Disk Electrode

At large current densities, the contribution of the ohmic potential drop to the applied potential must be considered. The ohmic resistance is a function of the distance between

the reference and working electrodes, the conductivity of the solution, and the geometry of the working electrode. Experimental errors in the measurement of ohmic drop could be reduced by setting the reference electrode at "infinity" with respect to the working electrode. The ohmic resistance is insensitive to changes in the position of the reference electrode when the latter is placed relatively far from the working electrode [3]. This simplifies the experimental apparatus (that is, no Luggin capillary is necessary) and allows some leeway on electrode placement.

A procedure for Ohmic potential drop correction was derived from Newman's analysis of the current and potential distribution on a disk electrode [3,4]. The current distribution can be described as primary or secondary depending on the applied potential. The term  $\Phi_{\text{eq}}$  can be neglected in Eq 2 when the applied potential is measured against a reference electrode of the same kind as the working electrode. The concentration overpotential  $\eta_c$  can also be neglected at high convection rates. Each of the remaining terms vary with radial position to keep the  $\Phi_{\text{app}}$  constant over the entire disk.

A uniform potential in the solution adjacent to the electrode surface is obtained when both  $\eta_c$  and  $\eta_s$  are negligible. In this regime, the reaction rate constants are high and the current distribution is determined by the ohmic drop throughout the solution. The primary current distribution on an equipotential surface is

$$i = \frac{0.5i_{\text{avg}}}{\sqrt{1 - (r/r_o)^2}} \quad (6)$$

and the primary resistance is given by

$$\Phi_o = \frac{I}{4\kappa_{\infty}r_o} \quad (7)$$

where  $I$  represents the total current,  $\kappa_{\infty}$  is the solution conductivity, and  $r_o$  is the radius of the disk electrode [3].

The secondary current distribution applies when the surface overpotential cannot be neglected and the current at a point on the electrode becomes a function of the potential of the adjacent solution. The secondary current distribution under Tafel kinetics [4] is presented in Fig. 1 as a function of radial position with  $\beta\delta$  as the parameter where  $\delta$  is given by

$$\delta = |i_{\text{avg}}| \frac{zFr_o}{RT\kappa_{\infty}} \quad (8)$$

and represents the dimensionless average current density. For solutions with supporting electrolyte,  $z$  is defined to be equal to  $-n$ , the number of electrons transferred in the reaction. The term  $\beta z$  is the apparent cathodic or anodic transfer coefficient  $\alpha_c$  or  $\alpha_a$ . The current distribution is now determined by the requirement that the current at any location satisfy both Ohm's law, relating current to a gradient in potential at that location, and the kinetic expression relating current to the local value of the surface potential. This is in contrast to the primary case, in which the local value of current density need only satisfy Ohm's law. The potential in the solution for both primary and secondary distributions is governed by Laplace's equation. As  $-\beta\delta$  tends toward  $\infty$ , the current distribution approaches the primary distribution where the current density approaches infinity at the disk edge and is equal to one-half the average current value at the center of the disk. As

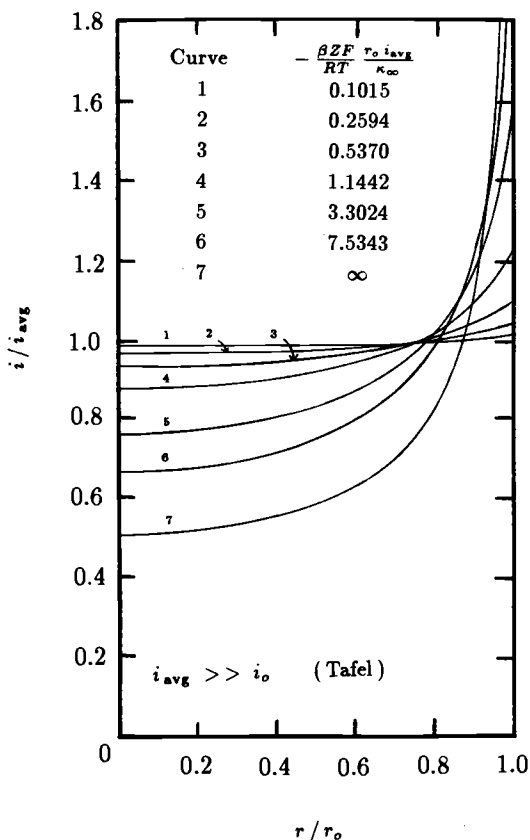


FIG. 1—Secondary current distribution on a disk electrode for Tafel kinetics (Ref 4, reprinted by permission of the publisher, The Electrochemical Society, Inc.).

$-\beta\delta$  approaches zero, the current distribution becomes uniform. This means that kinetic limitations to the electrode reaction cause the current distribution to become more uniform and cause the potential adjacent to the electrode surface to deviate from a uniform value to overcome the tendency of current to favor the edge of the electrode [4,5].

One consequence of the nonuniform secondary distribution for the potential of the solution adjacent to the electrode is that subtraction of the ohmic correction for a primary distribution applies strictly only for a single radial position on the disk, and the location of this position is a function of the average current density. One can, however, reference the ohmic potential drop and the current density to values appropriate for the center of the disk. This approach requires that the ohmic resistance be a function of the average current density. The primary ohmic potential drop is therefore corrected by a factor given in Fig. 2 as a function of the ratio of the current density at  $r = 0$  to the average current density. This factor is equal to unity for the primary current distribution (where the potential of the solution adjacent to the disk is uniform) and approaches 1.273 when the current distribution becomes uniform.

If one could obtain the ratio  $i/i_{avg}|_{r=0}$  from Fig. 1, the applied potential could be corrected for the ohmic drop to obtain the surface overpotential at the center of the disk elec-

trode, that is

$$\eta_s|_{r=0} + \Phi_{\text{corr}} = \Phi_{\text{app}} - \Phi_o|_{r=0} \quad (9)$$

or

$$\eta_s|_{r=0} + \Phi_{\text{corr}} = \Phi_{\text{app}} - \frac{I}{4\kappa_{\infty}r_o} \left[ \frac{\Phi_o 4\kappa_{\infty}r_o}{I} \right]_{r=0} \quad (10)$$

where  $I$  is the total current to the disk at an applied potential  $\Phi_{\text{app}}$  measured relative to a reference electrode. The term in the bracket is the correction factor for the primary resistance to the center of the disk electrode determined from Fig. 2.

### The Numerical Method for Ohmic Compensation

Data obtained from potentiostatic or potentiodynamic experiments may be corrected for ohmic potential drop at the center of the disk to acquire the surface overpotential and current density at  $r = 0$  using the procedure derived from Newman's treatment of the disk electrode. Reliable estimates for the ohmic contribution can be obtained since the calculations are referenced to a radial position where the ohmic potential drop and current density are known.

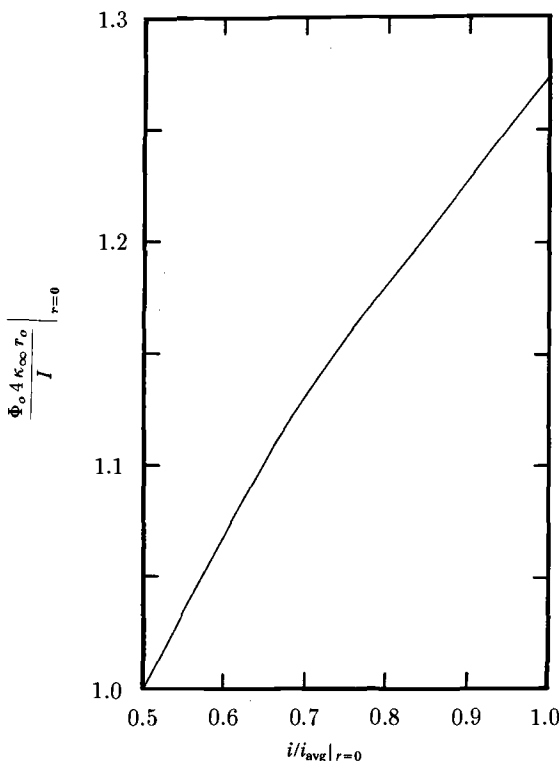


FIG. 2.—Correction factor for the primary resistance used to correct for the ohmic potential drop to the center of the disk electrode under a secondary current distribution (Ref 4, reprinted by permission of the publisher, *The Electrochemical Society, Inc.*).

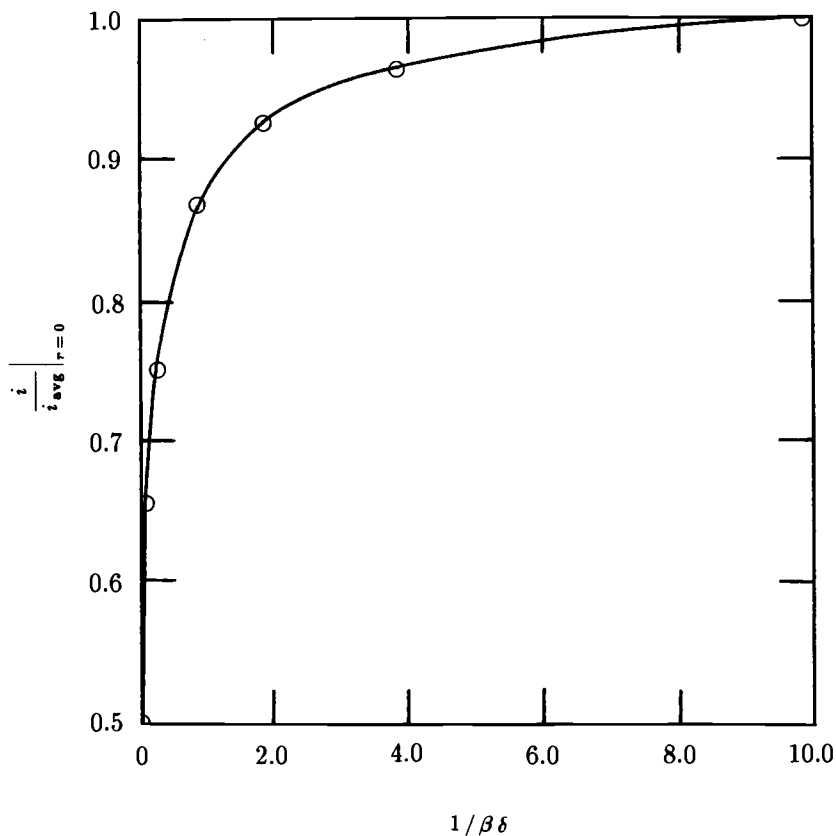


FIG. 3—Correction factor for the average current density used to obtain the current density at the center of the disk electrode under a secondary current distribution.

Values for  $i/i_{\text{avg}}|_{r=0}$  from Fig. 1 were plotted as a function of  $|1/\beta\delta|$  to yield Fig. 3. This plot shows that as  $|1/\beta\delta| \rightarrow 10$  the current distribution becomes nearly uniform. Since

$$\frac{1}{\beta\delta} = \frac{RT\kappa_{\infty}}{\beta nFr_o i_{\text{avg}}} \quad (11)$$

an expression for  $\beta$  can be related to the Tafel slope obtained from Newman's expression relating the current density to the surface overpotential. Therefore,

$$b = \frac{2.303RT}{\beta nF} \quad (12)$$

or

$$\beta = \frac{2.303RT}{bnF} \quad (13)$$

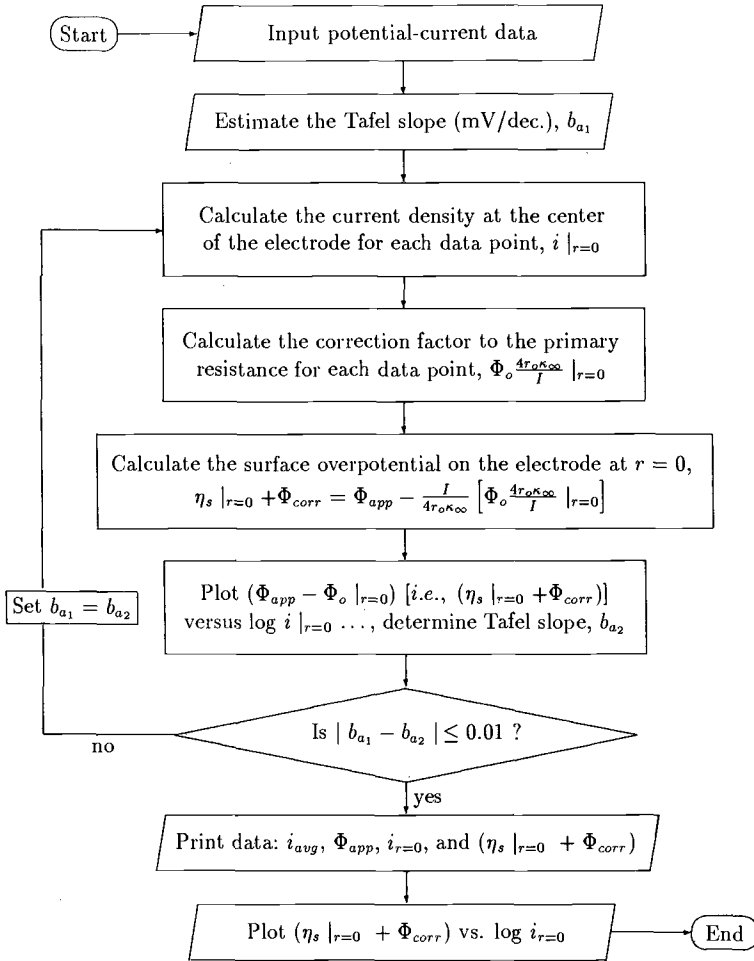


FIG. 4—The flowchart describing the ohmic drop correction algorithm.

With

$$i_{avg} = \frac{I}{\pi r_o^2} \tag{14}$$

Equation 13 becomes

$$\frac{1}{\beta \delta} = \frac{b \kappa_{\infty} \pi r_o}{2.303 I} \tag{15}$$

The iterative procedure used to obtain  $\eta_s |_{r=0}$  requires an initial guess for the Tafel slope and calculation of the parameter  $1/\beta \delta$  from Eq 15 for each pair of current-potential data. The corresponding value of  $i/i_{avg} |_{r=0}$  is subsequently obtained from a discretized version

of Fig. 3. The correction factor for the primary resistance at the center of the disk electrode is estimated from a curve-fit of Fig. 2, and the surface overpotential at  $r = 0$  is calculated from Eq 11. A new value for the Tafel slope is determined from linear regression of the adjusted data plotted as  $(\Phi_{\text{app}} - \Phi_o|_{r=0})$  [that is,  $(\eta_s|_{r=0} + \Phi_{\text{corr}})]$  versus  $\log(i|_{r=0})$  where

$$i|_{r=0} = \left[ \frac{I}{\pi r_o^2} \right] \left[ \frac{i}{i_{\text{avg}}} \right]_{r=0} \quad (16)$$

This procedure is repeated until the error criterion for the Tafel slope is achieved. A flow-chart describing the algorithm is presented as Fig. 4. The computer program prepared for this method is documented in Ref 1.

### Experimental Results

The use of this ohmic correction program is illustrated here in the analysis of current-potential data acquired potentiostatically for the dissolution of iron in deaerated acidic chloride solutions [1,2]. These data are presented in Figs. 5, 6, and 7 for chloride concentrations of 0.1, 1.0, and 4.5 M, respectively, in aqueous solutions with their pH adjusted with hydrochloric acid (HCl). The data points correspond to potentiostatic data obtained for individually polished electrodes held at the applied potential for between 15 and 45 min. The potential was measured relative to the saturated calomel electrode (SCE). These data are also shown as corrected by the iterative technique developed here. The ohmic correction procedure yielded a Tafel slope value of 39 mV/decade for the 0.1 M  $\text{Cl}^-$  system, while the higher concentrations of 1.0 M and 4.5 M  $\text{Cl}^-$  gave values of 58 and 60 mV/decade, respectively. These are consistent with reported results [1, 2].

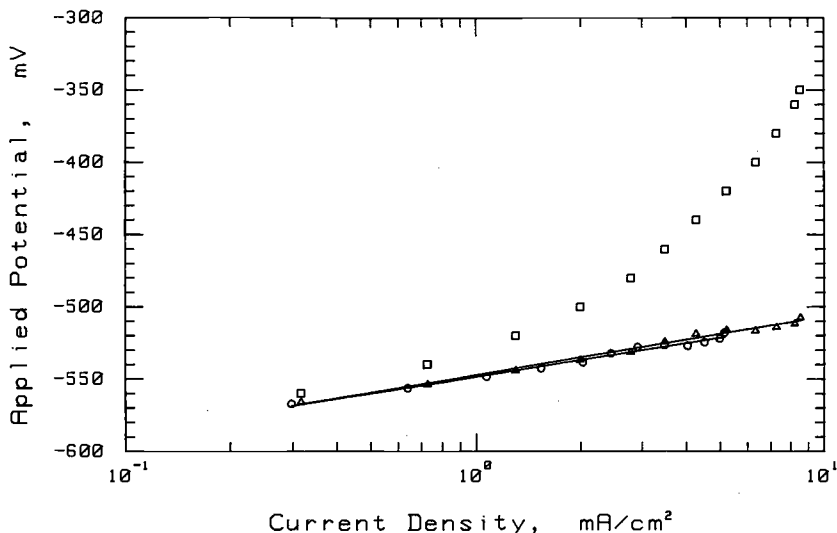


FIG. 5—Tafel plot for measured current density as a function of applied potential for the corrosion of an iron disk in a 0.1 M  $\text{Cl}^-$  solution with a pH of 2.  $\square$ , raw data, that is, averaged current density as a function of measured potential;  $\circ$ , data corrected by the iterative program, that is, current density as a function of overpotential appropriate for the center of the disk electrode; and  $\triangle$ , averaged current density as a function of overpotential obtained by a primary resistance correction, that is, the current-interrupt method.

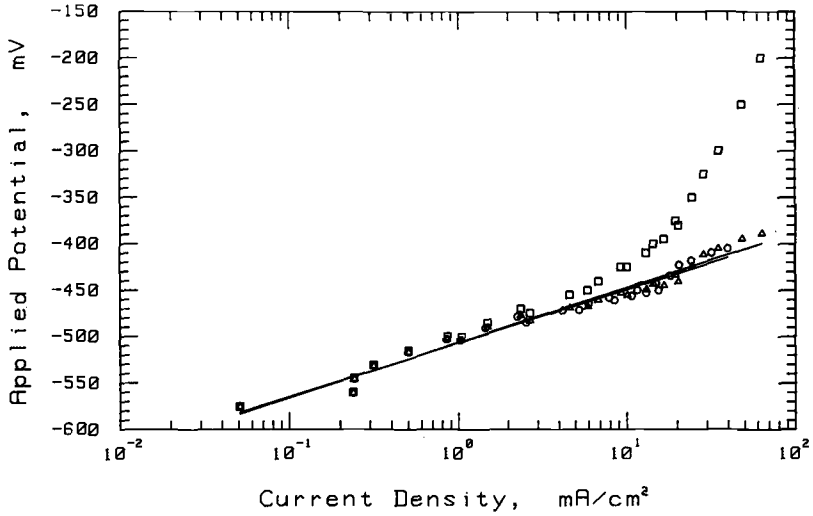


FIG. 6—Tafel plot for measured current density as a function of applied potential for the corrosion of an iron disk in a 1.0 M  $\text{Cl}^-$  solution with a pH of 2. Symbols as in Fig. 5.

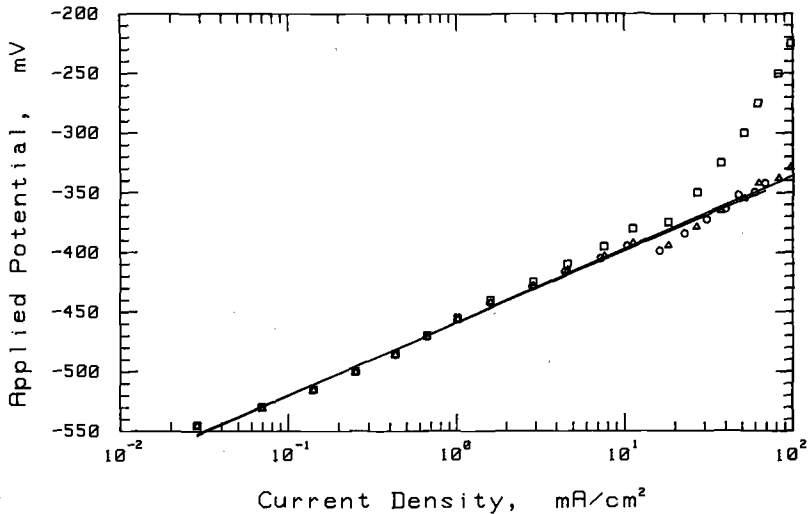


FIG. 7—Tafel plot for measured current density as a function of applied potential for the corrosion of an iron disk in a 4.5 M  $\text{Cl}^-$  solution with a pH of 2. Symbols as in Fig. 5.

The correction of data for the ohmic resistance by Newman's method was compared to that which would have been obtained by the current-interrupt technique. The ohmic drop measured by the current-interrupt technique corresponds to the primary resistance of the system being studied [16]. This is a consequence of the small time constant for the interruption, which does not allow time for the discharge of the nonuniformly charged double layer associated with a nonprimary current distribution. Therefore, to estimate the correction for the interrupter technique, the primary resistance was subtracted from the applied potential to give the surface overpotential, and the measured current was divided by the

electrode surface area to get the average current density. The results of this correction to the data are also shown in Figs. 5 through 7. The Tafel values based on the current-interrupt method differ by only 3 mV/decade for the 0.1 M Cl<sup>-</sup> solution and the agreement improves as the Cl<sup>-</sup> concentration increases. The difference is greater at lower conductivities because the ohmic solution resistance is larger under these conditions [16,17]. Close agreement is seen because the Ohmic correction factor approaches one at the high current densities at which ohmic resistance is most significant. The variation of the calculated correction factor for the primary resistance as a function of surface overpotential  $\eta_s|_{r=0}$  is presented in Fig. 8 for the three cases considered. The approach to a primary resistance at large overpotentials (or currents) is most apparent for the more dilute solutions where the ohmic correction is most important. At lower current densities the small total current makes the ohmic portion of the applied potential negligible, hence the surface overpotential is determined largely by the applied potential.

A unique feature of this IR-correction method is that the current distribution existing on a disk surface can be inferred from the corrected polarization data. The value of  $i/i_{avg}|_{r=0}$  at a given potential can be compared with those in Fig. 1. As this ratio approaches 1.0, a nearly uniform current distribution exists at the disk surface; nonuniformities at the edge become discernable for  $i/i_{avg}|_{r=0} < 0.95$ . Increasing solution conductivity makes the current distribution more uniform over a wider range of surface overpotentials, as illustrated in Fig. 9. When employing disk electrodes for erosion-corrosion studies, it is important to know whether the experiments are being performed in the region of uniform current density to distinguish between the effects of fluid flow and the current distribution at the applied potential.

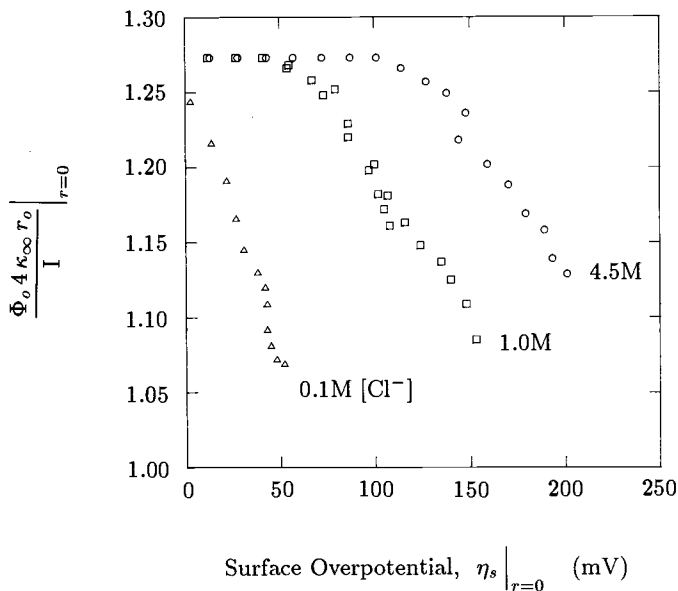


FIG. 8—Correction factor for the primary resistance used to correct for the Ohmic potential drop to the center of the disk electrode under a secondary current distribution for  $\Delta$ , 0.1 M Cl<sup>-</sup> solution [ $\Phi_{corr} = -570$  mV (SCE)];  $\square$ , 1.0 M Cl<sup>-</sup> solution [ $\Phi_{corr} = -558$  mV (SCE)]; and  $\circ$ , 4.5 M Cl<sup>-</sup> solution [ $\Phi_{corr} = -543$  mV (SCE)](Fig. 5, 6, and 7, respectively).

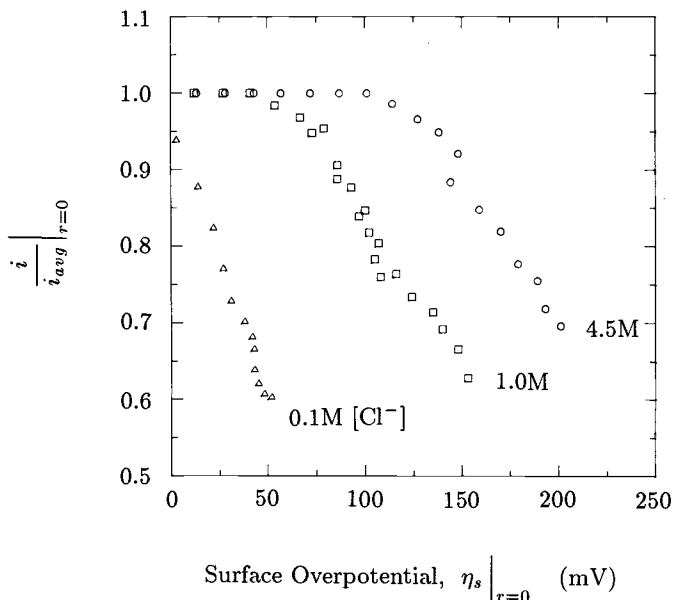


FIG. 9—Ratio of the current density at the center of the disk to the average current density  $i/i_{avg}|_{r=0}$  as a function of surface overpotential at the center of the disk electrode under a secondary current distribution. Symbols as in Fig. 8.

This correction procedure requires accurate values for the solution conductivity and electrode diameter. At the lower conductivities, such as those observed for the 0.1 M  $Cl^-$  solution, the magnitude of the Tafel slope was strongly dependent on the value of the conductivity. A variation of  $0.0005 \Omega^{-1}cm^{-1}$  (4%) in  $\kappa_{\infty}$  caused a variation in the calculated Tafel slope of as much as 20 mV/decade. At higher concentrations, small changes in the conductivity had little influence on the Tafel slope. The conductivities used in the calculations presented here were obtained in independent experiments.

The "tangent method" described by Asakura and Nobe [18] was also employed for the polarization data. The polarization data were fitted to a Tafel equation in which the surface overpotential was modified by an ohmic term corresponding to a constant solution resistance. The anodic Tafel slopes obtained (40, 56, and 59 mV/decade for the 0.1, 1.0, and 4.5 M  $Cl^-$  systems, respectively) were comparable to those obtained through the iterative calculations.

## Conclusions

The numerical technique for correcting polarization data for the ohmic resistance corresponding to a secondary current distribution on a disk electrode provides a useful tool for the analysis of experimental data. The analysis is conducted after data are taken and does not require the interruption of an experimental condition. This technique is most useful when it is desirable to account for the nonuniform nature of the current and potential distribution at a disk electrode surface. The referencing of corrected current-potential data to the center of the disk is convenient in comparing it with the results of one-dimensional models of rotating disks, and the results of the correction procedure provide information on the current distribution and the extent of nonuniformity across the disk elec-

trode. This information cannot be obtained from other ohmic potential compensation procedures. As can be done with other ohmic correction techniques, the results of the correction can be used to obtain  $i_{\text{corr}}$  and  $\Phi_{\text{corr}}$  through Tafel extrapolation of anodic and cathodic regions. The values obtained for Tafel slopes and corrosion current densities and potentials agree closely with other ohmic correction techniques such as current interruption.

The time required for calculation on a microcomputer is not excessive. Iterative treatment of 3000 data pairs with a program written in interpretive BASIC 4.0 on an Hewlett Packard-310 computer requires about 3 min, and the treatment of 25 data pairs requires only a few seconds. The time required can be further reduced when the algorithm is rewritten in compiled Basic or Pascal. The use of this technique is restricted to the Tafel regime for cases where the rotation speed does not influence the measured current at a given applied potential and where the reference electrode is located far from the disk electrode. Accurate values are also needed for solution conductivity and electrode diameter.

### Acknowledgment

This work was supported in part by the Chemicals and Metals Department of DOW Chemical, by the Institute for Materials Science and Engineering of the Virginia Center for Innovative Technology, Grant No. MAT-86-028, and by the Office of Naval Research under Contract Number N00014-87-K-0042.

### References

- [1] Lowry, M. M., "Corrosion of Iron in Acidic Chloride Solutions," M.S. Thesis, University of Virginia, 1988.
- [2] Lowry, M. M., Joyce, L. A., Moghissi, O. C., Diem, C. B., and Orazem, M. E., "Corrosion of Iron in Acidic Chloride Solutions," in preparation, 1988.
- [3] Newman, J., "Resistance for Flow of Current to a Disk," *Journal of the Electrochemical Society*, Vol. 113, pp. 501-502.
- [4] Newman, J., "Current Distribution on a Rotating Disk Below the Limiting Current," *Journal of the Electrochemical Society*, Vol. 113, pp. 1235-1241.
- [5] Newman, J., *Electrochemical Systems*, Prentice-Hall, Inc., NJ, 1973.
- [6] Wagner, C. and Traud, W., *Z. Electrochem.*, Vol. 44, p. 391.
- [7] Stern, M. and Geary, A. L., "Electrochemical Polarization: I. A Theoretical Analysis of the Shape of Polarization Curves," *Journal of the Electrochemical Society*, Vol. 104, pp. 56-63.
- [8] Mansfeld, F. and Oldham, K. B., "A Modification of the Stern-Geary Linear Polarization Equation," *Corrosion Science*, Vol. 11, pp. 787-796.
- [9] Mansfeld, F., "Simultaneous Determination of Instantaneous Corrosion Rates and Tafel Slopes from Polarization Resistance Measurements," *Journal of the Electrochemical Society*, Vol. 120, pp. 515-518.
- [10] Mansfeld, F., "Tafel Slopes and Corrosion Rates from Polarization Resistance Measurements," *Corrosion*, Vol. 29, pp. 397-402.
- [11] Mansfeld, F., "Some Errors in Linear Polarization Measurements and Their Correction," *Corrosion*, Vol. 30, pp. 92-96.
- [12] Gershakove, S. M., Udey, L. R., and Mansfeld, F., "An Improved Method for Analysis of Polarization Resistance Data," *Corrosion*, Vol. 37, pp. 696-700.
- [13] Barnartt, S., "Two-point and Three-point Methods for the Investigation of Electrode Reaction Mechanisms," *Electrochimica Acta*, Vol. 15, pp. 1313-1324.
- [14] Barnartt, S., "Tafel Slopes for Iron Corrosion in Acidic Solutions," *Corrosion*, Vol. 27, pp. 467-470.
- [15] McLaughlin, B. D., "A New Approach for Determining Corrosion Currents and Tafel Slopes," *Corrosion*, Vol. 37, pp. 723-726.

- [16] Newman, J., "Ohmic Potential Measured by Interrupter Techniques," *Journal of the Electrochemical Society*, Vol. 117, pp. 507-508.
- [17] Nisancioglu, K., "The Error in Polarization Resistance and Capacitance Measurements Resulting from Nonuniform Ohmic Potential Drop to Flush-Mounted Probes," *Corrosion*, Vol. 43, pp. 258-265.
- [18] Asakura, S. and Nobe, K., "Electrodissolution Kinetics of Iron in Chloride Solutions. Part I. Neutral Solutions," *Journal of the Electrochemical Society*, Vol. 118, pp. 13-18.

## Application of Numerical Simulations to Evaluate Components of Potential Difference in Solution

---

**REFERENCE:** Farozic, V. and Prentice, G., "Application of Numerical Simulations to Evaluate Components of Potential Difference in Solution," *The Measurement and Correction of Electrolyte Resistance in Electrochemical Tests, ASTM STP 1056*, L. L. Scribner and S. R. Taylor, Eds., American Society for Testing and Materials, Philadelphia, 1990, pp. 142-153.

**ABSTRACT:** Computer simulation of the potential distribution in an electrochemical cell is a useful technique for estimating the ohmic drop and the potential gradient at any point in solution. Results of such simulations can be used in several applications. Since optimal location of a reference electrode depends, in part, on avoiding large potential gradients, calculations can be useful in determining where substantial gradients occur. One can alter the current and potential distribution by changing the cell geometry; the effects of changes can be quantitatively determined from a simulation. Knowledge of ohmic drop in the electrolyte is also of interest in applications such as cathodic protection, where large potential losses can lead to insufficient protection.

In this paper we illustrate the use of computer simulation for the computation of potential and current distributions from which we evaluate ohmic drop and surface overpotential. We used the finite-difference technique for several problems in which both field effects and electrode kinetics were important. Approximations introduced to reduce the complexity were assessed by comparing numerical results with analytical solutions.

Electrochemical systems of practical interest, the disk electrode and plane electrodes with gas bubbles in the electrolyte, were studied. In one variation, we showed the effect of recessing a disk electrode in the insulating plane. In a second set of calculations, we simulated a gas bubble layer near an electrode and determined the effects of increasing void fraction in the bulk electrolyte.

**KEY WORDS:** current density, current distribution, electrochemical measurement, experimental design, finite difference theory, IR drop, mathematical models, numerical methods, ohmic compensation, potential distribution

### Nomenclature

- $f$  void fraction; dimensionless
- $i$  current density A/cm<sup>2</sup>
- $i_o$  exchange current density, A/cm<sup>2</sup>
- $K_m$  exchange current density, A/cm<sup>2</sup>
- $L$  characteristic length, cm
- $Wa$  Wagner number; dimensionless
- $\beta$  Tafel slope in V/decade
- $\Delta h$  change in node spacing, cm
- $\eta$  overpotential, V
- $\kappa$  conductivity,  $\Omega^{-1}\text{cm}^{-1}$
- $\phi$  electrical potential, V

<sup>1</sup> Graduate student and professor, respectively, department of chemical engineering, Johns Hopkins University, Baltimore, MD 21218.

## Introduction

In many electrochemical systems, it is useful to locate areas of high and low potential gradient. Because a slight error in placement may cause a large error in measured potential, an experimenter usually wishes to avoid area of high potential gradient when positioning a reference electrode. Landau et al. [1] analyzed several aspects of reference electrode placement with computer models. They studied ohmic drop in parallel electrode configurations, and they assessed the effect of shielding (interference offered by the reference electrode to current flow) on the working electrode. A review of developments in reference electrode placement, including placement through the back of the electrode, is also presented in their article.

If the cell geometry displays a high degree of symmetry, it is possible that the potential drop in the electrolyte can be calculated from published results [2]. Usually, only an estimate of the ohmic drop can be obtained, since the current and potential distributions are a function of the electrode kinetics; frequently, it is the activation overpotential which one is attempting to measure and, therefore, the relation between current density and overpotential is not precisely known in advance.

For simple geometries, analytic solutions of the primary current distribution problem, which only account for electric field effects, may suffice to help investigators place reference electrodes. Configurations such as the concentric cylinder and parallel plate electrode systems are used for investigative studies for just this reason. Rotating disk electrodes are popular for their well-characterized hydrodynamics; for this system, the primary potential distribution is available [3], but this distribution serves only as an approximation in cases in which electrode kinetics or mass transport limitations become important. For more complex situations such as a dispersed phase in the electrolyte, some analytic solutions exist, but these are highly dependent upon the perception of the makeup of the dispersed phase. For example, Maxwell's [4] analysis only applies to a dilute dispersion of nonconductive spheres.

We simulated the potential distribution in several cell geometries of experimental and industrial interest using a finite difference scheme. Development of such computer routines as they apply to electrochemical systems was first carried out by Klingert et al. [5]. To estimate the accuracy of the method, we compared our numerical results to the analytic solutions available for the concentric cylinder system. The effects of relatively minor alterations in the geometry of a cell were determined. We chose the disk electrode imbedded in a larger insulating disk to illustrate the change in potential distribution resulting from recessing the electrode. In a third set of simulations, we assessed the effect of including a dispersed, nonconducting phase as a model for gas evolving electrodes.

## Governing Equations

In situations in which the system can be decoupled into a homogeneous electrolyte and a thin layer near the electrode where kinetic limitations are important, Laplace's equation governs the potential distribution in solution

$$\nabla^2\phi = 0 \quad (1)$$

The current density  $i$  is proportional to the potential gradient

$$i = -\kappa\nabla\phi \quad (2)$$

where  $\kappa$  is the electrolyte conductivity. The information needed for a computer analysis is the system geometry, the electrolyte conductivity, and some other information that describes the current-voltage behavior of the electrodes, such as a potentiostatic polarization curve. If the system is kinetically controlled, an expression such as the Tafel equation may be applicable

$$\eta = \beta \log (i/i_o) \quad (3)$$

where  $\beta$  is the Tafel slope,  $\eta$  is the surface overpotential, and  $i_o$  is the exchange current density. Other relations, such as a linear relation, the Butler-Volmer expression, or a function that fits an experimental current-overpotential curve, may also be appropriate. The relative importance of the system kinetics is characterized by the Wagner number

$$Wa = \kappa(\partial\eta/\partial i)/L \quad (4)$$

where the partial derivative is evaluated at the average current density, and  $L$  is a length characteristic of the system such as the electrode separation. A Wagner number greater than zero indicates a finite kinetic resistance at the electrode interface and hence a secondary current distribution. We developed a general finite-difference routine to calculate the potential distribution in solution for large classes of two-dimensional and axisymmetric problems. The basic concept of the finite-difference method is to subdivide the domain into smaller elements. Laplace's equation is solved in each subdomain through an iterative process. When the values of the potentials in all subdomains change by less than a small, prescribed amount between iterations, a converged solution is assumed.

Significant simplification results from assuming that the boundary can be approximated by a series of line segments connecting the nodes. This approximation, which we refer to as the "nearest-node approximation," was used in all simulations where applicable. Computation time on a Micro VAX computer was less than 15 min for all cases considered.

## Results

The configurations considered were chosen to illustrate the power and limitations of the finite-difference method for potential distribution calculations. To this end, we investigated two systems, the disk electrode and the plane parallel electrode with a dispersed layer of nonconducting elements, representing bubbles.

One major advantage of computer simulation is that with proper coding, changes in geometry are easily made. For low Wagner numbers, the current distribution on a disk electrode is nonuniform with a minimum current density near the center of the electrode and a maximum current density at the edge of the electrode [6]. The geometry chosen for this discussion was a disk 2 mm in diameter with a planar counterelectrode 2 cm away from the disk. Figure 1a is a vector diagram that shows this nonuniformity, which is characteristic of the primary current distribution. Note that if the kinetics are sluggish enough (i.e., if high kinetic resistance is present), this distribution tends to be more uniform (Fig. 1b), while in other situations, such as metal dissolution reactions obeying Tafel kinetics at high discharge rates, the distribution tends to be more primary in character. This can be demonstrated if one considers that the Wagner number for Tafel kinetics is given by  $\kappa\beta/i_{\text{avg}}L$ . Thus, at higher current densities, the Wagner number becomes smaller as the current and potential distributions become more primary.

One of the characteristics of a primary current distribution is that the current density approaches an infinite value where an electrode and an insulator intersect at an obtuse

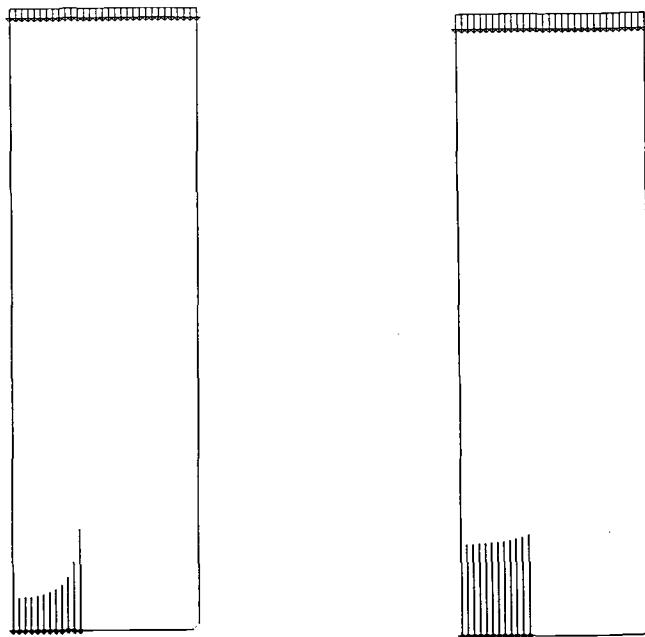


FIG. 1—(a) Primary current distribution vector program; disk electrode; radial symmetry about the left boundary; largest vector corresponds to  $i = 0.155 \text{ A/cm}^2$ ;  $W_a = 0$ . (b) Secondary current distribution vector diagram; disk electrode; radial symmetry about the left boundary; largest vector corresponds to  $i = 0.038 \text{ A/cm}^2$ ;  $W_a = 0.1$ .

angle. At the edge of a disk electrode imbedded in an insulator, the current density for the primary distribution is infinite. In an actual cell, kinetic and mass-transport limitations offer resistances that reduce the current density at the disk edge to finite values. A more uniform potential and current distribution can be produced by recessing the electrode in the insulator. Such an arrangement may be desirable in an experimental cell. From a simulation we can quantify the effect of varying the depth of recess. Figure 2 shows that a recess of 1 mm causes the primary current distribution of the system in Fig. 1 to have a maximum variation of 10% of current density around the average value and that much greater leveling in this worst-case distribution is not attained even when the disk is recessed 2 mm. The case in which a linearly polarizable disk electrode, denoted by  $\eta = 10i$ , is used shows less improvement in an already very uniform distribution.

The more uniform current density of a recessed disk implies that the potential gradient near its edge is lower, which is advantageous if a reference electrode is placed near that location because exact placement of the reference electrode is then not as crucial. Figures 3 and 4 illustrate the primary equipotential lines for the flush disk and for the disk recessed 1 mm. This lower gradient enables a researcher to minimize ohmic drop between reference and working electrodes by allowing placement of the reference electrode in this area near the recessed electrode in the plane of the insulator. The flush-mounted system has a steep potential gradient in this area; a small imprecision in reference electrode placement would cause a large error in ohmic compensation. Hence, the recessed disk is the preferred system if accurate determination of ohmic compensation is of primary importance.

Variations in electrolyte conductivity can also be accommodated in a finite-difference

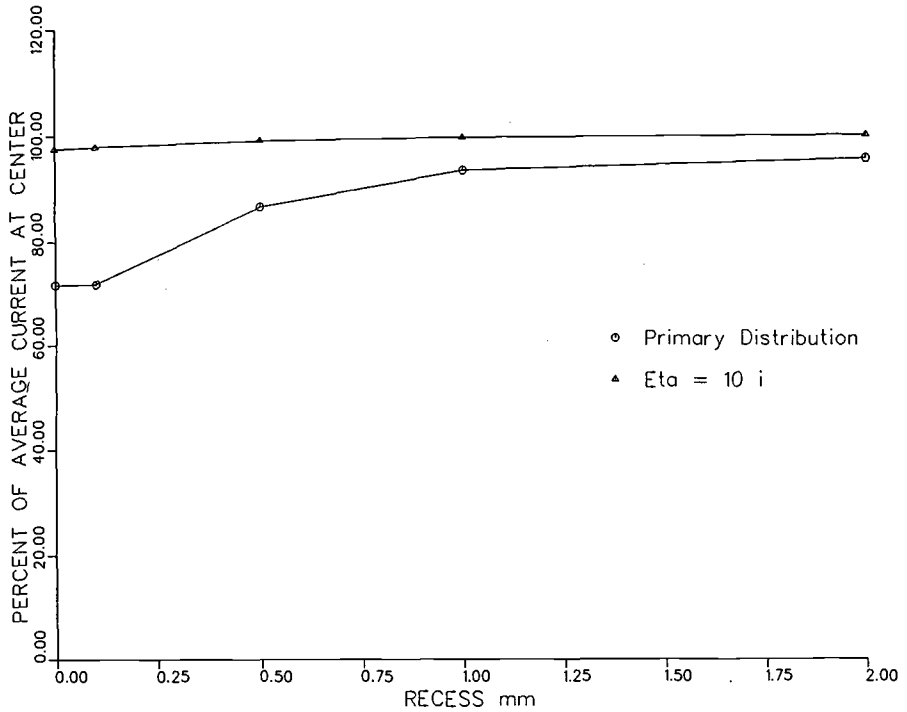


FIG. 2—Percent of average current versus recess depth; disk electrode.

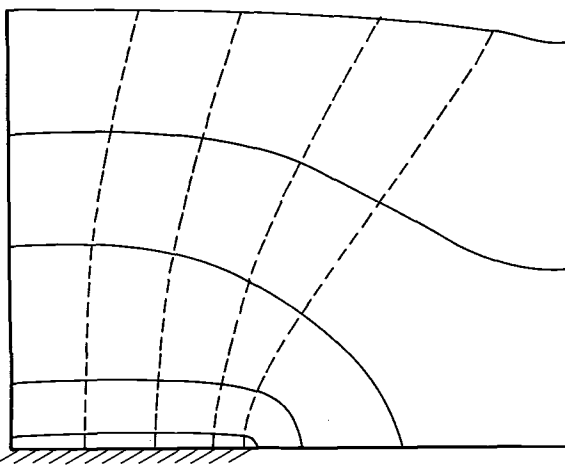


FIG. 3—Equipotential (solid lines) and current flow (dashed lines) for disk electrode flush mounted in insulator; radial symmetry about the left boundary; each equipotential contour corresponds to 0.2 V; primary distribution.

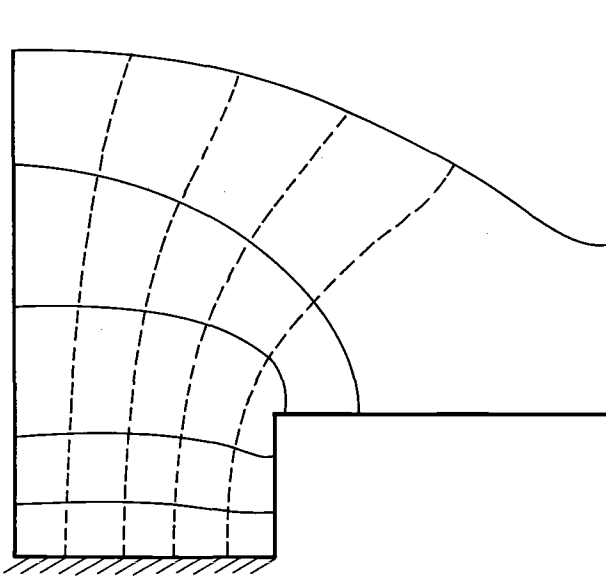


FIG. 4—Equipotential (solid lines) and current flow (dashed lines) for disk electrode recessed 1 cm into insulator; radial symmetry about the left boundary; each equipotential contour corresponds to 0.2 V; primary distribution.

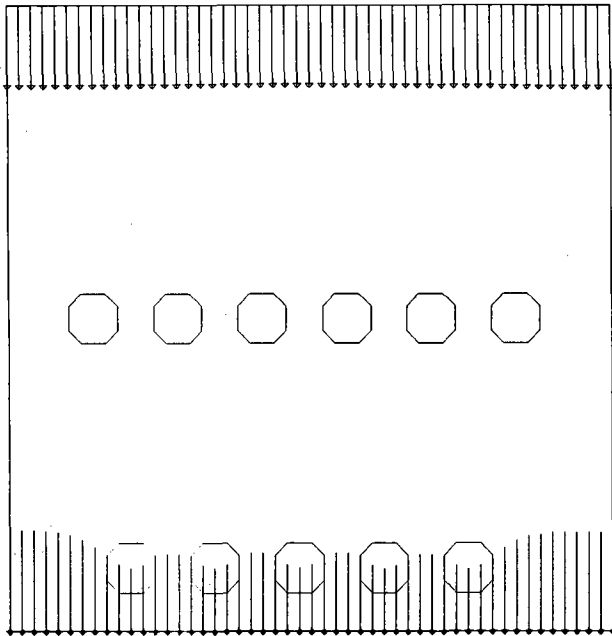


FIG. 5—Primary current distribution vector diagram; parallel plane electrodes with octagonal voids; void fraction 0.101; largest vector corresponds to  $i = 0.100 \text{ A/cm}^2$ ;  $W_a = 0$ .

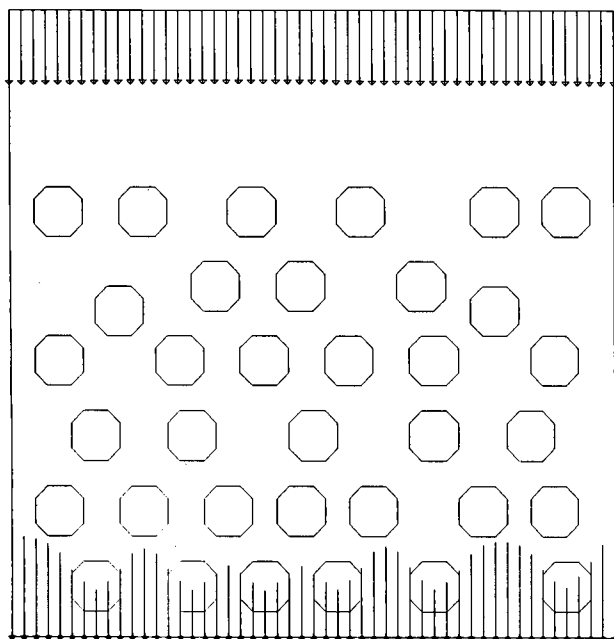


FIG. 6—Primary current distribution vector diagram; parallel plane electrodes with octagonal voids; void fraction 0.322; largest vector corresponds to  $i = 0.090 \text{ A/cm}^2$ ;  $W_a = 0$ .

simulation. The presence of bubbles reduces the current flow in a constant potential cell. Changes in the effective conductivity as a function of void fraction have been previously characterized by numerous investigators. The incremental resistance owing to a dilute, random suspension of spheres was first calculated by Maxwell [4] in the 1800s with this result

$$K_m = (1 - f)/(1 + f/2) \quad (5)$$

The effective conductivity,  $K_m$ , is defined as the ratio of conductivity in a system with voids to that of a void-free system;  $f$  is the system void fraction. Sides [7] has reviewed many of the subsequent developments. These systems are of interest because many industrial electrolyzers produce gaseous products. Figure 5 shows one layout for simulated bubbles, a rectangular Cartesian cut approximating spheres in solution with the indicated void fraction. The test system has a 1-cm interelectrode separation, a bulk electrolyte conductivity of  $0.1 \Omega^{-1} \text{ cm}^{-1}$ , and an applied potential difference of 1 V. Because we chose to simplify the problem by performing the simulation in Cartesian coordinates, the system can more realistically be considered as a series of cylinders in a duct. Thus, our system is fundamentally different from Maxwell's. Figure 6 shows another void fraction studied. Significant perturbations in the locations of these voids indicated that void placement did not change the total current passed by more than 1%. The relationship of effective conductivity versus void fraction in the system appears in Fig. 7. In the low void-fraction region, our results agree with those derived from the Maxwell model, while at higher void-fractions, deviations are undoubtedly caused by the differences in underlying assumptions. Intuitively, we expect the interactions between voids to reduce the effective conductivity more than that predicted by the Maxwell equation, but for our particular simulation, just the opposite

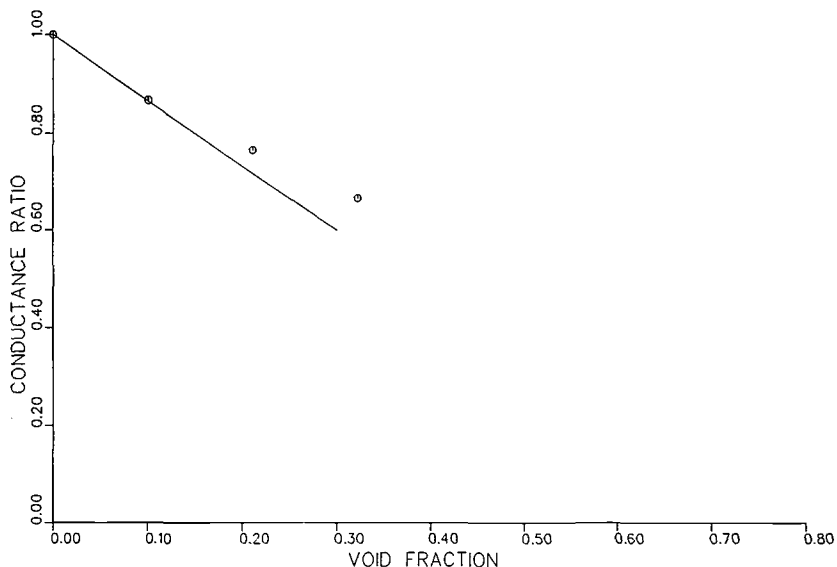


FIG. 7—Conductance ratio versus void fraction; solid line from Maxwell.

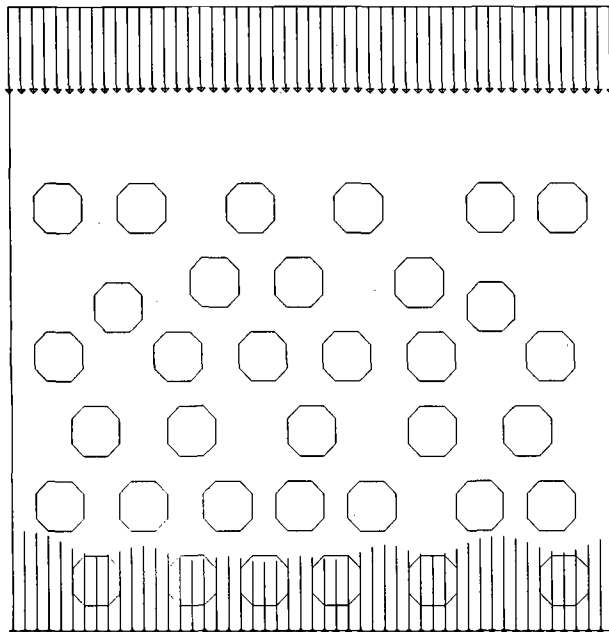


FIG. 8—Primary current distribution vector diagram; parallel plane electrodes with octagonal voids; void fraction 0.322; Tafel kinetics; largest vector corresponds to  $i = 0.055 \text{ A/cm}^2$ ;  $Wa = 0.1$ .

effect was observed. This relative increase in effective conductivity probably resulted from the fact that we did not have a random void distribution. The simulation illustrates the importance of knowing the void distribution (rather than just the volume fraction of the voids) to make an accurate calculation. Figure 8 shows the same geometry as in Fig. 6 with Tafel kinetics. This simulation demonstrates the increased uniformity of the current distribution as the Wagner number increases.

It is interesting to note the real implications of the presence of voids in a cell. If a reference electrode is placed 0.18 cm from the upper electrode in the sample cell, the measured potential is 0.82 V in a system without voids. However, as the void fraction increases to 0.1, 0.2, and 0.3, the voltage increases to 0.85, 0.87, and 0.89, respectively. The ohmic drop in a solution with voids then depends strongly upon the system void fraction and any calculation for this drop must incorporate some means of measuring the void fraction.

### Error Analysis

We can assess the effect of certain approximations that are commonly made to reduce the complexity of the problem. A finite-difference routine can be considerably simplified by requiring that the boundary coincide with nodes on a regular gridwork. This implies that curved surfaces may only be approximated with a series of straight lines. The space between nodes in the mesh also limits the accuracy that may be attained.

Since geometry is a critical part of the simulation, one must try to quantify the errors introduced by the nearest-node assumption and the inherent approximations made by discretizing partial derivatives. To do this, we chose the concentric cylinder electrode system, an arrangement that has been theoretically characterized, as our basis for comparison. The dimensions for the cylinders studied were a 2-cm inner diameter, a 6-cm outer diameter, and a 10-cm height. To quantify the effect of node spacing alone, a primary current distri-

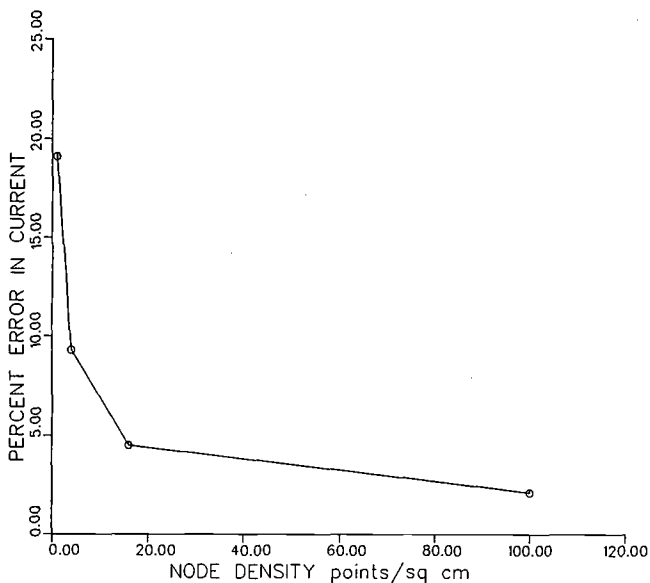


FIG. 9—Percent current error versus node density; concentric cylinders modeled in radial coordinates.

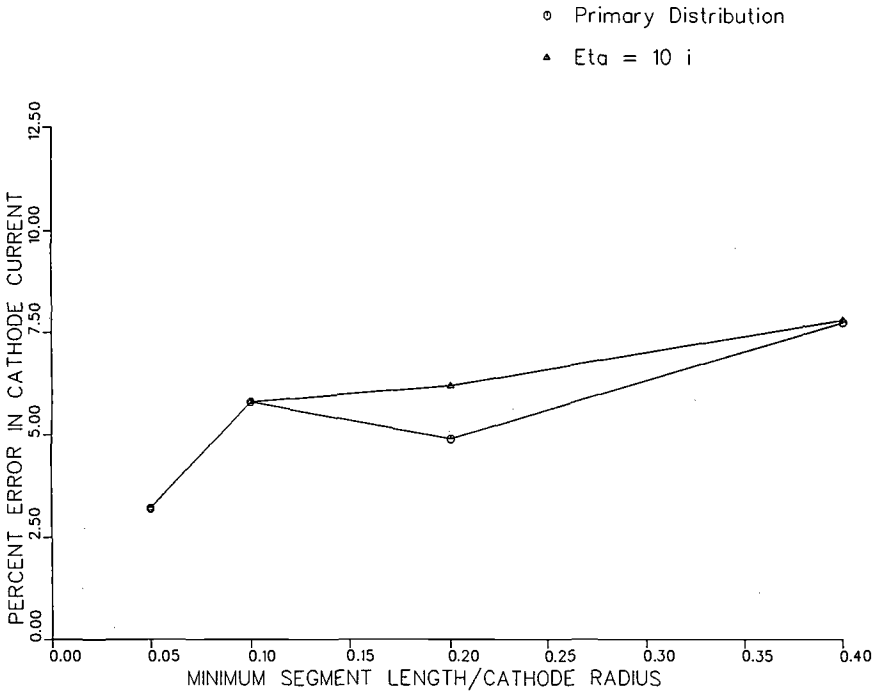


FIG. 10—Percent current error versus scale ratio; concentric cylinders with nearest node approximation; normalized for node density error.

bution was simulated on a radially symmetric domain with several different mesh spacings. The results of these simulations are shown in Fig. 9 with the percent error in total current plotted as a function of node density. From this plot, it is clear that there is a tradeoff between accuracy and computer time. For this type of simulation, the computer time is proportional to the square of the node density for a two-dimensional field. Errors in total current of approximately 2% can be attained for this system without demanding significantly more computer time than that required for 10% error. On the other hand, an experimenter who desires 0.1% error would require considerably more computer time for the simulation.

The nearest-node approximation to a curved surface was tested by modeling the same concentric cylinder system in Cartesian coordinates while varying the node spacing. The approximation to the actual geometry improves as segment length to radius ratio decreases. Figure 10 shows that the percent error in the cathode current decreases as this ratio decreases for both primary and secondary current distributions. It is important to note that these results have been corrected for the error owing to node density. An approximation of a surface to the nearest node has inherent in it errors owing to the finite node spacing as well as inaccuracies occurring because the exact geometry is not modeled. Since these simulations were run at different node densities, this error was subtracted to give a true representation of what the error caused by nearest node approximation alone contributes. This is the normalized error that is shown in Fig. 11, which indicates that taking a nearest node approximation introduces approximately another 5% error into the calculation. It also demonstrates that the dependence upon scale ratio is very weak, with the pri-

mary contribution to the error at uncorrected, high scale ratios coming from the node density rather than from the nearest node approximation itself.

Overall, it seems that a value of 20 for the node density normalized by the minimum radius of curvature gives an error in total current of less than 7% without making extreme demands on the computer. This normalization is the product of the node density and the minimum radius. Hence, this product must be at least 20 to meet this guideline. For a guide to the placement of reference electrodes where knowledge of areas of high potential gradient is of primary significance, this should be more than sufficient.

Another shortcoming strongly manifest in finite difference schemes is that discontinuities or singularities cannot accurately be represented by such methods. This shortcoming occurs because the finite difference expressions for partial derivatives are Taylor expansions, which are truncated to give an error in potential at each node proportional to the square of the node spacing [5]. Thus, the method attempts to fit a linear gradient between adjacent nodes. As the mesh spacing decreases, such singularities as corners and edges of disk electrodes in primary distributions become better approximated as the node spacing decreases.

The effect of a singularity is shown in our model of the disk electrode at the edge of the disk. This current density is theoretically infinite. Also, it is noted [3] that the theoretical current density at the center of the disk electrode is equal to half the average current density for the system. Neither of these values was observed in our system. The truncation error mentioned in the previous paragraph explains the finite edge current density. The reasons for the center current density not equaling half the average current density for the system in part stem from this effect; the integration, which yields the average current density, never incorporates large enough current density vectors near the edge. Another reason the current densities differ from Newman's solution is that the systems are fundamentally different. Newman calculated the current distribution on a working electrode imbedded in an insulating plane with a hemispherical counter electrode at infinity. Our system contains an insulating cylinder perpendicular to the plane of the disk electrode with a plane parallel counter electrode at a finite distance.

## Conclusions

Current and potential distribution modeling is a useful tool in the study of electrochemical systems. An investigator can use computer simulation to determine the position of optimal placement of reference electrodes and to determine which geometric modifications improve its characteristics in terms of potential and current distribution. For the systems presented in this study, errors arising from mathematical approximations can be estimated and are invariably smaller than errors inherent in parameter estimation.

## Acknowledgment

We are grateful to our sponsors, who have provided funding for our projects in the modeling and simulation of electrochemical systems. Current sponsors include The Baltimore Gas and Electric Company, Castle Technology Corporation, and the Office of Naval Research. Portions of this work were performed in the Corrosion and Electrochemistry Research Laboratory (CERL) at The Johns Hopkins University.

## References

- [1] Landau, U., Weinberg, N. L., and Gileadi, E., *Journal of the Electrochemical Society*, Vol. 135, pp. 396-403.

- [2] Prentice, G. A. and Tobias, C. W., *Journal of the Electrochemical Society*, Vol. 129, pp. 72-78.
- [3] Newman, J., *Journal of the Electrochemical Society*, Vol. 113, pp. 501-502.
- [4] Maxwell, J. C., *A Treatise on Electricity and Magnetism*, Vol. 1, 2nd Ed., Clarendon Press, Oxford, 1881.
- [5] Klingert, P., Lynn, S., and Tobias, C. W., *Electrochimica Acta*, Vol. 9, 1964, pp. 297-311.
- [6] Newman, J. S., *Journal of the Electrochemical Society*, Vol. 113, pp. 1235-1241.
- [7] Sides, P. J., *Modern Aspects of Electrochemistry*, J. O'M. Bockris, Ed., Vol. 18, Plenum Publishing, New York, 1986.

# **Applications**

Daniel Abraham,<sup>1</sup> Denny A. Jones,<sup>1</sup> Michael R. Whitbeck,<sup>2</sup> and Clinton M. Case<sup>2</sup>

## Ohmic Compensation in Desert Soil Using a Galvanostatic DC Bridge

---

**REFERENCE:** Abraham, D., Jones, D. A., Whitbeck, M. R., and Case, C. M., "Ohmic Compensation in Desert Soil Using a Galvanostatic DC Bridge," *The Measurement and Correction of Electrolyte Resistance in Electrochemical Tests*, ASTM STP 1056, L. L. Scribner and S. R. Taylor, Eds., American Society for Testing and Materials, Philadelphia, 1990, pp. 157-167.

**ABSTRACT:** A modified wheatstone bridge circuit has been used with success to compensate ohmic interferences in soil and other high resistivity corrosive solutions during galvanostatic (current controlled) dc measurements. Previous applications of the circuit have been reviewed and details of operation described. The most current use in our laboratories has been a study of corrosion in desert soils at the Nevada Nuclear Test Site (NNTS). A profile of desert soils samples with depth was obtained for electrochemical testing of lead and steel, which are construction materials for low level nuclear waste containers at NNTS. The soils were of naturally high resistivity, requiring compensation of ohmic interferences during electrochemical polarization measurements for corrosion rate (polarization resistance) determinations and cathodic protection requirements. Results are described briefly on effects of sulfate, chloride and carbonate, all of which can be derived from variations of soil composition with depth. Effects of added moisture content on all soil samples are also discussed.

**KEY WORDS:** corrosion, lead, steel, desert soil, electrochemical polarization, bridge circuit, ohmic compensation, polarization resistance

Electrochemical polarization measurements have been used to study the corrosion behavior of metals in soil [1-3]. These methods, besides furnishing quantitative corrosion rates for buried metal throughout its exposure, allow as estimate of its performance based on tests of short duration [4].

The purpose of the present investigation was to study the corrosion rates of lead and mild steel in soils from the Nevada Nuclear Test Site (NNTS) in southern Nevada. These metals are being used for containers to store low level radioactive waste. Because the corrosion rates were expected to be very low, electrochemical techniques were used in view of their well documented sensitivity [5-8].

Electrochemical studies are difficult in high resistivity soils because of the presence of the high ohmic or  $IR$  polarization incurred when a polarizing current  $I$  passes through  $R$ , the solution resistance between the specimen and the reference electrodes. This ohmic polarization obscures the Tafel behavior of the metal. As a result, the desired activation overvoltages cannot be accurately determined. A bridge circuit was used to compensate for the high ohmic effects of the desert soils. Subsequently, the effects of soil chemistry and moisture content on the buried metal specimens were investigated in detail.

<sup>1</sup> Graduate research assistant and professor, respectively, Department of chemical and metallurgical engineering, University of Nevada-Reno, Reno, NV 89557.

<sup>2</sup> Associate research professor and research professor, respectively, Desert research institute, University of Nevada-Reno, Reno, NV 89557.

### Experimental Apparatus and Materials

A selection of the desert soil samples from NNTS was obtained for electrochemical testing along with measured chemical compositions, pH and specific conductivity values. The values are listed in Table 1 in order of depth. The soils were generally alkaline and had specific conductivity values ranging from 103  $\mu\text{S}/\text{cm}$  in the surface layer to 2810  $\mu\text{mhos}/\text{cm}$  in the high sulfate zone. The moisture content of each soil was measured in the as received condition, using ASTM Method for Laboratory Determination of Water (Moisture) Content of Soil, Rock, and Aggregate Mixtures (D 2216) in which moisture was measured by weight loss during baking. As received moisture contents were found to be very low, between 0.5 and 2.0% of the total soil weight. Because of the restricted quantity of soil samples available, information on the corrosion rate variation with chemical composition and depth could be obtained only for lead and not for steel.

Corrosive properties of soil are, in general, dependent on the particle or grain size. Smaller grain sizes yield larger surface areas which retain moisture more easily and hence increase corrosivity. The soil samples were sieved and only the portion finer than 2000  $\mu\text{m}$  was used in the study.

The polarization cell shown in Fig. 1 consisted of a two inch OD copper tube capped on one end by a rubber compression stopper, which was expanded in position by a bolt and wing nut combination. The working electrode was either lead wire or a steel nail, 3.556 mm ( $\frac{1}{8}$  in.) in diameter, encased in heat shrunk Teflon exposing 1.5 to 2  $\text{cm}^2$ . The copper tube served as the auxiliary electrode, and the large corroding zinc surfaces of the galvanized bolthead and underlying washer served as the reference electrode. Anodic polarization by conventional anodic currents did not yield expected Tafel behavior. Polarization was quite high compared to the derived anodic curves which are shown. We believe this high polarization and the high derived Tafel constants may be caused by inhibitive effects of anions in the soil combined with low transport in the pore volumes adjacent to the surfaces.

The working electrode was centrally positioned vertically and the soil sample poured into the cell. The soil was then gently compacted with the end of a  $\frac{1}{8}$  in. diameter steel rod. The bulk density [9], which gives the degree of soil compaction was calculated from the soil mass and volume (approximately 100  $\text{cm}^3$ ) and found to be in the range 1.5 to 1.6 gms/cc for all samples.

The bridge circuit [7] shown in Fig. 2 was used to conduct the polarization measurements. The filtered DC power supply provided direct current through the circuit. A battery powered electrometer measured the current level. The potentiometer ( $P$ ) measured the potential of the working electrode (WE) with respect to the reference electrode, which was

TABLE 1—Average values of chemical composition, pH, specific conductivity for the soil samples tested.

Soil Type	Number of Samples	Depth, ft	Chemical Composition			pH	Specific Conductivity, $\mu\text{s}/\text{cm}^2$	Material Exposed
			$\text{HCO}_3^-$ , ppm	$\text{Cl}^-$ , ppm	$\text{SO}_4^-$ , ppm			
1	3	0 to 2.5	200.9	7.11	13.4	9.01	111	Lead
2	1	5.5	197.5	355	139	9.17	438	Lead
3	1	15.5	74.5	214	8550	8.08	2810	Lead
4	3	22 to 36	266.7	170.5	414	9.6	348	Lead
5	3	20 to 41	247.6	156.2	198.5	9.59	360	Steel

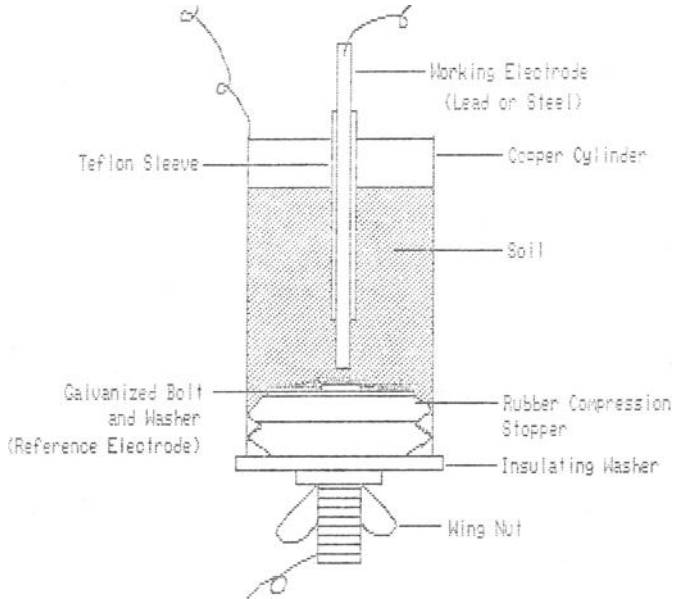


FIG. 1—Schematic cross section of polarization cell.

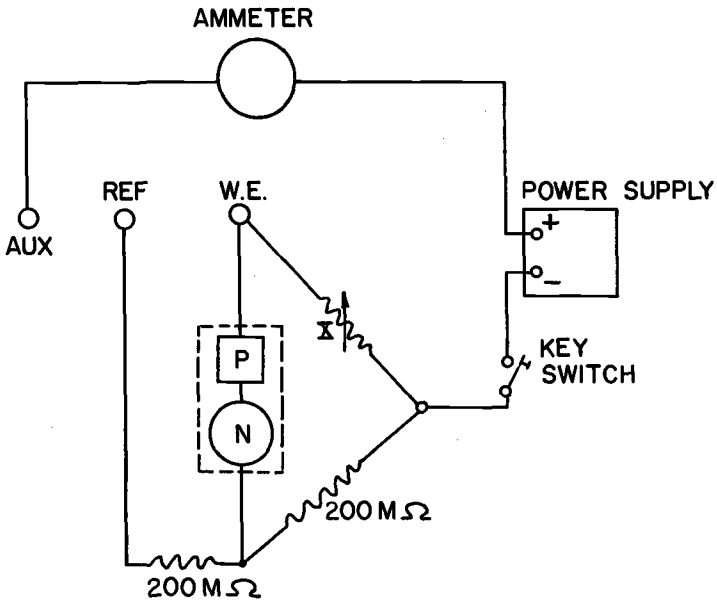


FIG. 2—Bridge circuit for polarization measurements on buried specimens.

connected through a line operated electrometer acting as a null detector  $N$ . The large values of  $S$  and  $T$ , 200 M $\Omega$  each, prevented polarization of the reference electrode. The variable resistor,  $X$ , was adjusted to compensate the ohmic effects. The key switch,  $K$ , provided a means of current interruption.

### Experimental Procedure and Results

Initial measurements were made to check the stability of the zinc reference electrode in the time period of the polarization measurement. The readings were taken in a representative soil versus a saturated calomel electrode (SCE). The drift over a period of 24 hours was found to be about 1 mv. Since the polarization measurements lasted up to a maximum of one hour, the reference electrode was considered sufficiently stable. The zinc measured 0.4 V active (negative) with respect to the SCE. No further measurements with respect to SCE were conducted in subsequent experiments.

In general, the zinc reference electrode measured active with respect to the lead and steel working electrodes. Under conditions of excessive water ponding a reversal of potential was observed in case of both lead and steel electrodes, and both showed an active potential with respect to the zinc reference. Both Romanoff [10] and Schwerdtfeger [11] observed similar reversals in water and soil and attributed the effect to the formation of a zinc silicate film on the metal.

In each soil sample, the moisture content was increased from the dry state to levels of 10, 15, 20, and 25% of the total soil weight and finally under saturation with water ponding over the soil surface. Water content was selected as a parameter for the study because it was expected to have a major effect on increasing the corrosion rate at the NNTS.

After addition of the water, the soil samples in their polarization cells were equilibrated for two days minimum in a high humidity chamber to minimize evaporation. Polarization measurements were then conducted using the circuit shown in Fig. 2. The procedure described in Ref 7 was used to balance the bridge circuit. A relatively high value of the current (2  $\mu\text{A}/\text{cm}^2$ ) was selected and the polarized potential was allowed to stabilize. The current was interrupted momentarily by pressing the key switch. In cases of overcompensation, the potential briefly jumped to a more negative value before rapidly increasing back to the unpolarized corrosion potential. The resulting "blip" on the strip chart record of potential versus time disappeared when  $X$  was adjusted equal to the resistance between reference and working electrodes. It was observed that as the water content of the soil increased, the resistance  $X$  necessary for compensation decreased as expected, from a few hundred k $\Omega$  for dry samples to approximately 10 k $\Omega$  with 10% water, and finally to less than one k $\Omega$  in saturated samples.

After the compensating resistance was determined, the system was given a few hours to stabilize. Galvanostatic techniques [8] were then used to generate first polarization resistance by cathodic polarization followed by cathodic Tafel curves under further cathodic polarization. The specimens were cathodically polarized to potentials more negative than the open circuit potential and sufficient data points to obtain a Tafel line. In general, it was observed that steady state polarized potential was attained within one minute to five minutes at each current step.

The corrosion rates were determined both by Tafel extrapolation and polarization resistance methods [12]. Typical examples of experimental cathodic polarization curves are shown in Fig. 3 for lead and Fig. 4 for steel. The Tafel line was extrapolated back to the corrosion potential to obtain the value of the corrosion current density. In most cases, the linear Tafel behavior extended over a decade. However, under conditions of water ponding on the soil surface, the results obtained varied from cell to cell, indicating in some cases,

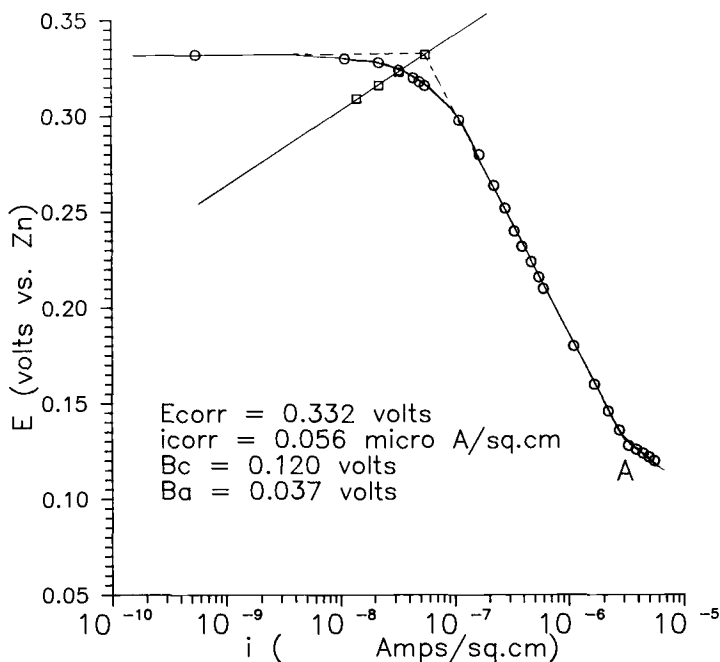


FIG. 3—Typical Tafel plot for lead (exposed area = 1.82 cm<sup>2</sup>). Soil No. 2. Water content = 20% of soil weight

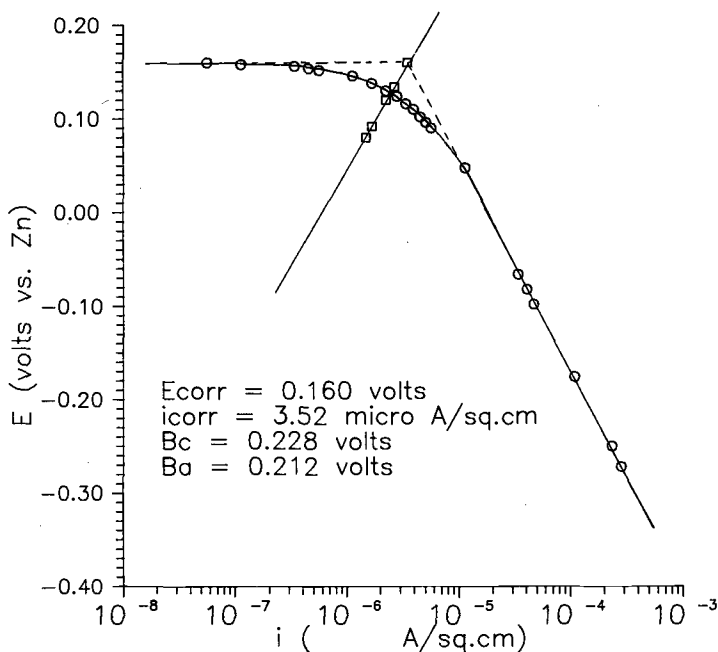


FIG. 4—Typical Tafel plot for steel (exposed area = 1.76 cm<sup>2</sup>). Soil No. 5. Water content = 20% of soil weight.

a limiting diffusion current, and in some cases the electrolyte evolution of hydrogen from water at higher cathodic overvoltages.

In both lead and steel specimens, a levelling off, or decrease in the rate of polarization was observed at higher currents (Pt.A in Fig. 3). This behavior had also been observed in an earlier study [1], and the reason remains undetermined.

In Fig. 3, the Tafel line extended over a decade and a half. The cathodic Tafel Slope,  $B_c$  was found to be 0.12 V. Tafel extrapolation showed the corrosion current density to be  $5.6 \times 10^{-8}$  A/cm<sup>2</sup>. Since the polarization resistance equation required the determination of the anodic slope,  $B_a$  for the calculation of the corrosion current density, the anodic polarization curve was extrapolated from the cathodic polarization values, using the relation,  $i_a = i_c - i_{\text{applied}}$ , where  $i_a$  and  $i_c$  are the anodic and cathodic current densities respectively and  $i_{\text{app}}$  is the current density applied for the cathodic polarization [13,14].  $B_a$  was found to be 0.037 volts. The corresponding values for steel were  $B_c = 0.228$  volts and  $B_a = 0.212$  volts. Anodic polarization by conventional anodic currents did not yield expected Tafel behavior. Polarization was quite high compared to the derived anodic curves which are shown. We believe this high polarization and the high derived Tafel constants may be caused by inhibitive effects of anions in the soil combined with low transport in the pore volumes adjacent to the surfaces.

A plot of overvoltage less than 10 mV as a function of applied current density yielded the polarization resistance curve. Typical curves are shown in Fig. 5 for lead and Fig. 6 for steel. The corrosion rate,  $i_{\text{corr}}$ , expressed as a function of applied current density was related to the slope at the apparently linear portion of the curve at the origin by the usual relation

$$R_p = \frac{B_a B_c}{2.3 i_{\text{corr}} (B_a + B_c)} \quad (1)$$

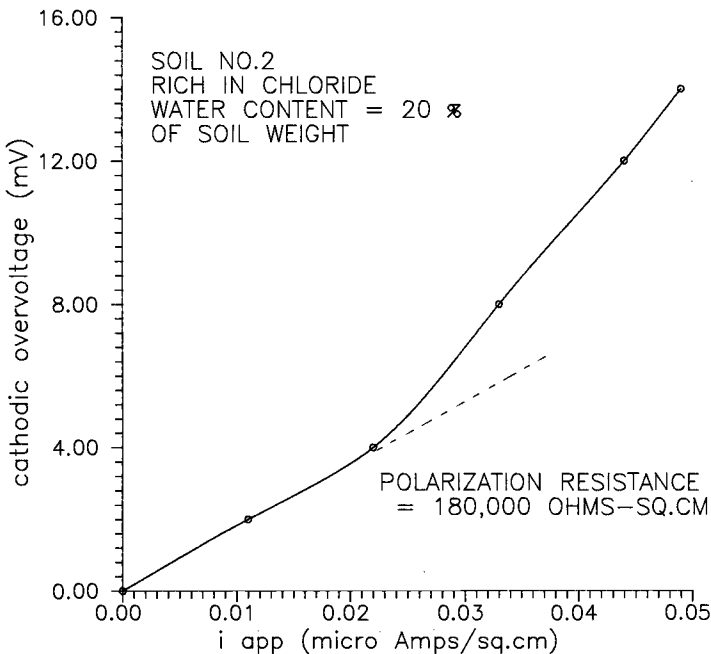


FIG. 5—Typical resistance polarization curve for lead.

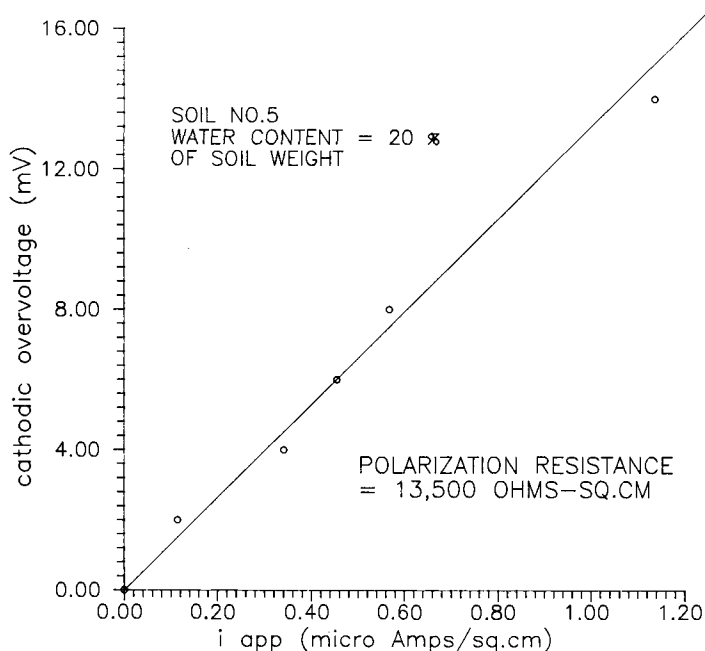


FIG. 6—Typical resistance polarization curve for steel.

Since,  $B_a$  and  $B_c$  were already known,  $i_{corr}$  was calculated. Figure 5 yields an  $R_p$  value of  $180\,000\ \Omega\text{ cm}^2$ . From Fig. 3, we have  $B_a = 0.037$  and  $B_c = 0.12\ \text{V}$ .

Hence

$$i_{corr} = 6.76 \times 10^{-6}\ \text{A/cm}^2\ \text{for lead}$$

A similar process for steel yields  $i_{corr} = 3.53 \times 10^{-6}\ \text{A/cm}^2$ .

For lead, the variation of corrosion rates with respect to water content in the soil pores is shown in Figs. 7a and 7b. The values indicated are an average over the number of samples considered for each soil type as shown in Table 1. In almost all cases the corrosion rates were found to increase with increasing water content and then decrease rapidly as the water content approached the saturation value. This effect was found to be relatively pronounced in the upper layer soils that were rich in bicarbonate (Soil Type number 1). In this case, the corrosion rates increased from about  $0.12\ \mu\text{A/cm}^2$  in the soil with the 10% moisture content to about  $2.9\ \mu\text{A/cm}^2$  in the approximately saturated soil. Surprisingly, Soil Type number 3, with the high sulfate content did not show the high corrosivity expected from its relatively high specific conductivity. The corrosion rates in this case varied from about  $0.15\ \mu\text{A/cm}^2$  in the soil with the 10% moisture content to a maximum of  $0.5\ \mu\text{A/cm}^2$  and then dropped to less than  $0.1\ \mu\text{A/cm}^2$  under conditions of ponding. Soil Type number 4, with the three anions, bicarbonate, sulfate, and chloride present in relatively high proportions also showed no unusual corrosivity. In this case the values ranged from a minimum of  $0.2\ \mu\text{A/cm}^2$  to a maximum of  $0.45\ \mu\text{A/cm}^2$ .

Figure 8 shows the corresponding results for steel in Soil Type number 5, which had some of all three anions mentioned above. The corrosion rates varied from about  $2\ \mu\text{A/cm}^2$  to about  $10.35\ \mu\text{A/cm}^2$  when 70% of the soil pores were filled.

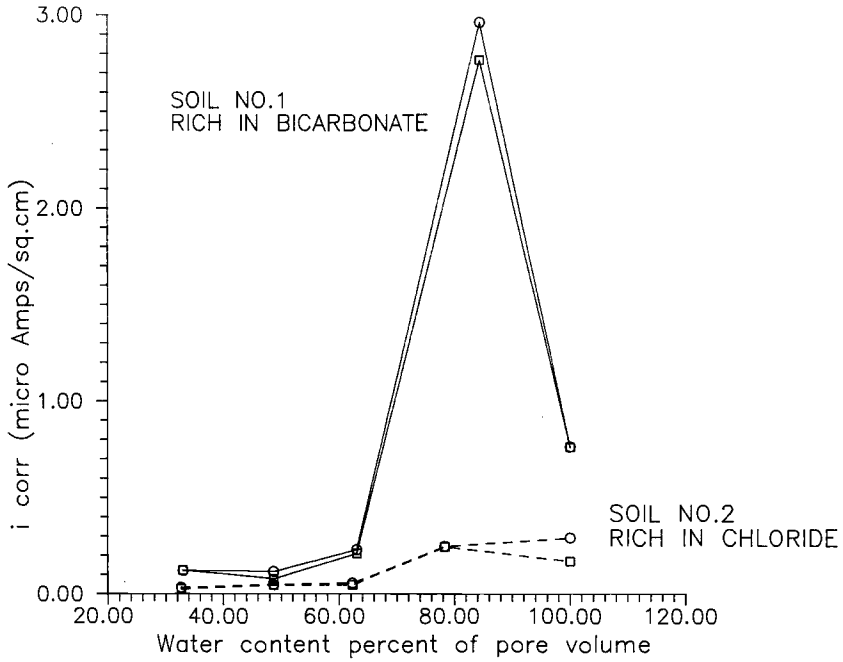


FIG. 7a—Variation of lead corrosion rate with water content in Soil Type 1 and Soil Type 2.

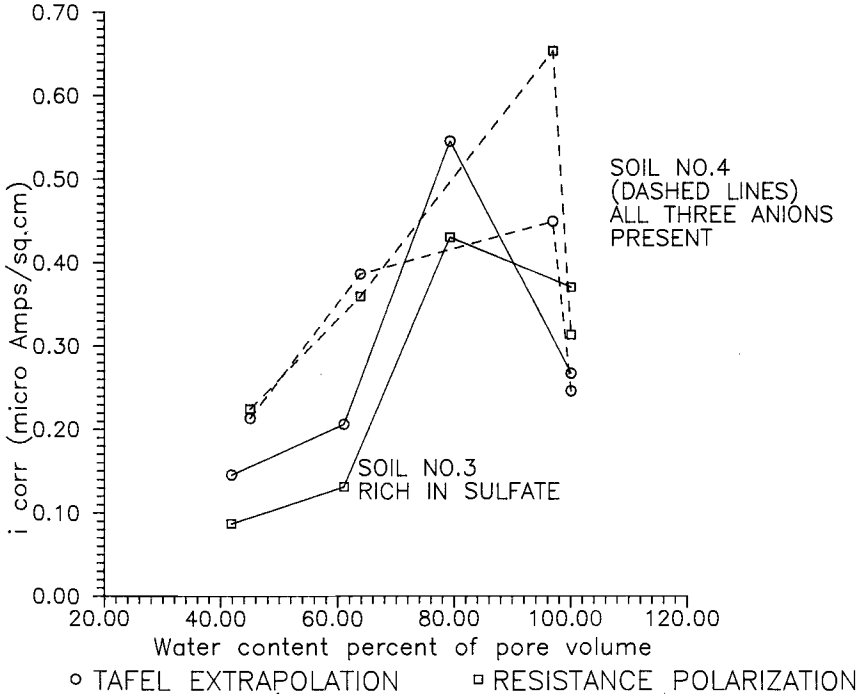


FIG. 7b—Variation of lead corrosion rate with water content in Soil Type 3 and Soil Type 4.

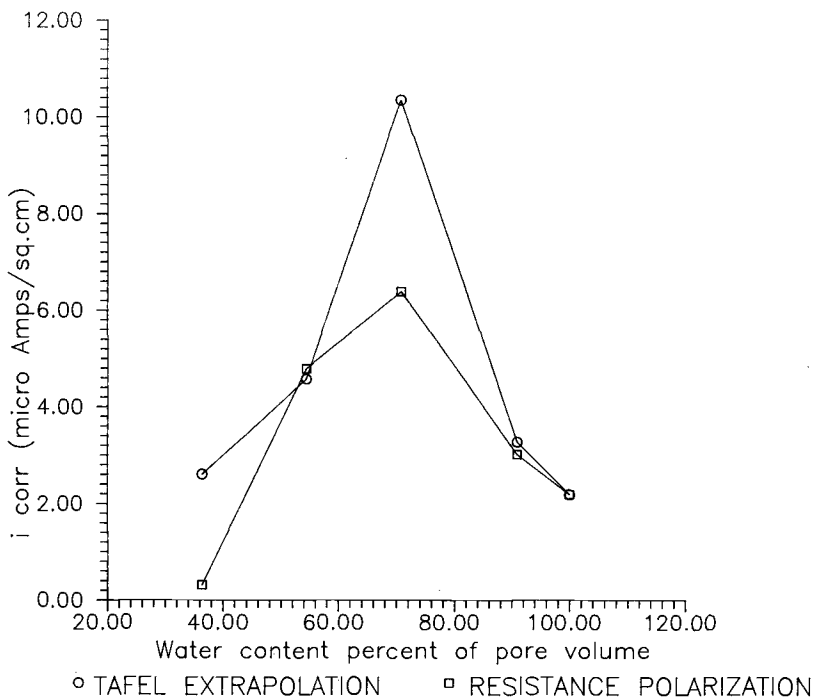


FIG. 8—Variation of steel corrosion rate with water content in Soil Type 5.

In general, there was a good correlation of corrosion rate values obtained by the Tafel extrapolation and the resistance polarization methods as shown in Fig. 7a. However, Figs. 7b and 8 shown deviations at certain points. This difference in values is probably due to variations in calculated Tafel slopes. The corrosion rate values calculated by either method differed by a factor of two or less.

The variation of corrosion rates with depth for lead is shown in Fig. 9. These data should be interpreted only as the corrosion rates in samples taken from these depths. The actual corrosion rates at these depths at any time is a function of the amount of moisture and oxygen available, besides other features of the microscale environment, such as particle size.

## Discussion

The availability of dissolved oxygen and effects of soil composition are expected to control the corrosion process. The soil water plays a very important role in the regulation of air supply. If the pore volume of the soil is only partly filled with water, transfer of oxygen to the metal surface occurs along the major part of the transport pathway by means of diffusion in the gaseous phase, a comparatively rapid process. With an increase in the water content of the soil, corrosion rate will first increase due to a larger wetted surface area and improved conductivity. On the other hand, in cases of saturation and water ponding, the pore volume of the soil is completely filled with water. This acts as a seal and strongly obstructs the supply of air to the metal surface. Oxygen can then reach the metal surface only through the pore water, in which diffusion is very slow as compared even to bulk

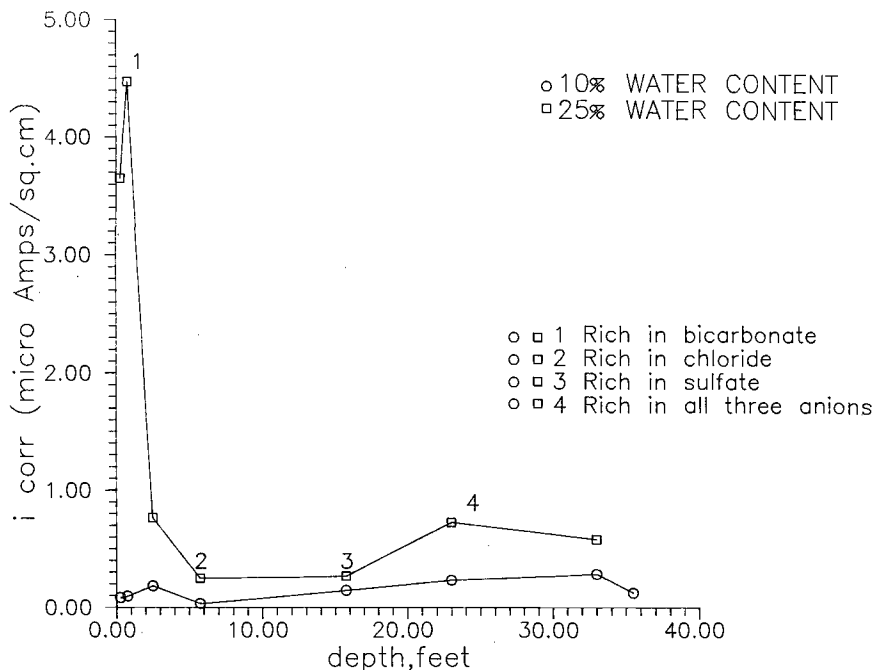


FIG. 9—Variation of soil composition and lead corrosion rate with depth.

water [15,16]. Hence under conditions of ponding, the corrosion rates decrease rapidly due to a strongly obstructed supply of oxygen. This explains the peak observed in Figs. 7 and 8. One of the soils (number 2), that is the soil relatively rich in chloride did not show this sharp peak. However, the corrosion rates observed in this case were extremely small. There may have been other microscale effects which masked the expected behavior. The presence of the peak at intermediate water contents indicates that conditions of alternate wetting and drying which would maintain water in the soil pores at intermediate levels could have the most deleterious effect on the buried metal.

Romanoff has discussed the inhibitive action of anionic species and the effects of their concentrations on the corrosion behavior of lead [16]. He reports that the presence of sulfates, carbonates, chlorides and silicates in relatively high concentrations can have a strongly inhibitive effect on lead. This reduction in the corrosion rates is attributed to anodic polarization from the deposition of corrosion products of low solubility in close proximity to the anodic areas. This along with the intrinsic surface oxide film, explains the low corrosion rates observed of lead in the various soils, especially in the zone with the high sulfate contents. The observance of relatively higher corrosion rates in the soil richer in bicarbonate anions at intermediate water contents may be due to the presence of anions in amounts, insufficient to cause passivation [16]. The corrosion rates of the steel specimens are relatively high because of the absence of a protective surface oxide film.

Some general comments on metallic corrosion *in situ* are warranted at this point. First, the accuracy of these measurements is dwarfed by the natural day to day variability of exposure conditions in the real world. Second, measurements of initial corrosion rates have been made in the laboratory. In general, corrosion rates may be reduced from these initial high rates due to the accumulation of a protective coating of corrosion products.

Third, metallic corrosion in soil depends on particle grain size; smaller and grain size, greater the expected corrosion rate. In our experiments we sieved the soil through a 2000 micron sieve to reduce this to a controlled variable. Finally, metal exposed to different soil regimes (different moisture contents, oxygen contents, etc.) will experience the highest corrosion rates due to the formation of differential aeration cells [15], which have not been considered in the above experiments.

### Summary

A profile of desert soil samples with depth was obtained from the Nevada Nuclear Test Site for the electrochemical corrosion testing of lead and steel, which are construction materials for low level radioactive waste containers. The soils were of high resistivity and required compensation of ohmic interferences during the electrochemical polarization measurements for corrosion rate determination.

Galvanostatic (controlled current) DC measurements were made on buried lead and mild steel specimens using a modified Wheatstone Bridge circuit. Comparison of corrosion rates observed by Tafel extrapolation and polarization measurements showed good agreement. In most cases, corrosion rates were found to increase initially with increasing water content, and then to decrease rapidly. The low corrosion rates observed under conditions of ponding, indicate restricted availability of oxygen at the metal surface. Sulfate and chloride ions showed a strongly inhibitive action on lead corrosion. Whereas, at intermediate water contents, the bicarbonate anions stimulated a relatively higher rate of corrosion. This behavior may be due to its presence in amounts insufficient to cause passivation of the lead surface.

In situ corrosion of the buried containers is expected to be very small because of the very low moisture levels present. It may be observed that conditions of alternate wetting and drying which corresponds to the filling and emptying of the soil pores could have the most deleterious effect on the buried metal.

### References

- [1] Jones, D. A., and Lowe, T. A., *Journal of Materials*, vol. 4, No. 3, Sept. 1969, pp. 600-617.
- [2] Scully, J. R. and Bundy, K. J., *Materials Performance*, April 1985, pp. 18-25.
- [3] Scully, J. R. and Bundy, K. J., *Materials Performance*, July 1984, pp. 50-55.
- [4] Serra, E. T. and Manheimer, W. A., *Underground Corrosion*, Escalante E., Ed., Philadelphia, STP 741, 1981, p. 111.
- [5] Fontana, M. G., *Corrosion Engineering*, 3rd ed., McGraw-Hill, New York, 1986, pp. 499-503.
- [6] Jones, D. A. and Greene, N. D., *Corrosion*, Vol. 22, July 1966, pp. 198-205.
- [7] Jones, D. A., *Corrosion Science*, Vol. 8, 1968, pp. 19-27.
- [8] Jones, D. A., *Corrosion*, Vol. 39, No. 11, Nov. 1983, pp. 444-448.
- [9] Hillel, D., *Fundamentals of Soil Physics*, Academic Press, 1980, pp. 6-20.
- [10] Romanoff, M., *Underground Corrosion*, National Bureau of Standards, Circular 579, 1957, pp. 115-117.
- [11] Romanoff, M., *Underground Corrosion*, National Bureau of Standards, Circular 579, 1957, p. 79.
- [12] Dean, Jr., S. W., "Electrochemical Techniques of Corrosion Testing," National Association of Corrosion Engineers 1976, p. 52.
- [13] Jones, D. A., *Corrosion Science*, Vol. 11, 1971, pp. 439-451.
- [14] Jones, D. A., *Corrosion*, Vol. 28, No. 11, Nov. 1972, pp. 421-423.
- [15] Wranglen, G., *An Introduction to Corrosion and Protection of Metals*, Chapman and Hall Publishers, New York, 1985, pp. 124-139.
- [16] Romanoff, M., *Underground Corrosion*, National Bureau of Standards Circular 579, 1957, p. 89.

## Measurements of IR-Drop Free Pipe-to-Soil Potentials on Buried Pipelines

---

**REFERENCE:** Thompson, N. G. and Beavers, J. A., **Measurements of IR-Drop Free Pipe-to-Soil Potentials on Buried Pipelines,** *The Measurement and Correction of Electrolyte Resistance in Electrochemical Tests, ASTM STP 1056*, L. L. Scribner and S. R. Taylor, Eds., American Society for Testing and Materials, Philadelphia, 1990, pp. 168-179.

**ABSTRACT:** The purpose of this paper is to examine current interruption methods of estimating the level of polarization (off-potential) on a buried pipeline and to indicate some of the specific problems associated with field measurements. Data are reviewed that indicate the magnitude of the voltage (IR-drop) errors associated with potential measurements on buried pipelines. Oscilloscope tracings of pipe-to-soil potential waveforms are presented and a "spiking" condition is discussed which can significantly affect the ability to make an off-potential measurement at the instant of interruption. Stray currents and long-line currents, which can affect the ability to measure the level of polarization on an operating pipeline, are discussed. Methods of detecting stray currents and long-line currents are briefly presented.

**KEY WORDS:** cathodic protection, off-potential, current interruption, voltage error, IR-drop, IR error, pipe-to-soil potential, voltage waveforms, oscilloscope, pipelines, buried pipe, steel, soil, long-line current, stray current, potential spike

The estimation of voltage error (IR-drop) in potential measurements of a polarized electrode is not a new technology. Circuits which interrupt the applied current and measure the potential immediately following interruption, have been available for some time [1-9]. With these circuits, it is desired to measure the potential following interruption but prior to any depolarization of the electrochemical interface, such that only the instantaneous IR-drop is removed. Other methods for IR-drop correction include bridge circuits [10-12] and AC techniques [13,14]. The bridge circuits are primarily laboratory methods and have not been developed for the field. An AC technique that can determine the resistive component of IR-drop is usually of little benefit in the field because the current component can typically not be measured and estimates at best are very poor. However, the AC technique developed by Camitz, et al. [13] was designed for interference situations in the field.

There has been a significant increase in interest over the past five years, within the cathodic protection industry, concerning the measurement of the IR-drop in pipe-to-soil potential readings. This interest, in large part, was created by the on-going reevaluation of the National Association of Corrosion Engineers (NACE) criteria for cathodic protection, Recommended Practice RP-01-69 [15]. The reevaluation of the criteria was driven, in part, by an increased awareness that IR-drop may introduce a sizable error in a pipe-to-soil potential measurement in many circumstances.

---

<sup>1</sup> President and vice-president, respectively, Cortest Columbus, Inc., 2704 Sawbury Blvd., Columbus, OH 43235.

The acknowledgment that IR-drop in pipe-to-soil potential measurements can be a problem in determining the level of polarization on a cathodically protected pipe has been universally agreed upon for a long time. The magnitude of the IR-drop and the likelihood that a large IR-drop is present is often debated. It is true that, on many pipelines, little or no IR-drop exists in the pipe-to-soil potential measurements. However, there are quite a few circumstances in which relatively large IR-drops in pipe-to-soil potentials exist [16]. Figure 1 shows results of a study by Thompson, et al., in which 115 sites on operating pipelines across the U.S. were examined and on- and off-potentials were measured [17]. It should be noted that sites of high IR-drop were requested, such that this did not represent a random sampling. Figure 1 shows the number of sites (readings) that fall into the different percentage classifications of IR-drop error, given as the percent difference between on- and off-potential. These data show that the magnitude of IR-drop error can be quite significant. In this particular study, 64% of the 115 sites tested had IR-drops which constituted 30% or more of the pipe-to-soil potential measurement.

In this paper, ideas and data are presented which have been gathered over several years of field work. Therefore, the structure of the paper is different from a standard research paper. The discussion includes data that have been previously published, but are discussed in this paper in the specific context of IR-drop correction in pipe-to-soil potential measurements. Any previously published data are clearly referenced.

## Discussion

### Off-Potential Measurements

Some of the commonly used "pipeline" terminology and their definitions are presented below since these terms are not generally used in other areas of corrosion. The pipe-to-soil potential refers to the measurement of the potential of the buried pipe with respect to a reference electrode generally placed at ground level above the pipe. The on-potential refers

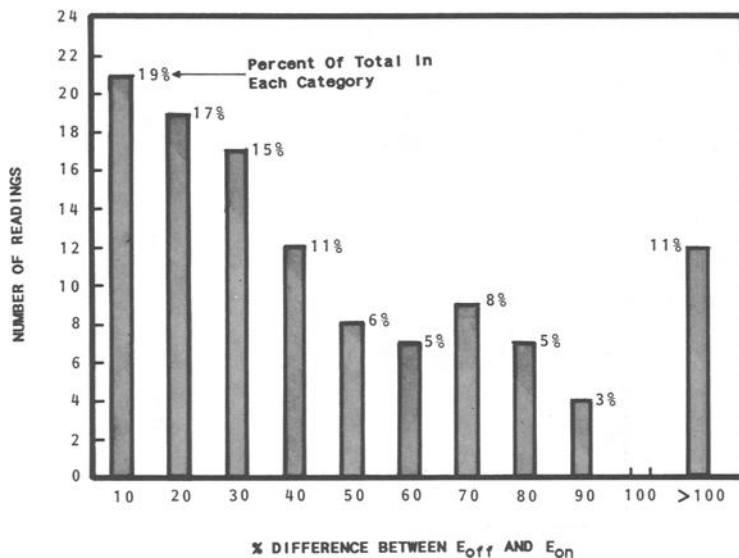


FIG. 1—Percent difference between the off-potential and the on-potential for several locations on operating pipelines.

to the pipe-to-soil potential measured with the cathodic protection (CP) system on, that is, IR-drop is included. The off-potential (sometimes called the instant-off potential) refers to the estimate of the polarized level of the pipe surface, that is, IR-drop free potential. The term off-potential is related to the technique by which it is measured.

Although there are several variations and schemes for IR-drop determination, there are two general methods of practically correcting for IR-drop in a pipe-to-soil potential measurement on an operating pipeline: (1) interrupting the CP current to the pipe ( $I = 0$ ) or (2) placing the reference probe near the pipe surface ( $R \sim 0$ ). The process of placing a reference electrode near the pipe surface is difficult and time consuming to accomplish, in addition to being limited in its application to bare pipe. For coated pipe, the reference electrode would have to be placed at the exact location of the holiday and, furthermore, be small enough to be placed very near the pipe surface.

The most common method of correcting for IR-drop in a pipe-to-soil potential measurement is interrupting the CP system, measuring the instantaneous drop in potential, and estimating the level of polarization of the pipe surface (off-potential) by subtracting this instantaneous potential drop from the on-potential. Figure 2 shows this measurement technique indicating the on- and off-potential values and the IR-drop. In this paper, the discussion is limited to interruption of the CP current for estimating IR-drop.

In general, the two methods used for recording current interruptions are oscilloscopes and strip chart recorders. These two methods will be discussed in detail later. Briefly, for many of the operating pipeline conditions, strip chart recorders are better for recording the interruption event because the significant ac interference often masks the interruption process on an oscilloscope. Interrupting the CP system of a pipeline causes the current to the pipe to become zero at that instant. The electrochemical (soil-steel) interface at the pipe surface has a capacitive component which gives the potential-time transient, depolarization, an exponential decay. Figure 2 shows this schematically. On operating pipelines, however, the break between the instantaneous drop (IR-drop) and depolarization is not as clear as the sharp break shown in Fig. 2. Figure 3 shows a more typical potential-time transient following interruption measured using a strip-chart recorder with a full-scale response time of 1 s and a chart speed of 1 cm/s. In this case, there is no clear break following the instantaneous drop. Different methods of selecting the IR-drop from a strip chart recording have been used. The following is a simple method used by the authors in both field and laboratory studies which removes some of the ambiguous nature of selecting IR-drops from strip-chart recordings. A straight edge is placed, or line is drawn, along the linear portion

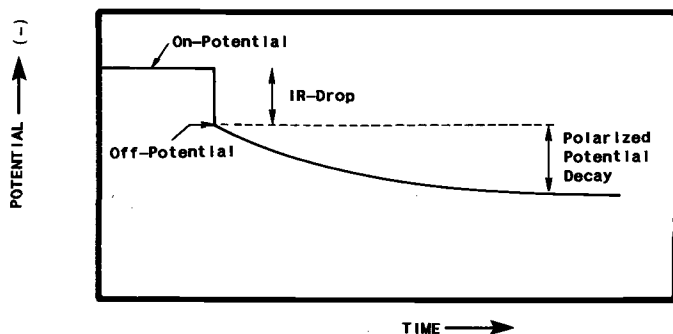


FIG. 2—Schematic diagram of a potential-time transient following interruption of a CP system, indicating on- and off-potentials.

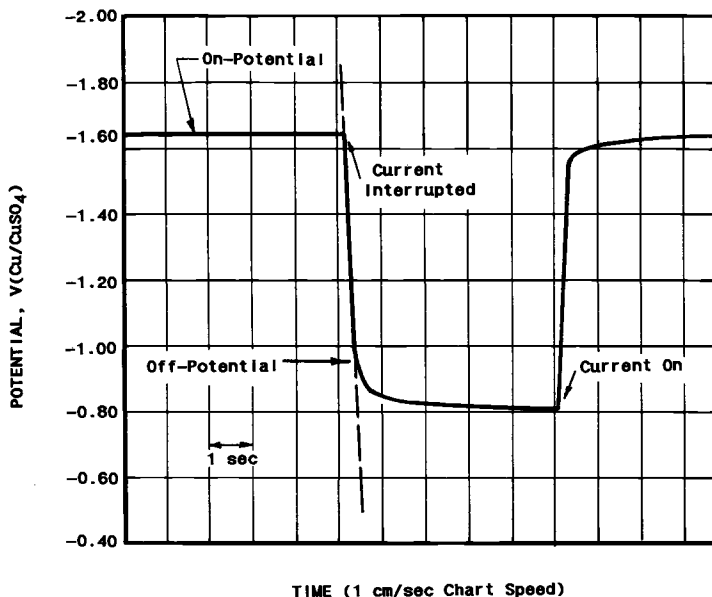


FIG. 3—Strip-chart recording of a potential-time transient following interruption during a typical pipe-to-soil potential measurement.

of the initial transient. The point at which the potential time curve deviates from this straight line denotes the break between IR-drop and depolarization (see Fig. 3). This method has been used in both the field and laboratory along with an oscilloscope and has proven to be quite reliable.

On operating pipelines, one of the primary issues is to ensure that all of the current to the pipe has been interrupted. Although there are some specific methods in which rectifiers are interrupted in sequence [18], it is generally required that all rectifiers, which supply current to the area of pipe being measured, be interrupted simultaneously. There are synchronous interrupters available for this purpose. At a minimum, the rectifiers on either side of the test point should be interrupted, and more typically, the three or four closest rectifiers should be interrupted. Past experience can be used in selecting rectifiers for interruption. Obviously, a small CP system, involving a single rectifier for an isolated section of pipe, is a much easier system on which to work.

One parameter which must be considered is the on and off cycle for interruption. If the CP system remains off for significant time periods, the amount of cathodic polarization of the pipe will decrease and a condition is established where the measurement method alters the potential of the pipe. This, of course, is very undesirable. The on- and off-interruption cycle is selected to fit the rate at which off-potential measurements are to be taken. The largest practical on-to-off cycle ratio is desired. As a rule-of-thumb, the on cycle is selected to be a minimum of three to five times the length of the off cycle. A typical cycle time for a manual reading of the interruption is 5 to 10 s off—25 to 50 s on.

Methods of recording IR-drops that have been used, and are being used, range from visual examination of analog or digital meters to sophisticated data processing systems. The process of visually selecting an off-potential from an analog or digital meter is by far the most subjective method. It is the authors' opinion that visual selection methods should be used only when no other means exist. On the other hand, strip-chart recorders are suf-

ficient to establish the off-potential for most pipeline conditions. It is possible that the response of a strip-chart recorder would not be able to differentiate very fast depolarization from IR-drop, and the off-potential value determined would be more positive than the true polarized level of the pipe. However, these conditions have not been confirmed in the field. Pipe-to-soil potential waveforms measured using oscilloscopes are discussed in greater detail later. As previously stated, the AC noise picked up on the pipeline makes the use of an oscilloscope to measure off-potentials very difficult in many circumstances.

Automated data processing systems with synchronous interrupters are becoming more prevalent. In general, these systems capture data and select a potential at some time interval following interruption, which can be a few milliseconds to several hundred milliseconds. Some of these automated systems permit the time following interruption at which the off-potential is selected to be varied by the user. The exact selection process, criteria, and data averaging or filtering depends on the specific manufacturer. These types of systems are designed for both test site location measurements and long-line surveys. One consideration, which will become more apparent in the following discussion of waveforms, is the existence of a spike in the pipe-to-soil potential immediately following interruption [17,18]. The spike condition makes selection of the time interval between current interruption and the off-potential measurement very important.

A device that is just coming onto the market, which was developed by Thompson, et al. [17] for the Gas Research Institute (GRI), was named the Waveform Analyzer by its developers (its marketed name may be different). This device utilizes internal computer algorithms for estimating the off-potential and does not require synchronous interrupters. However, special interrupters are required for each rectifier from which IR-drop correction is performed. The special interrupters are placed in the rectifiers in a similar manner to standard interrupters. The Waveform Analyzer is used in much the same way a standard voltmeter is used except that the internal algorithms sample the pipe-to-soil potential waveform and estimate the off-potential. The algorithms are designed to optimize the time interval for selection of the off-potential with respect to the spiking condition discussed in the following section. Because of the time required for data processing, the off-potential measurements made by the Waveform Analyzer probably take longer than those required by other automated off-potential devices.

### *Analysis of Pipe-To-Soil Potential Waveforms*

Much of the work performed by Dr. Thompson during the GRI project [17] centered around the measurement of pipe-to-soil potential waveforms using an oscilloscope or data processor at over one hundred field sites on operating pipelines. Although several of the waveforms were previously presented [18], their direct impact on the measurement of off-potentials has not been clearly discussed.

In the field, the standard CP power supply consists of either a full-wave or half-wave rectifier and the output is applied between the pipeline and anode bed. In the rectified AC signal, the current output goes to zero 120 (or 60) times a second for the full-wave (or half-wave) rectifier. Thereby, the standard rectifier itself acts as a fast interruption circuit. This rectified signal is manifested in the pipe-to-soil potential measurement as shown in Fig. 4. The on-potential is related to the RMS value of the voltage waveform. The off-potential is the DC level obtained when the current goes to zero. Therefore, theoretically, the off-potential can be measured from the pipe-to-soil potential waveform without any external interruption. Figure 5 shows an actual pipe-to-soil potential waveform which exhibits near ideal behavior. The off-potential measured with a strip-chart recorder is indicated in the figure. It is seen that the off-potential from a strip-chart recorder is similar to the off-potential or

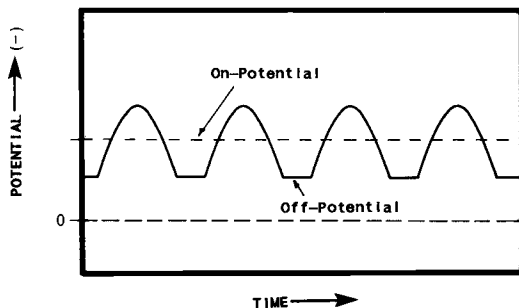


FIG. 4—Schematic diagram illustrating a rectified dc signal and the corresponding off-potential and on-potential.

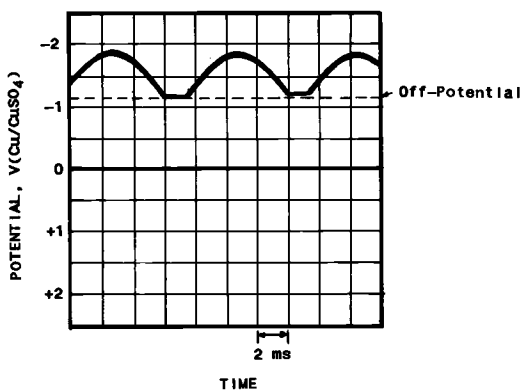
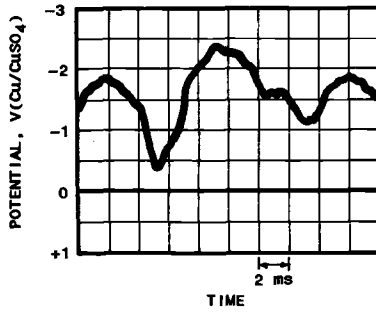


FIG. 5—Near ideal rectified pipe-to-soil potential waveform.

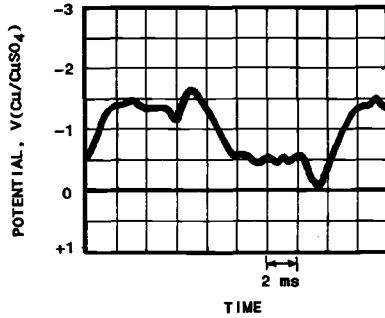
DC potential level when the rectified current goes to zero. This particular waveform was measured on a small (less than 30 meters) isolated length of pipe with a single rectifier CP system using a remote anode bed. This example indicates that “ideal” pipe-to-soil potential waveforms do exist, but it should be noted that only a few of these were observed, two or three out of 115 sites examined.

Unfortunately, a high percentage of pipe-to-soil potential waveforms have a significant degree of AC noise. A typical waveform containing AC noise is shown in Fig. 6. From Fig. 6a (rectifier on) it is obvious that an off-potential cannot be selected from the waveform. Furthermore, because AC noise exists with the rectifier off (Fig. 6b), it is also very difficult, if not impossible, to determine an off-potential from the oscilloscope using an external interruption method. To establish an off-potential, a filtering system is required such that most of the AC noise is filtered out and interruption is performed utilizing the DC signal. A strip-chart recorder provides just such a filtering system via the mechanical movements comprising the strip chart recorder. The limitation of the strip-chart recorder is in the response time of the recorder, which limits its ability to distinguish between the instantaneous IR-drop and very fast depolarization of the potential-time transient.

In addition to the AC noise problem, there is another phenomena, a spiking condition, which exacerbates the problem of measurement of off-potentials [17,18]. Figure 7 shows a pipe-to-soil waveform that is relatively free of AC noise, but has a small potential perturbation (spike) at the beginning of what should be a constant potential DC level (compare



(a) Rectifier On



(b) Rectifier Off

FIG. 6—Typical pipe-to-soil potential waveform showing a c noise of different frequencies.

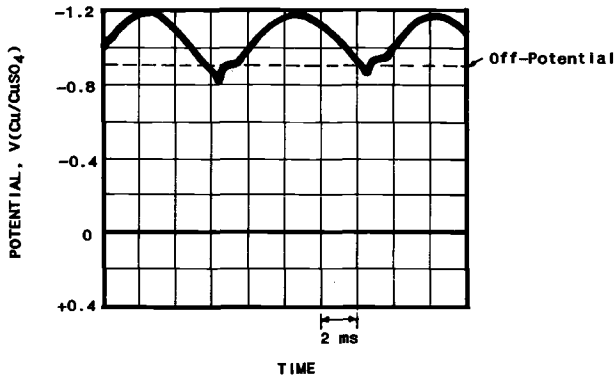


FIG. 7—Pipe-to-soil potential waveform showing a small spiking condition.

Fig. 7 with Fig. 5). For this particular waveform, the plateau region for the off-potential remains visible so that the spike does not mask the off-potential. Figure 8 shows a severe spiking condition in which the spike travels through zero. There is no clear relationship between the waveform and the off-potential measured using synchronous interruption of multiple rectifiers and a strip-chart recorder. In the previously referenced GRI study [17], 39% of the 115 pipe locations measured exhibited some form of a spiking condition in the pipe-to-soil potential waveform.

It was also shown in the GRI study that the spiking condition persists even when the rectifier is interrupted externally. Figure 9 shows a schematic of the waveform following external interruption with the 60 Hz and higher frequency noise removed. The difference between Fig. 9 and Fig. 2 is the time scale over which the schematic corresponds. In Fig. 9, the time scale is on the order of 500 ms while, in Fig. 2 the time scale is 10 to 20 s. On a strip-chart recorder, the response of the recorder is typically not fast enough and/or the mechanical filtering too extensive to pick up the spiking condition. Only once during the examination of 115 pipe locations in the GRI study and well over 100 locations in other

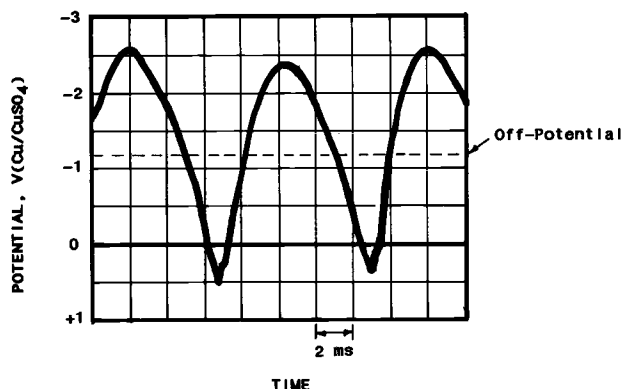


FIG. 8—Pipe-to-soil potential waveform showing a severe spiking condition.

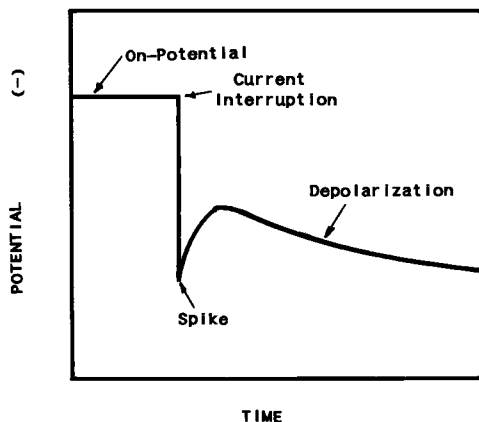


FIG. 9—Schematic diagram of a potential-time transient following interruption with all 60 Hz and its harmonics removed and corresponding to a time scale of 50 to 500 ms.

miscellaneous field work, have the authors observed a small spike on a strip-chart recording.

Because the spike alters the waveform even with 60 Hz and greater frequencies removed, the spiking condition can have a significant impact on the ability to measure off-potentials at very short time intervals following interruption. The mechanical filtering inherent in the strip-chart recorder and the chart speed, which determines resolution on the time scale (approximately 1 cm/s), makes the strip-chart recorder a good instrument for measuring off-potentials on operating pipelines. With faster data processing devices or devices with less filtering, care must be taken when measuring off-potentials in the presence of the spiking condition.

It is speculated that the spiking condition is a result of an induction component of the pipeline-CP system. In fact, very little work has been performed for the purpose of understanding the cause of the spike condition. Until more is known as to the cause of the spiking condition, attempts to extract the value of the real polarized level of the pipe surface at the instant of interruption will probably not be successful.

#### *Factors That Affect Accuracy of Off-Potentials*

It is emphasized that the off-potential is an estimate of the polarized potential and the accuracy of this estimation depends on several factors including (1) the instrumentation used to measure the instantaneous potential drop following interruption and (2) the rate of activation depolarization. For example, the larger the time constant for the capacitive potential decay, the slower the instrument can be for measuring an accurate off-potential. In the field, the rate of potential decay (depolarization) can vary greatly depending on the type of soil, moisture content of the soil, level of CP previously applied, and length of time CP has been applied.

In addition to the above variables which can affect the measurement of the off-potential, there are several special considerations specific to long buried pipelines. The two primary considerations are stray currents and long-line currents. The IR-drop created by these currents can either add to or subtract from the value of a pipe-to-soil potential, depending on the direction of current flow in the soil. Interference and stray currents are often caused by the proximity of pipelines (in the same right-of-way or crossing) owned and operated by different companies. Quite often, the different pipelines are bonded together to help prevent interference and stray currents. All of this makes current interruption very difficult, if not impossible, on certain portions of pipelines.

Stray current is just what the name implies, a DC current in the soil which is not associated with the CP system of the pipe being measured; for example, current from a separate CP system to a nearby pipeline or tank, or a current associated with a DC transit or rail system. Stray current can be current flowing past the pipe or can be current being picked up on the pipe or discharged from the pipe.

A long-line current is created when a potential gradient exists on the pipeline. This is the rule more often than the exception because of the heterogeneous nature of the environment in which the pipe is buried, for example, resistivity of the soil varies, stream/river crossings, etc. When a potential gradient exists, a differential cell couple is created and positive current flows through the ground from the more negative potential area (anodic) to the more positive potential area (cathodic). Thereby, long-line currents are produced that can cause IR-drop in the soil.

Long-line and stray currents are difficult to quantify since IR-drop is a vector quantity. IR-drop due to long-line and stray currents can be detected by ground level cell-to-cell measurements, that is, the placement of two reference electrodes 3 to 10 m apart and the

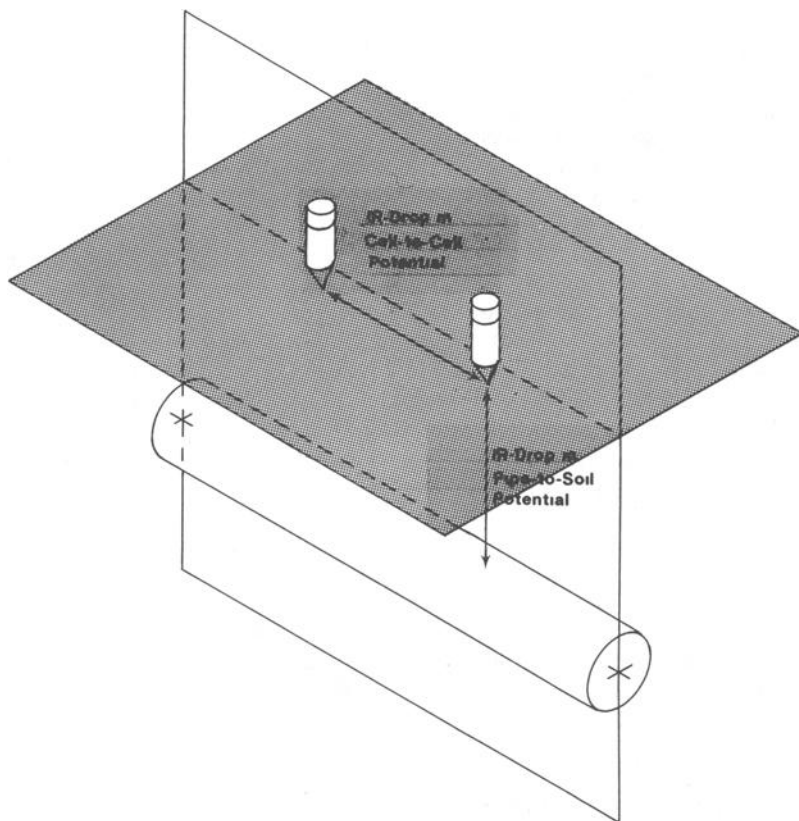


FIG. 10—Schematic illustration showing the vector nature of IR-drop.

measurement of the potential difference. However, IR-drop measurements made on the surface of the ground cannot be directly related to the IR-drop in a plane perpendicular to the surface; the latter is the plane in which the IR-drop occurs in a pipe-to-soil potential measurement (see Fig. 10). For example, if current is flowing with a vector which is longitudinally along the pipe, no IR-drop due to that current would be measured in the pipe-to-soil measurement, even though the IR-drop in the cell-to-cell measurement made at ground level longitudinally along the pipe could be significant. Although a direct comparison is not possible, cell-to-cell potential measurements made with the CP system off are useful in establishing whether stray or long-line currents are present. To check for stray or long-line currents, cell-to-cell measurements should be made both longitudinally along the pipe and transverse to the pipe.

Quite often, cell-to-cell potential measurements are made over top of a pipeline (transverse and longitudinal) to determine if interference currents exist or to determine whether all current to the pipeline has been interrupted. To make the measurement, the potential difference between two reference electrodes is measured in an environment that has no current flow to establish a reference potential difference (should be 5 mV or less). Next, the reference electrodes are placed in the ground and the magnitude of the potential difference is proportional to the current flow in the ground and the sign (plus/minus) indicates direction.

The following discussion illustrates how long-line currents can affect the ability to estimate the polarized level of a pipe (off-potential) utilizing interruption methods. Cell-to-cell potential measurements were made transverse to the pipe with one reference cell over the pipe and the other reference cell 6 m transverse to the pipe. With the CP system on, the cell-to-cell potential was on the order of 0.5 V, with the (negative) lead of the meter connected to the cell over the pipe (current was flowing toward the pipe). When the CP system was interrupted, the cell-to-cell potential immediately (visually examining a digital meter) went to approximately  $-0.4$  V. This indicated that the net current toward the pipe reversed upon interruption. This was likely due to long-line currents in which the area of pipe being tested was more negative (anodic) to other sections of pipe upon interruption. The significance of this is that the IR-drop at this particular location went from a negative component to a positive component immediately upon interruption. It is possible that an oscilloscope (which was not available) could have established the IR-drop if no AC interference was present. Although the majority of locations on a pipeline will not exhibit such extreme conditions, it is clear that off-potentials are not a foolproof measurement. In certain circumstances, other measurements are necessary, such as cell-to-cell potential measurements, to establish whether stray or long-line currents exist.

### Conclusions

1. Off-potentials determined using interruption methods generally provide a good measure of the level of polarization on a pipeline with CP applied.
2. It must be remembered that off-potentials are estimates of the polarized level of the pipe surface and can be complicated by stray currents, long-line currents, the "spiking" condition, and the ability to interrupt all rectifiers supplying current to the portion of pipe being measured.
3. A "spike" frequently is present in the pipe-to-soil potential waveforms upon external interruption of the current or during the normal rectifier operation, 60 or 120 Hz, cycle. The consequence of the "spike" is that off-potentials more positive than the polarized level of the pipe surface may be predicted if the spike is not considered.
4. The cause of the spike is not fully understood and methods of compensating for its presence in pipe-to-soil potential transients following interruption typically are not available.
5. There are several instrumentation configurations for determining the off-potential of a cathodically protected pipe. The limitations of the instrumentation must be understood, especially in consideration of the "spiking" condition.

### References

- [1] Hickling, A., "Studies In Electrode Polarization; Part I—The Accurate Measurement Of The Potential Of A Polarized Electrode," *Transactions, Faraday Society*, Vol. 33, 1937, p. 1540.
- [2] Darnielle, R., "Measurement Of Electrode Potentials And Polarization In Soil Corrosion Cells," *Journal of Research National Bureau of Standards*, Vol. 25, 1940 (RP1336), p. 421.
- [3] *Underground Corrosion*, Logan, K. H., National Bureau of Standards, Circular C450, 1945, p. 182.
- [4] Miles, J. A., "Eliminating IR-Drops From Potential Measurements," *Corrosion*, Vol. 28, 1972, p. 4.
- [5] Britz, D. and Brocke, W. A., "Elimination Of IR-Drop In Electrochemical Cells By The use Of A Current Interruption Potentiostat, *Electroanalytical Chemistry and Interfacial Electrochemistry*," vol. 58, 1975, p. 301.
- [6] "Technology of Measurement," *Handbook Of Cathodic Protection*, Edited by W. von Baeck-

- mann and W. Schwenk, English translation by E. Neufeld and P. Neufeld, Portcullis Press, Ltd., England (1975), p. 90.
- [7] Kasahara, K., Sato, T., and Adachi, H., "An Improved Method For Measuring Pipe-To-Soil Potential And Current Density At Cathodically Protected Pipelines," *Materials Performance*, vol. 18, no. 3, 1979, p. 79.
- [8] Kasahara, K., Sato, T., and Adachi, H., "Results of Polarization Potential And Current Density Surveys On Existing Buried Pipelines," *Materials Performance*, vol. 19, no. 9, 1980, p. 45.
- [9] Williams, L. F. G. and Taylor, R. J., "IR Correction; Parts I—A Computerized Interrupt Method," *Journal of Electroanalytical Chemistry*, 1980, p. 293.
- [10] Pearson, J. M. "Null Methods Applied To Corrosion Measurements," *Transactions of the Electrochemical Society*, vol. 81, 1942, p. 485.
- [11] Newberry, E., "Reversible Overvoltage," *Transactions of Faraday Society*, vol. 43, no. 127, 1947, p. 127.
- [12] Kordesh, K. and Marko, A., "Sine Wave Pulse Current Testor For Batteries," *Journal of the Electrochemical Society*, Vol. 107, No. 6, 1960, p. 480.
- [13] Camitz, G., Mattsson, E., Carre, G., and Linder, B., "Measurement Techniques For Determining Interference Effects," *Materials Performance*, Vol. 20, No. 11, 1980, p. 35.
- [14] Mansfeld, F., Kendig, M. W., and Tasi, S., "Corrosion Kinetics in Low Conductivity Media—I. Iron in Natural Waters," *Corrosion Science*, Vol. 22, No. 5, 1982, p. 455.
- [15] National Association Of Corrosion Engineers (NACE) Recommended Practice RP-01-69, "Control Of External Corrosion On Underground Submerged Metallic Piping Systems."
- [16] Barlo, T. J. and Fessler, R. R., Annual Report on Project PR-3-93, American Gas Association, Arlington, VA, Catalog L51394 (1979).
- [17] Thompson, N. G., Ruck, G. T., Walcott, K. J., and Koch, G. H., Annual Report on "Phase IV—Effectiveness Of Cathodic Protection," *Gas Research Institute Report GRI87/0020*, March, 1987.
- [18] Thompson, N. G., Walcott, K. J., and Burnham, K. B., "Instruments To Monitor The Level of Cathodic Protection On Buried Pipelines," *Proceedings 1986 International Gas Research Conference*, Toronto, Canada, Sept. 1986.

## Elimination of IR Error in Measurements of Corrosion in Concrete

---

**REFERENCE:** Escalante, E., "Elimination of IR Error in Measurements of Corrosion in Concrete," *The Measurement and Correction of Electrolyte Resistance in Electrochemical Tests*, ASTM STP 1056, L. L. Scribner and S. R. Taylor, Eds., American Society for Testing and Materials, Philadelphia, 1990, pp. 180-190.

**ABSTRACT:** The deterioration of concrete bridge decks owing to the corrosion of imbedded steel has generated interest in developing techniques to measure the corrosion of steel in this high-resistivity environment. Several electrochemical polarization methods have been used successfully in the laboratory. This paper describes the use of current interruption to eliminate the IR that arises in measuring the potential of steel during polarization measurements.

Polarization measurements were carried out using a small, portable computer system that controlled and monitored the potential of the steel and the applied current. Current was cycled on and off, with the potential measured during the off cycle and the current during the on cycle. The duty cycle was 2.2 s on and 0.4 s off, and sampling of the voltage occurred approximately 75 ms after the current was interrupted. Results indicated that 95% of the error is eliminated using this technique.

**KEY WORDS:** bridge deck corrosion, corrosion of steel, corrosion rate measurement, IR error, polarization resistance, steel in concrete

Measuring the corrosion rate of a metal in a poorly conducting electrolyte is a problem that has captured the interest of corrosion scientists for some years, and in each case the motivation for that interest has been different [1,2]. More recently, the deterioration of steel reinforced structures resulting from the corrosion of the imbedded steel, has motivated us to focus our attention on the corrosion process in concrete, a highly resistive media. However, this time technology, in the form of portable computers, has made it possible to apply well-established laboratory techniques to measurements in the field.

The use of an electrochemical polarization method for the measurement of corrosion is attractive because it is nondestructive and several approaches have been used successfully in the laboratory [3,4,5]. In a resistive media where a direct current,  $I$ , is used to change the potential of a working electrode (WE), some means must be used to eliminate or compensate for the error in potential,  $IR$ , that results when the potential of the WE is measured. The source of this resistance,  $R$ , is the sum of all resistive components between the WE and the reference electrode (REF). Positive feedback circuits to compensate for this error in the presence of a direct current have been investigated [6]. Other workers have used current interruption techniques for eliminating  $IR$  from the measurement [7,8,9]. This study describes the use of a portable computer system that applies polarization resistance and current interruption to measure the corrosion of steel in concrete in laboratory and field situations.

<sup>1</sup> Metallurgist, National Institute of Standards and Technology, Gaithersburg, MD 20899.

**Approach**

Preliminary studies, using manually controlled equipment, indicated that the corrosion of steel in concrete can be measured by using polarization techniques [10,11]. However, the manually controlled procedure used is very slow and tedious, and not at all suited for rapid field measurements. Furthermore, IR compensation is always difficult and, at times, questionable with these manually controlled methods. The use of portable computer equipment opens new avenues to the application of laboratory methods to field measurements, especially where a highly resistive medium is encountered.

**System Description**

The computer controlled device operates by modulating the current applied between the WE and the counter electrode (CE) to maintain a potential difference ( $\Delta E$ ) between the WE and the reference electrode (REF),  $E_w - E_r$ , that is 10 mV less than the same potential difference at open circuit (OC)

$$(E_w - E_r) - (E_w - E_r)_{OC} = -10 \text{ mV} = \Delta E \tag{1}$$

The voltage measurement, however, is taken during a brief period while the current is interrupted so that the potential owing to the IR drop is absent, but soon enough after the interruption of the current so that the potential owing to polarization of the WE has not yet decayed significantly.

Figure 1 is a schematic diagram showing the relationship of the three electrodes, the current control switches, and the power supply. The details of the operation of the computer controlled system are as follows. First, the three potentials  $V_1$ ,  $V_2$ , and  $V_3$  are measured in the open circuit condition. A voltage  $V$  equal and opposite to  $V_1$  is then applied by the power supply. The switch,  $S_1$ , in series with a 4.7-K  $\Omega$  resistor, closes, and the

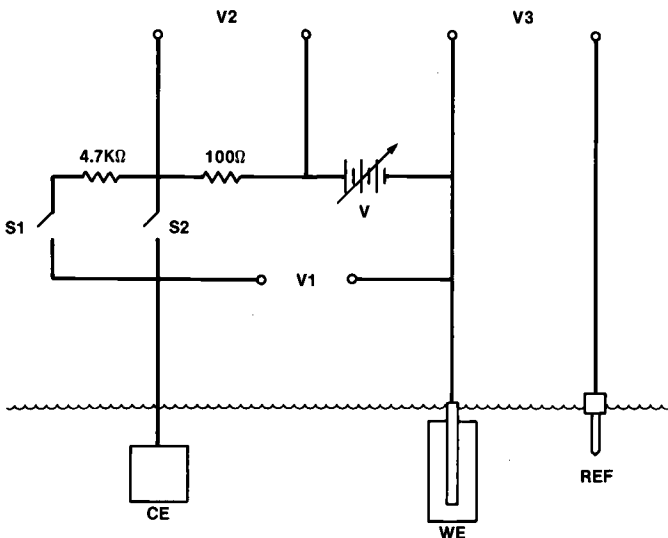


FIG. 1—Schematic diagram of the three electrode system, power supply, switches, and measurement points.

applied current,  $I_2$ , through the circuit is determined by measuring  $V_2$  across a  $100\text{-}\Omega$  resistor ( $I_2 = V_2/100$ ). The power supply voltage  $V$  is then adjusted to make  $I_2$  equal to zero so that applied current at the start of the measurement is zero. This current zeroing process is repeated more accurately when the second switch,  $S_2$ , is closed. The entire current zeroing procedure occurs in less than 10 s and prepares the system for the polarization measurement.

Briefly, the measurement of corrosion occurs in two stages, as follows. Immediately after the open circuit potential is measured, the first stage, called the "setting" stage, begins, and it is during this period of time that the WE electrode is polarized to  $(DE) = -10\text{ mV}$ . Once the computer senses that the preselected target voltage of  $-10\text{ mV}$  is reached, it enters the second stage, called the "holding" stage, where the applied current is controlled to maintain the WE potential at  $-10\text{ mV}$  for a preselected period of time (3 min). The open circuit potential and the series of readings of polarized potential and applied current taken during the holding stage are stored in memory and used to calculate corrosion current. An example of the potential and current traces as observed with a digital oscilloscope during a measurement sequence are shown in Fig. 2. Figure 3 is an idealized drawing of the oscilloscope trace identifying the setting and holding stages. Not easily visible in Figs. 2 and 3 is the current interruption taking place during the measurement.

By magnifying the wave forms of current and potential, the details of current interruption events can be readily examined. A magnified view of the oscilloscope trace of the current applied during the "holding" portion of the measurement is shown in Fig. 4. The idealized wave form of this trace is shown in Fig. 5, and illustrates more clearly the application of current as a function of time. This figure shows that the duty cycle is 2.2 s with the current on and 0.4 s with the current off. The current is measured at the end of the

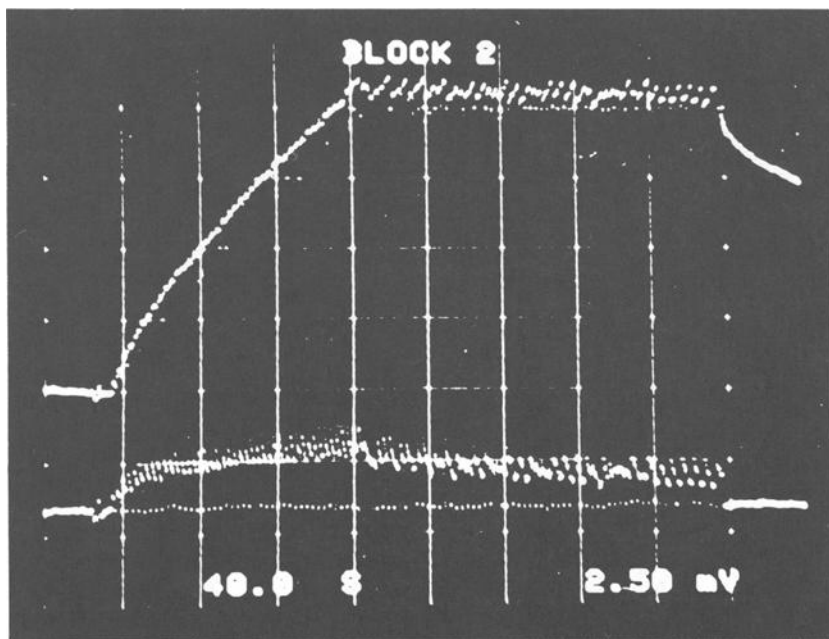


FIG. 2—Example of the potential and current traces, as a function of time, observed with a digital oscilloscope during a complete measurement sequence.

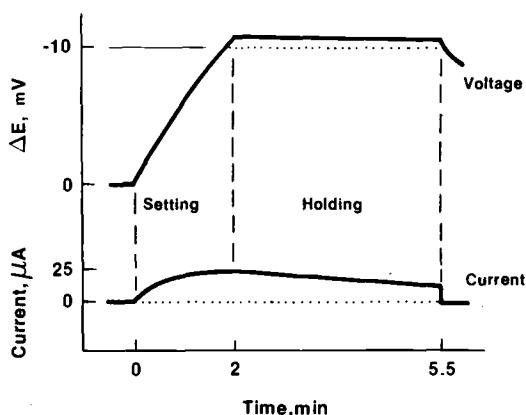


FIG. 3—An idealized drawing identifying the stages of the measurement shown in Fig. 2.

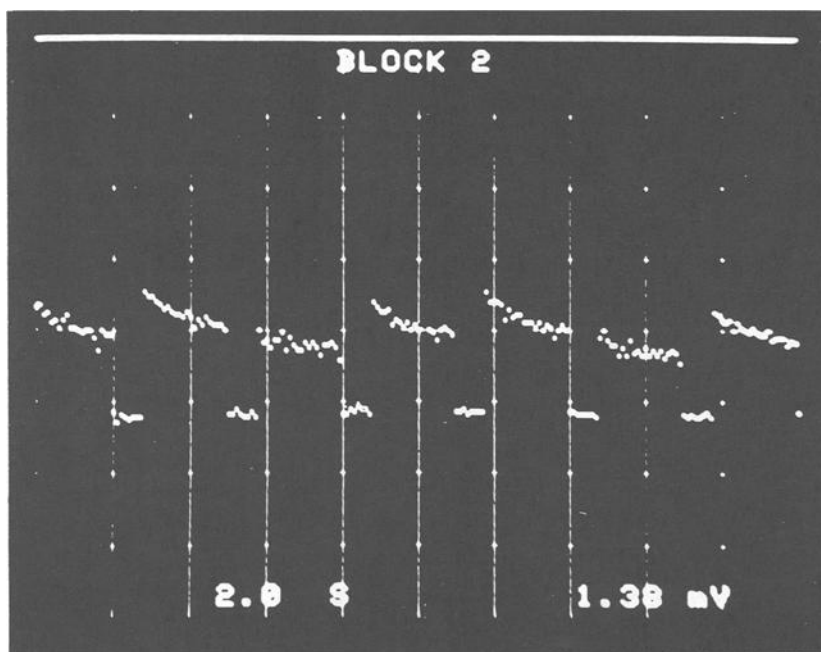


FIG. 4—A magnified view of the current trace, as a function of time, during the holding stage shown in Fig. 2.

current decay curve, just before the current is turned off. As indicated earlier, the current is modulated during the “holding” stage to maintain the polarized potential at the target voltage of  $(DE) = -10$  mV. This modulation can be seen on close examination of Fig. 4, which shows slight changes in current from one cycle to the next as the current acts to maintain the WE potential at the target voltage.

The response of the WE potential to the applied current is shown in the oscilloscope trace of Fig. 6. Figure 7 is the idealized illustration of the potential trace showing the

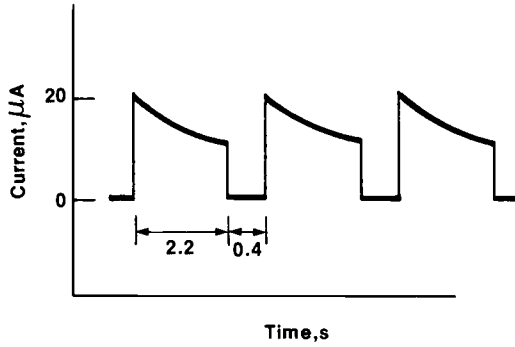


FIG. 5—An idealized drawing of the current trace shown in Fig. 4.

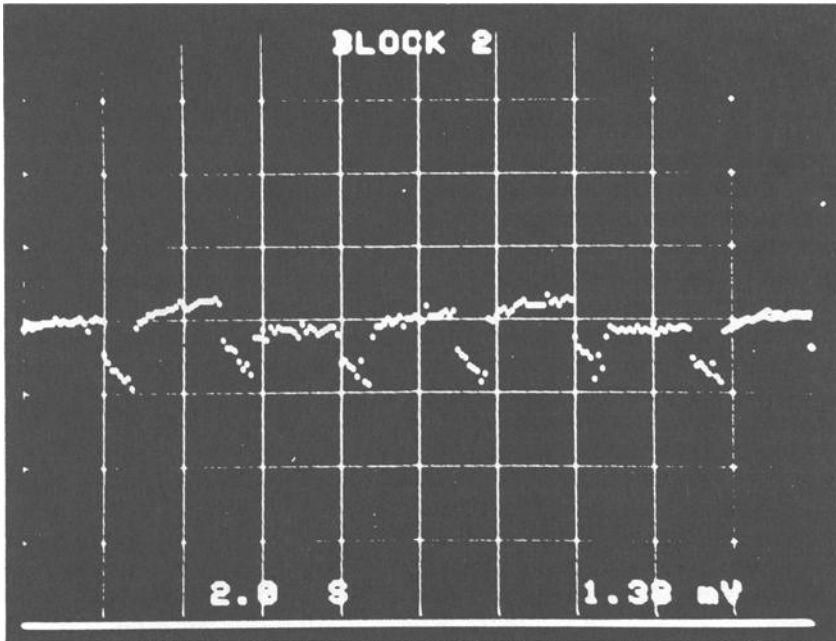


FIG 6—A magnified view of the potential trace, as a function of time, during the holding stage shown in Fig. 2.

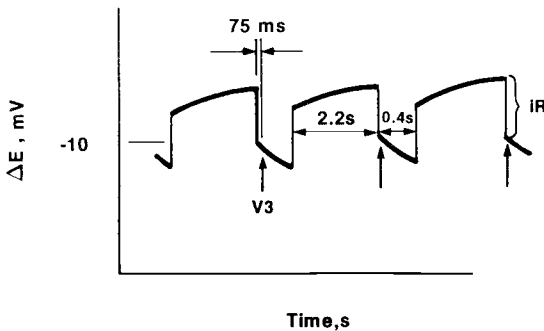


FIG. 7—An idealized drawing of the potential trace shown in Fig. 6.

instant change in potential (IR) as current is applied, followed by a time-dependent change as the WE is polarized during the 2.2 s of current application. When the applied current is turned off, the IR component of the potential is eliminated and the polarized potential of the WE can be measured. This IR-free measurement of potential, identified as V3 in Fig. 7, occurs 75 ms after the current is turned off. The cycle is then repeated 0.4 s later as illustrated.

To evaluate the computer system's ability to eliminate IR error, a circuit simulating the WE, CE, and REF in a concrete environment was constructed as illustrated in Fig. 8. The resistive R component in IR (not shown) was added in series with the WE. Using known values of the resistance, R, in the range from 1 to 5000  $\Omega$ , we determined that 95% of the IR error is eliminated throughout the resistance range as shown in Fig. 9. The straight line represents an ideal elimination of IR, and the six data points are the actual values eliminated by the computer system. The details of the computer hardware and software are available in another publication [12].

**Laboratory Procedure**

Initial measurements were made in the laboratory as the software and hardware were in the stages of development. Cleaned and weighed steel rods 1.3 cm in diameter and 15.2 cm long encased in cast concrete cylinders were used for laboratory measurements. The surface area of steel embedded in the concrete was approximately 62 cm<sup>2</sup>. Concrete mixes with and without chloride added were used. Electrical contact with the steel was made via an insulated copper wire soldered onto the exposed side of the rod, which was then overcoated with a primer and rubber-based coating. The steel in concrete specimens were immersed in simulated pore solution, simulated pore solution saturated with sodium chlo-

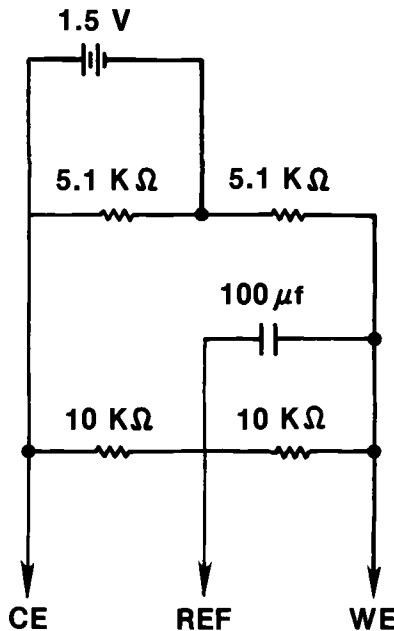


FIG. 8—An electrical circuit used to simulate the WE, CE, and REF in a concrete environment.

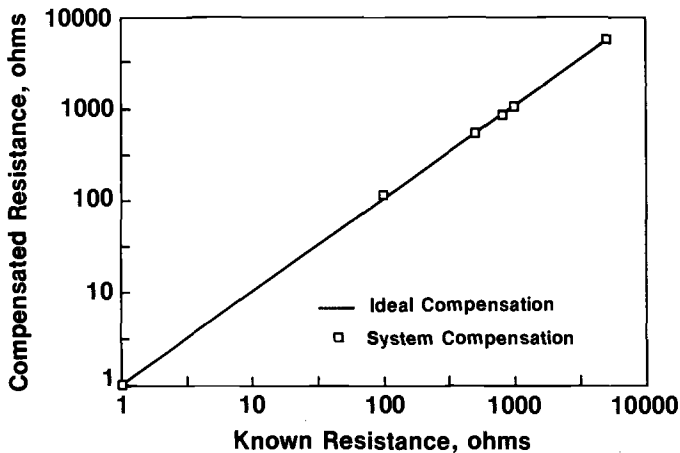


FIG. 9—A plot of the computer compensated ohmic resistance component in IR and the actual value of the resistance.

ride, or a saturated solution of sodium chloride. Some specimens were continuously immersed, while others were immersed 2 h per day and allowed to air dry the remaining 22 h. The solutions were kept in stainless steel containers that also served as counter electrodes during the measurements. Saturated calomel electrodes (SCE) were used as references in the laboratory. Specimens were exposed for a total period of 115 to 148 days, and measurements were made on each specimen once a day, five days a week. Weight loss measurements were carried out in accordance with ASTM Practice for Preparing, Cleaning, and Evaluating Corrosion Specimens (G 1).

## Results and Discussion

As an example of the results obtained on a day to day basis, the calculated corrosion rates of three specimens (#1, #3, and #7) are plotted on a logarithmic scale as a function of time and illustrated in Fig. 10. Specimen #1 was exposed to chloride-free conditions, and displayed the lowest corrosion rate throughout the entire period. Specimen #7 underwent the most severe corrosion, as expected, since it was cast in chloride-containing concrete and alternately immersed in a chloride-containing solution. A corrosion rate between the two extremes was displayed by specimen #3, which was cast in a chloride-free concrete but alternately immersed in a chloride-containing solution. After the exposure period, the steel rods were cleaned and weighed. These gravimetric weight loss data were compared to the weight loss calculated from the polarization data, and the results are shown in Fig. 11.

The IR observed in the laboratory environments ranged from 0.5 to 3 mV, and the Resistance, R, calculated ranged from 65 to 200 ohms. The highest resistances (175 to 200  $\Omega$ ) were those for which chloride-free concrete was used. With chloride in the concrete, the calculated resistances ranged from 63 to 115  $\Omega$ . The resistivities of the solutions ranged from 30 to 50  $\Omega$  cm, and the resistivity of the concrete in these solutions was as low as 900  $\Omega$  cm when soaked and as high as 10 000  $\Omega$  cm when allowed to dry in laboratory air for a month. The maximum applied polarizing current in all cases was less than 1 mA.

## Field Procedure

Three bridges in Frederick County, MD, were chosen for the study on the basis of age, known history, and condition. Thus, bridge number 10029 was a 54-year-old structure with

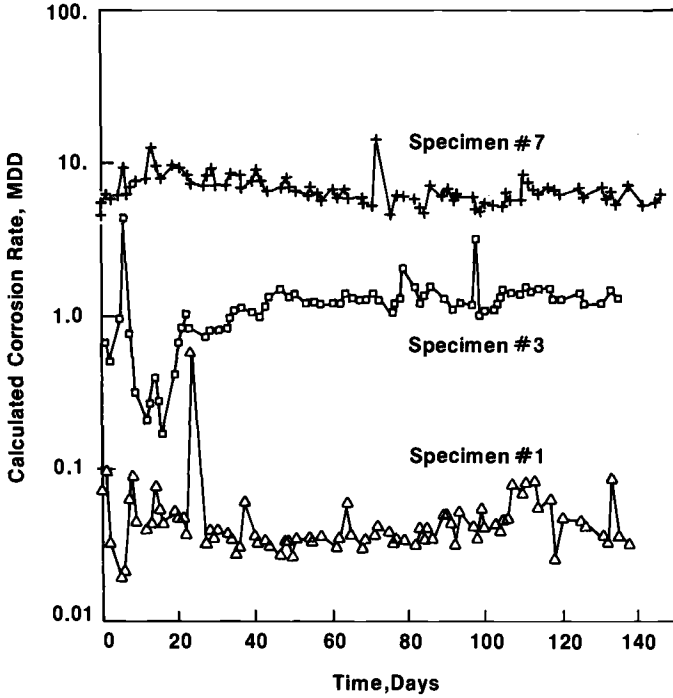


FIG. 10—A plot of corrosion rate of steel in concrete with three conditions of chloride contamination.

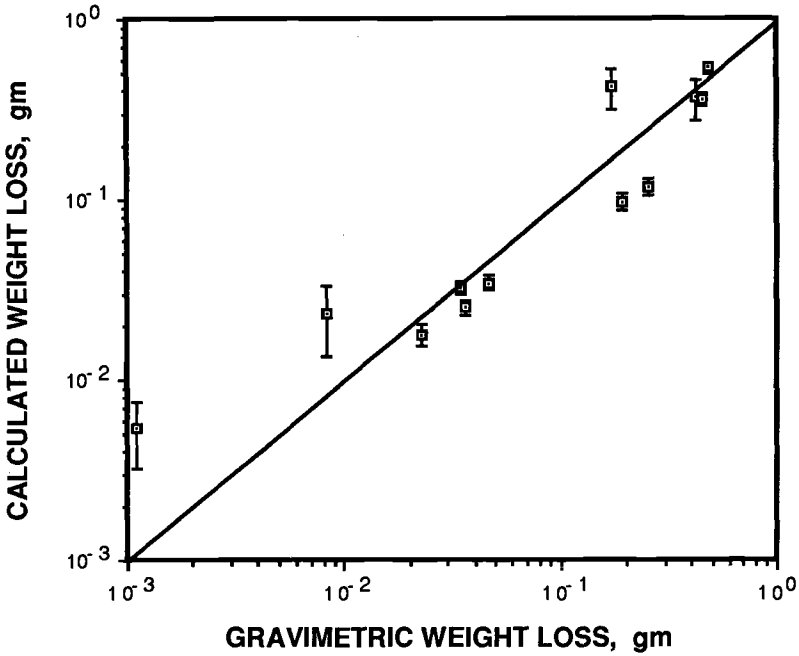


FIG. 11—A plot of the gravimetric weight loss of steel in concrete versus the calculated weight loss obtained with the portable computerized system.

fine cracks scattered over the surface of the deck, but otherwise in good condition. Bridge number 10100, along a major interchange, was 17 years old and appeared to be in excellent condition. The newest bridge, number 10059, was 13 years old and also in good condition, but cracks are beginning to appear along the rebar position. Deicing salts for snow removal are used on all three decks.

The procedure for making measurements in the field was essentially identical to that used in the laboratory. The differences were mostly physical. For example, the configuration of the electrodes in the field was as illustrated in Fig. 12, which a Cu/CuSO<sub>4</sub> reference electrode, a lead (Pb) ring used as a counter electrode, and a steel reinforcing bar in the concrete bridge deck used as the working electrode. Note that the CE and the REF are on a wetted, absorbent material (towel or sponge) and are supported by a clear plastic holder that facilitated alignment of the electrodes. A 1% solution of liquid detergent in tap water was used as a wetting agent. Scrubbing of the concrete surface with a wire brush to break-up the oil film on the surface proved useful. Along the side of the deck, a small area of concrete (15 by 15 cm) was removed to expose the reinforcing bar so that good contact could be made with the WE. This was a precaution on our part, since the bridge engineers assured us that every exposed metal bridge component (drains, guard rails, etc.) was grounded to the reinforcing steel. Measurements between the metal components and the reinforcing steel verified this continuity. The most serious problem encountered in the field

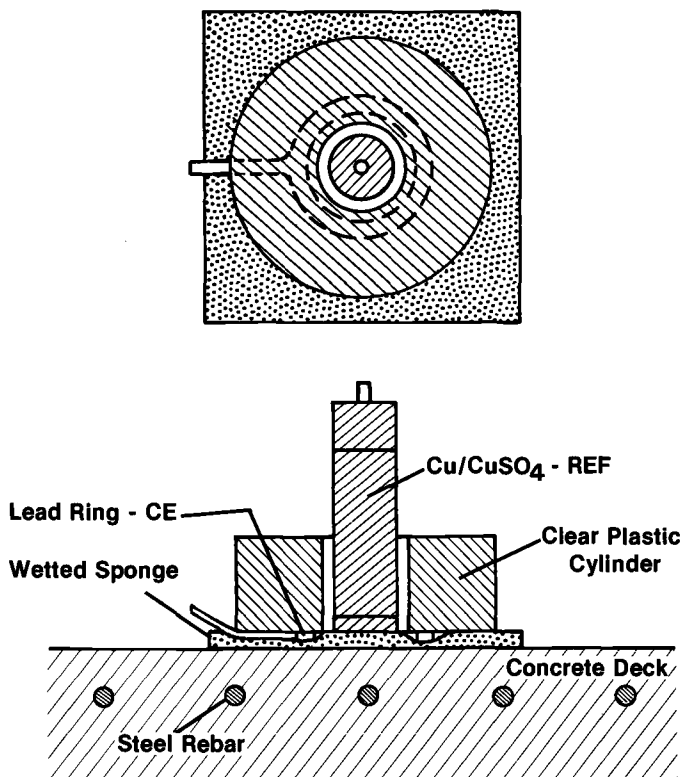


FIG. 12—Configuration of the Cu/CuSO<sub>4</sub> reference electrode, lead (Pb) ring, sponge, and plastic support, during field measurements.

measurements was electronic equipment damage resulting from mechanical vibration generated during transportation. Using the dummy cell described in Fig. 8, the equipment and cables were checked before and after every series of measurements. Three measurements were made on each bridge span every two weeks over a four month period during the summer. The location of each measurement was permanently marked on the bridge deck surfaces so that the measurements could be repeated at the same location each time.

Measurements of current distribution through concrete indicated that the current from the counter electrode to the working electrode was limited to an area only slightly larger than the CE over a wide range of concrete resistivities [11]. Calculations of the corrosion rate on the bridge decks were based on an area of rebar that was twice the area of projection of a 6 cm diameter CE on a 1.6 cm rebar. The tafel slopes used for these calculations were obtained from polarization measurements in concrete, and were about 150 mV. Details of these calculations have been described [12].

## Results and Discussion

The first 90 days of the four 4 month period were spent in improving the equipment and developing our ability to make measurements in the field. One problem encountered, not yet mentioned, involved eliminating electrical noise, and unfortunately, this process was time consuming. Only one source of noise will be mentioned here, and that arose from the irreproducibility of the WE potential. Lengthy investigation revealed that the corrosion of the steel counter electrode was generating a stray current that seriously affected the potential measurement of the WE. By using trial and error, we discovered that a lead (Pb) CE, which had a negligible corrosion rate in the detergent solution, reduced or eliminated the effect.

After this initial period, measurements were continued, and the results show that the 54-year-old bridge, number 10029, exhibited the lowest average corrosion rate (0.5 MDD)(mg/dm<sup>2</sup>day) of the three bridges. The 17-year-old bridge, number 10100, had an average corrosion rate of 1.1 MDD, and the 13-year-old bridge, Number 10059, exhibited the highest average corrosion rate of 1.9 MDD. However, it is difficult to assess the reliability or accuracy of the data obtained through these preliminary field measurements. Examination of the reinforcing steel by borings was not carried out because the limited amount of data collected did not warrant such a destructive action. However, the results can be compared with the visual appearance of the bridge deck surfaces in the immediate vicinity of the measurements. On this basis, the following observations can be made. The 54-year-old bridge, though it has suffered wear and tear through the years, is in surprisingly good condition, with small cracks randomly scattered over the surface of the deck. The 17-year-old bridge appears to be relatively crack-free with little evidence of wear to the surface. The 12-year-old bridge, in general, looks good, but close examination of the surface reveals cracking of the concrete above and in line with many of the reinforcing steel bars. This crack alignment is not evident on the other two bridges. Thus, the visual appearance of the bridge surfaces tends to support the electrochemical data. However, because of the limited amount of useful data obtained, we are reluctant to attribute much significance to these field results.

Measurements of resistivity were made on steel reinforced concrete slabs outdoors. Based on these measurements, we estimated that the resistivity of bridge decks can range from 5000 to 50 000  $\Omega$  cm, depending on moisture and temperature. The IR generated in the laboratory environments was low compared to those observed in the field measurements. The field IR values were as low as 30 mV and as high as 150 mV, with calculated resistance values of 740 to 1000  $\Omega$ . Large values of IR do not necessarily correspond to

large values of resistance, since the applied current,  $I$ , and the resistance,  $R$ , are independent of each other. The maximum applied current in the field measurements was less than 1 mA in every case.

### Summary

We used portable, battery-operated computerized equipment to apply laboratory measurement techniques to practical field situations. To do this, we developed a procedure that uses the techniques of polarization resistance and current interruption to measure the corrosion of steel in concrete. We found that the IR error component in the laboratory measurement of the potential is significant, but it can be eliminated. Measurements carried out in the laboratory revealed a relationship between weight loss calculated from electrochemical data and weight loss measured by gravimetric means. The approach was then extended to include measurements of the corrosion of reinforcing steel in three concrete bridge decks located in Frederick County, MD. In the field measurements, the IR error component was larger than the polarized potential of the working electrode, but the technique of current interruption eliminated this error. The results of the field study indicate that the problems encountered in the field can be overcome and corrosion measurements can be performed successfully.

### References

- [1] Schwerdtfeger, W. J., "Current and Potential Relations for the Cathodic Protection of Steel in a High Resistivity Environment," *Journal of Research, National Bureau of Standards -C*, Vol. 63C, No. 1, p. 37.
- [2] Jones, D. A., "Polarization in High Resistivity Media," *Corrosion Science*, Vol. 8, p. 19.
- [3] Matsuoka, K., Kihira, H., Ito, S., and Murata, T., "Monitoring of Corrosion of Reinforcing Bar in Concrete," National Association of Corrosion Engineers, Paper No. 121, March 1987.
- [4] Locke, C. E. and Siman, A., "Electrochemistry of Reinforcing Steel in Salt-Contaminated Concrete," *Corrosion of Reinforcing Steel in Concrete*, ASTM STP 713, American Society for Testing and Materials, Philadelphia, 1980, p. 3.
- [5] Gonzalez, J. A., Molina, A., Escudero, M. L., and Andrade, C., "Errors in the Electrochemical Evaluation of Very Small Corrosion Rates—II Other Electrochemical Techniques Applied to Corrosion of Steel in Concrete," *Corrosion Science*, Vol. 25, No. 7, p. 519.
- [6] Sarma, N. S., Sankar, L., Krishnan, A., and Rajagopalan, S. R., "Short Communication—IR Compensation in Potentiostat," *Electroanalytical Chemistry and Interfacial Electrochemistry*, Vol. 41, p. 503.
- [7] Britz, D. and Brocke, W. A., "Elimination of  $iR$ -Drop in Electrochemical Cells by the Use of a Current Interruption Potentiostat," *Electroanalytical Chemistry and Interfacial Electrochemistry*, Vol. 58, p. 301.
- [8] Williams, L. F. G. and Taylor, R. K., " $iR$  Correction, Part I. A Computerised Interrupt Method," *Journal of Electroanalytical Chemistry*, p. 1980, 293.
- [9] Miles, J. A., "Eliminating IR Drops from Potential Measurements (technical note)," *Corrosion*, Vol. 28, No. 4, 1972.
- [10] Escalante, E., Ito, S., and Cohen, M., "Measuring the Rate of Corrosion of Reinforcing Steel in Concrete," NBSIR 80-2012, National Bureau of Standards, March 1980.
- [11] Escalante, E., Cohen, M., and Kahn, A. H., "Measuring the Rate of Corrosion of Reinforcing Steel in Concrete," NBSIR 84-2853, National Bureau of Standards, April 1984.
- [12] Escalante, E., Whitenton, E., and Qiu, F., "Measuring the Rate of Corrosion of Reinforcing Steel in Concrete—Final Report," NBSIR 86-3456, National Bureau of Standards, Oct. 1986.

## Comparison of Current Interruption and Electrochemical Impedance Techniques in the Determination of Corrosion Rates of Steel in Concrete

---

**REFERENCE:** Berke, N. S., Shen, D. F., and Sundberg, K. M., "Comparison of Current Interruption and Electrochemical Impedance Techniques in the Determination of Corrosion Rates of Steel in Concrete," *The Measurement and Correction of Electrolyte Resistance in Electrochemical Tests, ASTM STP 1056*, L. L. Scribner and S. R. Taylor, Eds., American Society for Testing and Materials, Philadelphia, 1990, pp. 191–201.

**ABSTRACT:** Steel reinforced concrete is a widely used construction material. It is often the material of choice in bridges, parking garages, and marine structures because of its good durability and resistance to corrosion. However, over time, even well designed concrete is susceptible to chloride intrusion from deicing or marine salts or both, resulting in corrosion of embedded steel.

By the time corrosion of steel in concrete is readily noticeable, major repairs are often required. A nondestructive means of determining the corrosion rate of inaccessible steel is thus needed. Electrochemical techniques such as polarization resistance are useful, however resistivities of concrete range from 1000 to greater than 30 000 ohm-cm. Furthermore, reference electrodes are usually greater than 25 mm from the working electrode (rebars). Thus, large ohmic electrolyte resistance is present, even at the low current densities associated with steel in concrete, and must be accounted for to accurately measure corrosion rates.

In this paper we compare the use of current interruption correction for ohmic resistance to an electrochemical impedance measurement at 20 KHz. In general, we find a good correlation between the two techniques, and demonstrate that substantial ohmic resistances are present.

**KEY WORDS:** concrete resistivity, current interruption, electrochemical impedance, polarization resistance, reinforcing steel, ohmic electrolyte resistance, ohmic electrolyte compensation

The magnitude of chloride induced corrosion of reinforced concrete is staggering. Nearly half of the 500 000 plus U.S. Highway bridges are in need of repair [1]. Repairs in relatively new reinforced concrete parking facilities can range from \$50 000 to \$1 000 000 [2]. Recently, the Strategic Highway Research program pointed out that \$450 to \$550 million per year can be saved by correcting corrosion problems in current bridges [3]. As a result of the large number of corrosion related problems, there is an increasing amount of research into measuring corrosion rates of steel in concrete. A number of methods have been used in the past to study this [4]. Naturally, the nondestructive test methods are desirable.

<sup>1</sup> Senior research engineer associate, senior technician specialist, and marketing specialist, respectively, W. R. Grace & Co., Construction Product Division, 62 Whittemore Ave., Cambridge, MA 02140.

In this paper we examine the use of polarization resistance to determine the corrosion rates of steel in concrete. Because of the high resistivities of concrete, we used the current interruption technique.

Independently, we determined the ohmic drop with electrochemical impedance, and show that the current interruption technique accurately corrected for this drop.

Two nondestructive electrochemical techniques for monitoring corrosion rates are polarization resistance and electrochemical impedance. Both methods are based on the equation developed by Stern and Geary [5]

$$i_{\text{corr}} = B/R_p \quad (1)$$

where

$B$  = a constant,

$i_{\text{corr}}$  = the corrosion current density, and

$R_p$  = polarization resistance.

During polarization resistance experiments, the potential is swept at a relatively slow scan rate (for example, 0.1 mV/s). The current response is recorded. Linear polarization resistance,  $R_p$ , is defined as the slope of the voltage versus current density curve ( $\Delta i/\Delta V$ ) at zero current ( $i = 0$ ). Typical curves are shown in earlier publications [6,7]. This method of monitoring corrosion rates is simple and used quite often. It has been used to study the corrosion rates of steel in concrete as well as other systems [4,6-12].

Although polarization resistance is a well-accepted method of monitoring corrosion, the technique is complicated by high electrolytic resistance [13]. Because concrete resistivities are high (1000 to >30 000  $\Omega$  cm), means should be employed to minimize errors in the determination of  $R_p$  [14]. Two methods of compensating for high resistivity are "positive feedback" and "current interruption."

Positive feedback has been a very popular method of instrumental correction of the potential error caused by uncompensated resistance [15]. A proportion of the potential output of a current-to-voltage converter is fed back into the input of the potentiostat. The main problem with this type of compensation is that the amount of potential redirected to the input is subjective. Different experimental setups require different amounts of compensation, and the amount is not easily determined. The biggest advantage of positive feedback is that it is continuous. Hence, this method can be used during fast electrochemical experiments (scan rates of 100 mV/s or greater).

Another method used to correct for uncompensated resistance is current interruption. In this method, the potential error that results from uncompensated resistance is measured and corrected. At given time intervals, the current flowing through the cell is dropped to zero. At that instant, the only potential across the cell is caused by the double layer. The initial rapid potential drop is the error resulting from uncompensated resistance (Fig. 1).

The advantages of using this method are:

1. Essentially 100% of the potential error caused by uncompensated resistance will be corrected.
2. Changes during the scan will be accounted for.
3. Adjustments are made by the equipment on demand (that is, they are not subjective).

Due to the nature of this type of compensation, that is, it is done at finite time intervals, it is not suitable for scan rates greater than 500 mV/s. It is not recommended for scan rates greater than 100 mV/s [15].

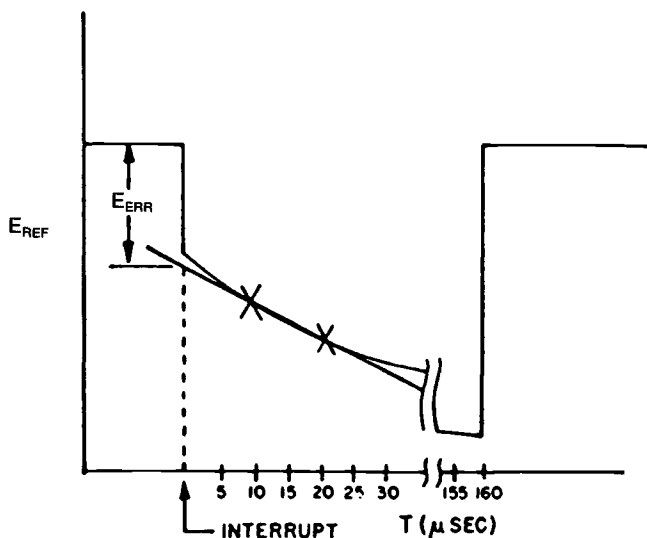


FIG. 1—This figure depicts the ideal voltage waveform for a current interrupt cycle.  $E_{ERR}$  is the potential that the current interruption method compensates for Ref 15.

Electrochemical impedance is a technique that determines the impedance,  $Z(\omega)$ , where

$$Z(\omega) = E(\omega)/I(\omega) \tag{2}$$

where

- $E(\omega)$  = an ac potential,
- $I(\omega)$  = the ac current associated with  $E(\omega)$ , and
- $\omega = 2\pi f$ ,  $f$  the frequency of the change in  $E$ .

A Randles circuit can be used as a simplified model for steel reinforced concrete (See Fig. 2).  $R_\Omega$  is the concrete resistance,  $R_t$  is the charge transfer resistance and  $C_{dl}$  is the double layer capacitance of the rebar, where the rebar is the electrode. The data are usually displayed as either a Nyquist plot (Fig. 3) or as a Bode plot (Fig. 4). At high frequencies, the impedance is the ohmic resistance,  $R_\Omega$ . More detailed descriptions are found in the literature [4,13,16].

**A.C. IMPEDANCE PROFILE FOR  
A SIMPLE ELECTROCHEMICAL SYSTEM**

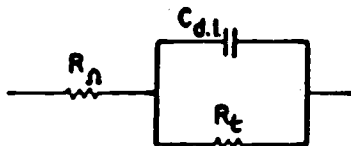


FIG. 2—A Randles circuit is shown here. This is a simplified electrochemical model of steel reinforced concrete where the rebar is the electrode.

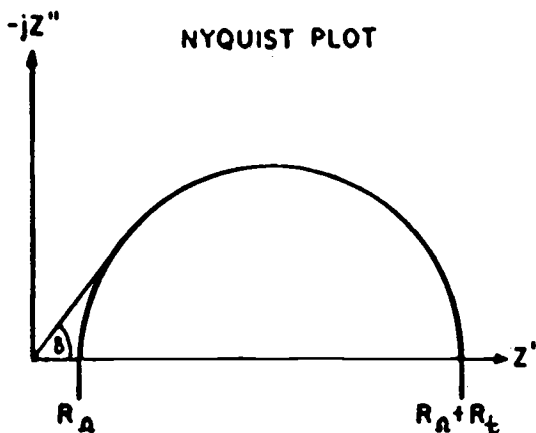


FIG. 3—A Nyquist plot is shown here.

### Idealized Bode Plot

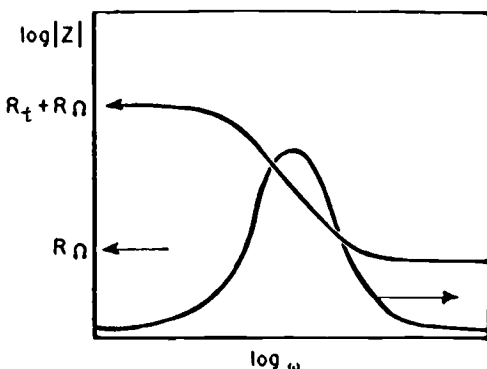


FIG. 4—Another method of plotting impedance data is with the Bode plot.

### Experimental Procedure

#### Materials

Each specimen was a wire brushed No. 3 (0.95 cm diameter) steel reinforcing bar 30.5-cm (12-in.) long embedded in a concrete cylinder 7.6 cm (3 in.) in diameter by 15.2 cm (6 in.) high. These concrete/rebar specimens had 10.2 cm (4 in.) of exposed rebar that were not isolated with Devcon® Epoxy Sealer 100, or electroplaters tape #470 from 3M.

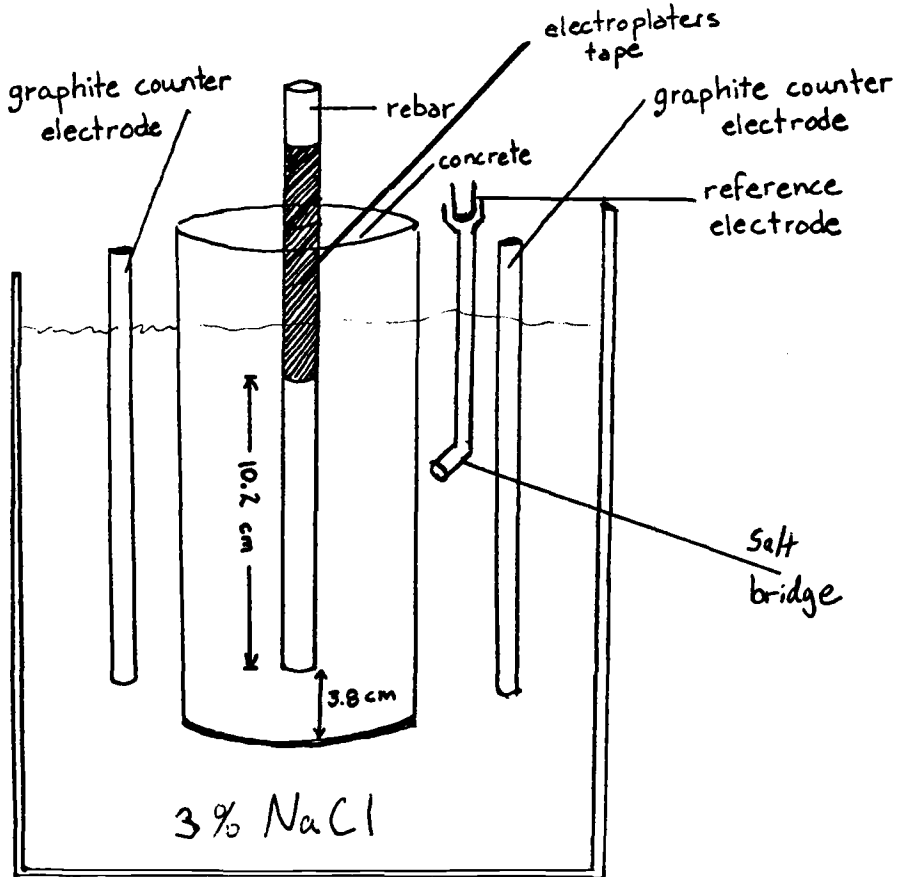
Concrete mix designs are listed in Table 1.

#### Test Details

Polarization resistance tests were performed using an EG&G model #351 corrosion measurement system. This system includes 2 model #272 potentiostat/galvanostats, a model #273 potentiostat and a model #1000 computer. The scan rate was 0.1 mV/s, and it began at  $-20$  mV versus the corrosion potential ( $E_{corr}$ ). The maximum positive potential

TABLE 1—*Mix designs for the concrete.*

#, Samples	Type of Cement	cf kg/ m <sup>3</sup> (pcy)	Fly Ash kg/m <sup>3</sup> (pcy)	W/C	Calcium Nitrite %, s/s Cement	Microsilica %, s/s Cement
3284—Mix 1	I—II	339 (573)	0	0.45	1.7	0
3284—Mix 2	I—II	336 (568)	0	0.45	1.7	0
4348—Mix 1	I—II	388 (655)	0	0.34	3.1	0
4348—Mix 2	I—II	398 (672)	0	0.34	3.1	0
5684—Mix 1	I—II	393 (664)	0	0.34	0	0
5684—Mix 2	I—II	401 (677)	0	0.34	0	0
12384—Mix 1	I	295 (499)	0	0.56	0	0
12384—Mix 2	I	240 (406)	72 (122)	0.66	0	0
12384—Mix 5	I	240 (406)	72 (122)	0.66	1.5	0
9685—Mix 1	I	311 (525)	0	0.50	0	0
9685—Mix 2	I	242 (409)	47 (79.5)	0.74	0	10.7
9685—Mix 8	I	242 (409)	47 (79.2)	0.74	0.8	10.7

FIG. 5—*Schematic of specimens and corrosion cell.*

was +20 mV versus  $E_{\text{corr}}$ . Typically, the scan stopped at +10 mV versus  $E_{\text{corr}}$  to minimize the corrosion of the specimen. Tests were conducted with and without the built in current interruption, as described in Ref 15.

Electrochemical impedance tests were performed using an EG&G #5206 two phase lock in analyzer, an EG&G #173 potentiostat, and an Apple IIe. The voltage amplitude  $\leq 10$  mV versus  $E_{\text{corr}}$ . The real impedance at 20 KHz was used as an approximation of the ohmic resistance of the concrete and solution. A sample of the cell is given in Fig. 5. The high conductivity of the 3% sodium chloride (NaCl) solution compared to the concrete allows us to treat the system as one of two concentric cylinders (one of the rebar diameter and the other of the concrete diameter:) with the resistivity of the concrete as the cause of the measured resistance. In such a geometry the resistance between electrodes is

$$R = - \frac{\ln (r_1/r_2)}{2\pi L} \rho$$

where

$r_1$  = the rebar radius,

$r_2$  = the concrete cylinder radius, and

$L$  = the rebar length.

Note that the resistance,  $R$ , multiplied by the rebar surface area gives  $R_p$ .

TABLE 2—Results of polarization resistance and electrochemical impedance tests.

ID of Lollipop	Polarization Resistance					Electrochemical Impedance	
	$E_{\text{corr}}$ (mV)	$R_{p1}^a$ (K $\Omega\text{cm}^2$ )	$E_{\text{corr}}$ (mV)	$R_{p2}$ (K $\Omega\text{cm}^2$ )	$R_{p2}-R_{p1}$ (K $\Omega\text{cm}^2$ )	$E_{\text{corr}}$ (mV)	$R_{\Omega}$ (K $\Omega\text{cm}^2$ )
	YES			NO			
12 384							
141	-616	10	-615	11	1	-613	3
244	-572	22	-586	25	3	-567	13
542	-290	84	-308	91	7	-275	12
543	-472	28	-490	40	12	-463	12
3 284							
141	-504	24	-501	31	7	-502	6
241	-343	17	-342	27	10	-339	5
242	-274	38	-274	49	11	-262	6
9 685							
141	-509	22	-502	27	5	-497	8
142	-472	23	-463	27	4	-459	6
143	-503	23	-496	27	4	-496	7
241	-382	168	-380	199	31	-366	33
242	-384	172	-379	224	52	-371	35
243	-371	153	-371	190	37	-362	32
841	-451	50	-454	61	11	-443	17
842	-459	26	-459	40	14	-448	15
843	-376	56	-377	72	17	-374	17

<sup>a</sup>  $R_{p1}$  is the  $R_p$  value determined with current interruption engaged.  $R_{p2}$  is the  $R_p$  value found without using the current interruption technique.

## Results and Discussion

### Concrete Resistance

Polarization resistance tests were run two ways.  $R_p$  values were calculated from polarization curves both with and without current interruption. The data are listed in Table 2.  $R$  is the difference between the  $R_p$  calculated from the experiments run without current interruption and the  $R_p$  calculated from the experiment run with current interruption. Electrochemical impedance was conducted on the same samples.

$R_p$  values calculated at 20 KHz are also listed in Table 2.

### Comparison of Two Methods

As described above, we used both current interruption and electrochemical impedance to measure the resistivity of concrete. By conducting polarization resistance tests with and without compensating for concrete resistivity, we determined the ohmic drop across the concrete. In Table 2, this is compared to the values found using electrochemical impedance.

Examining Table 2 we find that the  $R_p$  values determined by the two methods compare favorably. Only two samples, 12384-244 and 9865-242, have  $R_p$  values that differ. All other pairs are in agreement within a few Kohm-cm<sup>2</sup>. This demonstrates that the methods are interchangeable. If current interruption is unavailable (for example in the field), a measurement of  $R_p$  at 20 000 Hz could be used to correct  $R_p$ . Capacitance effects must be negligible. This agreement is not surprising, since polarization is occurring within  $\pm 20$  mV of the corrosion potential in either case.

Note that samples 12384-244 and 9865-242 had relatively high  $R_p$  values indicating that corrosion rates are extremely low. For these samples a slower scan rate would have been more appropriate [14]. However for our purposes the scan rate employed readily indicates passivity and differentiates corrosion rates of corroding specimens [7].

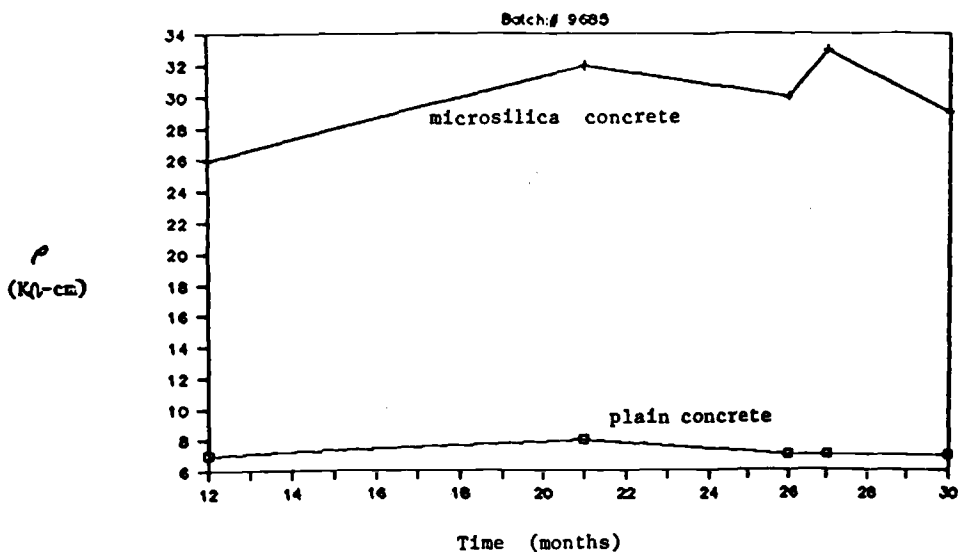


FIG. 6—Concrete resistivity is plotted as a function of time for plain concrete and concrete containing microsilica.

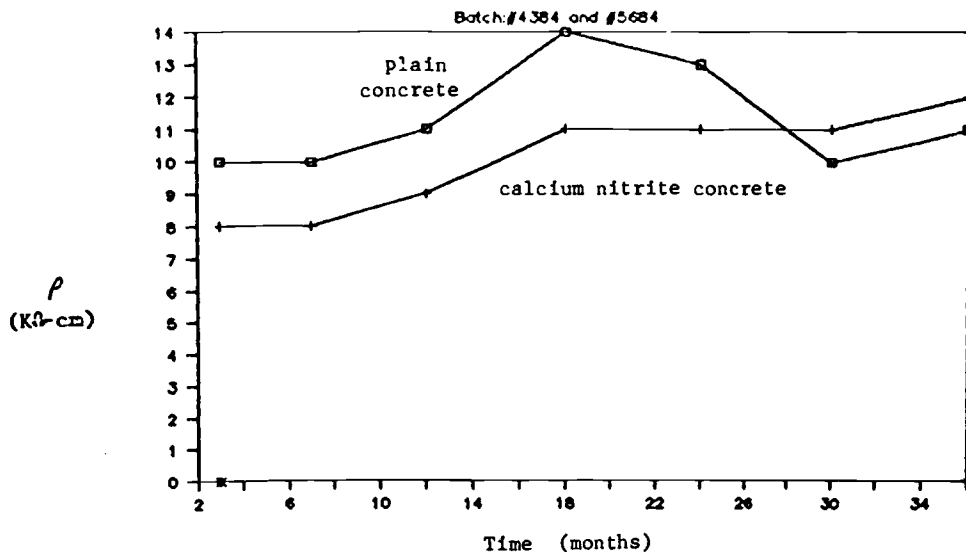


FIG. 7—Concrete resistivity is plotted as a function of time for plain concrete and concrete containing calcium nitrite.

#### Changes in Concrete Resistivity with Time

In Figs. 6 and 7, concrete resistivity,  $\rho$  (K $\Omega$ -cm), is plotted as a function of time. Figure 6 shows data for a plain concrete and a similar mix containing microsilica. Microsilica has substantially increased concrete resistivity, and steel in concretes with resistivities greater than 30 k $\Omega$ -cm generally does not severely corrode [17]. Figure 7 compares plain concrete with concrete containing calcium nitrite corrosion inhibitor. The resistivities in Fig. 7 are higher than those for plain concrete in Fig. 6 because of a decrease in water-to-cement (w/c) ratio.

#### Corrosion Rates

Corrosion rates were monitored by measuring  $R_p$  over time. Based on Eq. 1, the rates are indirectly proportional to  $R_p$ .

Comparisons of corrosion rates for concrete with and without microsilica are shown in Fig. 8. The corrosion rate of steel in microsilica concrete is significantly lower than that of the steel in concrete without microsilica. This is due both to the increased resistivity, Fig. 6 [17], and a reduction in chloride content at the steel [18].

Note that  $1/R_p$  values greater than 20  $\mu$ mhos/cm<sup>2</sup> correlate well with the onset of severe corrosion [6–8], as observed by breaking specimens open and examining the reinforcement for corrosion.

Corrosion rates over time of steel in concrete with and without calcium nitrite are shown in Fig. 9. Even though concrete resistivities were similar (Fig. 7), the rate of corrosion in concrete containing calcium nitrite is significantly lower. Note that the differences between the plain concretes shown in Figs. 8 and 9 are due to different w/c ratios (reducing w/c lowers the corrosion rate).

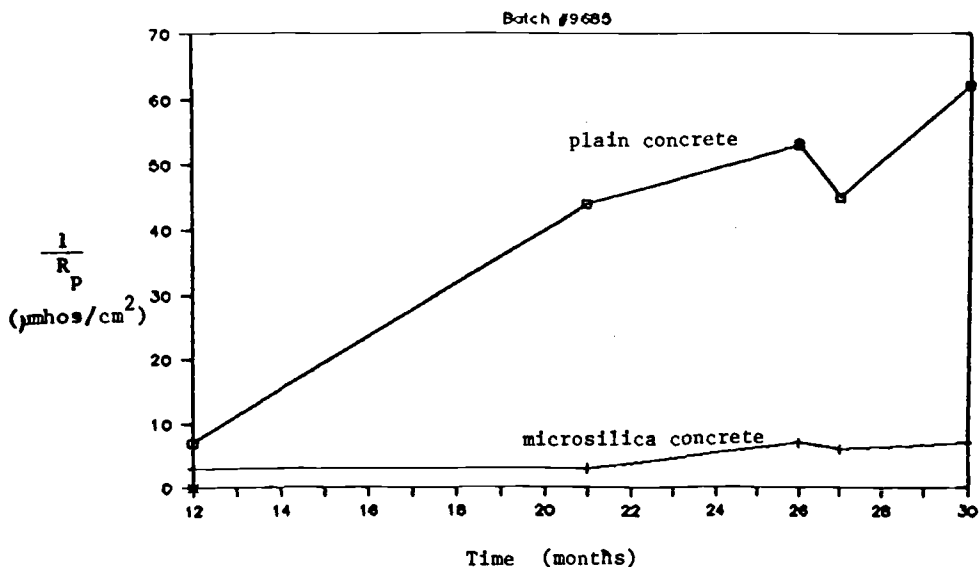


FIG. 8—Corrosion rates are shown in this figure for plain concrete and microsilica concrete. Values of more than 20  $\mu\text{mhos}/\text{cm}^2$  indicate corrosion.

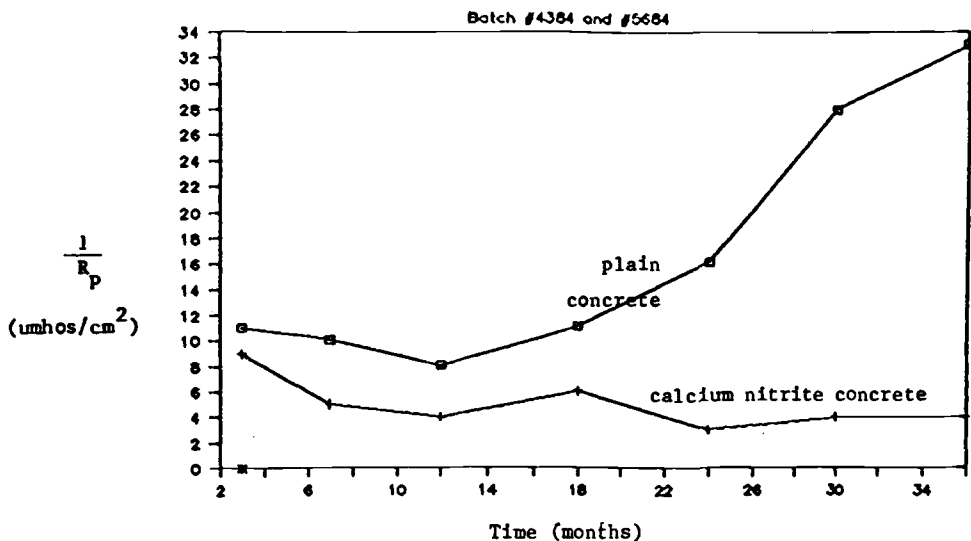


FIG. 9—Corrosion rates are shown in this figure for plain concrete and calcium nitrite concrete. Values of more than 20  $\mu\text{mhos}/\text{cm}^2$  indicate corrosion.

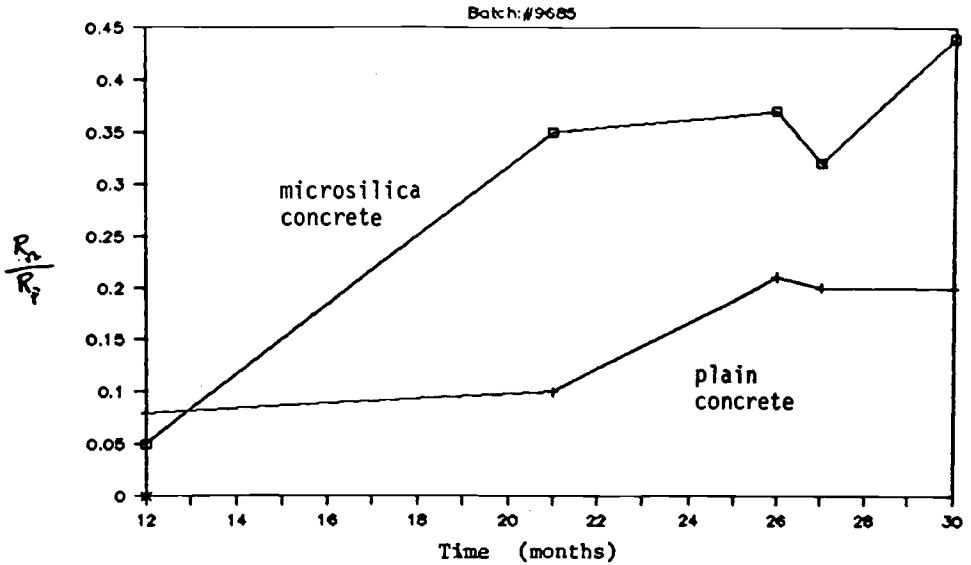


FIG. 10—This plot shows the change of  $R_0/R_p$  with time for plain and microsilica concrete.

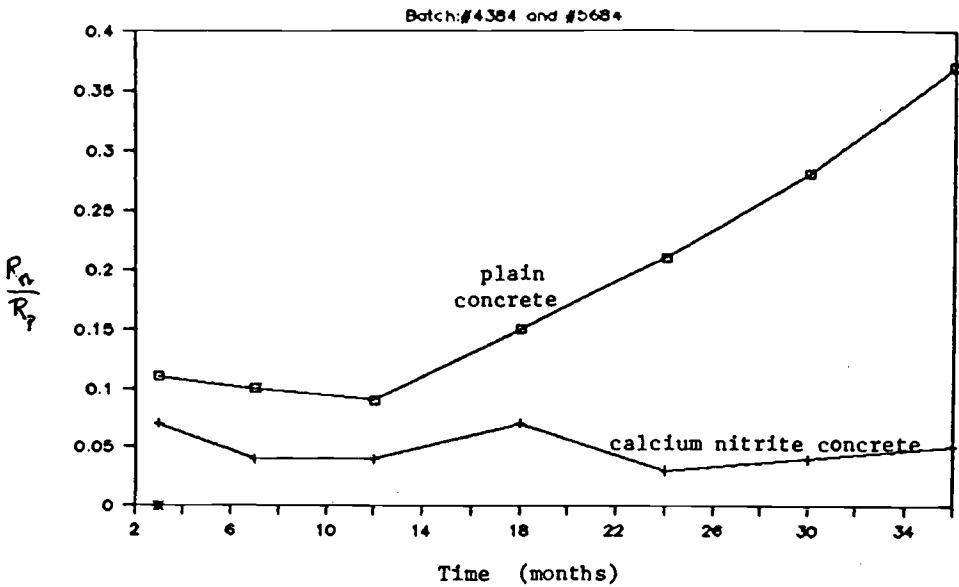


FIG. 11—This plot shows the change of  $R_0/R_p$  with time for plain concrete containing calcium nitrite.

### *Significance of Ohmic Drop to Corrosion Rate Measurements*

When there is no compensation for the electrolytic resistance of the concrete, the error is reflected in the corrosion rate measurement. Uncompensated resistance is measured as  $R_{\text{tot}}$ , where  $R_{\text{tot}} = R_p + R_\Omega$ . Figures 10 and 11 demonstrate the significance of this error. The amount of error in  $R_p$  is represented as  $R_\Omega/R_p$ . Thus at low  $R_p$  values or high  $R_\Omega$  values, considerable error can be present due to electrolytic resistance. Since the corrosion rate is indirectly proportional to  $R_p$ , significant underestimating of the corrosion rate can occur.

### Conclusions

Based upon the work presented, the following conclusions are made:

- The current interruption technique accurately corrected for ohmic resistance of concrete.
- Corrosion rates can be significantly underestimated if electrolyte resistance is not corrected for. This is especially true when high concrete resistivities or high corrosion rates or both are present.
- A single measurement of ohmic resistance at 20 000 Hz can be used to correct uncompensated polarization resistance values, in conditions similar to those of this experimentation.
- Steel in concrete containing calcium nitrite or microsilica showed improved resistance to corrosion compared to plain concrete, based on results presented here.

### References

- [1] Strategic Highway Research Program, Participant Workbook—National Workshop, Strategic Highway Research Program: Washington, DC, Sept. 1985, p. TRA 4-1.
- [2] Tracy, R. and Nehil, T., "Parking," The National Parking Assn., Washington, DC, Summer 1981.
- [3] *Focus*, Special Edition, Strategic Highway Research Program, Washington, DC, 18–20 Sept., 1985.
- [4] Dawson, J. L. "Corrosion Monitoring of Steel in Concrete," *Corrosion of Reinforcement in Concrete Construction*, A. P. Crane, ed., Ellis Horwood Ltd., London, Eng., 1983, p. 175.
- [5] Stern, M. S. and Geary, A. J., *Journal of Electrochemical Society*, Vol. 105, 1958, p. 638.
- [6] Berke, N. S., "The Effects of Calcium Nitrite & Mix Design on the Corrosion Resistance of Steel in Concrete (Part 1)," National Association of Corrosion Engineers Corrosion 85, Paper No. 273, Boston, Massachusetts, March 1985.
- [7] Berke, N. S., "The Effects of Calcium Nitrite and Mix Design on the Corrosion Resistance of Steel in Concrete (Part 2)," National Association of Corrosion Engineers Corrosion 87, Paper No. 132, San Francisco, California, March 1987.
- [8] Berke, N. S., "Corrosion Rates of Steel in Concrete," *ASTM Standardization News*, March 1986, p. 57.
- [9] Berke, N. S. and Stark, P., "Calcium Nitrite as an Inhibitor: Evaluating and Testing for Corrosion Resistance," *Concrete International*, September, 1985, p. 42.
- [10] Hughes, B. P., Soleit, A. K. O., and Brierly, R. W., "New Technique for Determining the Electrical Resistivity of Concrete," *Magazine of Concrete Research*, Vol. 37, 1985, p. 133.
- [11] Wheat, H. G. and Eliezer, Z., *Corrosion*, Vol. 41, No. 11, 1985.
- [12] Andrade C. and Castelo, V., *British Corrosion Journal*, Vol. 19, No. 2, 1984, p. 98.
- [13] Dawson, J. L., Callow, L. M., Hladky, K. and Richardson, J. A., *Corrosion* 78, paper #125.
- [14] F. Mansfeld, *Corrosion*, Vol. 37, No. 5, 1981, p. 301.
- [15] EG&G, Princeton Applied Research, Electrochemical Instruments Division, Technical Note #101.
- [16] Atimtarey, E. and Ferguson, P. M., *American Concrete Institute Journal*, Sept. 1973, p. 606.
- [17] Hope, B. B., Ip, A. K., and Manning, D. A., "Corrosion and Electrical Impedance in Concrete," *Cement and Concrete Research*, Vol. 15, 1985, p. 523.
- [18] Berke, N. S., "Microsilica and Concrete Durability," Paper No. 870275, presented at the 1988 Transportation Research Board meeting, 11–14 January, 1988, Washington, D.C.

C. C. Streinz,<sup>1</sup> R. G. Kelly,<sup>1</sup> P. J. Moran,<sup>1</sup> J. Jolson,<sup>2</sup>  
J. R. Waggoner,<sup>3</sup> and S. Wicelinski<sup>2</sup>

## Measurement of the Components of the Ohmic Resistance in Lithium/Iodine (P2VP) Batteries

**REFERENCE:** Streinz, C. C., Kelly, R. G., Moran, P. J., Jolson, J., Waggoner, J. R., and Wicelinski, S., "Measurement of the Components of the Ohmic Resistance in Lithium/Iodine (P2VP) Batteries," *The Measurement and Correction of Electrolyte Resistance in Electrochemical Tests*, ASTM STP 1056, L. L. Scribner and S. R. Taylor, Eds., American Society for Testing and Materials, Philadelphia, 1990, pp. 202–210.

**ABSTRACT:** It is well known that at high discharge rates (approximately 200  $\mu\text{A}/\text{cm}^2$ ) the (Li/I<sub>2</sub>) (P2VP) battery suffers severely increased polarization. Recently, through the use of electrochemical impedance spectroscopy, it has been demonstrated that for cells with pelletized cathodes this increased polarization is dominated by ohmic effects. It has also been shown that monitoring the ohmic impedance throughout discharge provides an excellent means for understanding battery behavior. This is further illustrated in this paper. In this study cells containing only cathode material are utilized to determine the contribution of the cathode to the total cell ohmic impedance. It is demonstrated that prior to discharge the cathode impedance contributes greater than 60% of the full cell ohmic impedance. During discharge both the magnitude and the changes in the measured ohmic impedance are shown to be dominated by the LiI electrolyte layer. Further, it is concluded that the impedance of the cathode increases with increasing molecular weight of the P2VP polymer used in the cathode. As a result, the relative contributions of the cathode and electrolyte to the total ohmic impedance are a function of P2VP molecular weight.

**KEY WORDS:** lithium iodine battery, lithium batteries, solid electrolyte batteries, pacemaker batteries, electrochemical impedance spectroscopy, ohmic impedance, rate limiting mechanisms

Since 1970, when it was first reported in the literature [1], the lithium iodine battery has become an important power source for the biomedical, especially pacemaker, industry. Valuable features, such as its long shelf life, high reliability, long operating life, high energy density and lack of gassing during discharge, have made it an ideal pacemaker source. However, the use of the lithium/iodine (Li/I<sub>2</sub>) battery for higher rate applications has been severely limited due to the increased polarization suffered during high-rate discharge.

For a detailed introduction to the fabrication procedures and the discharge performance characteristics of the battery system, the interested reader is referred to two comprehensive review texts [2,3]. Briefly, the Li/I<sub>2</sub> battery is a solid electrolyte cell consisting of a lithium anode, a cathode mixture of iodine and an organic polymer, poly(2-vinylpyridine)(P2VP), and a lithium iodide electrolyte. The electrolyte layer forms *in-situ* from the direct combination of the products of the electrode reactions. A cathode mixture of iodine and P2VP is used because they form a one-to-one charge transfer complex which has a significantly higher conductivity than iodine alone [4]. The cathode preparation procedure used to pro-

<sup>1</sup> Corrosion and Electrochemistry Research Laboratory, Department of Materials Science and Engineering, The Johns Hopkins University, Baltimore, MD 21218.

<sup>2</sup> Catalyst research, A Division of Mine Safety Appliances, Owings Mills, MD 21117.

<sup>3</sup> Current Address: Gates Energy Products, P. O. Box 114, Gainesville, FL 32602.

duce the cells for this study involves pressing a mixture of iodine and P2VP powders into the form of a pellet. This cathode pellet is then placed directly into the battery can in direct contact with the lithium anode. Cathodes prepared in this manner possess a resistivity on the order of  $10^4 \Omega \text{ cm}$  [5].

During discharge lithium ions diffuse through the polycrystalline lithium iodide electrolyte layer under the influence of both potential and concentration gradients to the cathode where they combine with reduced iodine to form more lithium iodide. This results in a continually increasing lithium iodide (LiI) volume throughout discharge until end-of-life when the cathode becomes sufficiently depleted in iodine, decreasing its conductivity dramatically. As the discharge rate increases, the cell suffers severely increasing polarization until it is such that it dominates the operating voltage, which falls to unusable levels. Recent advances in the biomedical industry, such as the development of chronic pain control and drug infusion devices, have led to the need for cells with the favorable characteristics of the  $\text{Li}/\text{I}_2$  cell, but capable of delivering increased power. The development of such a  $\text{Li}/\text{I}_2$  cell would most certainly lead to numerous other applications for the  $\text{Li}/\text{I}_2$  battery system.

Recently, Kelly, and Moran [6,7] have performed studies aimed at elucidating the rate limiting mechanisms of  $\text{Li}/\text{I}_2$  batteries with pelletized cathodes. They utilized electrochemical impedance spectroscopy (EIS) to develop an equivalent circuit model (see Fig. 1). The model described the two electrode reactions and the electrolyte layer as three parallel resistor-capacitor (RC) circuits in series. Each electrode also contained a Warburg impedance. In addition, the three RC circuits are in series with a resistor representing the true ohmic resistance of the cell, assumed to be dominated by the cathode. The approach utilized by Kelly and Moran [7] enabled the separation of the ohmic, activation and concentration overpotentials to the total cell overpotential. However, the high frequency limit, 100 kHz, of the measuring system used in this study was not sufficiently high to separate the contributions of the lithium iodide ( $R_{\text{LiI}}$ ) and cathode ( $R_{\text{cath}}$ ) impedances to the total cell impedance. Therefore the influence of these on the ohmic overpotential could not be directly determined and their sum is referred to as  $R'_\Omega$ .

It was established that a dramatic increase in the ohmic overpotential during high rate discharges is the dominant factor in the cells poor performance. Using cells with internal reference electrodes positioned between the cathode and electrolyte layers it was demonstrated that the measured ohmic impedance is dominated by  $R_{\text{LiI}}$  at all discharged capacities of interest. It was also demonstrated that the impedance of the formed LiI electrolyte layer is discharge rate dependent. Specifically, it was determined that the cells discharged at high rates (approximately  $300 \mu\text{A}/\text{cm}^2$ ) possess an electrolyte layer with a resistivity three times greater than those discharged at low rates (approximately  $40 \mu\text{A}/\text{cm}^2$ ).

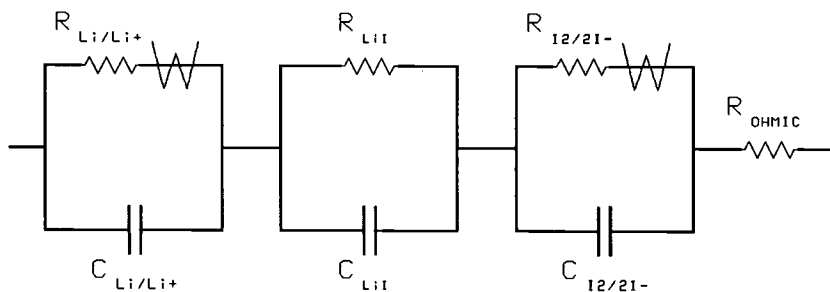


FIG. 1—The equivalent circuit model developed by Kelly and Moran [7].

To further verify the above conclusions, Kelly [8] performed EIS measurements over a broader frequency range (up to 1 MHz) in an attempt to separate the contributions of  $R_{\text{cath}}$  and  $R_{\text{LiI}}$ . It was shown that even 1 MHz was not sufficient to resolve the cathode impedance plateau; however, an analysis of the data illustrated that the 1 MHz impedance was less than 20% of the 1 kHz value for most of the discharge. It was thus surmised that  $R_{\text{cath}}$  is negligible compared to  $R_{\text{LiI}}$  at all discharged capacities. This study, however, did not clearly demonstrate that the contributions of the cathode and LiI could be separated in frequency.

It is known that the cathode in these cells has limited conductivity, which is a function of the ratio of molecular iodine to P2VP. As the cell is discharged, iodine is consumed and the conductivity reaches a maximum at a molar ratio of approximately 3:1  $\text{I}_2$ :P2VP [5]. This occurs about 55 mAh into discharge for the cells used in this study, with further discharge decreasing the cathode conductivity rapidly until end-of-life. In the studies by Kelly and Moran [6,7,8] only one P2VP polymer molecular weight was used, one which produced a cathode with a relatively high conductivity. In this study two different cathodes were used: one identical to that used by Kelly and Moran and one containing a higher molecular weight P2VP polymer. Based upon the knowledge of cathode conductivity stated above, an alternate approach to delineate the contribution of the cathode to  $R'_\Omega$  and  $\Delta R'_\Omega$  during discharge is to determine the conductivity of the cathode alone. This was accomplished by constructing cells which contained only cathode material and determining their ohmic impedances relative to those measured for complete cells. The difference between these two measurements was the contribution of the LiI to the total cell ohmic impedance.

### Experimental Procedure

The cells used in this study were dimensionally equivalent to the commercially available Catalyst Research S2-P15 button cell [9]. The external dimensions can be seen in Fig. 2. Through a reduction in the quantity of cathode material used, the cells nominal capacity was decreased from 120 mAh to 74 mAh. The cathodes had an initial iodine: P2VP weight ratio of 19:1 and were pressed to an initial thickness of 13 mils. Cells were constructed with P2VP polymers of either 22 000 (cell used by Kelly and Moran) or 54 000 average molecular weights. The cells with the P2VP molecular weight of 22 000 will herein be referred to as 22K cells, while those with the P2VP molecular weight of 54 000 will be referred to as 54K cells. In addition cells were constructed which contained a nickel elec-

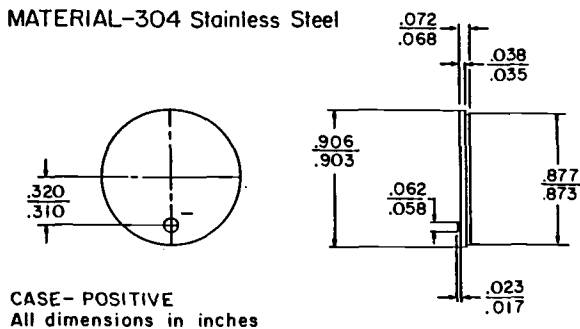


FIG. 2—Schematic of Catalyst S23-P15 button cell. The nominal capacity was reduced from 120 to 74 mAh for this study.

trode, instead of a lithium anode, and a standard cathode (26 mils thickness) so that the impedance of the cathode could be directly measured.

Nominally identical cells containing either 22K or 54K molecular weight P2VP polymer were characterized via (EIS). Cells containing only cathode material were also characterized via EIS in order to quantify the contribution of the cathode impedance to the full cell  $R'_\Omega$  in a nondischarged cell. In addition both 22K and 54K cells were discharged across constant 5 k $\Omega$  resistive loads. During discharge, at approximately every 10 mAh, impedance spectra were generated while the cells were potentiostatically held at their closed circuit potential. The cells were returned to discharge immediately after the completion of the impedance measurement. The measured ohmic impedances were then compared to those measured for the cells containing only the cathode material. All experiments were performed at ambient temperature.

The EIS system utilized in this study was a PAR Model 368-4 Impedance Measurement System. It consists of a Model 5208EC Lock-in Analyzer, a Model 273 Potentiostat and an Apple IIe computer which enables the automated measurement of the electrochemical impedance of the cells over a frequency range of 100 kHz to 0.1 mHz. An AT&T Personal Computer was sometimes used instead of the Apple IIe computer to automate the system. There were no noticeable differences in the measured impedances. The accuracy of this system was checked and verified using dummy cells, made up of resistors and capacitors of known values. The EIS procedure used in this study assumed the same equivalent circuit developed by Kelly and Moran [7]. All impedance spectra were generated over a frequency range of 100 kHz to 100 mHz.

## Results and Discussion

Figures 3a and 3b show the discharge behavior of the newly constructed 22K and 54K cells respectively across a constant resistive load of 5 k $\Omega$ . The three curves in each figure illustrate the separation of the total overpotential into its ohmic, activation and concentration components at various depths of discharge. The bottom curve is the operating potential versus discharged capacity, while the differences between the curves correspond to the indicated overpotentials. These overpotentials are determined using the method employed by Kelly and Moran [7]. It can be seen at this relatively high discharge rate (approximately 140  $\mu\text{A}/\text{cm}^2$ ) that the ohmic overpotential is the dominant overpotential.

The studies performed on the cells containing only cathode material indicate that the cathode impedance constitutes most of the measured  $R'_\Omega$  in the predischarged state. This is illustrated in Table 1 which shows that the cathode in the 22K cells contributes 60% or more of the fresh cell ohmic impedance. The impedances of the cathode material given in Table 1 correlate well with the cathode resistivity of pelletized cathodes determined by Surd et al. [5]. This result is in contrast with the high frequency work of Kelly [8] which concluded that the cathode contributed at most 20% of the measured  $R'_\Omega$ . In that study he assumed that the impedance contribution from the cathode alone could be determined by evaluating the impedance at higher frequencies where the LiI impedance would be shorted. The measurements made in this study were direct measurements of the cathode impedance as a function of frequency, and indicate that  $R_{\text{LiI}}$  and  $R_{\text{cath}}$  cannot be separated by this approach. This has been accommodated by modifying the circuit model developed by Kelly and Moran [7]. The modified model treats the LiI and cathode as inseparable components.

This modification is illustrated in Fig. 4. This model is identical to the Kelly and Moran model except that it now includes resistive and capacitive components from the cathode as well as the LiI electrolyte layer because they are inseparable in frequency. This effect

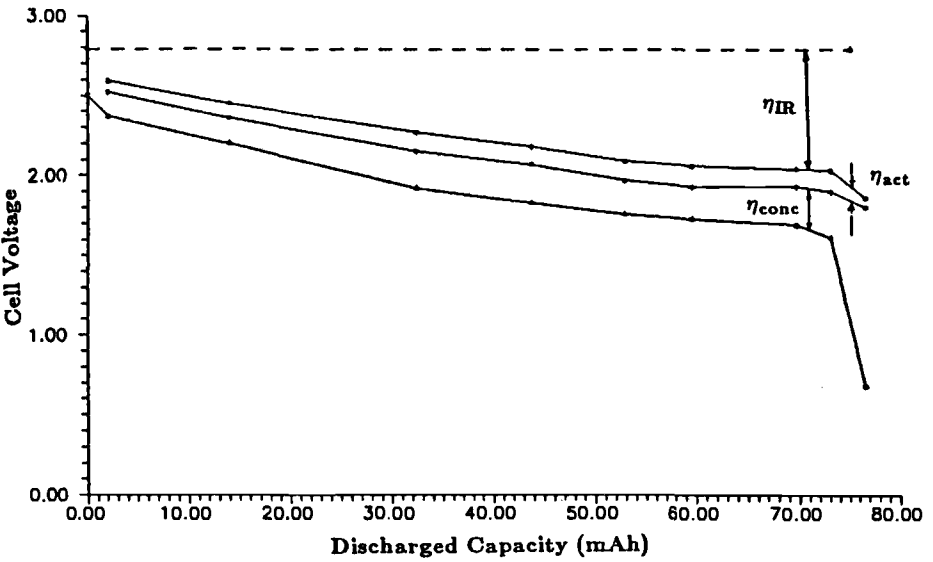
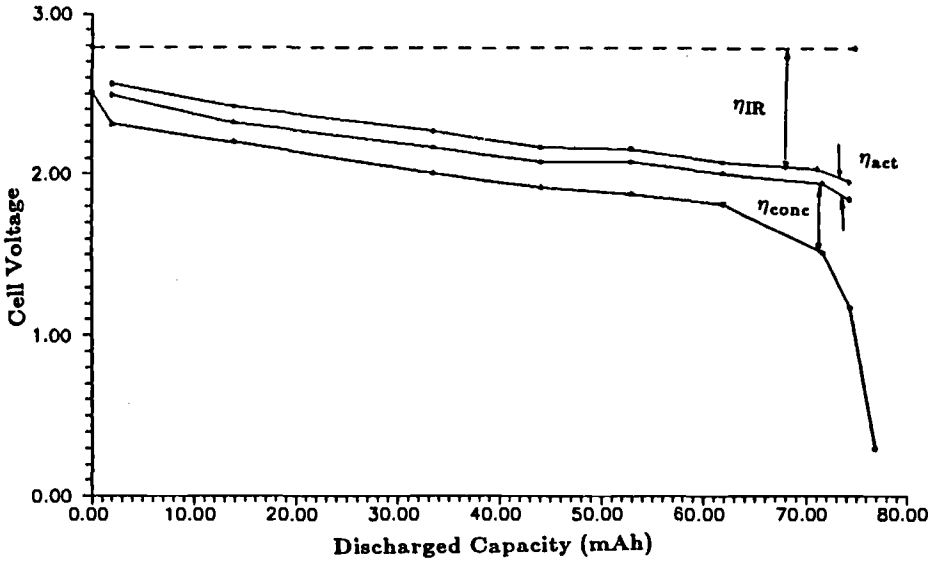


FIG. 3—Typical overpotential versus discharged capacity curves of newly constructed cells with cathode molecular weights of (a) 22K and (b) 54K discharged across 5 k $\Omega$ . The contributions of each of the individual overpotentials are shown. The bottom of the three curves are the operating cell voltage versus discharged capacity. Note that for both cell types the total overpotential is dominated by the ohmic contribution.

TABLE 1—Initial cathode and full cell impedance.

Molecular Weight	Cathode Cell	Complete Cell
22K Cathode	$106 \pm 6$	$165 \pm 22$
54K Cathode	$442 \pm 112$	$412 \pm 65$

probably occurs because the cathode, like the electrolyte, has a capacitance associated with it, making it necessary to model the cathode as an RC combination. If the time constant of this combination is similar to the time constant of the LiI RC combination then  $R_{\text{cath}}$  and  $R_{\text{LiI}}$  cannot be separated without the use of cells containing reference electrodes. It is also possible that since the LiI electrolyte forms into the remaining polymer framework of the cathode that the cathode and electrolyte are not physically separable, making it impossible to directly measure  $R_{\text{cath}}$  and  $R_{\text{LiI}}$  without an additional electrode. In either case, the modified model accommodates this by lumping the cathode and electrolyte together into one RC combination.

Table 1 also illustrates that the 54K cathode has an ohmic impedance that is approximately a factor of four greater than the 22K cathode. It has been proposed that this is due to an increase in the quantity of liquid phase present in the 22K cathode due to the lower molecular weight of the polymer [10]. It has been shown that the iodine-P2VP mixture forms a eutectic in the temperature and composition range of interest whose conductivity increases with increasing quantity of liquid phase [11]. Therefore it is evident that the cathode in the 54K cell dominates the fresh cell impedance to an even greater extent than in the 22K cell. An explanation for the 54K cathode impedance appearing greater than the 54K complete cell impedance is that a few of the cathode only cells had contact problems and thus very high impedances. The high standard deviation supports this.

While the impedance of the cathode thoroughly dominates the fresh cell ohmic impedance, the increase in ohmic impedance and the total ohmic impedance measured during discharge are dominated by the resistive LiI electrolyte layer, except near end of life. This is consistent with the results of Kelly and Moran [6,7]. Figure 5 illustrates that discharge of a 22K cell for only one mAh (less than 2% of cell capacity) increases the ohmic impedance by approximately a factor of three. Subsequent discharge increases the ohmic impedance to values more than an order of magnitude greater than in the predischarged state. Since this impedance is the sum of the LiI and cathode impedances and the cathode impedance is decreasing, this increase can only be explained by an increasing thickness of the LiI

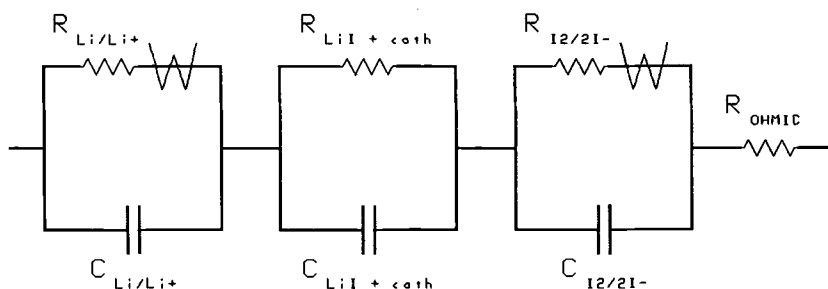


FIG. 4—The modified equivalent circuit model. This model is identical to the model developed by Kelly and Moran except that it now contains resistive and capacitive components from the cathode as well as the LiI layer.

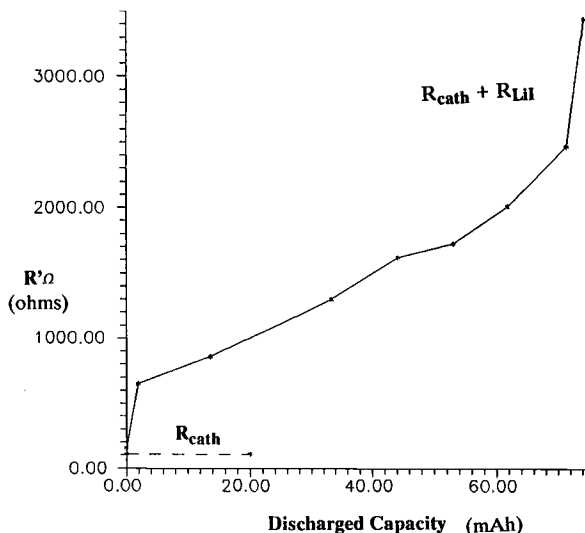


FIG. 5— $R'_o$  versus discharged capacity for the discharge shown in Fig. 2a (22K cell). The dashed line is the initial measured cathode impedance using the cathode only cell. It is used as an overestimation of the true cathode impedance at any time during discharge. Note that the full cell ohmic impedance becomes significantly larger than that measured for the cathode.

during discharge. Therefore the impedance measured in the 22K cell quickly becomes dominated by the impedance of the LiI layer. This is supported by the fact that the resistivity of the cathode material has been demonstrated to decrease with decreasing iodine:P2VP ratio until a critical molar ratio of about 3:1, which is not reached until near end-of-life in the battery system studied [5]. In addition, Kelly and Moran [6] have shown that the LiI layer does increase in thickness with discharge and that the cathode thickness decreases with discharge. Decreasing cathode thickness also results in decreasing cathode impedance. Therefore, it is clear that the cathode impedance decreases with discharge until near end-of-life when it becomes severely depleted in iodine. (In Figs. 5 and 6 the cathode impedance is approximated as constant at its initial value as an overestimation.) Further evidence supporting LiI dominance is the approximately linear increase in  $R'_o$  with discharged capacity. This is consistent with the linearly increasing thickness of the LiI during constant current discharge. While these discharges are not exactly constant current discharges, it can be seen in Fig. 2 that between 1 mAh and 65 mAh, discharge current can be approximated as constant.

Figure 5 illustrates the increase in ohmic impedance with discharge for the 54K cell discharged across a 5 k $\Omega$  resistive load. For the same reasons as in the 22K cells the 54K cell ohmic impedance is dominated by the impedance of the LiI electrolyte. However, the dominance is not as severe as for the 22K cell simply because the impedance of the 54K cathode is greater than the 22K cathode. This indicates that as the P2VP polymer molecular weight increases, increasing the resistance of the cathode, the degree of dominance of the ohmic impedance of the LiI decreases. Thus, it is probable that pacemaker cells, which use polymer with molecular weights approaching 400 000, are partially limited by the high resistance of the cathode. As stated above this is due entirely to the increasing magnitude of the cathode impedance with increasing molecular weight. It should be noted that,

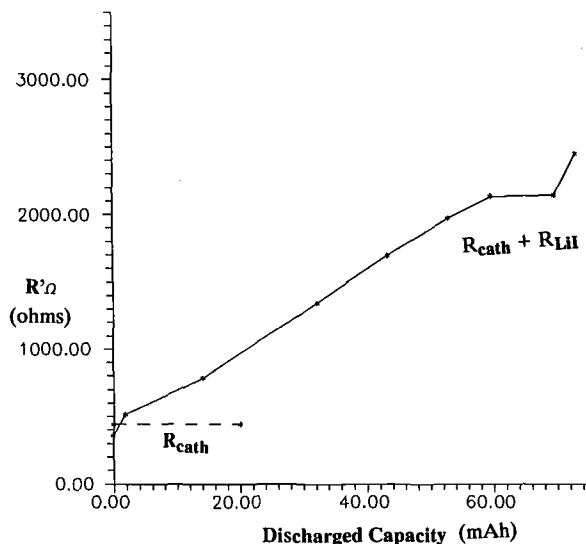


FIG. 6.— $R'_\Omega$  versus discharged capacity for the discharge shown in Fig. 2b (54K cell). The dashed line is the initial measured cathode impedance using the cathode only cell. It is used as an overestimation of the true cathode impedance at any time during discharge. Note that in the 54K cell the cathode contributes more significantly to the total  $R'_\Omega$ , than in the 22K cell.

regardless of the molecular weight of the P2VP polymer, the increasing ohmic impedance with discharge is due entirely to the formation of LiI.

## Conclusion

Electrochemical impedance spectroscopy can be utilized to monitor ohmic changes in the lithium/iodine (P2VP) battery system. In this system, owing to its solid state nature, ohmic losses are the dominant factor controlling the rate capabilities of the cell. At high discharge rates ( $300 \mu\text{A}/\text{cm}^2$ ), ohmic losses dominate the operating voltage such that it falls to unusable levels. In previous work performed in this laboratory, Kelly and Moran [6,7] showed a correlation between the morphology and resistivity of the formed electrolyte. Specifically, it was demonstrated that higher discharge rates produce an electrolyte layer that is less homogeneous and more resistive. It was concluded that the formation of a highly resistive electrolyte was the rate limiting mechanism for these cells.

In this study it has been shown, through the use of cells containing only cathode material, that the resistance of the cathode dominates the measured  $R'_\Omega$  prior to discharge for the cells used. As a result, a modification of the developed equivalent circuit model has been proposed to accommodate the fact that  $R_{\text{cath}}$  and  $R_{\text{LiI}}$  do not appear to be separable in frequency. This modification in no way changes the conclusions drawn by Kelly and Moran [6,7] especially with regard to the rate limiting mechanisms in these cells. It has also been shown that the 54K cell consists of a more resistive cathode which governs the fresh cell  $R'_\Omega$  to a greater extent than in the 22K cell. Consistent with the work of Kelly and Moran [6,7], it has been concluded that  $R_{\text{LiI}}$  becomes considerably larger than  $R'_\Omega$  early in discharge (less than 2% cell capacity for the 22K cell). Owing to the increased magnitude of  $R_{\text{cath}}$  in the 54K cell dominance of  $R_{\text{LiI}}$  occurs later in discharge than for the 22K cell;

however, all changes in the measured  $R'_\Omega$  during discharge for both cell types are controlled by  $R_{Li}$ .

### Acknowledgments

This research was performed in cooperation with and supported by Catalyst Research, a Division of Mine Safety Appliances, Owings Mills, Maryland. The technical assistance in manufacturing these cells provided by Henry Sunel is greatly appreciated. EG&G Princeton Applied Research is acknowledged as a sponsor of CERL.

### References

- [1] Schneider, A. A., Moser, J. R., Webb, T. H., and Desmond, J. E., "Proceedings of the 24th Power Sources Symposium," Atlantic City, NJ, 19-20 May 1970, pp. 27-30.
- [2] B. B. Owens and N. Margalit, Eds., "Power Sources for Biomedical Implantable Applications and Ambient Temperature Lithium Batteries," The Electrochemical Society Softbound Proceedings Series, Princeton, NJ (1980).
- [3] Editor, B. B. Owens, "Batteries for Implantable Biomedical Devices," Plenum Press, New York, 1986.
- [4] Lewkowitz, S., Untereker, D., Holstrom, K., and Phillips, G., Abstract 22, p. 61, The Electrochemical Society Extended Abstracts, Vol. 77-2, Atlanta, GA, 9-14 Oct. 1977.
- [5] Surd, D., Jolson, J., Yang, N. L., and Hou, C. J. Presented at the 1985 Power Sources Conference, Cherry Hill, NJ, 1985.
- [6] Kelly, R. G., and Moran, P. J., *Journal of the Electrochemical Society*, Vol. 134, 1987, p. 25.
- [7] Kelly, R. G. and Moran, P. J., *Journal of the Electrochemical Society*, Vol. 134, 1987, p. 31.
- [8] Kelly, R. G., *Journal of the Electrochemical Society*, Vol. 134, 1987, p. 55C.
- [9] Schneider, A. A., Bowser, G. C., and Foxwell, L. H., U. S. Pat. 4, 148,975 (1979).
- [10] Streinz, C. C., Kelly, R. G., Moran, P. J., and Waggoner, J. R., "Proceedings of the Symposium on Primary and Secondary Ambient Temperature Lithium Batteries," Editors J. P. Gabano, P. Bro, and Z. Takehara, The Electrochemical Society, 18-23 October (1987).
- [11] Phillips, G. M. and Untereker, D. F., "Power Sources for Biomedical Implantable Applications and Ambient Temperature Lithium Batteries," B. B. Owens and N. Margalit, Ed., *The Electrochemical Society Softbound Proceedings Series*, Princeton, NJ 1980, pp. 195-206.

## The Importance of Ohmic Potential Drop in Crevice Corrosion

---

**REFERENCE:** Shaw, B. A., "The Importance of Ohmic Potential Drop in Crevice Corrosion," *The Measurement and Correction of Electrolyte Resistance in Electrochemical Tests, ASTM STP 1056*, L. L. Scribner and S. R. Taylor, Eds., American Society for Testing and Materials, Philadelphia, 1990, pp. 211-219.

**ABSTRACT:** The IR drop along the length of a crevice plays an important role in crevice corrosion. Two examples of how crevice corrosion can be induced by IR drop are presented and discussed. The first example involves crevice corrosion of a passive film forming metal whose polarization characteristics *do not* need to be altered to establish crevice corrosion. The second example involves the crevice corrosion of a passive film forming metal whose anodic polarization characteristics *do* need to be altered to establish crevice corrosion and the alteration results from chemistry changes within the crevice. Polarization behavior in environments representing those found inside and outside the crevice will be used to illustrate the role of IR drop in crevice corrosion.

**KEY WORDS:** ohmic potential drop, IR drop, mechanism of crevice corrosion, stainless steel, iron, polarization curves

Crevice corrosion is a localized form of corrosion inherent in metals and alloys that are easily passivated (e.g., stainless steels, aluminum and aluminum alloys, titanium and titanium alloys, and nickel and nickel-based alloys). Iron and steel are also susceptible to crevice corrosion in highly oxidizing or passivating environments. The objective of this paper is to illustrate the importance of the role that IR, or ohmic potential drop, plays in a crevice corrosion.

Crevice corrosion involves accelerated attack in the creviced region of a metal or alloy and is usually attributed to compositional differences of the electrolyte within the crevice relative to the bulk. This was evident even in the early literature, in which differential aeration [1,2] metal ion concentration [2], inhibitor concentration [2-4], and hydrogen ion concentration [5] cells were proposed to explain crevice corrosion. It has also been evident that a potential difference develops between the metal in the crevice and that in the bulk solution [6,7] because of the electrolyte composition change. Because of the typically large surface area of the metal exposed to the bulk environment relative to that exposed to the crevice solution, we would expect that the potential of the creviced region would be polarized substantially toward the bulk potential. Loss of passivity and the ensuing attack within the crevice can then be explained by one or two depassivation mechanisms. In the first depassivation mechanism, which will be referred to as the breakdown mechanism, the crevice potential is polarized to a value at which passivity is locally broken down. In other words, the breakdown potential,  $E_{bd}$ , for the metal in the crevice environment is exceeded [8,9]. For this mechanism, the IR associated with the crevice might actu-

<sup>1</sup> Materials Engineer, Martin Marietta Laboratories, Baltimore, MD, 21227.

ally serve to lessen attack in the crevice by limiting the extent of anodic polarization of the crevice. While the breakdown mechanism may be applicable to less corrosion-resistant metals because of their susceptibility to  $\text{Cl}^-$ , it cannot explain the observed crevice corrosion of very corrosion resistant metals, for which breakdown is very difficult. Additionally, the breakdown mechanism cannot explain crevice corrosion that occurs in the absence of an aggressive species, such as chloride ions [10–13], or crevice corrosion that occurs in concentrated oxidizing acids.

A second depassivation mechanism, which will be referred to as the IR induced mechanism, occurs when the crevice potential rests at a value in the active region of the active-passive polarization curve. The rate of propagation of attack depends on the current densities that can be attained in this active region of the polarization curve. For this mechanism, the IR drop down the crevice is a necessity, as it is responsible for the potential of the crevice, or at least part of the crevice, being in the active region of the active-passive portion of the polarization curve. We will show that the IR induced mechanism can explain crevice corrosion that occurs in the absence of an aggressive species and can also explain the crevice corrosion of highly resistant metals.

The IR drop along the length of the crevice is an important factor that has been overlooked in many crevice corrosion mechanism studies. For tight or deep crevices or both, or crevices containing entrapped hydrogen bubbles, the resistance value,  $R$ , in this term can be quite high. Resistances on the order of 100 000  $\Omega$  are possible, even in highly conductive, concentrated crevice solutions [14]. The resistance of the narrow electrolyte path in the crevice is directly proportional to the crevice length and inversely proportional to the crevice tightness. Kain [15–17] has documented crevice gaps for a number of practical applications and observed dimensions ranging from 10  $\mu\text{m}$  to less than 1  $\mu\text{m}$ . Gaps of these dimensions are produced when deformable materials, such as nitrile rubber o-rings, are compressed between metallic surfaces. Combining the high resistance of a narrow electrolyte path with passive currents on the order of a few  $\mu\text{A}$  to tens of mA results in significant ohmic potential drops.

A unified crevice corrosion mechanism [18] combining several of the concepts identified above was proposed in the midsixties. This mechanism was proposed specifically to explain the crevice corrosion of stainless steels exposed in neutral pH environments containing chloride ions. The unified mechanism consists of four stages:

- (1) depletion of oxygen in the crevice,
- (2) an increase in the chloride ion content and acidity of the crevice solution,
- (3) permanent loss of passivity for the metal inside the crevice, and, finally
- (4) propagation of attack within the crevice.

Initially, the anodic reaction of slow alloy dissolution and the cathodic oxygen reduction reaction occur both inside and outside the crevice. In time, the oxygen within the crevice is depleted faster than it can be replenished by diffusion, and the cathodic reaction moves outside the crevice, where it can be supported by the higher dissolved oxygen content of the bulk solution. Slowly, metal ions concentrate in the crevice and  $\text{Cl}^-$  ions migrate into the crevice to maintain charge neutrality. The hydrolysis of metal chloride complexes in the crevice leads to the formation of  $\text{H}^+$  ions, dropping the pH of the crevice solution. A point is reached when the metal in the crevice becomes active and propagation of attack within the crevice ensues. Rapid dissolution of the metal inside the crevice is driven by the oxygen reduction reaction outside the crevice and, if thermodynamically possible, some hydrogen evolution inside the crevice.

The unified mechanism just described was proposed to explain the crevice corrosion of

stainless steels exposed to neutral chloride solutions and is, therefore, not applicable to all cases of crevice corrosion. For a process as complex as crevice corrosion, it is unlikely that a single mechanism exists that is capable of explaining all cases of crevice corrosion. Loss of passivity in the crevice is usually attributed to compositional changes occurring in the crevice. However, the majority of the literature concerned with crevice corrosion is unclear as to the depassivation mechanism involved. In fact, the idea of IR induced depassivation has received little attention when it is possibly the most common mechanism.

### The Role of IR in Crevice Corrosion

#### Example 1—No Change in Anodic Polarization Behavior Required

Case 1 describes the crevice corrosion of a passive film forming metal whose anodic polarization characteristics *do not* need to be altered to establish crevice corrosion. In other words, the breakdown potential ( $E_{bd}$ ), the passivating potential ( $E_{pp}$ ), the passive current density ( $i_p$ ), and the critical current density ( $i_{crit}$ ) for the metal in the crevice do not need to be altered by the build up of a high chloride/low pH environment to establish crevice corrosion. Some practical examples of this case include: crevice corrosion of iron in a concentrated oxidizing acid [3,4], crevice corrosion of iron in a solution containing an oxidizing (passivating) inhibitor [4,19–21], and crevice corrosion of a stainless steel in aerated sulfuric acid [22]. Consider the example of crevice corrosion of iron (Fe) in an oxidizing acid such as concentrated nitric acid ( $\text{HNO}_3$ ). Initially, the reduction of  $\text{HNO}_3$  is responsible for the passivation of the metal surfaces inside and outside the crevice. The anodic

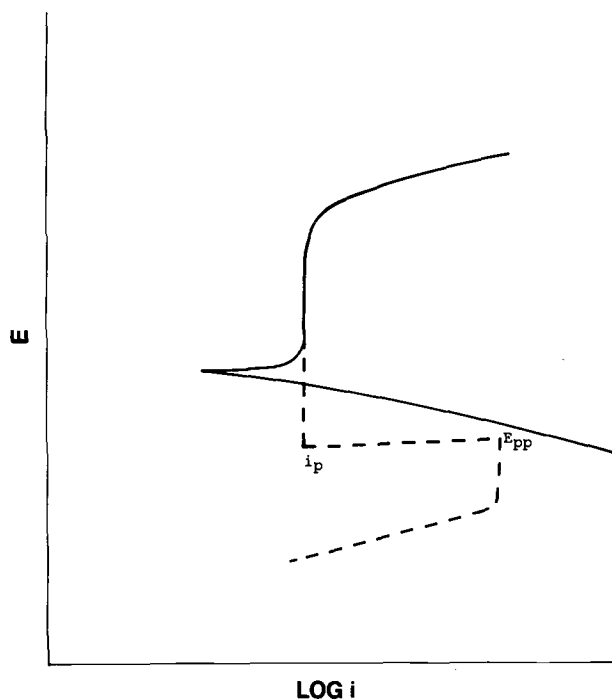


FIG. 1—Anodic and cathodic polarization curves for iron in concentrated  $\text{HNO}_3$  (dotted curve shows underlying Evans diagram for anodic dissolution of iron).

and cathodic polarization behavior for the iron in the concentrated  $\text{HNO}_3$  is presented in Fig. 1. The dotted curve in this figure reveals the underlying Evans diagram for the anodic polarization curve. The passivity of the metal outside the crevice is maintained by a fresh supply of  $\text{HNO}_3$  to the metal surface. Inside the crevice, however, the supply of  $\text{HNO}_3$  to the metal surface is impeded by the geometry of the crevice. In time, the  $\text{HNO}_3$  within the crevice is reduced to nitrous acid ( $\text{HNO}_2$ ), and ultimately, to  $(\text{NO})$  [23], diminishing the oxidizing capacity of the solution. As the oxidizing capacity of the crevice solution is reduced, the open circuit potential of the iron in the crevice shifts in the electronegative direction as illustrated in Fig. 2 (ignoring for the moment the influence of the "galvanic" couple to the area outside the crevice). When the oxidizing power of the solution in the crevice is diminished to a value below the passivating potential, the iron in the crevice becomes active. This transition from passive to active occurs because of the loss of oxidant and the corresponding cathodic polarization of the metal in the crevice, and not because the polarization characteristics of the metal have been altered.

The differences in the oxidizing capability of the solution inside and outside the crevice result in the formation of a "crevice couple," which can be evaluated using a mixed potential approach. Analysis of the "crevice couple" is made based on the current ( $I$ ) rather than the current density ( $i$ ) because the cathodic and anodic areas in a crevice situation are seldom equal. Superimposing the cathodic polarization curve in the bulk concentrated  $\text{HNO}_3$  from Fig. 1 onto the anodic polarization curve for iron in the nonoxidizing acidic environment within the crevice results in Fig. 3. If no crevice were present, the current at

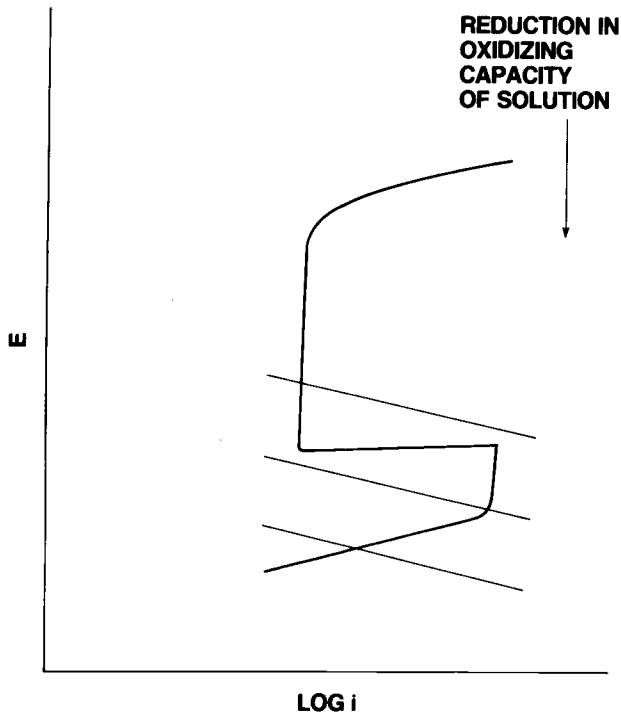


FIG. 2—Evans diagram for iron in acid illustrating the effect of solution oxidizing capacity.

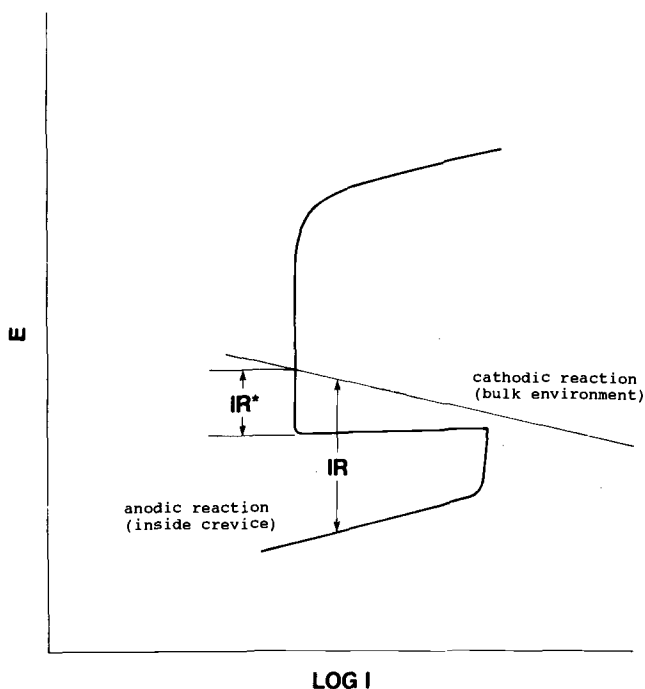


FIG. 3—Mixed potential analysis of iron/oxidizing acid—iron/nonoxidizing acid crevice couple.

the cross-over point would represent the corrosion rate of the iron. When a crevice is present, the high resistance of the narrow electrolyte path results in an  $IR$  drop along the length of the crevice. Figure 3 illustrates that if the potential drop associated with the crevice is larger than  $IR^*$ , the only region where the  $IR$  drop can be accommodated between the anodic and cathodic curves is in the active region of the anodic polarization curve.

#### Example 2—Changes in Anodic Polarization Behavior Required

Case 2 involves the crevice corrosion of a passive film forming metal whose anodic polarization characteristics *do* need to be altered to establish crevice corrosion. In other words, a change in the characteristic features ( $E_{pp}$ ,  $E_{bd}$ ,  $i_{crit}$ ,  $i_p$ ) of the anodic polarization curve for the metal in the crevice is needed. Crevice corrosion of a highly alloyed stainless steel or a nickel-based alloy in seawater exemplifies case 2 crevice corrosion [24,25]. Crevice corrosion is most commonly encountered in neutral pH environments, such as seawater, and specific experimental results supporting an  $IR$  induced mechanism for the crevice corrosion of a nickel-based alloy in seawater are presented in another paper [26].

To illustrate this case, consider the example of crevice corrosion of a highly alloyed stainless steel in aerated seawater. Initially, oxygen reduction and metal dissolution reactions occur both inside and outside the crevice. The rate of these reactions is determined by the passive current density of the particular stainless steel in seawater. For tight crevices (crevice gaps of about a micron), the oxygen within the crevice would be depleted within minutes and the cathodic reaction would move outside the crevice, where it could be supported by the higher dissolved oxygen content. As metal ions accumulate within the crevice, chlo-

ride ions migrate into the crevice to maintain charge neutrality, and hydrolysis of these ions and metal chloride complexes within the crevice lowers the pH of the solution in the crevice. As a result of these changes in the chemistry of the crevice solution, the shape of the anodic polarization curve for the stainless steel inside the crevice is altered. Acidification of the crevice solution shifts the passivating potential in the electropositive direction [27,28] and increases the critical current density [18] and the passive current density [28]. The increasing chloride content of the crevice solution also increases the passive current density [29] and the critical current density [18] and usually leads to an electronegative shift in the breakdown potential [29]. The degree of the shift in  $E_{bd}$  depends on the composition of the stainless steel, with the more corrosion-resistant materials exhibiting a greater resistance to electronegative shifts in  $E_{bd}$ . [29].

Representative anodic and cathodic polarization behavior for the stainless steel in the bulk seawater environment are presented in Fig. 4. Again, the dotted curve in this figure shows the underlying Evans diagram for anodic polarization of the metal. In this environment, the stainless steel is self passivating and exhibits a low passive current density and a relatively high breakdown potential. The cathodic curve in aerated seawater typically exhibits a limiting current density before experiencing hydrogen evolution. The characteristic features of the anodic polarization curve change as the crevice solution becomes more aggressive. Figure 5 illustrates the changes that occur in the polarization curve as a result of the formation of this low-pH, highly concentrated chloride solution within the crevice. As the pH of the solution drops,  $E_{pp}$  shifts electropositively and  $i_p$  increases. As the chloride

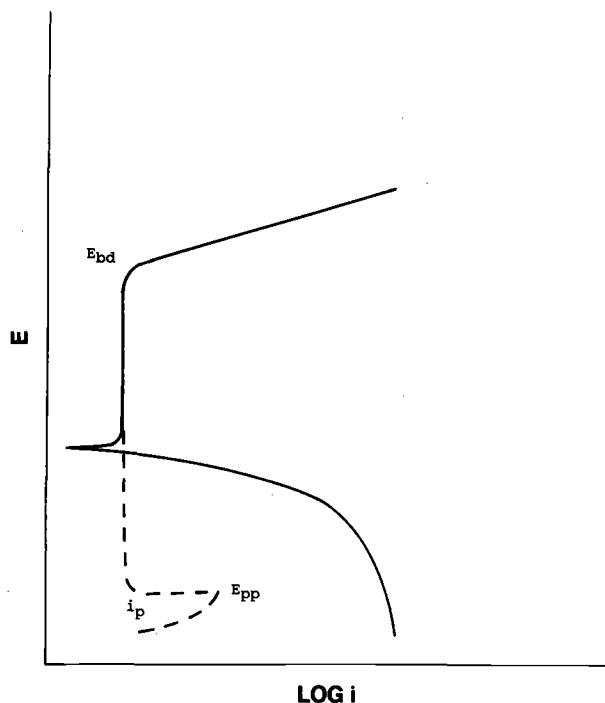


FIG. 4—Anodic and cathodic polarization curves for a highly alloyed stainless steel in seawater (dashed curve illustrates underlying Evans diagram for anodic dissolution of stainless steel).

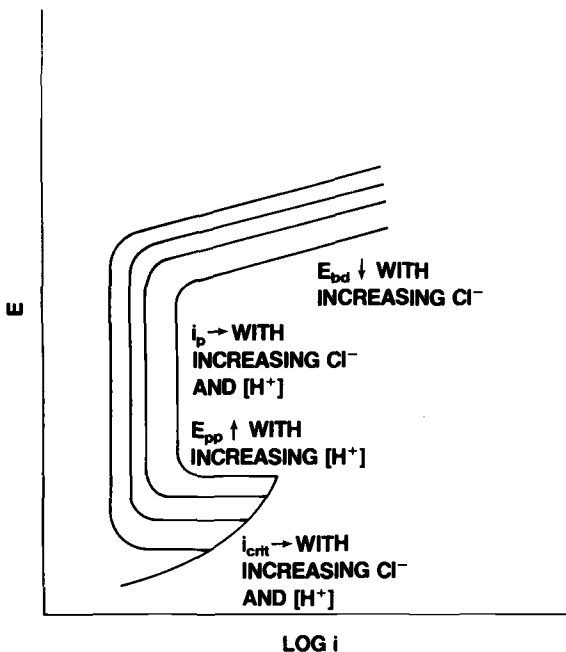


FIG. 5—Changes in anodic polarization behavior resulting from increasingly aggressive solution forming within the crevice.

ion concentration of the solution increases,  $i_{crit}$  increases,  $i_p$  increases, and  $E_{bd}$  shifts electronegatively.

The effects of IR on the crevice couple are best illustrated using a mixed potential evaluation. Figure 6 shows the anodic polarization curve in the aggressive crevice environment superimposed on the cathodic polarization curve in the bulk environment. Again, analysis of the “crevice couple” is based on current rather than current density because the cathodic and anodic areas for a crevice corrosion situation are seldom equal. The cross-over point for the two curves is in the passive region of the anodic curve. If no crevice is present, then the current at the cross-over point represents the corrosion rate of the stainless steel. When a crevice is present, the IR drop must be applied to the polarization curves to determine the rate of attack inside the crevice. Assuming that the passive current density is independent of potential as shown in Fig. 6, an IR drop equal to  $IR^*$  could be accommodated between the anodic and cathodic curves in the passive region; however once  $IR > IR^*$ , the only place where the IR drop can be accommodated in Fig. 6 is in the active region of the anodic polarization curve. Crevice corrosion is initiated because the IR drop down the crevice shifts the potential inside the crevice to a region where active dissolution of the metal occurs. Once initiated, crevice corrosion is maintained by the IR drop.

### Summary

Two examples of IR induced crevice corrosion were presented. In the first example, the polarization characteristics of the passive film forming metal *did not* need to be altered to establish crevice corrosion. The crevice corrosion of iron in concentrated  $HNO_3$  was presented as an example. A mixed potential analysis of this case demonstrated that once the

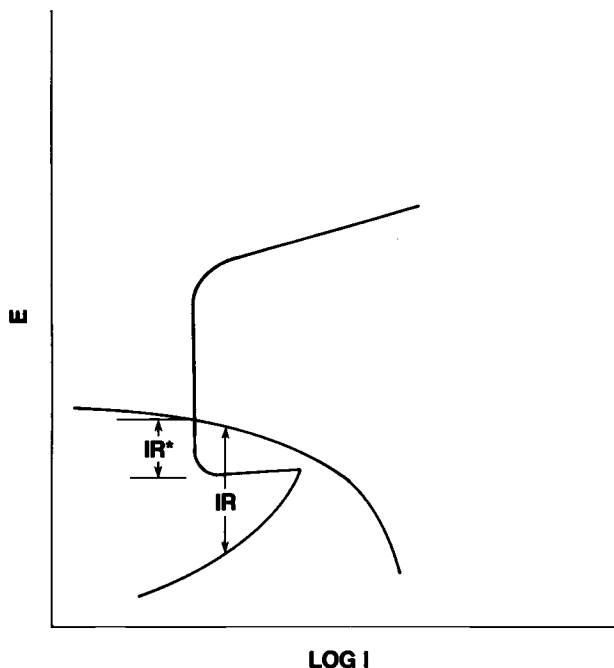


FIG. 6—Mixed potential analysis of crevice couple formed when a highly alloyed stainless steel is exposed in seawater.

oxidizing capacity of the acid within the crevice had been depleted, the IR drop along the length of the crevice was responsible for the establishment of crevice corrosion. In the second example, the polarization characteristics of the passive film forming metal *did* need to be altered to establish crevice corrosion. The crevice corrosion of a stainless steel in seawater was presented as an example. In this case, the polarization characteristics of the metal in the crevice are altered by low-pH, high-Cl<sup>-</sup> environment that forms within the crevice. As the passive current density increases in the low-pH, high-chloride environment, a point is reached at which the IR drop is greater than IR\* and crevice corrosion is initiated. In both the examples presented, the IR drop associated with the restricted geometry of the crevice was a necessary condition for the establishment of crevice corrosion.

In much of the literature, the exact depassivation mechanism (i.e., IR-induced or breakdown) for crevice corrosion initiation is not specified. I believe that more experimental evidence exists to support IR-induced crevice corrosion than to support crevice corrosion resulting from a breakdown mechanism. Hopefully, this paper has clarified the importance of the role that IR plays in initiating and maintaining crevice corrosion. This work also supports the assertion of Pickering [31] that an IR mechanism is responsible for many, if not all, cases of localized corrosion.

## References

- [1] Evans, U. R., *The Corrosion of Metals*, Arnold, London, 1926, p. 93.
- [2] West, J. M., *Electrodeposition and Corrosion Processes*, Van Nostrand, London, 1965, p. 55.
- [3] Evans, U. R., *An Introduction to Metallic Corrosion*, Arnold, London, 1948, p. 52.
- [4] Rosenfeld, I. L. and Marshakov, I. K., *Corrosion*, Vol. 20, No. 115.

- [5] Myers, J. R. and Obrecht, M. F., 27th Annual Conference National Association of Corrosion Engineers, Chicago, 1971, paper 90.
- [6] Korovin, Y. M. and Ulanovski, I. B., *Corrosion*, Vol. 22, No. 16.
- [7] Wranglen, G., *An Introduction to Corrosion and Protection of Metals*, Chapman Hall, London, 1985, p. 99.
- [8] Krougman, J. M and Ijsseling, F. P., Fifth International Congress on Marine Corrosion.
- [9] Dawson, J. L. and Ferreira, M. G. S., *Corrosion Science*, Vol. 26, p. 1027.
- [10] Rosenfeld, I. L., *Localized Corrosion*, K. W. Staehle, Ed. National Association of Corrosion Engineers, Houston, 1974, p. 373.
- [11] Uhlig, H. H. and Reeve, R. W., *Corrosion and Corrosion Control*, John Wiley & Sons, New York, 1985, p. 316.
- [12] Pickering, H. W., Joint United States—German Meeting on Electrochemical Passivity, to be published in *Corrosion Science*.
- [13] France, W. D., Localized Corrosion—Cause of Metal Failure, *ASTM STP 516*, American Society for Testing and Materials, Philadelphia, 1972, p. 164.
- [14] Shaw, B. A., Moran, P. J., and Gartland, P. O., *Corrosion 88*, Research Symposia Abstract, National Association of Corrosion Engineers, St. Louis.
- [15] Kain, R. M., *Corrosion 82*, paper 66, National Association of Corrosion Engineers (1982).
- [16] Kain, R. M., Tuthill, A., and Topsy, E., *Journal of Materials for Energy*, Vol. 5, No. 205.
- [17] Kain, R. M., *Metals Handbook*, Vol. 13, ASM International, Metals Park, 1987, p. 111.
- [18] Fontana, M. and Greene, N., *Corrosion Engineering*, McGraw-Hill, New York, 1978.
- [19] Karlberg, G. and Wraglen, G., *Corrosion Science*, Vol. 11, p. 499.
- [20] Ijsseling, F. P., *British Corrosion Journal*, Vol. 15, p. 51.
- [21] Shreir, L. L., *Corrosion*, Vol. 1, No. 18, p. 17.
- [22] Kain, R. M., *Metals Handbook*, Vol. 13, ASM International, Metals Park, 1987, p. 110.
- [23] Evans, U. R., *The Corrosion and Oxidation of Metals: Scientific Principles and Practical Applications*, Arnold, 1960, p. 328.
- [24] Hack, H. P., *Materials Performance*, Vol. 22, p. 24.
- [25] Streicher, M. A., *Materials Performance*, Vol. 22, p. 37.
- [26] Shaw, B. A., Moran, P. J., and Gartland, P. O., to be submitted to *Corrosion Science*.
- [27] Vetter, K. J., *Electrochemical Kinetics*, Academic Press, New York, 1967, p. 751.
- [28] Kaeschre, H. *Metallic Corrosion—Principles of Physical Chemistry and Current Problems*, National Association of Corrosion Engineers, Houston, 1985, p. 237.
- [29] Sedriks, A. J., *Corrosion of Stainless Steels*, John Wiley and Sons, New York, 1979.
- [30] Shreir, L. L., *Corrosion*, Vol. 1, p. 3:58, Newnes Butterworth, London 1976.
- [31] Pickering, H. W., *Proceedings of the International Conference on Localized Corrosion*, H. Isaacs, Ed., National Association of Corrosion Engineers, Houston, to be published.

## Author Index

### A-C

Abraham, D., 157  
 Beavers, J. A., 168  
 Berke, N. S., 191  
 Case, C. M., 157  
 Chen, Y. C., 95

### E-F

Erhardt, W. C., 27, 78  
 Escalante, E., 180  
 Esteban, J. M., 127  
 Farozic, V., 142

### H-K

Hack, H. P., 5  
 Jolson, J., 202  
 Jones, D. A., 157  
 Kelly, R. G., 202

### L-N

Lowry, M., 127  
 Mansfield, F., 95

Moran, P. J., 5, 202  
 Nisancioglu, K., 61

### O-P

Orazem, M. E., 127  
 Prentice, G., 142

### S

Scribner, L., editor, 1  
 Scully, J. R., 5  
 Shaw, B. A., 211  
 Shen, D. F., 191  
 Shih, H., 95  
 Streinz, C. C., 202  
 Sundberg, K. M., 191

### T-W

Taylor, R., editor, 1  
 Thompson, N. G., 68  
 Waggoner, J. R., 202  
 Whitbeck, M. R., 157  
 Wicelinski, S., 202

# Subject Index

## A-B

AC impedance, 5, 24, 61  
 Analytical solutions, 143  
 Battery behavior, 203  
 Breakdown mechanism, 211  
 Bridge deck corrosion, 142, 180, 186  
 Buried pipelines, 168

## C

Cathodes, 202, 204, 209  
 Cathodic protection, 168, 170  
 Cell constant, 27, 31  
 Cell geometry, 29, 142  
 Chloride intrusion, 191  
 Computer methods, 78, 142, 144, 180, 186, 190  
 Concrete resistivity, 191, 197  
 Corrosion, 5, 27, 61, 78, 89, 180, 198  
   buried pipelines, 168  
   concrete, 95, 157, 180, 186, 191  
   crevices, 61, 211  
   in soils, 157, 163  
   in water, 27  
   probes, 27  
   steel, 27, 43, 180, 187, 191, 198, 201, 212  
 Corrosion testing, 5, 27, 61, 157  
 Crevice corrosion, 61, 67, 211, 213, 217  
 Current density, 127, 134, 142  
 Current distribution, 5, 17, 23, 27, 35, 61, 142  
 Current interpretation technique, 192  
 Current interruption, 19, 61, 78, 82, 86, 168, 191, 197, 201  
 Curve fitting, 27

## D

Depassivation mechanism, 211, 214  
 Desert soils, 157  
 Disk electrodes, 61, 142, 146, 152  
   insulating disk, 142  
 Dummy cells, 95, 101, 107

## E

Electrochemical cells, 28, 39  
 Electrochemical corrosion technique, 27, 37  
 Electrochemical impedance spectroscopy, 5, 96, 105, 202, 209  
 Electrochemical impedance test, 5, 27, 78, 83, 191, 196  
 Electrochemical measurements, 5, 16, 142  
 Electrode potential measurements, 1 (*See also* Disk electrodes, Cathodes, Gas evolving electrodes)  
 Electrolyte resistance, 5, 9, 13, 95  
 Error reduction, 27, 50, 61, 67, 96, 211  
   in electrode placement, 143  
   in field studies, 169  
   in low conductivity media, 96  
 Experimental design, 142

## F

Feedback, 78, 81, 85, 89  
 Field techniques, 168, 180, 186  
 Finite difference theory, 142, 144  
 Full polarization, 27

## G-H

Gas evolving electrodes, 143  
 High potential gradient, 143  
 Hydrazine, 95, 119

## I

Inherent resistance, 1  
 Instrumentation, (*See also* Computer techniques) 27, 78, 84  
 Interrupter technique, 95, 98, 102, 122  
 IR drop, 5, 142, 168, 211, 213  
   compensation, 5, 27, 40, 50, 78, 81, 168, 176, 180, 191  
   in corrosion studies, 27, 78, 168, 177, 213  
   in current density, 127, 142  
   in current distribution, 5, 27, 61, 142  
 IR error, 5, 7, 21, 168, 180  
 IR induced mechanism, 211  
 Iron, 211

## L

Laboratory methods, 180, 185, 195  
 Lead, 157, 162  
 Lithium iodine battery, 202, 207, 209  
 Long-line current, 168, 176  
 Low conductivity media, 61, 75, 95, 97, 169  
 Low potential gradient, 143

## M

Mathematical models, 142, 143  
 Maxwell's analysis, 143, 149  
 Moisture content of soil, 157

## N

Nondestructive techniques, 191  
 Nonuniform current distribution, 27  
 Nonuniform ohmic drop, 51, 61  
 Numerical methods, 127, 133, 139, 142  
 Nyquist plot, 193

## O

Occluded corrosion cells, 62  
 Off-potentials in buried pipelines, 168, 176, 178  
 Ohmic compensation, 157, 160  
 Ohmic drop, 95, 100, 142, 211  
 Ohmic electrolyte resistance, 191, 201  
 Ohmic impedance, 202, 207  
 Ohmic overpotential, 202  
 Ohmic potential drop, 64, 127, 180, 211  
   AC impedance technique, 61  
   current density, 127, 142  
 Ohmic resistance, 61, 127, 130, 191, 202  
 On- and off-potentials, 169, 173  
 Oscilloscope, 168

## P

Pacemaker batteries, 202, 208  
 Parallel electrode configuration, 143  
 Pelletized cathodes, 202  
 Pipe-to-soil potentials, 168, 170, 177  
 Placement of electrodes, 142  
 Plane electrodes, 142, 147  
 Polarization, 27, 38, 61, 78, 157, 180, 191, 211  
   in corrosion studies, 27, 40, 65, 157, 192, 213  
   in low conductivity media, 96  
 Polarization resistance, 191, 196  
 Positive feedback technique, 95, 97, 99, 123, 192  
 Potential difference, 142, 191, 211  
 Potential pulse methods, 61  
 Potential spike, 168  
 Potentiodynamic measurements, 96  
 Potentiostatic testing, 5, 18, 78, 95, 103, 122  
 Primary potential distribution, 143  
 Probe design, 61, 72, 76

## R

Randles circuit, 193  
 Rate limiting mechanisms, 202  
 Reference electrode position, 95, 108, 143, 180, 191, 195  
 Reinforcing steel, 191  
 Rotating disk electrodes, 62, 127, 130, 143

**S**

Scan rate error, 96  
Shielding, 143  
Small range polarization, 27  
Sodium perchlorate, 95  
Sodium sulfate, 95  
Soils, 157, 163, 168  
Solid electrolyte batteries, 202  
Solution resistance, 27, 78  
Spiking conditions, 168, 175, 178  
Stainless steel, 95, 116, 211, 216, 218  
Steel, (*See also* Corrosion) 27, 95, 157,  
163, 168, 180, 201  
Steel reinforced structures, 180, 191  
Stray current, 168, 174, 176

Supporting electrolytes, 95  
Surface overpotential, 127, 138

**T**

Tafel slopes, 27, 96, 127, 129, 157, 161  
Total cell overpotential, 203

**U-W**

Uncompensated resistance, 95  
Voltage error 168  
Warburg impedance, 203, 207  
Water conductivities, 27  
Wheatstone bridge, 157, 167  
Working electrode, 180

ISBN 0-8031-1283-1